Research Report
KTC-15-14/SPR10-408-1F
DOI: http://dx.doi.org/10.13023/KTC.RR.2015.14

Effect of Thermal Loads on Substructures: New Trammel Creek Bridge on KY-100 in Allen County, Kentucky

Our Mission

We provide services to the transportation community through research, technology transfer and education. We create and participate in partnerships to promote safe and effective transportation systems.

Kentucky Transportation Center
176 Oliver H. Raymond Building
Lexington, KY 40506-0281
(859) 257-4513
fax (859) 257-1815

www.ktc.uky.edu

Research Report
KTC-15-14/ SPR10-408-1F

EFFECT OF THERMAL LOADS ON SUBSTRUCTURES: NEW TRAMMEL CREEK BRIDGE ON KY-100 IN ALLEN CO., KENTUCKY

by

Zhihui Zhu
Visiting Professor, Kentucky Transportation Center
Department of Civil Engineering
University of Kentucky

Michael T. Davidson
Research Professor,
Department of Civil Engineering
University of Kentucky

Issam E. Harik
Professor of Civil Engineering and Head, Structures Section,
Kentucky Transportation Center
University of Kentucky

and

Charlie Sun
Senior Research Engineer,
Kentucky Transportation Center
University of Kentucky

Kentucky Transportation Center
College of Engineering, University of Kentucky

in cooperation with

Transportation Cabinet
Commonwealth of Kentucky

and

Federal Highway Administration
U.S. Department of Transportation

August 2015

Technical Report Documentation Page

1. Report No.	2. Government Accession No.	3. Recipient's Catalog No.
KTC-15-14/ SPR10-408-1F		

4. Title and Subtitle	5. Report Date
Effect Of Thermal Loads on Substructures: New Trammel Creek Bridge On Ky-100 In Allen Co., Kentucky	August 2015
	6. Performing Organization Code

7. Author(s): Zhihui Zhu, Michael Davidson, Charlie Sun, and Issam Harik.	8. Performing Organization Report No. KTC-15-14/ SPR10-408-1F

9. Performing Organization Name and Address	10. Work Unit No. (TRAIS)
Kentucky Transportation Center College of Engineering University of Kentucky Lexington, Kentucky 40506-0281	11. Contract or Grant No.
12. Sponsoring Agency Name and Address	13. Type of Report and Period Covered
Kentucky Transportation Cabinet State Office Building Frankfort, Kentucky 40622	Final
	14. Sponsoring Agency Code

15. Supplementary Notes

Prepared in cooperation with the Kentucky Transportation Cabinet and the U.S. Department of Transportation, Federal Highway Administration.

16. Abstract

When infrastructure is subjected to temperature changes, structural members that are either partially or fully restrained against motion can develop internal stresses. The phenomenon of temperature-induced internal stress development in superstructure members has prompted the American Association of State Highway and Transportation Officials (AASHTO) to include provisions for determining superstructure temperature load effects. However, little consideration has been given to explicitly quantifying the effect that thermal stresses have on foundation systems such as intermediate bridge piers. The objective of this study is to instrument a multi-span integral abutment bridge with temperature and bridge response monitoring devices, and ultimately, to make a comparative analysis between measurements of temperature-induced soil pressures with pressures derived using the AASHTO design provisions. Accordingly, the New Trammel Creek Bridge (002B00054N) along KY-100 in Allen County, Kentucky has been fitted with temperature and response instrumentation. Data has being continuously collected from the bridge site since May 2011, and can be viewed at: http://www.ktc.uky.edu/kytc/RemoteBridgeMonitoringInKY/ky100Allen.html. Included in the research is a detailed analytical study of the New Trammel Creek Bridge, performed simultaneously with a field-monitoring program. Finite element (FE) modeling and analysis of temperature loadings on the bridge have pointed to AASHTO superstructure-temperature provisions as the preferred method. Also called Method B, the AASHTO provisions led to adequate sizing of bridge foundation members.

17. Key Words	18. Distribution Statement
Thermal stresses, foundation pressures, bridge piers, instrumentation, temperature load effects	Unlimited with approval of Kentucky Transportation Cabinet

19. Security Classif. (of this report)	20. Security Classif. (of this page)	21. No. of Pages	22. Price
Unclassified	Unclassified	178	

EXECUTIVE SUMMARY

Background

When temperature fluctuations impact infrastructure, the structural members that are either partially or fully restrained against motion can develop internal stresses. Bridge structures make up a substantial portion of the U.S. infrastructure; they are regularly exposed to significant temperature changes. Shifts in temperature are driven by convection as local climatic variability causes ambient air temperatures to fluctuate in the vicinity of bridge sites. Further, bridge roadway materials are heated radiantly by direct sun exposure (in addition to the convective influence of ambient air temperatures), and are thus susceptible to larger periodic temperature oscillations after the materials cool at night. Temperature fluctuations that occur along bridge roadways positively correlate with the underlying structural members' temperature variability; this is due to the process of conduction, which affects members such as bridge decks and superstructure girders. Due to partial or full-restraint conditions typically incorporated into the design of bridge superstructure systems (e.g., diaphragms, fixed-bearings), temperature changes bridge decks and superstructure girders can lead to the emergence of internal stresses. The changes in these members can, in turn, induce stresses throughout underlying bridge piers, into foundation systems, and into the underlying soil.

A principal focus for this study is the American Association of State Highway and Transportation Officials (AASHTO) LRFD Bridge Design Specifications (AASHTO 2012). Temperature-induced internal stress development in superstructure members has prompted AASHTO to include provisions for determining superstructure temperature load effects on overall bridge design. Furthermore, for construction types such as integral abutment bridges, the design of intermediate piers can be strongly influenced or even primarily controlled by the AASHTO thermal loads requirements (depending on pier height). However, little research has attempted to quantify the effect that thermal stresses have on the foundations of these intermediate piers. This study addresses this need by accurately estimating thermal loads (as translated to effects on foundation members), as a means to achieve proper design.

Having the cooperation of bridge owners in the state of Kentucky (the Kentucky Transportation Cabinet, KYTC), given the necessity for determining the impact that thermal stresses in continuous superstructures can have on the foundations of intermediate piers, a multi-span, integral abutment bridge was fitted with instrumentation to undergo structural monitoring. This study concerns the structural responses of the New Trammel Creek Bridge (002B00054N) on KY-100 in Allen County, Kentucky. The New Trammel Creek Bridge (Fig. E.1) is a four-span (two-lane) integral abutment bridge with spans ranging from 80 ft to 120 ft in length. The bridge spans are supported at the bridge far ends by integral end bents made up of reinforced concrete wing walls, wall stems, and steel h-piles. Three evenly spaced (at 120 ft) reinforced concrete bridge piers support the intermediate spans of the integral abutment bridge, where each pier contains a large shear wall and three pier columns. Each pier column span terminates below onto a thick reinforced concrete spread footing. All bridge foundation members rest on good-to-relatively-high quality limestone bedrock.

Fig. E.1 New Trammel Creek Bridge over KY-100 in Allen Co, Kentucky.

Research Objective

The objective of this study is to instrument the New Trammel Creek Bridge with temperature and bridge response monitoring devices, and ultimately, to make a comparative analysis between measurements of temperature-induced soil pressures with pressures derived using the AASHTO design provisions and bridge finite element analysis (FEA).

Research Tasks

To achieve this research objective, the New Trammel Creek Bridge was fitted with pressure cells at select foundation locations (Fig. E.2). Tiltmeters were placed at pier top locations, while temperature gauges were located at the superstructure level to simultaneously monitor temperatures within the bridge's vicinity, intermediate bridge pier motion, and soil pressures beneath the instrumented pier foundations. Continuous data collection began in May 2011 and is ongoing. Instrumentation readings are available in real-time on a website (http://www.ktc.uky.edu/kytc/RemoteBridgeMonitoringInKY/ky100Allen.html) maintained by the Kentucky Transportation Center (KTC), housed at the University of Kentucky in Lexington Kentucky. This website also details the monitoring of six other Kentucky bridges.

Concomitant with the field-monitoring program, the research team performed an analytical study of the New Trammel Creek Bridge. By using finite element (FE) modeling and analyzing temperature loadings on the selected bridge, we estimated bridge pier motion and foundation pressures using methodologies provided in AASHTO design provisions. We then compared the estimates to pressures physically measured at the bridge site. This assessed the merit of current AASHTO provisions related to temperature-induced response at the study site. Additionally, we reviewed those portions of the AASHTO provisions pertaining to superstructure temperature loading. Of the three techniques available in the AASHTO provisions to determine temperature-load effects on bridges, Procedure B (given in Sec. 3.12 of the AASHTO provisions) was used in

the design of the New Trammel Creek Bridge. Therefore, this study is primarily concerned with evaluating the temperature-load effects for the New Trammel Creek Bridge that have arisen from using Procedure B.

Fig. E.2 Pressure cells placed beneath selected footings of the bridge piers.

Research Findings

The research team used on-site testing to determine foundation pressures under gravity and under ambient temperature loads. The aim of the field-testing was to establish the actual pressures; field-testing data were then used as the basis for calibrating a bridge FE model, which is detailed in Chapter 4. After obtaining responses from conducting combined gravity-load temperature analyses across a range of values, the research team identified the mechanism that influences foundation bearing pressures due to temperature fluctuations at the superstructure level – namely, changes in superstructure member temperatures induce axial elongation (or contraction). Due to the restrained, monolithic nature of the integral abutment bridge superstructure, temperature-induced axial deformations generated stresses along the span. In response to the span stresses and temperature-induced motions, the underlying bridge piers underwent rotation. The overall pier rotations led to significant changes in bearing pressures beneath portions of the spread footings under intermediate bridge piers.

Comparing bridge response quantities measured on-site to those generated by subjecting the bridge FE model to combined gravity-temperature loading yielded the following conclusions:

Finding 1: Shown below are the records of in-service pressure cell readings for the instrumented footings beneath the intermediate piers of the New Trammel Creek Bridge. The piers are designated as Pier 1 (Fig. E.3) and Pier 3 (Fig. E.4), respectively. For each plot, cell pressure readings were paired chronologically with the corresponding superstructure temperatures (also measured on-site) from May 11, 2011 to May 11, 2012. The data records indicated that the pier footings were designed to limit pressures to approximately one-half of the allowable bearing capacity for the bridge site (65 psi). Specifically, the maximum pressures which occurred in the instrumented footings of Pier 1 and Pier 3 were 36 psi and 29 psi, respectively.

Finding 2: Also shown below are the minimum and maximum foundation pressures obtained from subjecting the bridge FE model to combined gravity-temperature loading. The foundation pressures acquired from the FEA were generated by introducing the extreme temperature values specified in the AASHTO Method B provisions to the bridge FE model; this enabled the research team to determine temperature-induced bridge structural demands. Comparing the FEA-derived pressures and field data indicated that the AASHTO Method B produces conservative estimates of foundation design pressures for the New Trammel Creek Bridge.

Finding 3: Numerical (FEA) estimates of the contributions to foundation pressures in the instrumented footings when the bridge FE model was subjected to combined gravity-temperature loading are shown below. Vertical, compressive foundation bearing pressures that are attributed to design-level uniform superstructure temperature changes (in accordance with AASHTO Method B) can be significant relative to those pressures that are attributed to gravity loading. For example, in Fig. E.5, for the location of maximum total pressure in the Pier 1 footing (cell 4), the FEA-derived estimate of foundation pressure attributable to extreme temperatures changes was 69% (27.6 psi) of the total pressure (38.5 psi). Similarly, for cell 3 of Pier 3 (Fig. E.6), the temperature-induced pressure comprised 56% (18.2) of the total pressure (32.5 psi).

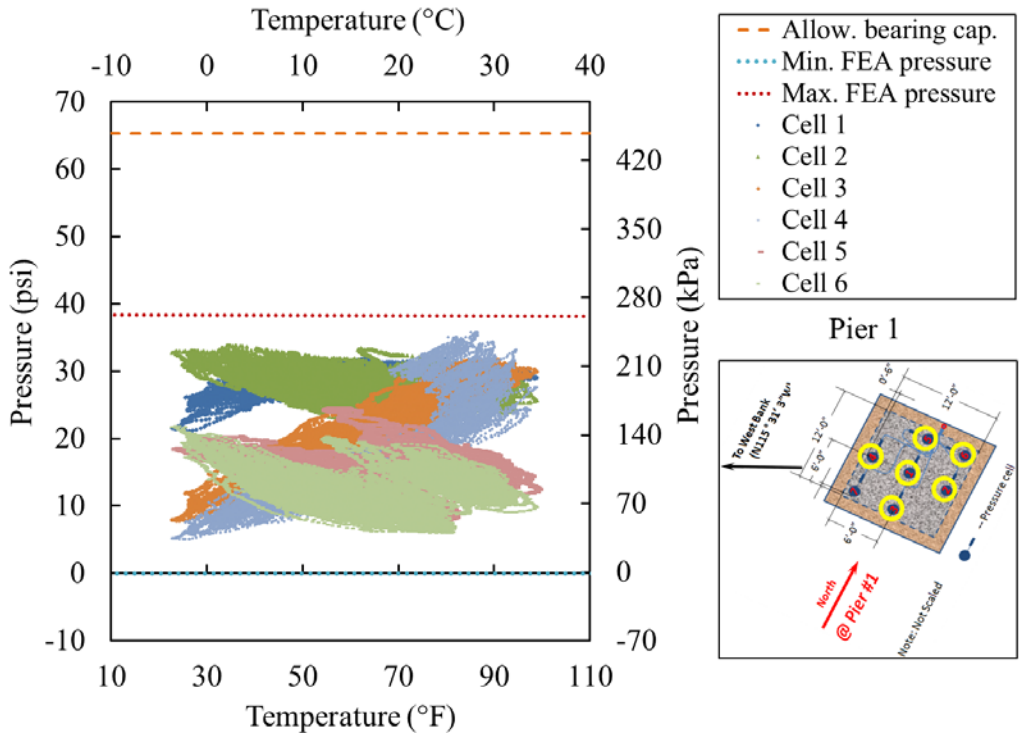

Fig. E.3 Pier 1 foundation bearing pressures versus temperature (Note: Cell 7 data are not available).

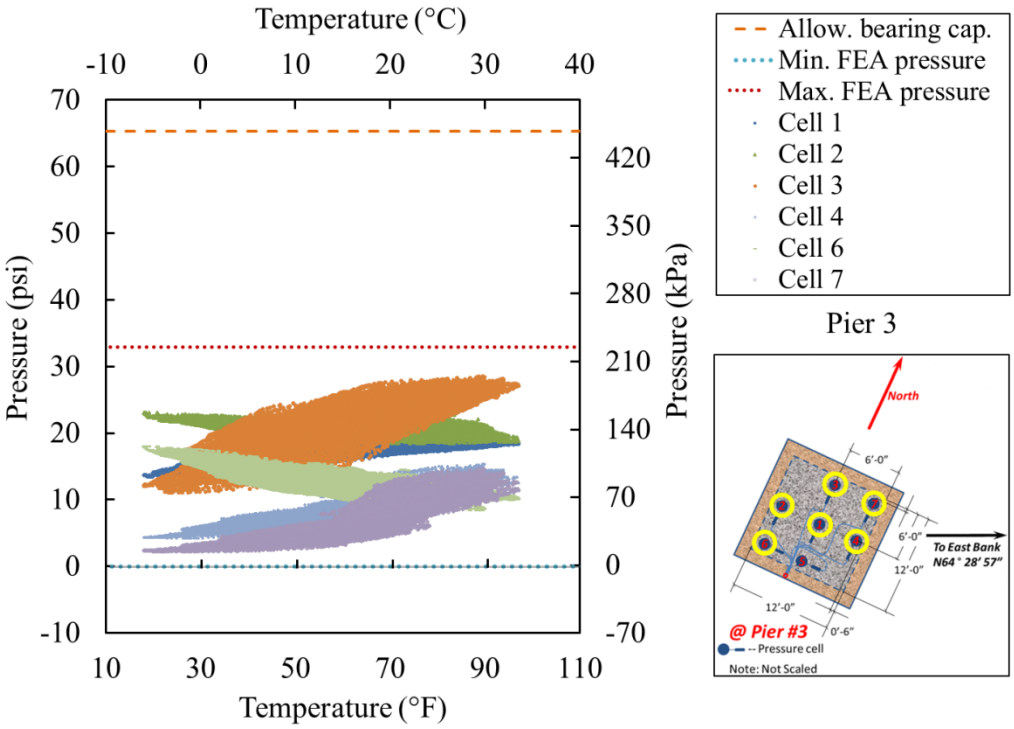

Fig. E.4 Pier 3 foundation bearing pressures versus temperature (Note: Cell 5 data are not available).

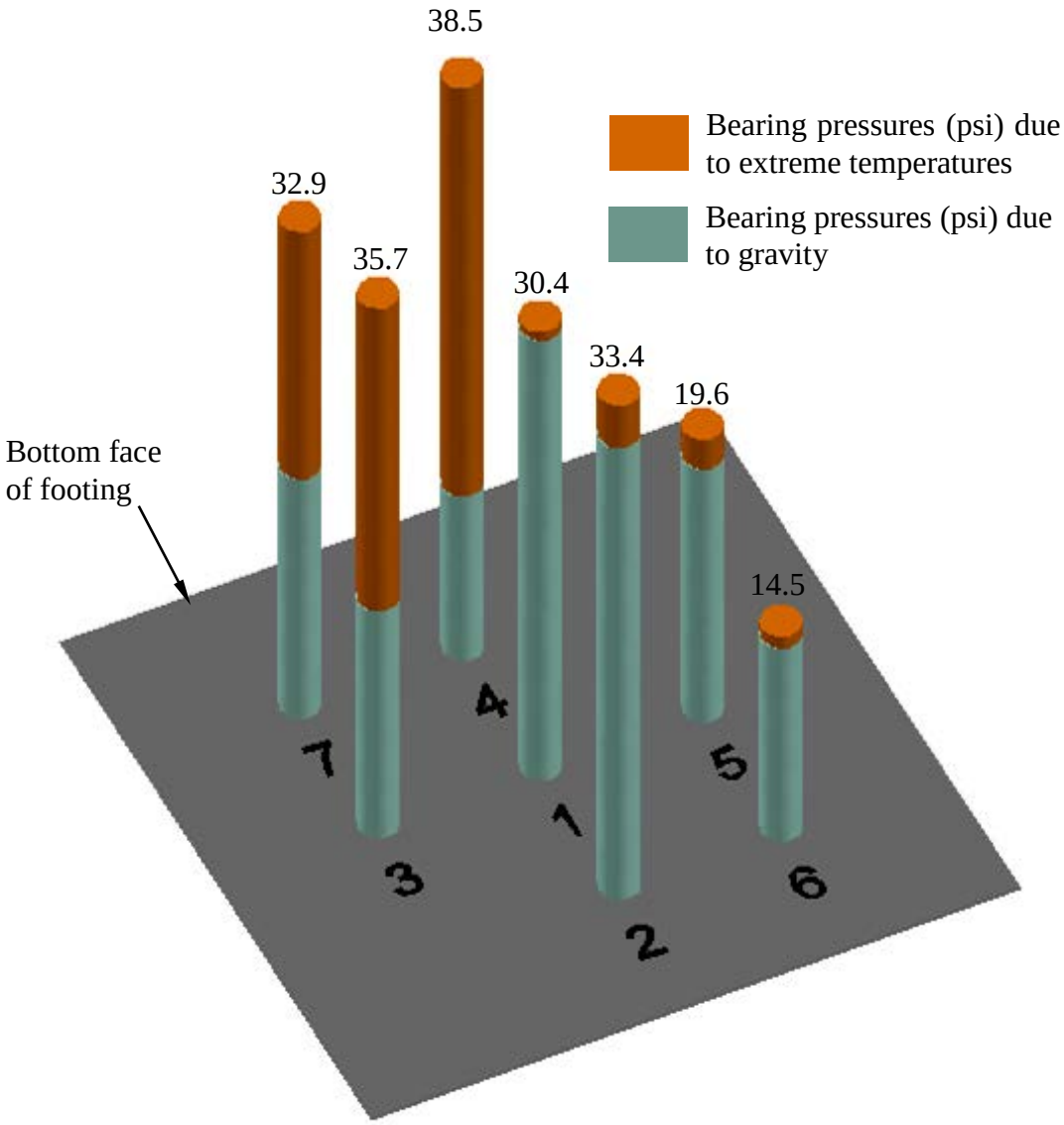

Fig. E.5 Distribution of gravity and extreme-temperature pressures on the bottom face of the instrumented Pier 1 footing (based on FEA results).

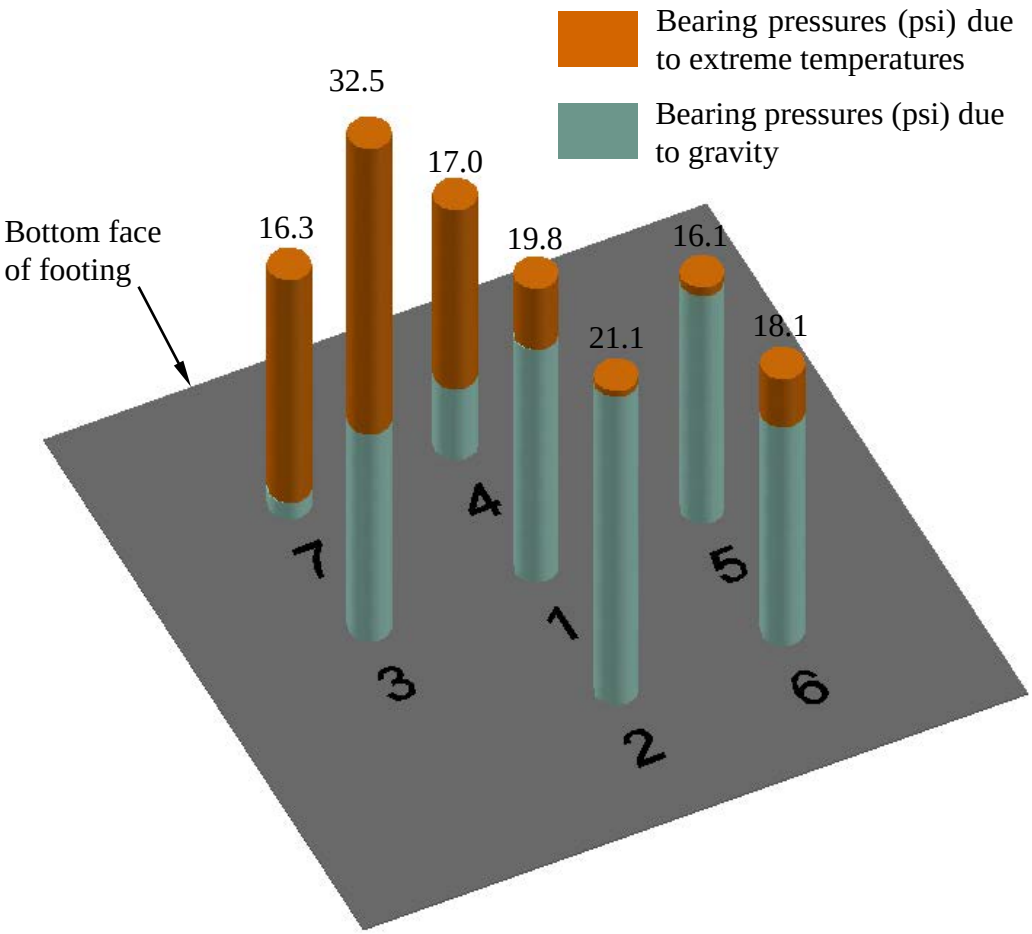

Fig. E.6 Distribution of gravity and extreme-temperature pressures on the bottom face of the instrumented Pier 3 footing (based on FEA results).

Recommendations and Conclusions

- The design-level pressures predicted using ASHTO Procedure B were compared to the temperature-induced foundation bearing pressures. This study verified the bridge motion in the piers and the foundation pressures obtained from FEA aligned with data taken at the bridge site; the combined gravity-temperature load foundation bearing pressures generated were conservative relative to the range of pressures that constitute the available, physical data record.
- The pier motions were rigid-body rotation, which resulted in increased bearing pressure beneath portions of the underlying footings, and resulted in pressure decreases along the opposite-edged portions of the footings. However, the design of the New Trammel Creek Bridge is consistent with the recommended safety factor for allowable bearing pressures in the spread footings.
- The components of vertical, compressive bearing pressure attributable to temperature changes at the superstructure level can be significant relative to those pressures that were traced to gravity loading. On the study bridge, portions of the footing developed

temperature-induced bearing pressures that were equal to or greater than pressures associated with gravity-loading.

- Very little research has addressed the issue of how to determine the base construction temperature for reinforced concrete structures. More insight could be gained into foundation response to temperature loading by investigating bridges that have been designed using one of the other two methodologies given in the AASHTO provisions.
- The study findings are specific to integral abutment bridges, which are constructed with relatively high levels of superstructure restraint. Similar instrumentation and analytical tasks could be carried out on bridges containing other superstructure types. Furthermore, the soil modeling included in this study was site-specific. Soil-structure interaction can play an important role in determining the distribution of loads to substructures such as individual piers. Therefore, a parametric study of soil strengths and types should be carried out to further examine the importance that soil-structure interaction plays in dictating substructure response to temperature loads.

ACKNOWLEDGEMENTS

The financial support is provided by the Federal Highway Administration (FHWA) and the Kentucky Transportation Cabinet (KYTC). The authors would also like to extend their gratitude towards Dr. Abheetha Peiris and Mr. Dan Eaton for their efforts in placing instrumentation throughout the New Trammel Creek Bridge. Finally, the authors would like to thank Mr. Kevin Sandefur for his assistance in providing design information for the bridge of interest in this study.

TABLE OF CONTENTS

LIST OF TABLES

LIST OF FIGURES

1 INTRODUCTION

1.1 General

Infrastructure containing structural members that are either partially or fully restrained against motion can develop internal stresses when those members are subjected to changes in temperature. Bridge structures constitute a substantial portion of the U.S. infrastructure; they are regularly exposed to significant temperature changes via convection, which is driven in part by microclimatological variability. Bridge roadway materials are also vulnerable to more significant periodic temperature fluctuations as roadways undergo radiant heating via direct exposure to sunlight (in addition to the convective influence of ambient air temperatures) during daylight hours, and then undergo convective cooling during non-daylight hours. Temperature fluctuations occurring along bridge roadways positively correlate with temperature fluctuations of immediately underlying structural members, due to conduction, which affects members such as bridge decks and superstructure girders. Due to partial or full restraint conditions that are typically incorporated into the design of bridge superstructure systems (e.g., diaphragms, fixed-bearings), temperature changes in members such as bridge decks and superstructure girders can lead to the development of internal stresses. These in turn induce stresses throughout underlying bridge piers, foundation systems, and ultimately into the underlying soil.

Many forms of bridge construction techniques are employed in the United States. Integral abutment bridges are constructed quite frequently. This technique integrates (e.g., monolithically casting) slab, stem wall, and other foundation members at bridge extents. It also uses rigid diaphragms atop intermediate piers, which reduces or eliminates the need for complex bearing systems or expansion joints at intermediate superstructure locations. Hence, integral abutment bridges are typically fitted with continuous superstructures. While numerous benefits are achieved from using integral abutment bridge construction techniques (e.g., reduced maintenance costs that would otherwise be necessary for the upkeep of the expansion joints and bearing systems), this type of bridge construction is not immune to the buildup of internal stresses that can arise from temperature changes that regularly occur in the continuous superstructure. A secondary effect from the build-up of temperature-induced internal (i.e., thermal) stresses in bridge superstructures are forces introduced into the piers and foundations of integral abutment bridges. Thermal stresses can be particularly large due to the additional restraint associated with the use of diaphragms atop intermediate piers.. Consequently, the forces that originate from heating or cooling of a continuous superstructure can influence the design of footings for integral abutment bridge piers.

The phenomenon of temperature-induced internal stress development in superstructure members has prompted the American Association of State Highway and Transportation Officials (AASHTO) to include provisions for determining superstructure temperature load effects on overall bridge design. Furthermore, for integral abutment bridges and similar construction types, the design of intermediate piers can be strongly influenced or even primarily controlled by the AASHTO thermal loads requirements (depending on pier height). However, little consideration has been given to explicitly quantifying the effect that thermal stresses have on the foundations of these intermediate piers. Therefore, it is critical that accurate estimates of the thermal loads (as translated to effects on foundation members) be achieved so as to ensure proper design.

One desirable means of fully assessing the impact that superstructure thermal stresses have on underlying foundation performance is through the direct, full-scale, long-term monitoring of temperatures and emergent stresses that develop at a selected, representative bridge site. Recent developments in remote monitoring technology permit the installation of sensors for the measurement of quantities such as temperatures and stresses; data collected by these sensors are read wirelessly in real-time and uploaded digitally for electronic data processing and analysis. Further, remote monitoring sensors are available in sufficiently compact configurations that work to minimize disruption to construction or instrumented bridge structural performance.

1.2 Objective

The objectives of this study are to 1) instrument, on a multi-span integral abutment bridge, the bottom horizontal surface at the base of selected footings from intermediate piers with soil pressure cells; 2) install temperature gages on the overlying superstructure's vertical face that continuously monitor temperatures; and 3) compare measurements of temperature-induced soil pressures taken on-site with pressures derived from AASHTO design provisions.

1.3 Tasks

With the cooperation of bridge owners in the state of Kentucky (the Kentucky Transportation Cabinet, KYTC), and given the need to determine the impact that thermal stresses in continuous superstructures can have on the foundations of intermediate piers, an integral abutment bridge was fitted with instrumentation to perform structural monitoring. More specifically, the New Trammel Creek Bridge along KY-100 in Allen County (southwest) Kentucky has been fitted with pressure cells at select foundation locations, with tiltmeters at pier top locations, and with temperature gages at the superstructure level to simultaneously monitor intermediate bridge pier motion. Soil pressures that develop beneath the instrumented pier foundations and temperatures in the vicinity of the bridges will also be measured. Over three years (from May 2011 through May 2014), data were collected from the bridge site. Concomitant with the field-monitoring program, the research team performed a detailed analytical study of the New Trammel Creek Bridge. Through finite element (FE) modeling and analysis of temperature loadings on the selected bridge, estimates of bridge pier motion and foundation pressures that would emerge according to the methodologies outlined in the AASHTO design provisions were made and were compared to those measured in full-scale at the bridge site. In this way, the merit of the current AASHTO provisions (as related to temperature-induced response for the selected bridge) was evaluated.

1.4 Background and Motivation

Bridge superstructure construction commonly entails the installation of expansion joints at pier top and abutment locations to facilitate attenuation of thermal stresses, where the expansion joints permit the superstructure spans to undergo longitudinal expansion and contraction as temperature fluctuations occur in the constituent members. Superstructure spans that are fitted with expansion joints are subject to large load concentrations due to truck passages (via axle and individual wheel loads), the accumulation of potentially deleterious substances (e.g., adulterated slush runoff as part of de-icing efforts), and to relatively large motions as a result of temperature-induced superstructure motion (Connal 2004). Consequently, expansion joints in bridges can

increase maintenance costs because they require periodic cleaning and even replacement. There are advantages, therefore, to employing bridge structural systems that eliminate the need for expansion joints, particularly in climates with extreme (low or high) temperatures. Many regions throughout the United States have climates that lead to temperatures falling below 32° F during the year. As a result of extreme temperature, bridge structural systems that eliminate the need for expansion joints (e.g., integral abutment bridges) have gained widespread use.

Although substantial upfront (construction stage) and maintenance (service stage) cost-savings can be realized through the use of integral abutment bridge construction, temperature fluctuations in superstructure members for those same types of bridges can bring about large secondary stresses in substructure members. Kappayil and Reed (1996) recognized — through a study of heat-transfer processes in superstructure members — that improved knowledge of the magnitudes of thermal movements and stresses could let bridge designers to make more rational selections when designing portions of bridges that transfer load from superstructure to substructure.

The phenomenon of thermal stresses that originate at the superstructure level, and pervade throughout a bridge structure has been investigated for integral abutment bridges. In particular, the effect of superstructure temperature changes on abutment foundation members at bridge extents has been assessed by Arsoy et al. (1999), who investigated the effect that bridge temperature changes had on the motion and forces in abutment walls. Paul et al. (2005) carried out an analytical investigation to quantify the effects of uniform superstructure temperature loading (a common analysis technique used as part of the design of certain bridge types) on stresses that develop in superstructure girders and abutment walls and abutment piles. Kim and Laman (2010) conducted an analytical study, wherein numerous bridge parameters were varied and supplied to a finite element bridge model, which was then subjected to superstructure temperature loading to ascertain those parameters that have the highest impact on internal forces that develop in piles distributed throughout the abutment locations. Kim and Laman (2010) found that temperature-induced forces in abutment foundation members were sensitive to the coefficient of thermal expansion attributed to superstructure members, the magnitude of bridge span lengths, and abutment pile-soil stiffness.

While there have been numerous studies focused on the effect of superstructure temperature changes in relation to abutment foundation forces, very few studies have examined the effects those same temperature changes can have on intermediate piers that may be placed along internal spans of integral abutment bridges. Furthermore, a scarcity of studies concerned with the effects of temperature loading on underlying piers persists, even though it has been recognized that abutments and piers must accommodate thermal superstructure movements (Schultz et al. 2011). As a further limitation, the AASHTO design provisions dedicated to assessing superstructure temperature load effects have been identified as suffering from ambiguities when fixed substructure-superstructure connections are present (Schultz et al. 2011). Additionally, other limitations have been identified that further complicate the study of integral abutment bridges, where research aimed at identifying the installation temperature for a bridge of interest (i.e., the temperature at which the bridge does not develop thermal stresses) has been relatively limited (as noted in Roeder, 2002; Roeder 2003).

This study simultaneously addresses the paucity of research on the thermal loading response of bridge piers situated within integral abutment bridges and the potential limitations of

AASHTO's existing temperature loading provisions. Installing monitoring devices and monitoring quantities such as superstructure temperatures, pier motions, and foundation pressures on the selected integral abutment bridge will lead to: 1) Substantial, quantitative insights into the thermal-stress sensitivity of foundation forces that are based on full-scale, in-service measurements; and, 2) The unprecedented creation of a dataset that can be used to make definitive comparisons to foundation pressures predicted using the AASHTO provisions.

The current study is also motivated by the United States Department of Transportation (US-DOT) and Federal Highway Administration (FHWA) joint program: Long-Term Bridge Performance (LTBP). Central to programs such as the LTBP is the need to quantify response metrics of in-service bridges over 3-year periods while these bridges are exposed to various types of loadings and deterioration due to corrosion, fatigue, and various climate conditions (Rodriguez 2012). In the current study, the monitoring period planned for the selected bridge is three years. The final motivation for the current study is to work toward overcoming visual, qualitative inspection methods, which although traditional, have been identified as antiquated, time-consuming, and expensive (Gastineau et al. 2009). By installing minimally invasive sensors, data acquisition systems, and establishing convenient, real-time monitoring protocols, the monitoring approach taken in the current study can be advocated for use in relevant structural health monitoring applications.

1.5 AASHTO Temperature Loading

Section 3.12 of the AASHTO LRFD Bridge Design Specifications (AASHTO 2012) encompasses determination of force effects due to superimposed deformations. More specifically, Sec. 3.12 of the AASHTO design specifications gives guidance for prescribing temperatures in bridge superstructure analyses, as part of bridge design process. In the AASHTO design provisions, two approaches are used: 1) The application of uniform temperature changes to the superstructure, and, 2) The application of a temperature gradient throughout the depth of the superstructure. Whereas certain aspects of the uniform temperature approach are associated with a more historic bridge design methodology, use of the more recently developed temperature gradient approach is not necessary for all types of structures (AASHTO 2012). In particular, the AASHTO provisions state that the bridge owner may choose to exclude the temperature gradient in the bridge design process, and further, that past experience and judgment can be helpful for determining whether uniform temperature or temperature gradient approaches should be used in the design of multi-beam bridges. Further, even though temperature fluctuations do not impact bridges uniformly across their entire span, their designs commonly assume uniform temperature changes (AASHTO 2012).

Given that the New Trammel Creek bridge is a multi-girder prestressed concrete bridge (as discussed in Chapter 2) and designed using the uniform temperature approach (Kevin Sandefur, personal communication, March 16, 2010), AASHTO's uniform temperature approach described in its provisions is of primary interest in the current study. In particular, predictions of foundation pressures for the New Trammel Creek bridge that were obtained using the uniform temperature approach are critical for comparison to selected field measurements of superstructure temperature and foundation pressures (in Chapter 5).

In AASHTO's specifications for determining design thermal movements, the uniform temperature approach is divided into two procedures: Procedure A and Procedure B. Procedure

A is a historic method used to identify extreme values of uniform temperature changes in bridge superstructures (AASHTO 2012). Procedure B is a calibrated procedure, where extreme values of uniform temperature change are applied during analyses for bridge design. The temperature ranges are based on an average history of 70 years of data (and minimum of 60 years of data) from many locations throughout the U.S. (Roeder 2002, AASHTO 2012). For this study, Procedure B was selected to generate comparisons, which uses full-scale bridge temperature and foundation pressure measurements.

Procedure B, which accounts for thermal loading during a bridge's design phase, works by prescribing span-longitudinal elongation (or contraction) at the superstructure level. After specifying the prescribed displacements, minimum and maximum (extreme) design temperatures (denoted $T_{MaxDesign}$ and $T_{MinDesign}$, respectively) are selected using temperature maps (Figs. 1.1-1.2). Then, to facilitate a bridge structural analysis, a bridge model is developed. Superstructure elements of the bridge model are then exposed to prescribed displacements to account for temperature loading, where the elongation (and separately, the contraction) magnitudes are calculated using the following equation:

$$\Delta_T = \alpha \cdot L \cdot (T_{MaxDesign} - T_{MinDesign}) \qquad \text{Eq. 1.1}$$

where Δ_T is the design thermal movement range, α is the coefficient of thermal expansion, and L is the length over which expansion can occur (e.g., the span length).

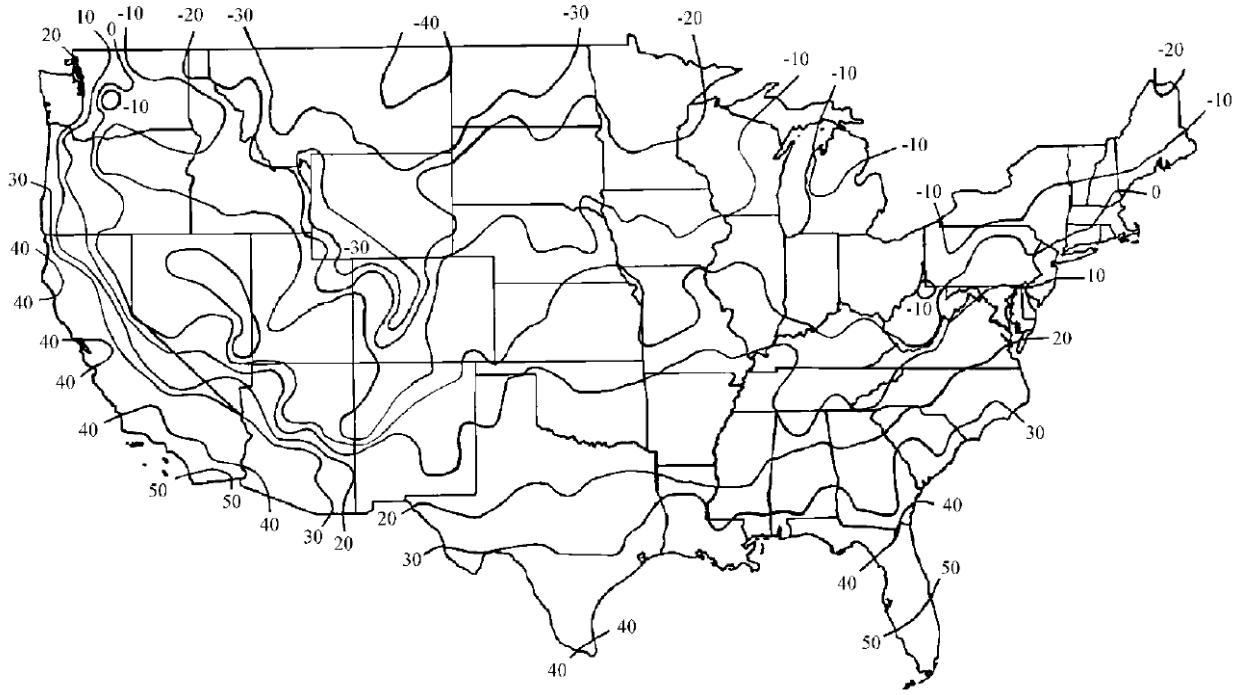

Fig. 1.1: Contour map for minimum design temperatures ($T_{MinDesign}$) for concrete girder bridges with concrete decks (AASHTO 2012).

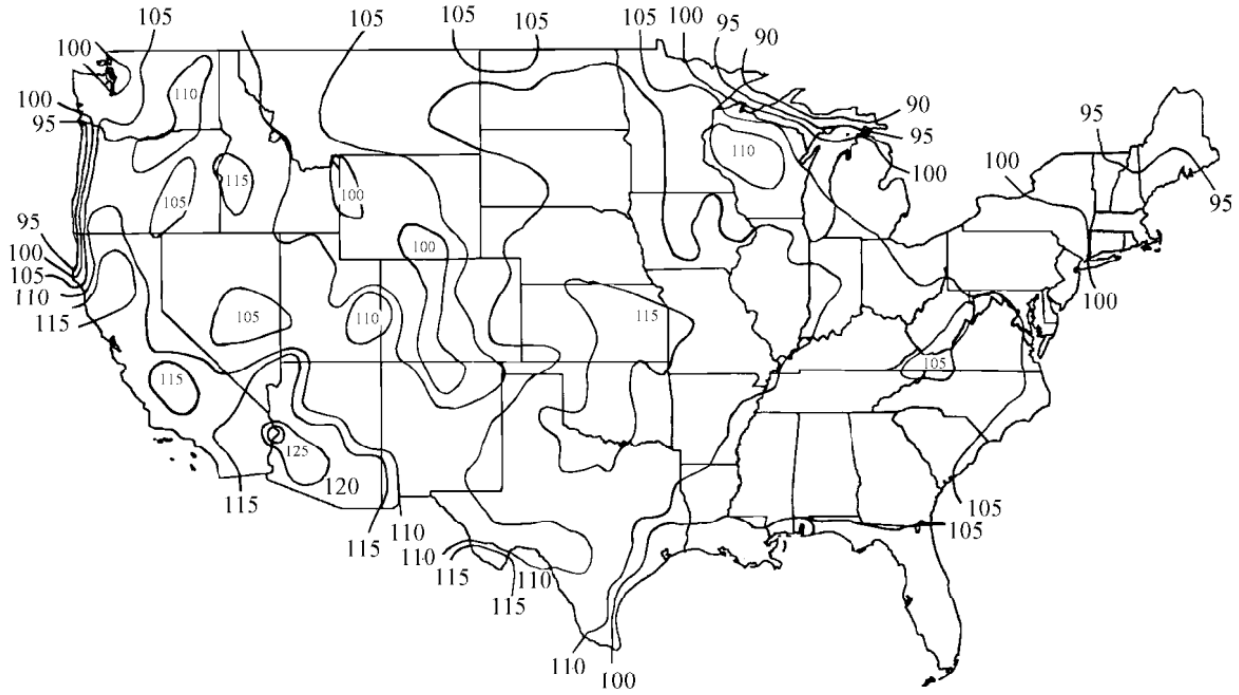

Fig. 1.2: Contour map for maximum design temperatures ($T_{MaxDesign}$) for concrete girder bridges with concrete decks (AASHTO 2012).

In Chapter 5, AASHTO's (2012) provisions for Procedure B are used to select the extreme temperatures that are appropriate for use in the design of the New Trammel Creek Bridge. The selected extreme temperatures are then used – as part of a series of finite element analyses – to induce thermal elongations (and contractions) in superstructure members so the corresponding extreme (i.e., design) values of foundation pressures can be computed at the intermediate piers of the New Trammel Creek Bridge.

1.6 Bridge Health Monitoring

Since 2007, bridge health monitoring has become an area of intense interest (Gastineau 2009). Structural health monitoring of bridges, with an overarching goal of incorporating structural monitoring devices to assess the integrity of in-service structures on a continuous, real-time basis has, in part, motivated this study. Therefore, as part of the construction of the New Trammel Creek Bridge on KY-100 (which was carried out in the Winter of 2010 and Spring of 2011), instrumentation has been installed at select locations (as discussed in Chapter 3) to facilitate the structural health monitoring of the bridge, with an emphasis on ascertaining performance-levels of the intermediate pier foundations, the motion of the piers, and the corresponding superstructure temperatures.

1.7 Scope of Work

The objective of this study is to apply instrumentation to a multi-span integral abutment bridge, the bottom horizontal surface at the base of the footing of selected piers with seven soil

pressure cells, the pier caps of selected piers with tiltmeters, and the vertical faces of the superstructure with temperature gages. The instrumentation will continuously monitor the soil pressure and temperatures and compare the soil pressures with ones derived using the AASHTO code. The data collected from the instrumentation will lead to more effective design of footings for bridge piers. The scope of the work entails the following tasks:

Literature review: A literature review will be conducted to determine the typical effects of thermal loads on substructures.

Procure and install bridge instrumentation: The instrumentation for the candidate bridge will be purchased, calibrated, installed, and maintained at the New Trammel Creek Bridge.

Data collection, reduction, and evaluation: The data from the instruments will be collected remotely at a server at the University of Kentucky. The data will be downloaded, reduced, and evaluated at regular intervals. During the course of the study, field data and design assumptions will be compared. Development of real-time monitoring website: Vested members of the public will be able to access the reduced data that was collected remotely from the bridge site. Data will be catalogued and made available for dynamic display through publication of a remote monitoring website.

Finite element modeling of New Trammel Creek Bridge: A high-resolution finite element model of the New Trammel Creek Bridge will be formed, calibrated using available field measurements made through the various construction stages of the New Trammel Creek Bridge, and used to make estimates of the design-valued foundation pressures that would be induced due to extreme changes in superstructure temperatures.

Comparison of AASHTO predictions of temperature-induced foundation pressures to field measurements and FEA predictions: Finally, the robustness of the AASHTO-based predictions of foundation pressures will be compared to the corresponding record of measurements collected from the instrumented bridge site and to those response quantities obtained using FEA.

2 NEW TRAMMEL CREEK BRIDGE AT KY-100 IN ALLEN COUNTY, KENTUCKY

2.1 General

The bridge selected for instrumentation is located within the State of Kentucky (Fig. 2.1) in the southeast United States. The study site is the New Trammel Creek Bridge, which spans Trammel Creek and is located in Allen Country, in south-central Kentucky (Fig. 2.2). Situated between a major interstate (I-65) and the town of Scottsville, the newly constructed New Trammel Creek Bridge is oriented as shown in Fig. 2.3. KTC researchers chose the site in cooperation with the Kentucky Transportation Cabinet (KYTC) with the aim of monitoring the bridge's response to fluctuating temperatures. To monitor this response, researchers instrumented selected footings of the bridge, which provided information during construction and after the bridge went into operation. The instruments monitored pier foundation pressures that arose due to temperature changes at the superstructure level. The discussion below describes the structural configuration details for each major bridge component.

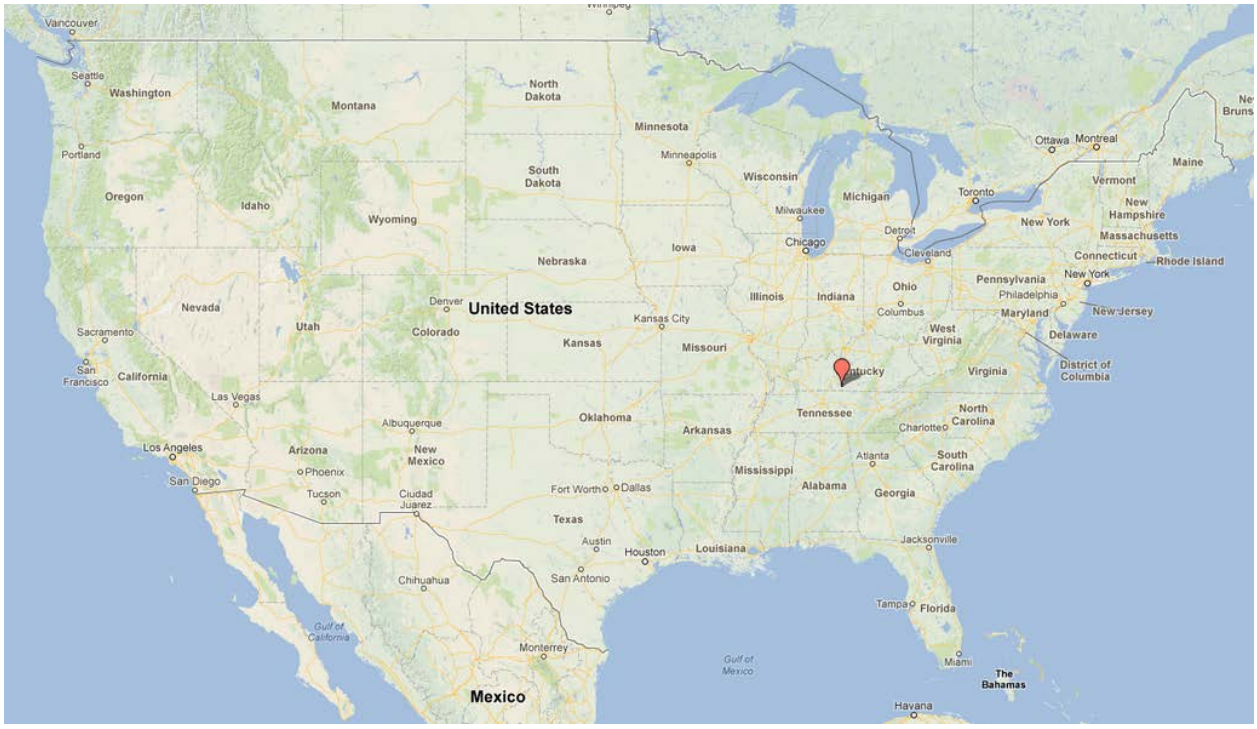

Fig. 2.1: Location of bridge site within the United States (source: Google Maps)

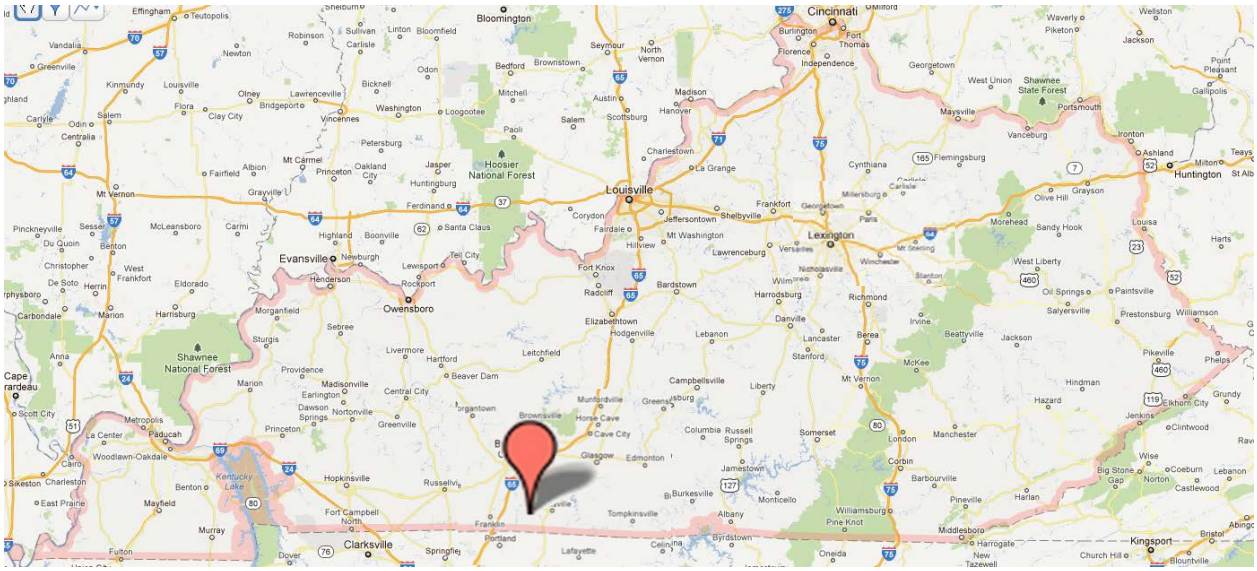

Fig. 2.2: Location of bridge site within Kentucky (source: Google Maps).

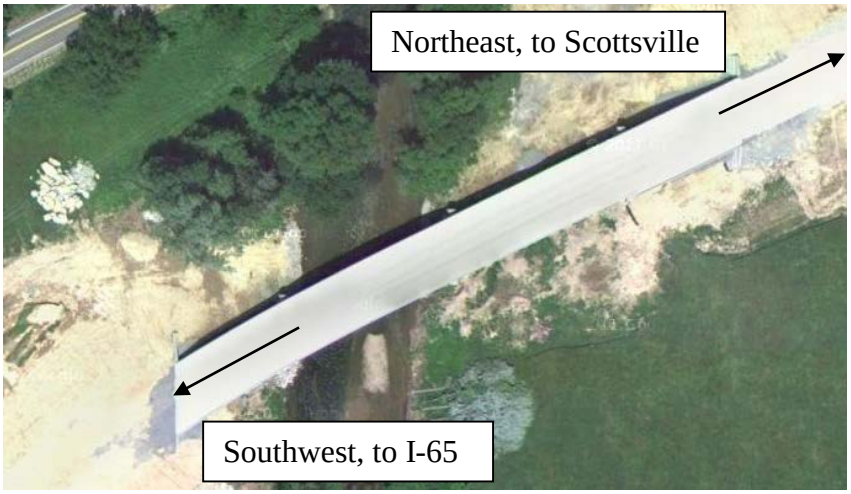

Fig. 2.3: Aerial view of bridge site (source: Google Maps).

2.2 Bridge Layout

Under normal flow conditions, Pier 1 and Pier 2 bound the stream edges. The bridge used integral abutment construction, with a monolithically cast bridge deck, stem caps, and wing walls located at each of the bridge far ends. Additionally, the bridge contains three internal piers that help support the spans, which in turn, consists of four spans. Six prestressed concrete girders of varying reinforcement configurations support each span of the two-lane concrete slab deck. The bridge's three piers are evenly spaced at 120 feet from one another, and the outermost piers (Pier 1 and Pier 3) are located 80 ft from the bridge abutments. The total bridge length is 403.5 feet.

The internal piers contain three columns and partial height shear walls, where each pier is supported by a spread footing. The two integral end abutments are each braced by a row of driven h-piles (Fig. 2.4a).

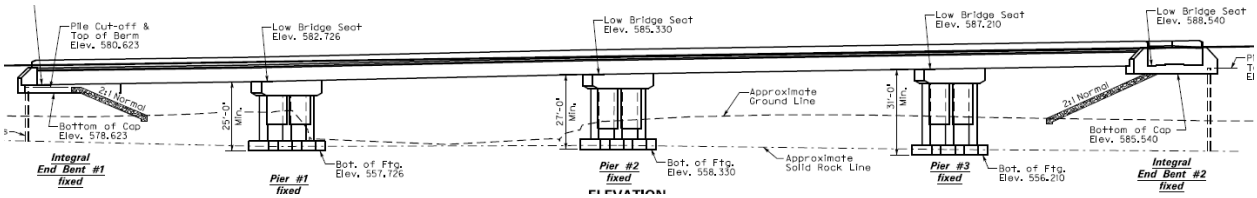

(a)

(b)

Fig. 2.4: Structural configuration: a) excerpt from structural drawings; b) as-built configuration.

2.3 Bridge Superstructure

The New Trammel Creek Bridge contains four spans, where the superstructure is comprised of an 8 in. thick prestressed concrete deck and six Type 5 PCI beams (PCI 2010). Each girder is spaced at 7.25 ft c.c., where each girder is fitted beneath a transverse bridge deck slope that varies from 2% to 6% (Fig. 2.5). The span longitudinal slope is relatively shallow; the end-bent nearest to Pier 1 contains a bridge seat elevation of 581.6 ft while the end-bent nearest to Pier 3 contains a bridge seat elevation of 588.4 ft. Horizontal curvature is built into the span located west of Pier 1 (i.e., span 1). The girders, with 28-day compressive strengths of 8500 psi, rest atop the piers and integral end bents at a uniform right-skew angle of 25°. The two-lane roadway and Type 3 reinforced concrete rails occupy a 43 ft width along the entire 403.5 ft bridge length. Two 80 ft spans extend from the (fixed) integral end bents to the externally located piers (Pier 1 and Pier 3), and pier-to-pier spans are 120 ft in length (Fig. 2.6). Reinforced concrete diaphragms (with 4000 psi 28-day comperssive strength), cast above all three internal piers, integrate the superstructure to the substructure in a fixed manner (Fig. 2.7).

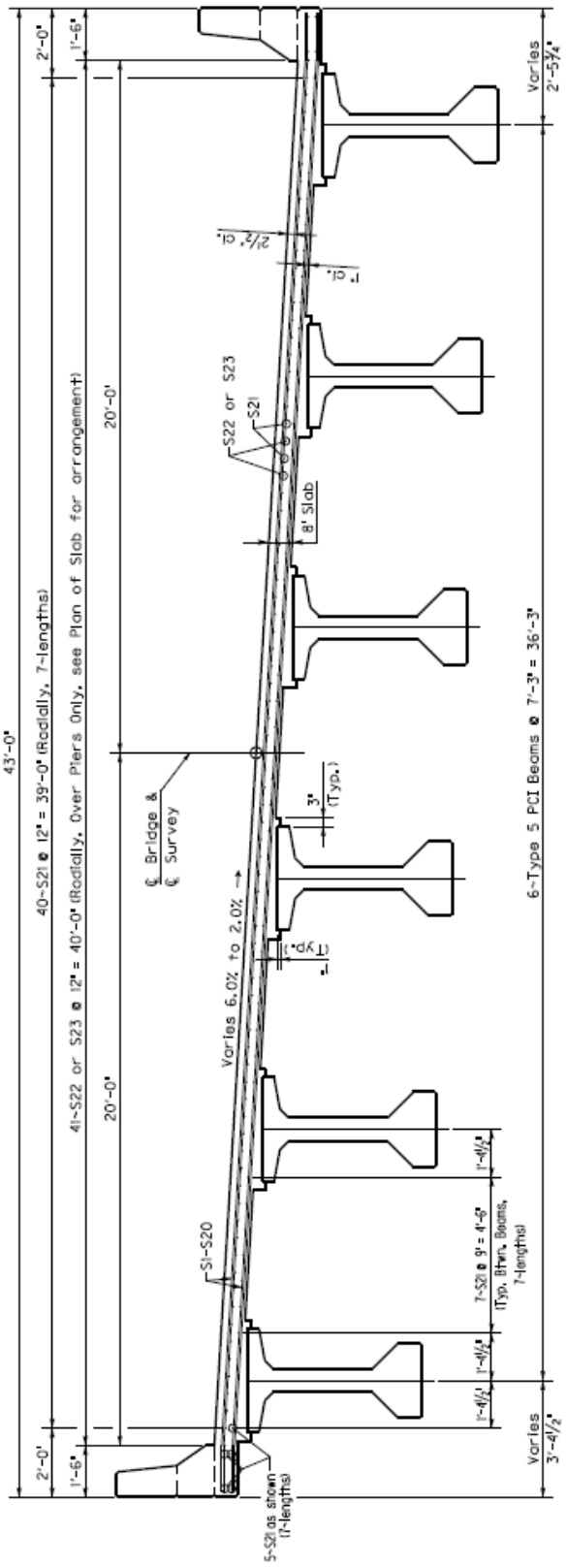

Fig. 2.5: Typical girder elevation.

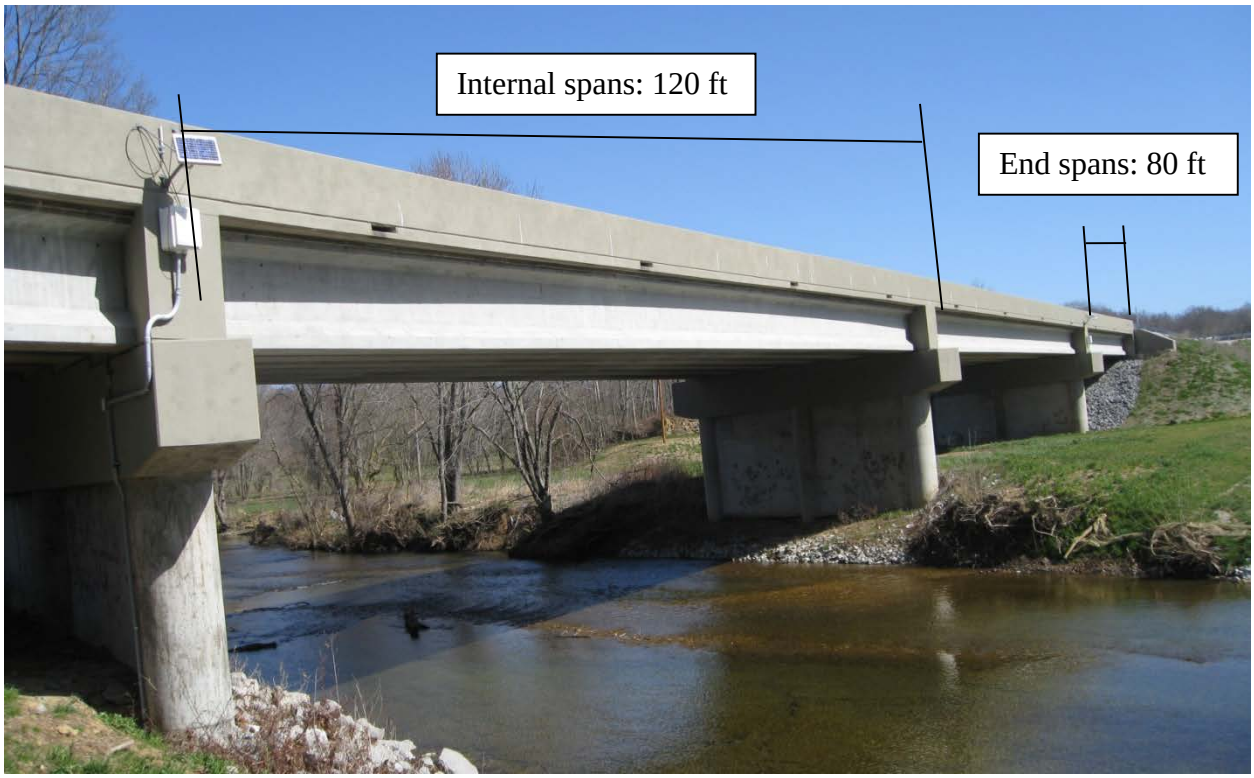

Fig. 2.6: Center spans (span 2 and span 3).

Fig. 2.7: Reinforced concrete diaphragms cast above the pier cap of each pier.

2.4 Elastomeric Bearing Pads

Both ends of each prestressed concrete girders rest upon Type 5F elastomeric bearing pads, placed in two rows atop each pier (Fig. 2.8), and placed in one row atop each integral end bent (Fig. 2.9). Individual bearing pads are oriented at the right-skew angle of 25,° with the pad short dimensions aligned parallel to the girder span direction. Installation of elastomeric bearing pads is shown for the two-row configuration atop Pier 1 in Fig. 2.10. This pad layout is typical for all of piers.

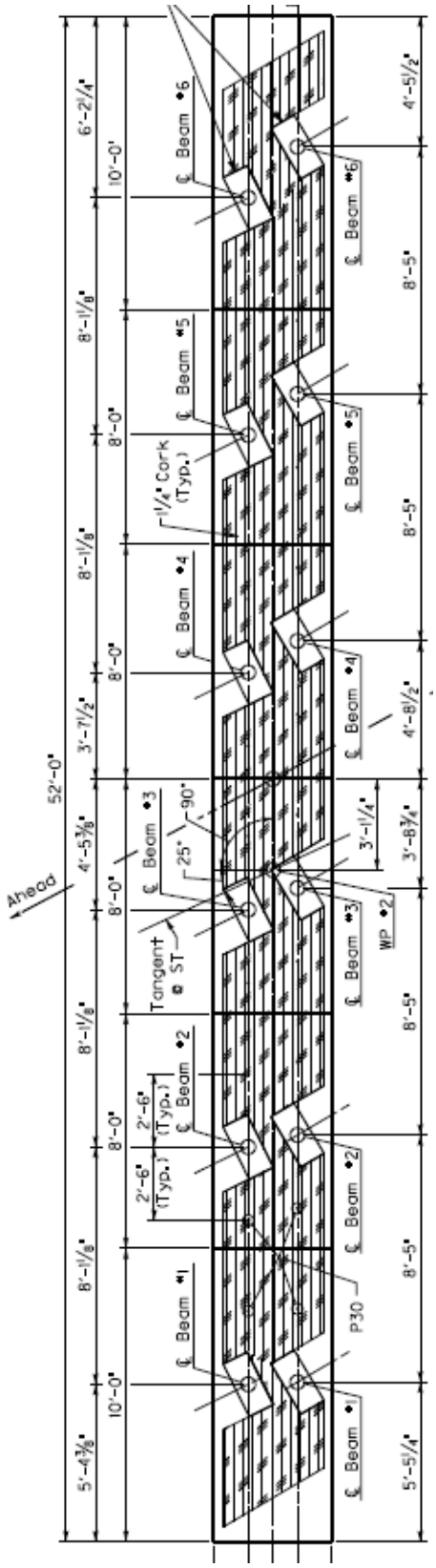

Fig. 2.8: Plan view of elastomeric bearing pad placement atop Pier 1.

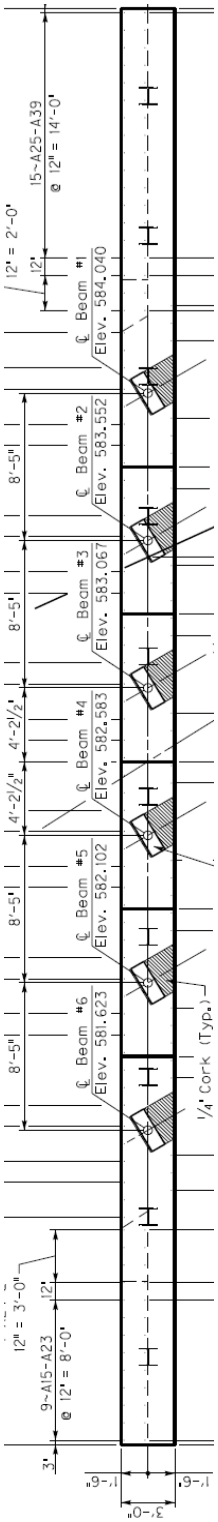

Fig. 2.9: Plan view of elastomeric bearing pad placement atop the southwest integral end bent.

Fig. 2.10: Elastomeric bearing pads placed atop Pier 1.

2.5 Bridge Substructure: Integral End Bents

The integral end bents for each of the southwest and northeast ends of the New Trammel Creek Bridge are shown in Fig. 2.11 and Fig. 2.12, respectively. At each end, integral construction is achieved by casting the bridge deck monolithically with a 3 ft thick (in the plan-longitudinal direction) by 82 ft wide (in the plan-transverse direction) reinforced concrete stem cap, with a 28-day compressive strength of 4000 psi. The cap rests immediately above ten driven h-piles (HP 12x53) on the southwest end and nine driven h-piles (HP 12x53) on the northeast end, where all piles are driven to bedrock. Reinforced concrete wing walls (with 3500 psi compressive strength) retain the in-situ soil immediately external to the stem cap and pile foundations, and simultaneously, the wing walls aid in retention of a 2:1 sloped retaining stone fill on the interior side of the stem cap and pile foundations.

Fig. 2.11: Integral end bent at southwest end of bridge.

Fig. 2.12: Integral end bent at northeast end of bridge.

2.6 Bridge Substructure: Piers

The three internal piers of the New Trammel Creek Bridge are uniformly spaced at 120 ft, and are oriented parallel to the span longitudinal direction (i.e., at a right-skew of 25°). Each pier contains three reinforced concrete columns spaced uniformly at 20 ft. Specifically, the outer two columns of each pier are of 3.5 ft diameter and the central columns are of 3.67 ft in diameter, as shown for Pier 1 in Fig. 2.12. Partial-height shear walls extend down from the cap of each pier, where, for Pier 1, the partial-wall height is 10.5 ft (Fig. 2.12). Similarly, the partial-wall heights are 14.5 ft for Pier 2 and 15 ft for Pier 3. However, the soil surface elevations are such that the shear walls are partially embedded in the soil for all piers. The total heights for Pier 1, Pier 2, and Pier 3 are 27.25 ft (Fig. 2.14), 27.67 ft (Fig. 2.15), and 31.25 ft (Fig. 2.16), respectively. All pier concrete is 4000 psi 28-day compressive strength.

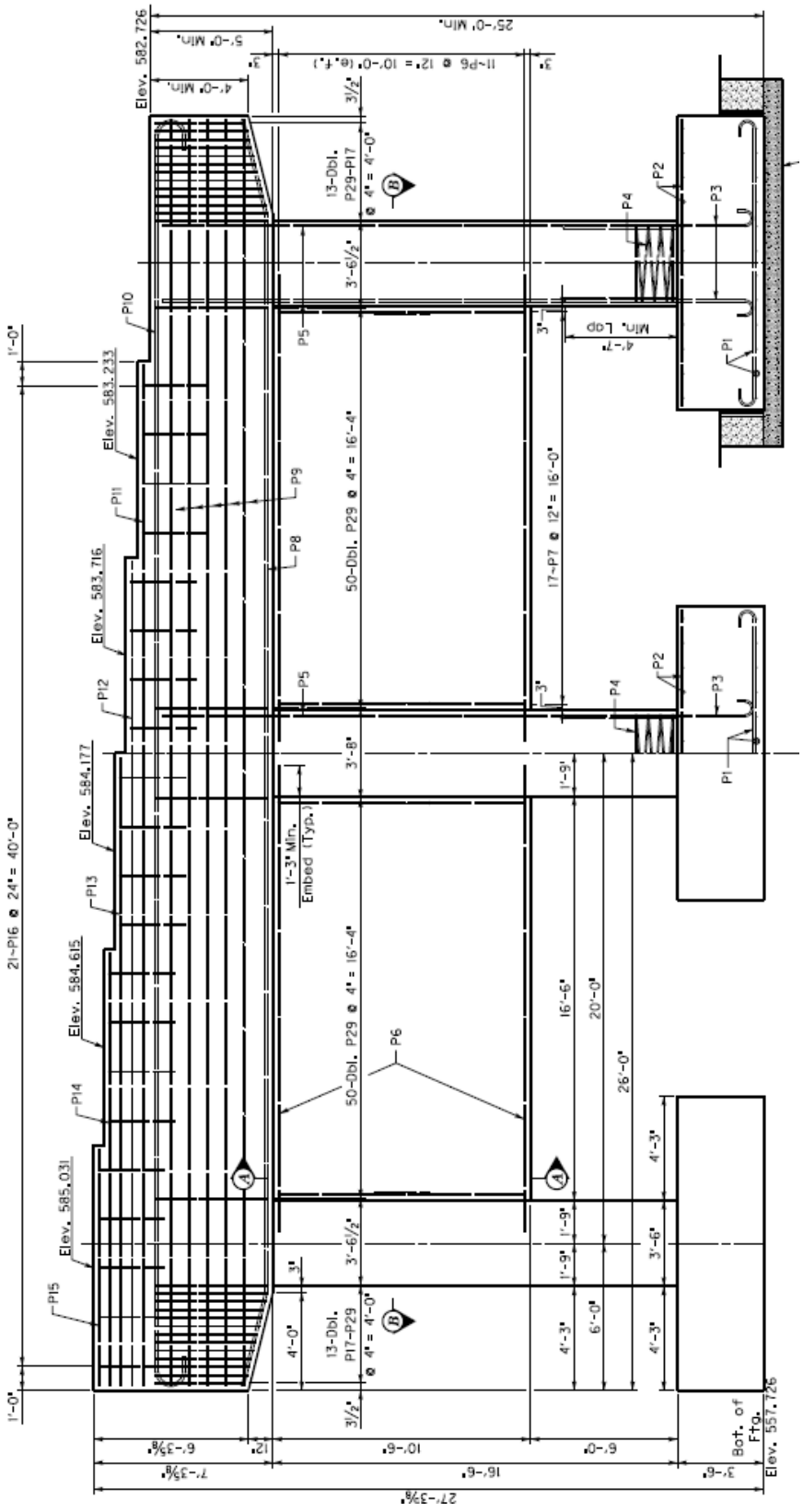

Fig. 2.13: Pier 1 dimensions.

Fig. 2.14: Pier 1 (prior to placement of superstructure).

Fig. 2.15: Pier 2 (prior to placement of superstructure).

Fig. 2.16: Pier 3 (prior to placement of superstructure).

2.7 Bridge Substructure: Footings

Shallow foundation reinforced concrete (spread) footings of 4000 psi 28-day compressive strength are positioned beneath each of the three New Trammel Creek bridge piers (Fig. 2.17). The footings are oriented consistently with the overlying piers (i.e., the footings are oriented parallel to the span longitudinal direction with right-skew angles of 25°). Each footing is 12 ft by 12 ft in plan (Fig. 2.17a), and 3.5 ft thick (Fig. 2.17b). Pier columns extend directly upward from — and are centered over — the footings. All footing excavation pits are dug down to limestone bedrock, and fill concrete is placed around the perimeter of all footing excavation pits up to the footing half-thickness (1.75 ft). As discussed in Chapter 3, selected footings were fitted with instrumentation to facilitate the study's completion.

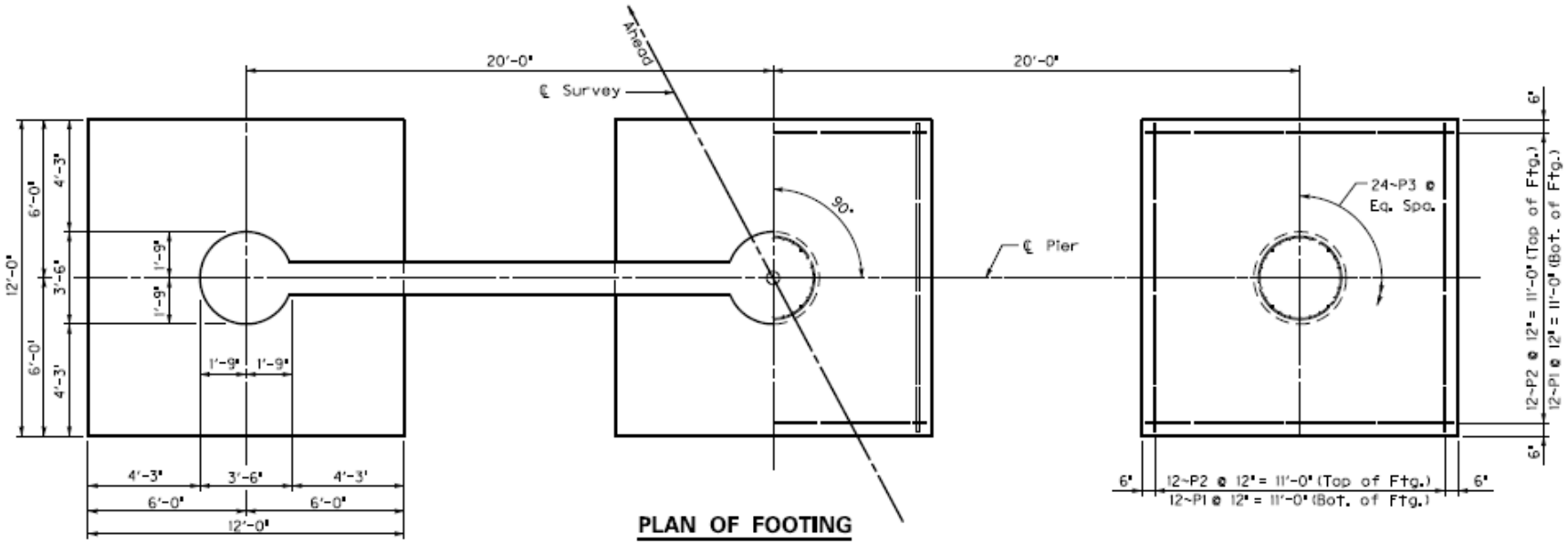

(a)

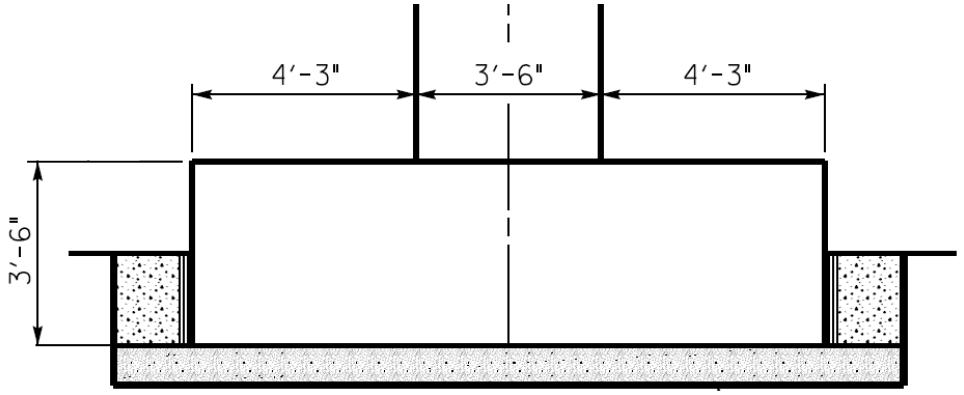

(b)

Fig. 2.17: Footings underlying Pier 1: a) Plan view; b) Section of typical footing (not to relative scale).

Fig. 2.18: Construction of the Pier 1 footings (prior to placement of soil fill).

3 BRIDGE MONITORING

3.1 General

After the New Trammel Creek Bridge was selected for the current study, the research team procured devices for measuring temperature, motion, and foundation pressure data. Immediately before the construction of the Pier 1 and Pier 3 foundations, two-dimensional spatial arrays were laid out in the footing excavation pits and pressure cells were installed in a prepared subsurface layer immediately below selected pier footings. Once the concrete bridge piers, abutments, and superstructure were constructed and set into place, temperature gauges were installed along the vertical faces of superstructure portions immediately overlying the tops of Pier 1 and Pier 3 to facilitate temperature monitoring at the superstructure level. Tiltmeters were also installed at the top and bottom of Pier 1 and Pier 3 pier caps after construction. Lastly, remote data acquisition systems were installed for each group of measurement devices. These were used to monitor and remotely store full-scale, real-time, in-service bridge response data. Assembling time series for foundation pressures, bridge pier motions, and superstructure temperatures can generate valuable insights about bridge performance, and allow for remote evaluations of the bridge's health.

3.2 Instrumentation

The monitoring devices placed on Pier 1 and Pier 3 included fourteen vibrating wire pressure transducers, two vibrating wire temperature gauges, and four vibrating wire tiltmeters. The specific installation locations for each sensor are delineated below. The following sections detail the installation procedures for the measurement devices, with special attention on how the installation fit within the context of bridge construction.

3.2.1 Pressure Cells

As shown in Fig. 3.1a, the southwest footing of Pier 1 and the northeast footing of Pier 3 were fitted with instrumentation to dynamically measure pressures that develop immediately beneath the two footings. As constructed, each instrumented footing of Pier 1 and Pier 3 rested atop a 9 in. layer of No. 10 crushed stone, which in turn, contained seven vibrating wire pressure cells. The two-dimensional arrays of pressure cells, embedded 3 in. below the top of the No. 10 crushed stone layer, were arranged as shown in Fig. 3.1b-c for the instrumented footings of Pier 1 and Pier 3. Each pressure cell was fitted with a data transmission cable, and all cables were fed into a 1.5 in. diameter conduit at a mid-corner of the footing gravel base. The conduit extended to a 14 in. x 16 in. weather-resistant enclosure that contained hardware for remote-monitoring data acquisition. As installed, the remote-monitoring data acquisition hardware was set to read the pressure cells at 5 min. intervals over a period of 3 years (May 2011 to May 2014). Pressure measurements were continuously cataloged on servers housed at the University of Kentucky in Lexington, Kentucky.

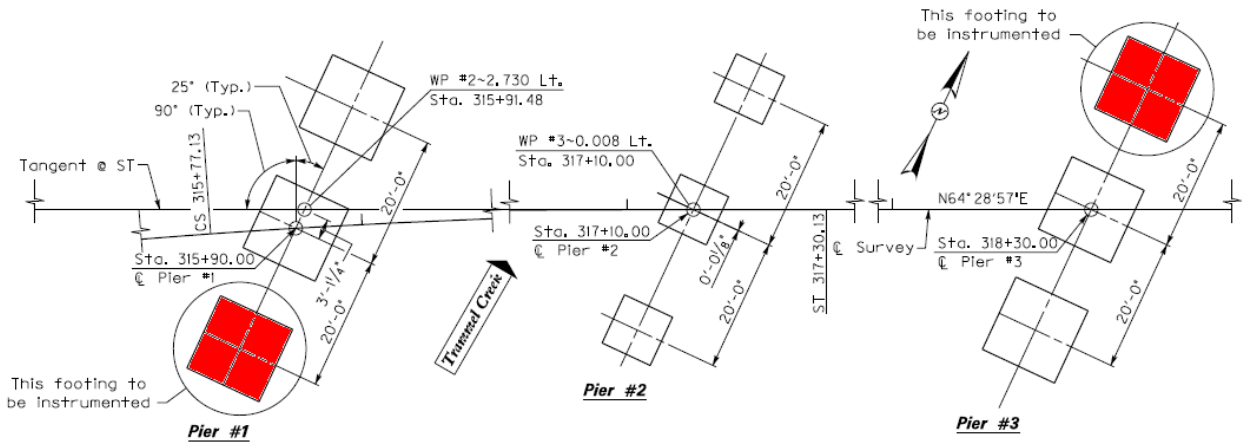

(a)

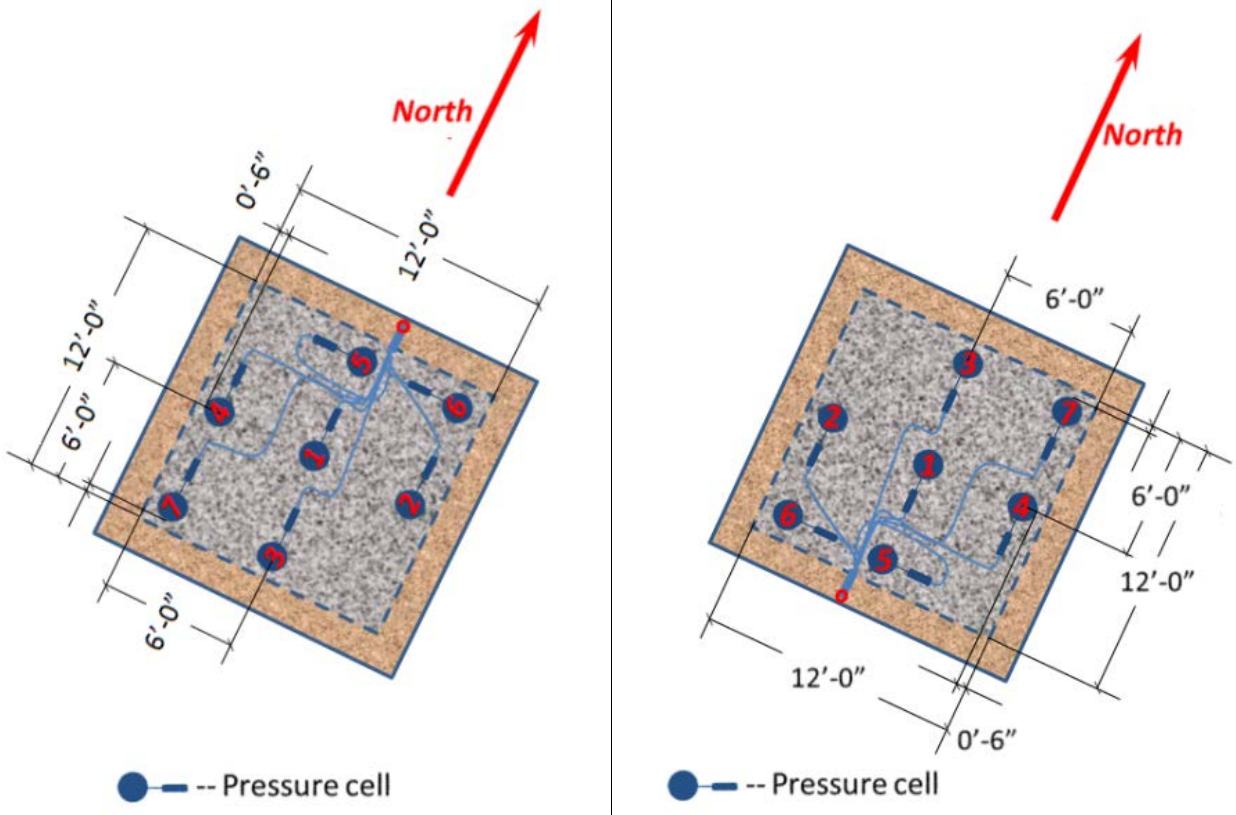

(b) **(c)**

Fig. 3.1: Pressure cell instrumentation schematic: a) Plan view of pier foundations with indication of instrumented footings; b) Pressure cell layout beneath Pier 1; c) Pressure cell layout beneath Pier 3.

Figs. 3.2 through 3.9 depict the vibrating wire pressure cell installation procedure. Note that placement of the crushed-stone layer was carried out for each of the footings in Pier 1 and Pier 3 (excluding the placement of pressure cells save for those footings identified in Fig. 3.1 above). In contrast, the footings of Pier 2 were cast to rest directly atop the underlying limestone bedrock.

To prepare for the construction of the instrumented spread footings beneath Pier 1 and Pier 3, 15 ft by 15 ft pits were excavated to a depth that corresponded to 9 in. below the footing bottom elevations (Fig. 3.2), where the pits were dug concentric to the respective footing locations. Before any structural members or instruments were placed, a 6 in. layer of No. 10 crushed stone was deposited in the excavation pits for each instrumented footing. [Note that all non-instrumented footings were constructed directly atop the excavation pit's limestone; no gravel was present beneath the non-instrumented footings.] The crushed stone was then compacted and leveled (Fig. 3.3). With the crushed stone surface prepared, the two-dimensional (i.e., constant elevation) array of seven pressure cells were placed on the surface of the compacted stone as shown in Fig. 3.4 for the southernmost and northernmost footings of Pier 1 and Pier 3. Importantly, the pressure cells were distributed so that pressures at the center of the footing, as well as those that develop throughout the mid-edge and corner regions, were included as part of the long-term bridge monitoring program. After emplacing the pressure cell array (Fig. 3.4), data transmission cables were connected to the pressure cells and collected at the mid-edge 1.5 diameter conduit.

Fig. 3.2: Pier column concentric 15 ft by 15 ft excavation to underlying limestone layer.

Fig. 3.3: Partial fill, compaction, and leveling of #10 crushed stone through a depth of 9 in. to 3 in. below the instrumented reinforced concrete footing.

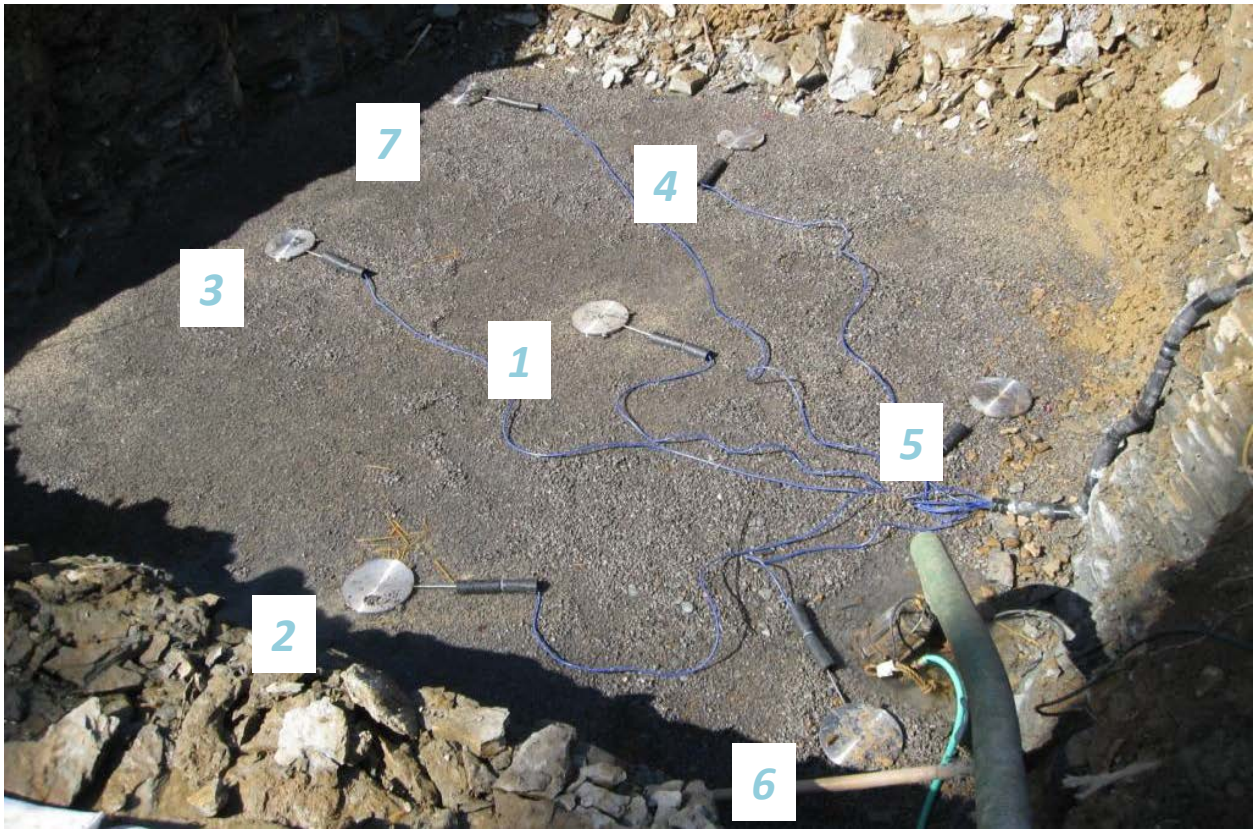

Fig. 3.4: Placement of seven vibrating wire pressure cells and data transmission cables.

Once the pressure cells were situated, an additional 3-inch layer of #10 crushed stone was deposited. Then, the entire composition was re-leveled and re-compacted using non-vibratory equipment. After this, the 9-inch layer of crushed stone containing the embedded pressure cells was covered using a Type I geotextile fabric cover (Fig. 3.5). Formwork and the spread footing reinforcement cages were then placed atop the fabric-shielded, crushed stone surface (Fig. 3.6). After pouring the footing concrete within the confines of the formwork (Fig. 3.7) and allowing the footing concrete to set, the formwork was removed from the footing periphery and replaced with 3 in. thick fiberboard. Finally, the excavation volume that remained around the perimeter of the footing was filled with filler concrete (Fig. 3.8). Note that the pressure cell data transmission-line conduit extends up from the edge of the footing and along the pier column, terminating at the remote monitoring data acquisition hardware in the weather-resistant enclosure. The finished pressure cell and data acquisition installation is shown for the instrumented footing of Pier 1 in Fig. 3.9.

Fig. 3.5: Placement of Type I Geotextile fabric cover.

Fig. 3.6: Installation of formwork and footing reinforcement.

Fig. 3.7: Pouring of footing concrete.

Fig. 3.8: Pouring of pier column and installation of data acquisition box.

Fig. 3.9: Pier 1 with pressure cells and data acquisition hardware installed.

3.2.2 Temperature gauges

To compare between field measurements and bridge response quantities associated with the extreme temperature conditions stipulated in the AASHTO provisions, vibrating wire temperature gauges were installed at the top of the superstructure directly above both Pier 1 and Pier 3 (Fig. 3.10). Temperature gauges selected for installation in the New Trammel Creek Bridge are capable of measuring temperatures ranging from -13° F to 122° F; this range conservatively envelopes the extreme temperatures given for the bridge location in the AASHTO provisions (extreme temperature values are identified in Chapter 5).

Each temperature gauge was installed after the prestressed concrete deck and superstructure rails were put into place. The temperature gauges were mounted along with a 20 W solar panel to the external (to roadway) face of the south-side superstructure rail (Fig. 3.11). Use of solar panels, which powered both the temperature and foundation pressure recording devices, was essential for the bridge monitoring system to be self-sustaining. As with the foundation pressure measurement recording interval, temperature readings were taken every 5 minutes from May 2011 to May 2014.

3.2.3 Tiltmeters

As an additional means of monitoring the in-service behavior of the New Trammel Creek Bridge, vibrating wire tiltmeters were installed at the top and bottom pier cap locations, directly above the southernmost columns of Pier 1 and Pier 3 (Fig. 3.12). Similar to the foundation pressure and temperature gauge monitoring intervals, relative inclinations of the pier caps for Pier 1 and Pier 3 were recorded at 5-minute intervals. As shown in Fig. 3.12, data transmission cables extend from each of the tiltmeters, into the 1.5 in. diameter conduits, and terminate at the white data acquisition box located on the exterior face of the overlying safety barrier (recall Fig. 3.11). Consequently, the tiltmeters were powered by the 20 W solar panels (such as the one shown above in Fig. 3.11).

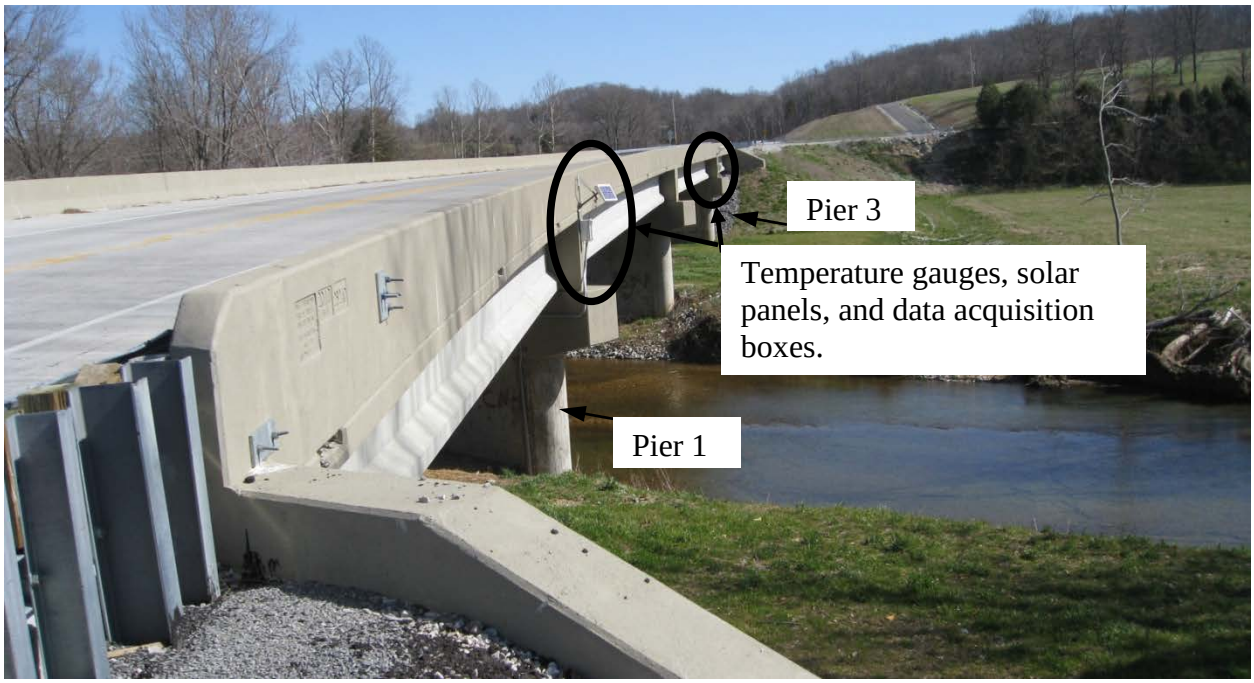

Fig. 3.10: Thermocouples, solar power cells, and data acquisition boxes atop pier caps of Pier 1 and Pier 3.

Fig. 3.11: Temperature gauge and solar panel mount to superstructure rail (typ.).

Fig. 3.12: Titlmeter installation to top and bottom of pier caps.

3.3 Data Record

Measurements of temperature, foundation pressures, and pier tilt have been recorded at 5-minute intervals since May 2011. Presented below are the time series data for each measurement device. Chapter 5 contains a detailed discussion of the pressures, motions, and temperatures measured, and relates the data to design-level estimates of temperature-induced bridge response obtained from the AASHTO provisions.

3.3.1 Pressure Cells

Fig. 3.13 shows the pressure readings through time (in 5-minute intervals) for pressure cell 1, which was placed beneath Pier 1. Data pertaining to pressure cells 2-7 of Pier 1 and to all of the pressure cells beneath the instrumented footing of Pier 3 are in Appendix A. Note that data are not available for pressure cell 7 of Pier 1 and pressure cell 5 of Pier 3. A collective examination of the pressure cell time-histories (shown in Fig. 3.13 and Appendix A) indicate that the spread footing beneath the southernmost column of Pier 1 is subjected to significantly higher pressures than those found beneath Pier 3.

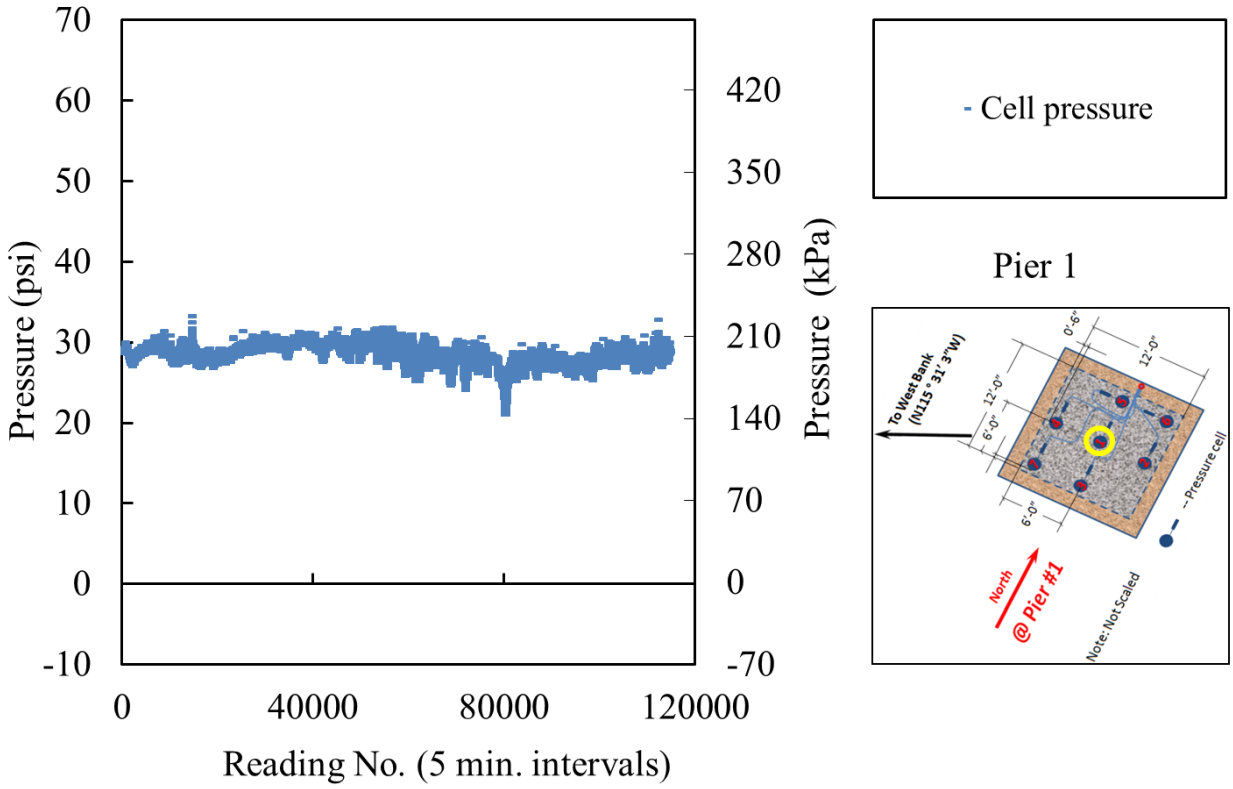

Fig. 3.13: Time-history of foundation pressures at Cell 1 of Pier 1 (note: reading No. 0 corresponds to May 11, 2011).

3.3.2 Tiltmeters

Shown in Fig. 3.14 and Fig. 3.15 are the tiltmeter readings through time (in 5-minute intervals) for the top and bottom tiltmeters, respectively, which have been placed atop Pier 1. Additionally, the corresponding measurements are given for the bottom tiltmeter atop Pier 3 in Fig. 3.16 (note that data are not available for the tiltmeter positioned at the top of the pier cap of Pier 3). Also note that, for the data presented in Figs. 3.14-3.16, a 20-point moving average has been applied to the raw field data.

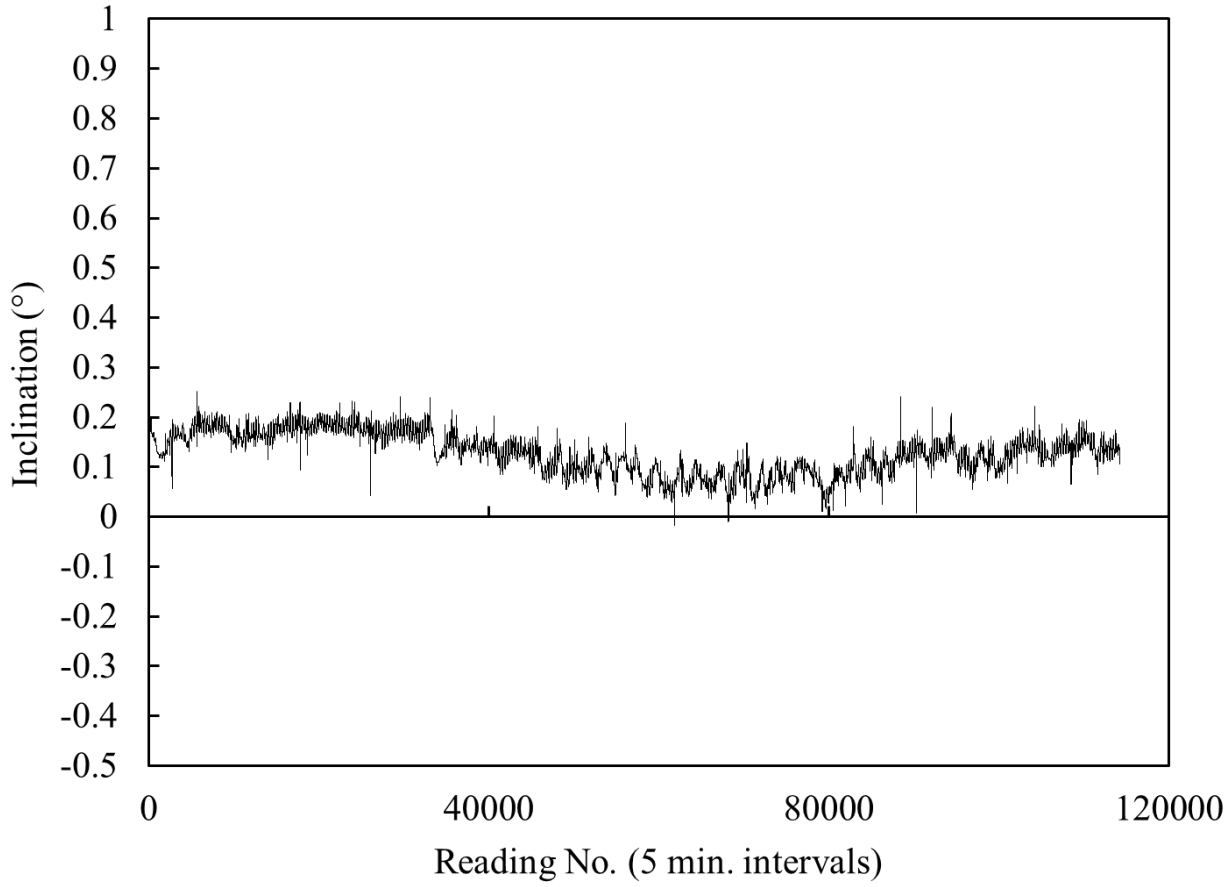

Fig. 3.14: Time-history of tiltmeter inclinations at the bottom of the pier cap on the south edge of Pier 1 (note: reading No. 0 corresponds to May 11, 2011).

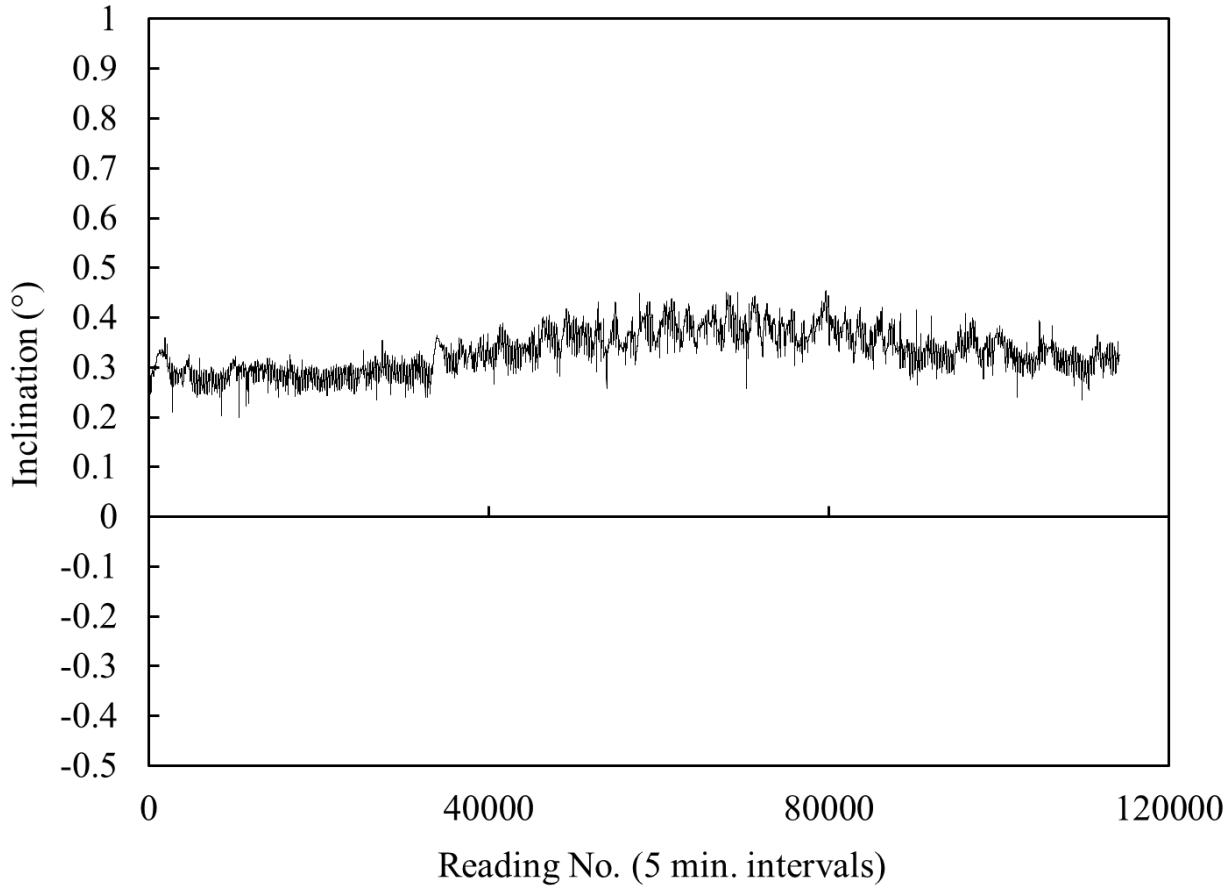

Fig. 3.15: Time-history of tiltmeter inclinations at the top of the pier cap on the south edge of Pier 1 (note: reading No. 0 corresponds to May 11, 2011).

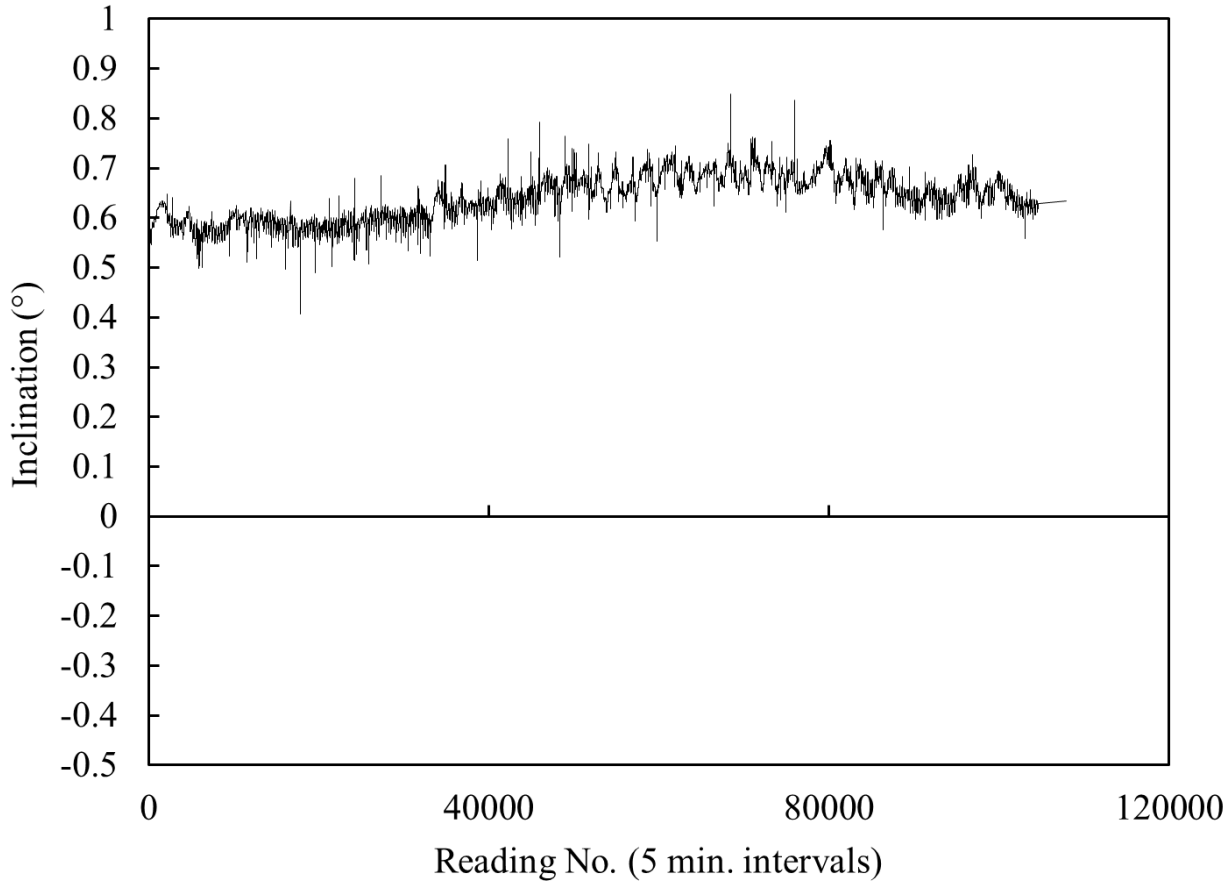

Fig. 3.16: Time-history of tiltmeter inclinations at the bottom of the pier cap on the south edge of Pier 3 (note: reading No. 0 corresponds to May 11, 2011).

3.3.3 Temperature gauges

Shown in Fig. 3.17 are the temperature readings through time (in 5-minute intervals) for the temperature gauge mounted at the superstructure level above Pier 1. Additionally, the corresponding temperature measurements are given for the temperature gage mounted at the superstructure level above Pier 3 in Fig. 3.18. As expected, the two collections of temperature readings show strong levels of correlation.

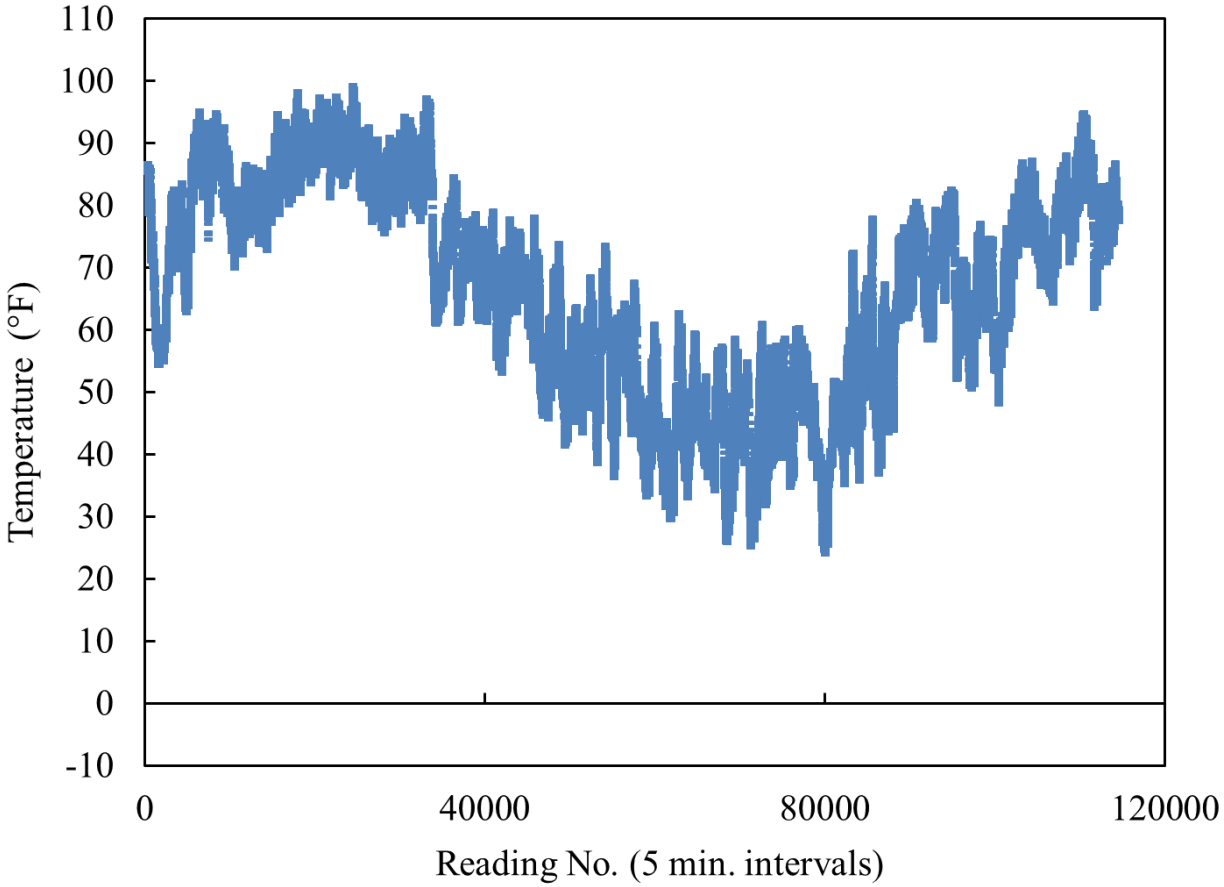

Fig. 3.17: Time-history of temperature readings taken at the superstructure level above Pier 1 (note: reading No. 0 corresponds to May 11, 2011).

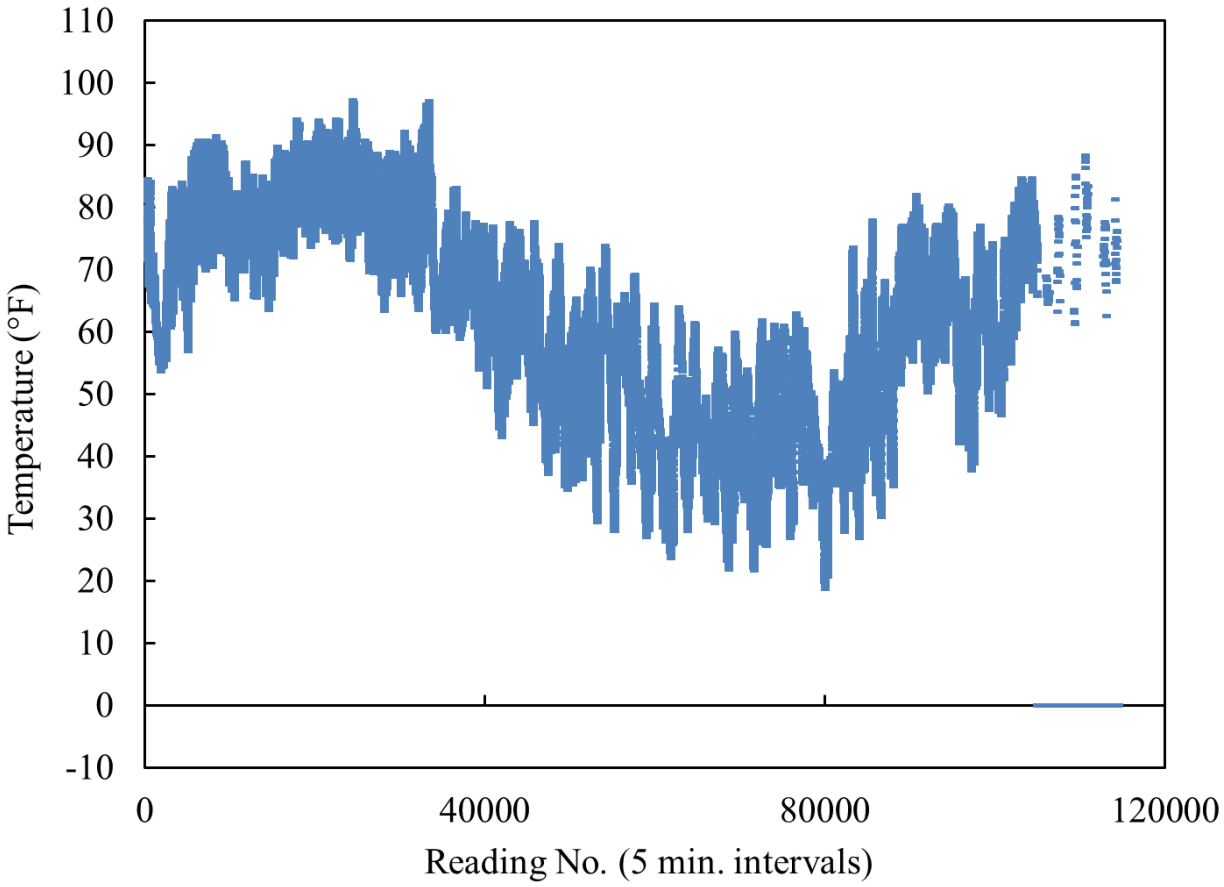

Fig. 3.18: Time-history of temperature readings taken at the superstructure level above Pier 3 (note: reading No. 0 corresponds to May 11, 2011).

3.4 Real-Time Monitoring of Data

This study contributes to wider efforts to establish remote bridge monitoring capabilities for numerous bridge sites throughout the state of Kentucky. As an integral facet of the remote monitoring functions, a dedicated website was developed that allows bridge owners, researchers, and members of the general public access to data that are continually being recorded at all bridge sites. Providing access to these datasets enables vested parties (researchers, owners) to remotely assess the structural health of the instrumented bridges. Additionally, the web interfaces act as a powerful tool in allowing the public to maintain research-product transparency and to engage in educational opportunities to explore the real-time, in-service behavior of bridge structures. The next sections of this report give a brief overview of the collective web pages that are dedicated to the instrumented bridge, and include the dedicated monitoring of temperatures, motions, and foundation pressures in the piers of the New Trammel Creek Bridge.

3.4.1 Remote Bridge Monitoring in KY Website

Remote monitoring studies like the one conducted at New Trammel Creek Bridge are currently underway at six bridge locations around the State of Kentucky. Instrumentation and remote monitoring hardware were installed at each bridge site, where hardware monitor s a variety of bridge-response data (http://www.ktc.uky.edu/kytc/RemoteBridgeMonitoringInKY has a complete listing). Website visitors will see a dynamic, interactive map from which individual-bridge websites can be accessed. The New Trammel Creek Bridge is highlighted below in Fig 3.19, which depicts a screenshot of the interactive map data is accessible from.

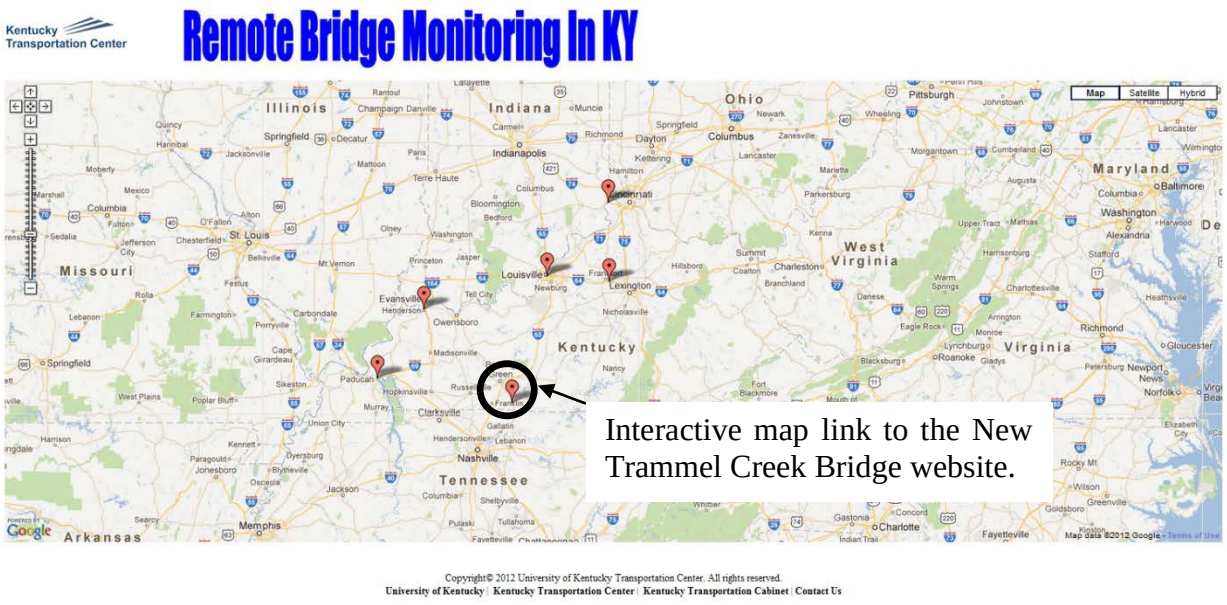

Fig. 3.19: Homepage of the Remote Bridge Monitoring in KY website (source: http://www.ktc.uky.edu/kytc/RemoteBridgeMonitoringInKY).

3.4.2 New Trammel Bridge over KY 100 in Allen Co., Kentucky

Upon accessing the interactive map link indicated above in Fig. 3.19, users are directed to a dedicated website that contains monitoring data from the New Trammel Creek Bridge: http://www.ktc.uky.edu/kytc/RemoteBridgeMonitoringInKY/ky100Allen.html. The home page for this specific remote monitoring effort is shown in Fig. 3.20. The website contains background information related to the bridge location and structural configuration. Additionally, an overview of the study objective and the relevant AASHTO temperature loading provisions is available for review (screenshots of the website contents are provided in Appendix B). Also, users may click on the links provided on the homepage to access all historical temperature, tiltmeter, and pressure cell data as well as more recent and real-time data. Further, the data are available for examination and for comparison to corresponding AASHTO foundation pressure estimates for piers of the New Trammel Creek Bridge. The data are presented via a dynamic plotting interface (see Appendix B for sample data plots), includes the pressure-temperature and tilt-temperature plots, both of which Chapter 5 discusses.

Fig. 3.20: Homepage of the Remote Bridge Monitoring in KY website dedicated to monitoring of the New Trammel Creek Bridge (source: http://www.ktc.uky.edu/kytc/RemoteBridgeMonitoringInKY/ky100Allen.html)

4 FINITE ELEMENT MODELING OF THE NEW TRAMMEL CREEK BRIDGE

4.1 General

This study explored temperature-induced loading and response of internally distributed bridge piers within integral abutment bridges using both full-scale in-service field measurements and high-resolution finite element analysis (FEA) of the New Trammel Creek Bridge. To date, this phenomenon has remained underexplored. The finite element (FE) bridge model was created using the general purpose FEA software ANSYS (2012). Structural members within the bridge FE model were created using dimensions and material properties listed in the associated bridge structural drawings.

Based on site-specific soil conditions and full-scale measurements of bridge pier foundation pressures – where measurements were taken throughout the various stages of bridge construction – FE model gravity and temperature loading responses were assessed to ensure that reasonable levels of agreement were achieved between numerical bridge response and field measurements taken at the bridge site. The following sections discuss the FE model structural configuration of the New Trammel Creek Bridge, where discrete modeling was employed on the bridge superstructure (bridge deck, girders), diaphragms, bridge piers, and pier footings. Further, the material properties and modeling for pier footing and span boundary conditions were delineated. Finally, as an assessment of the FE model capabilities, comparisons were made between the bridge FE model responses and those response quantities recorded during the bridge construction and in-service stages.

4.2 Bridge Finite Element Model

By making use of the structural drawings, site-specific soil conditions, and general stress-temperature characteristics of prestressed concrete bridges, an FE bridge model was developed in this study (Fig. 4.1) to assess temperature-stress relations. Particular emphasis was placed on using the FE model to make estimates of temperature-induced bridge pier foundation response. Dimensions of the bridge members included in the FE model matched those presented in Chapter 2. As discussed in detail in Chapter 2, the New Trammel Creek Bridge consists of four prestressed concrete slab-and-girder spans that are, in turn, supported by integral end bents at the bridge far ends. Reinforced concrete piers support the two internal bridge spans, where (as discussed in Chapter 3) the outermost piers were instrumented with temperature, pier cap motion, and foundation pressure monitoring devices. Since the emphasis of the study is to gain insight into the foundation pressures that develop in the *pier* substructures of integral abutment bridges, the FE model was developed to obtain the most detailed results within the pier footing regions. Consequently, the portions of the New Trammel Creek Bridge that were selected for discrete modeling included the internal bridge piers and the overlying (entire) superstructure (Fig. 4.2). The influence of the fixity conditions at the integral end abutments of the bridge were approximated using discrete stiffness beam elements and restrained boundary conditions.

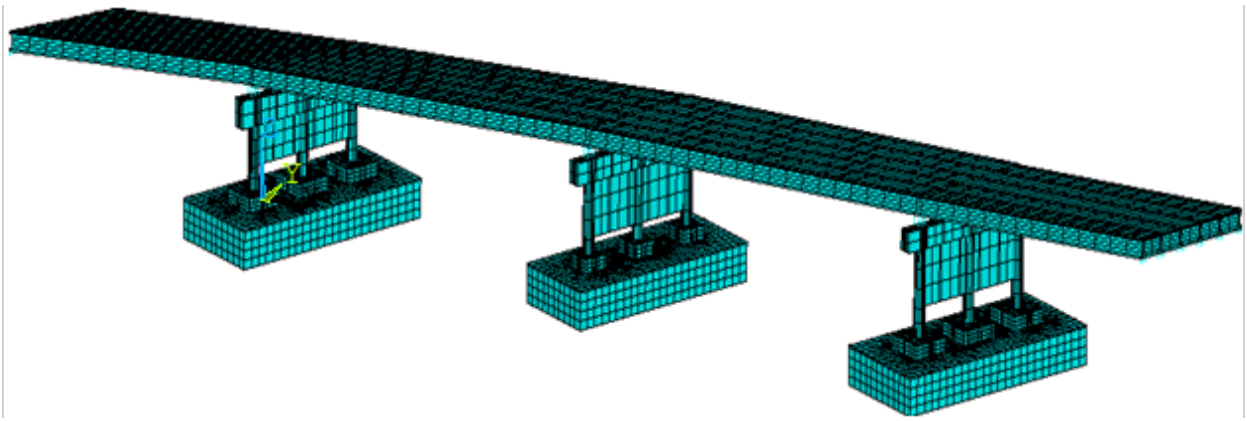

Fig. 4.1: Finite element model of the New Trammel Creek Bridge.

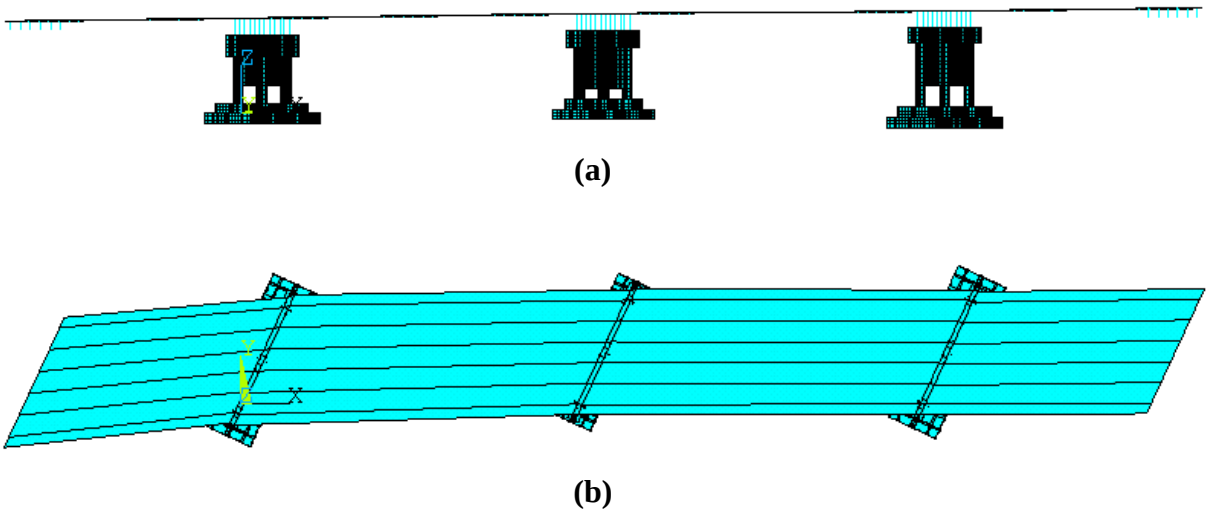

(a)

(b)

Fig. 4.2: Spans and piers included in the FE model: (a) Elevation view; (b) Plan view.

4.2.1 Structural Configuration

A three-dimensional linear elastic finite element (FE) model of the four-span New Trammel Creek Bridge was developed using the ANSYS finite element analysis (FEA) software package (ANSYS 2012). The full-bridge FE model was compiled by integrating separately modeled, major structural components (Span 1 through Span 4, diaphragms, bearing locations, and Pier 1 through Pier 3) as shown in Fig. 4.3. The major structural components and ANSYS element formulations employed in the FE model include:

1. The prestressed concrete superstructure slab was modeled using 5,037 four-node shell elements (SHELL63 elements), which possess three degrees-of-freedom (DOF) and three

rotational DOF at each node. Proper spatial alignment of the top and bottom surfaces of the slab elements was ensured by offsetting the centroid for stress-strain calculations within the shell elements relative to the respective shell element mid-thicknesses (Fig. 4.4).

2. The prestressed concrete superstructure Type 5 PCI girders were modeled using 33,582 twenty-node solid elements (`SOLID95` elements), which have three translational degrees of freedom (DOF) at each node (Fig. 4.4).
3. The reinforced concrete diaphragms were modeled using 1,080 twenty-node solid elements (`SOLID95` elements), which have three translational degrees of freedom (DOF) at each node (Fig. 4.5)
4. The elastomeric bearing pads were modeled using 36 two-node spring elements (`COMBIN14` elements), placed at every girder-pier (Fig. 4.6) and girder-abutment interface. The discrete spring elements contained three DOF at each node. For every bearing location, a collection of DOF-specific stiffnesses (Table 4.1.) was used to model horizontal, vertical and rotational DOF, where stiffness quantities were determined based on elastomeric bearing pad stiffness calculation procedures given in Podolny and Muller (1982).
5. The reinforced concrete piers and pier footings were modeled using 29,178 twenty-node solid elements (`SOLID95` elements), which have three translational DOF at each node. To incorporate the effective rigidity of the 3.5 ft thick reinforced concrete pier footings, linear elastic frame elements (`BEAM188`) representing mild steel reinforcement were distributed throughout each footing in accordance with the bridge structural drawings. Note that perfect bond was assumed between the reinforcement and surrounding concrete.

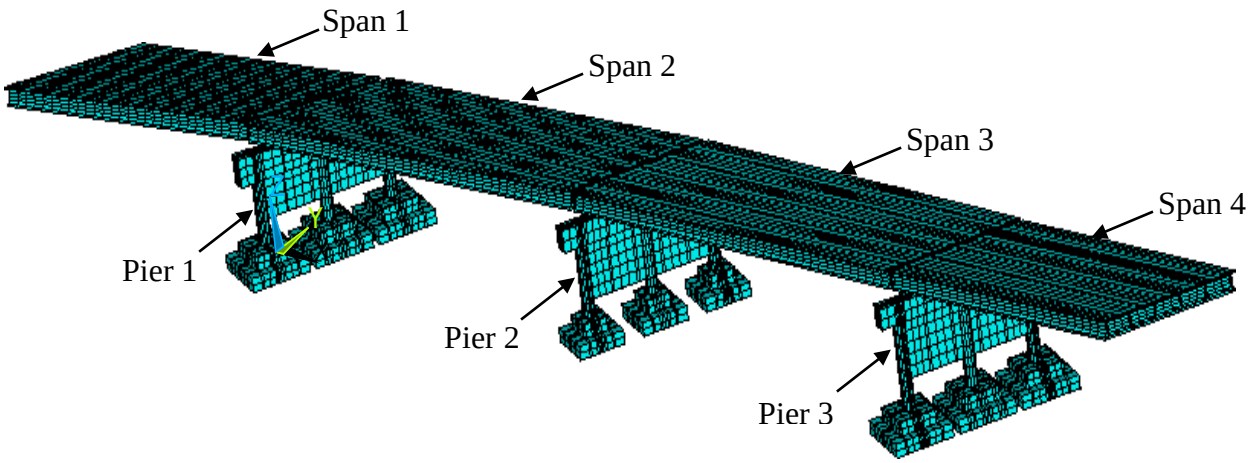

Fig. 4.3: Span and pier labels for the New Trammel Creek Bridge FE model.

4-node shell elements
(with thicknesses displayed)

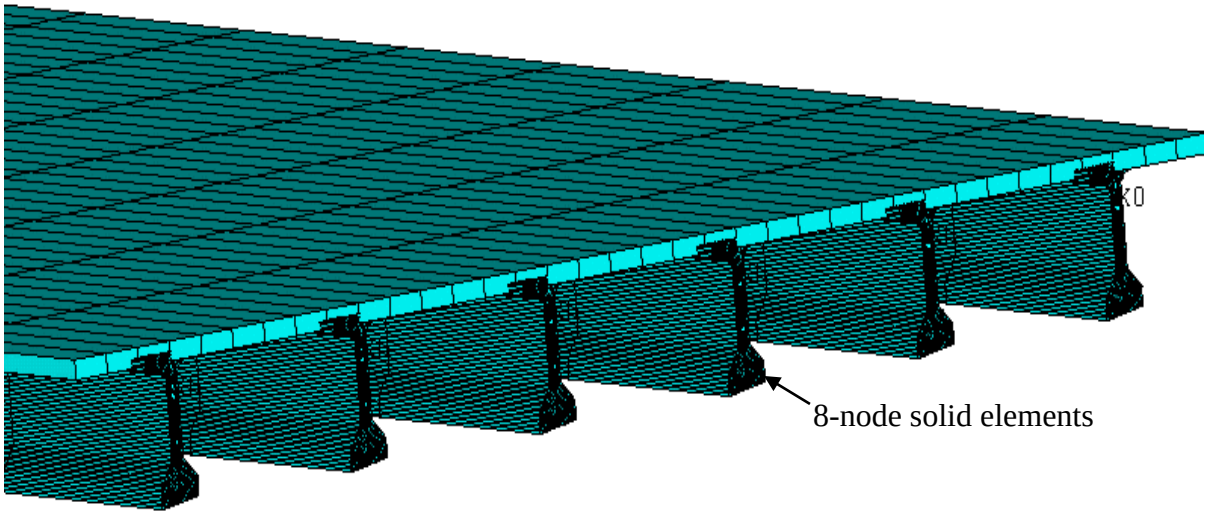

Fig. 4.4: Isometric-section view of discretely modeled bridge deck and girders.

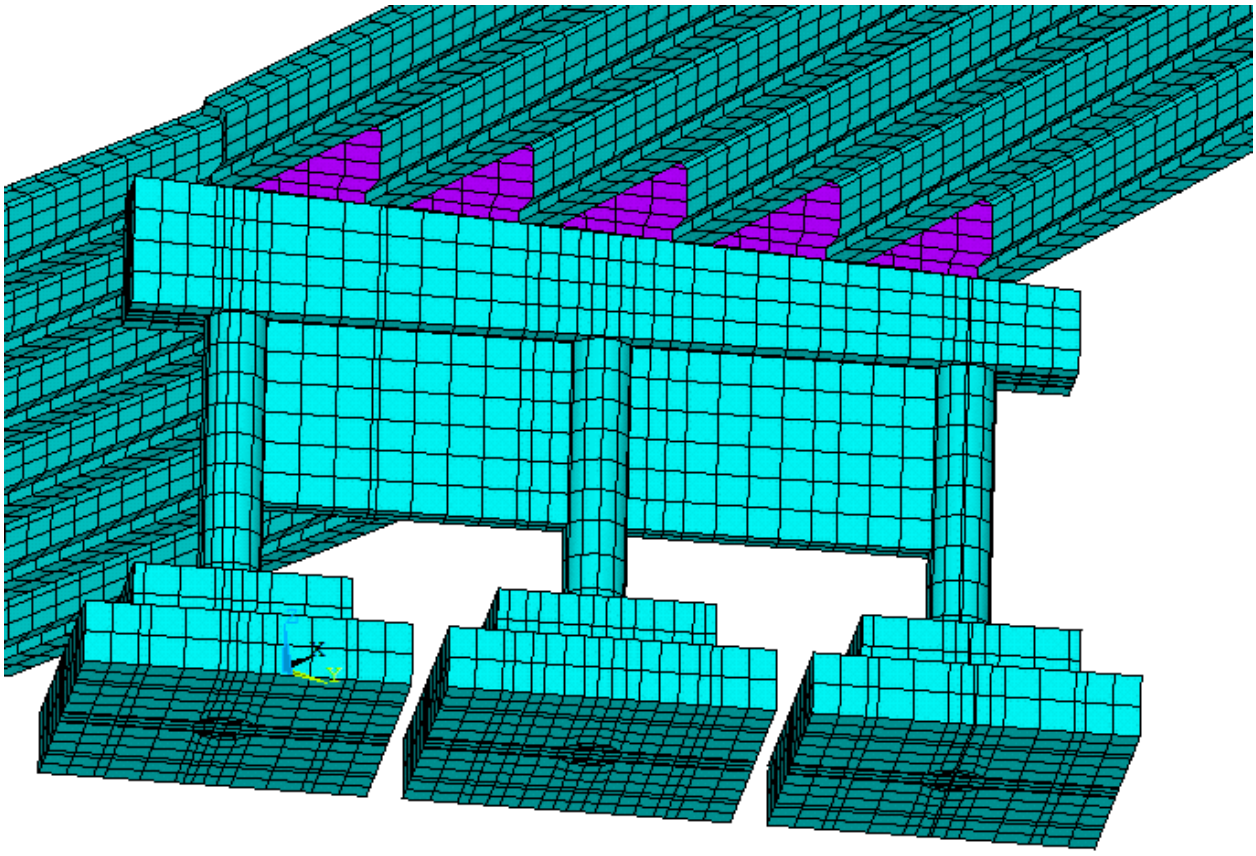

Fig. 4.5: Discrete modeling of reinforced concrete diaphragms above each pier.

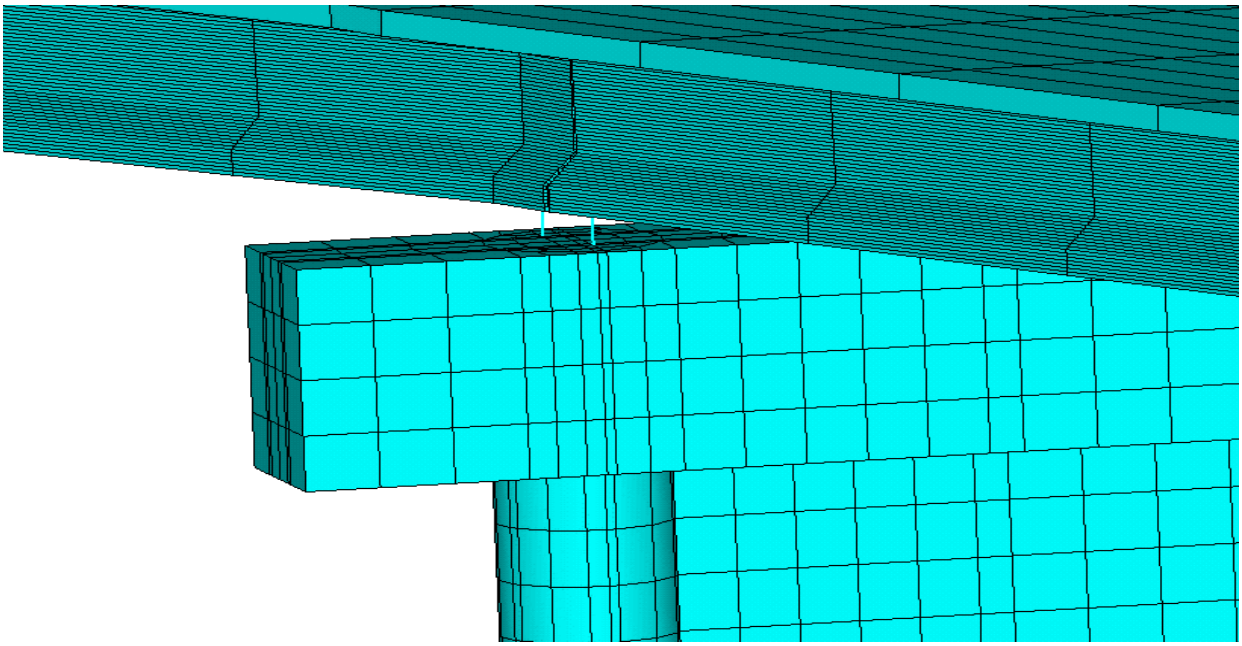

Fig. 4.6: Modeling of bearing force transfer at the substructure-superstructure interfaces above each pier

Table 4.1 Stiffness of elastomeric bearing pads (derived from Podolny and Muller 1982)

DOF	Stiffness (k/in and kip-in/rad)
Vertical stiffness (compression only)	3.2E+04
Horizontal stiffness (longitudinal shear)	2.9E+01
Rotational stiffness (longitudinal)	7.8E+04

The full three-dimensional FE bridge model is comprised of 69,129 elements, which corresponds to approximately 3,600,000 DOF.

4.2.2 Soil Modeling Beneath Pier Footings

Per the construction techniques employed during preparation of the bridge pier footing excavation pits (see Chapter 3 for a detailed discussion of the excavation pit surface preparation) and the boring log records given in the structural drawings, each instrumented footing of Pier 1 and Pier 3 rested on a 9 in. layer of #10 crushed stone. In contrast, all non-instrumented footings rest directly atop the limestone.

As shown in Fig. 4.7, the crushed stone layer was explicitly modeled for instrumented footings of Pier 1 and Pier 3. Immediately underlying the compacted crushed stone layer was a thick layer of limestone (all other footing model components bear directly on the underlying limestone layer). The site-specific, below-footing Kentucky rock quality designation (KY RQD) values ranged from 74% to 84% for the boring taken within the Pier 1 footprint; 76% to 84% for

the boring taken within the footprint of Pier 2; and, 59% to 98% for the boring taken in the immediate vicinity of Pier 3. Given that the relatively high-percentage KY RQD rates indicate predominately good to excellent rock quality (per Hawkins 1986) for the ubiquitous limestone layer, a thick (10 ft), monolithic slab of twenty-node solid elements were modeled beneath the footings of Pier 1, Pier 2, and Pier 3. The slabs of limestone are fully restrained throughout the bottom faces.

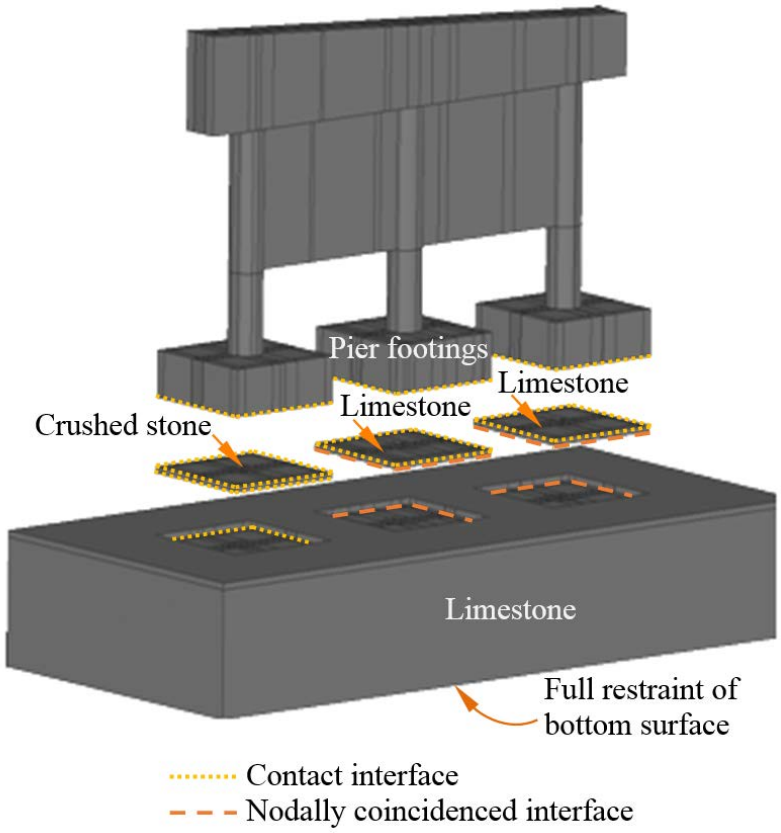

Fig. 4.7: Exploded model view of pier with emphasis on foundation modeling

Distributed throughout the element interfaces between each of the instrumented footing and underlying crushed stone layers of Pier 1 and Pier 3 were surface-to-surface contact definitions, which were employed to detect and prevent unrealistic penetration of either the respective faces of the footing elements or the faces of the solid elements representing the crushed limestone. An additional set of surface-to-surface contact definitions was included along the bottom face of the elements representing the crushed stone layer and the immediately underlying limestone layer elements. Note that the non-instrumented footings and underlying limestone layer were used to form a direct surface-to-surface contact definition, where no intermediary crushed stone layer was present. Coefficients of static and sliding friction along both the concrete-to-crushed stone, crushed stone-to-limestone, and concrete-to-limestone interfaces were taken as 0.636 (static, per Takayama 1992) and 0.5 (sliding, as estimated from Byerlee 1978). Employment of the surface-to-surface contact definitions allowed the FE model to undergo both bearing of the footing on the underlying limestone (under compressive loads) as well as separation (due to uplift).

4.2.3 Constitutive and Kinematic Modeling

Load levels considered in this study stemmed exclusively from naturally occurring temperature changes and the effects of gravity, and therefore, member stresses that were generated throughout the bridge FE model are expected to remain within the elastic range. Furthermore, bridge member displacements that developed as a result of load application were predicted to be small enough to employ linear approximations to the system kinematics. Hence, the elected use of linear elastic constitutive relationships and small displacement kinematics was considered appropriate for all analyses conducted.

Given the above, the parameters necessary to define the various member material models consisted of: elastic modulus, Poisson's ratio, and unit weight. Accordingly, the parameters attributed to each of the major structural model components (i.e., constructed bridge members) are listed in Table 4.2. Determination of constitutive parameters pertaining to the structural (reinforced and prestressed concrete) members was based on 28-day compressive strengths listed in the structural drawings. While the diaphragm, pier, and footing (normal weight) concrete compressive strength was listed at 3,500 psi, that of the superstructure slab concrete (normal weight) was specified at 4,000 psi. The 28-day compressive strength values were used in conjunction with the empirical expression given in ACI (2011), which determine the concrete elastic moduli (E_c) as:

$$E_c = [33 \cdot w_c^{1.5} \cdot f'_c{}^{0.5}] / 1000 \qquad \text{Eq. 4.1}$$

where E_c is the elastic modulus of the normal weight concrete in ksi, w_c is the concrete unit weight in pcf, and f'_c is the 28-day concrete compressive strength in psi.

Similarly, the prestressed concrete 28-day compressive strength for the girders was given in the structural drawings as 8,500 psi. Supplying the compressive strength (in psi) and unit weight (in psi) values to Eq. 4.2 (which was taken from ACI 1992) produced the prestressed concrete elastic modulus (in ksi) listed for the girders in Table 4.2.

$$E_c = (w_c/145)^{1.5} \cdot [1000 + 1265 \cdot (f'_c/1000)^{0.5}] \qquad \text{Eq. 4.2}$$

The Poisson's ratio and unit weight values for all concrete members, and the mild steel reinforcement, were selected from commonly used design values recommended in PCI (2010).

Table 4.2 Constitutive parameters for bridge structural model components

Model component	Elastic modulus (ksi)	Poisson's ratio	Unit weight (pcf)
Roadway slab	3644 [a]	0.20	150
Girders	4688 [a]	0.20	150
Diaphragms	3409 [a]	0.20	150
Piers	3409 [a]	0.20	150
Footings	3409 [a]	0.20	150
Mild steel reinforcement	29000	0.30	490

[a] - Unit weight (w_c) values of 145 pcf were used in calculating the elastic moduli of concrete members.

Foundation bearing stiffness parameters (i.e., elastic moduli) attributed to the limestone material models for elements beneath each pier footing are listed in Table 4.3. [Note that the

selection criteria of mechanical properties specified for the discretely modeled, crushed stone layers are discussed later in this chapter.] The elastic moduli magnitudes specified for the limestone layers were conservatively estimated for each pier by, first, interpolating between available KY RQD values for rock corings taken local to each pier within the immediate depth-vicinity of the footing bottom-elevations. The interpolated KY RQD values were then correlated to rock mass rating (RMR) values (Table 4.4) based on empirical expressions given in Turner (2006). Finally, the correlation-derived RMR values were used to estimate elastic moduli based on Eq. 4.3 (which is also referenced in Turner 2006):

$$E_M = 10^{\frac{RMR - 10}{40}}$$

Eq. 4.3, where E_M is intact mass modulus of the limestone in GPa.

Table 4.3 Constitutive parameters for foundation model components

Model component	Elastic modulus (ksi)	Poisson's ratio	Unit weight (pcf)
Soil (limestone) under Pier 1	3656	0.25	147
Soil (limestone) under Pier 2	3399	0.25	147
Soil (limestone) under Pier 3	3064	0.25	147

Table 4.4 KY RQD and RMR values used for determination of Limestone elastic moduli

Model component	KY RQD (interpolated)	RMR
Soil (limestone) under Pier 1	79%	66
Soil (limestone) under Pier 2	78%	65
Soil (limestone) under Pier 3	76%	63

Based on the unit weight values listed for limestone in Table 4.3, a recommended range of intact densities for limestone is given in Cobb (2009) of 131 pcf to 163 pcf. As an approximation, a simple average of the two range values (147 pcf) was used (as listed in Table 4.2) to specify limestone element unit weights in the FE model. A range of values for Poisson's ratio of limestone have been given as 0.2 to 0.3 (Kuiper et al. 1959), and accordingly, the Poisson's ratio supplied to the elements representing limestone in the model was taken as a simple average value of 0.25.

4.2.4 Model Components Beneath Integral End Abutments

The extents of the bridge FE model (Fig. 4.8a) corresponded to the interface between the prestressed concrete girder ends and the top of the h-pile supported stem-wall foundations located at the bridge far ends. The pile-supported end-bents were assumed to be relatively stiff compared to the pier spread footings. Accordingly, while the effect of the elastomeric bearing pads located beneath the girder ends were directly accounted for at the model extents through placement of discrete DOF spring elements for vertical translational, horizontal translational, and various rotational DOF (recall Table 4.1), vertical foundation (pile and soil) support were

accounted for by restraining the bearing pad bottom-node locations across each end-bent interface (Fig. 4.8b).

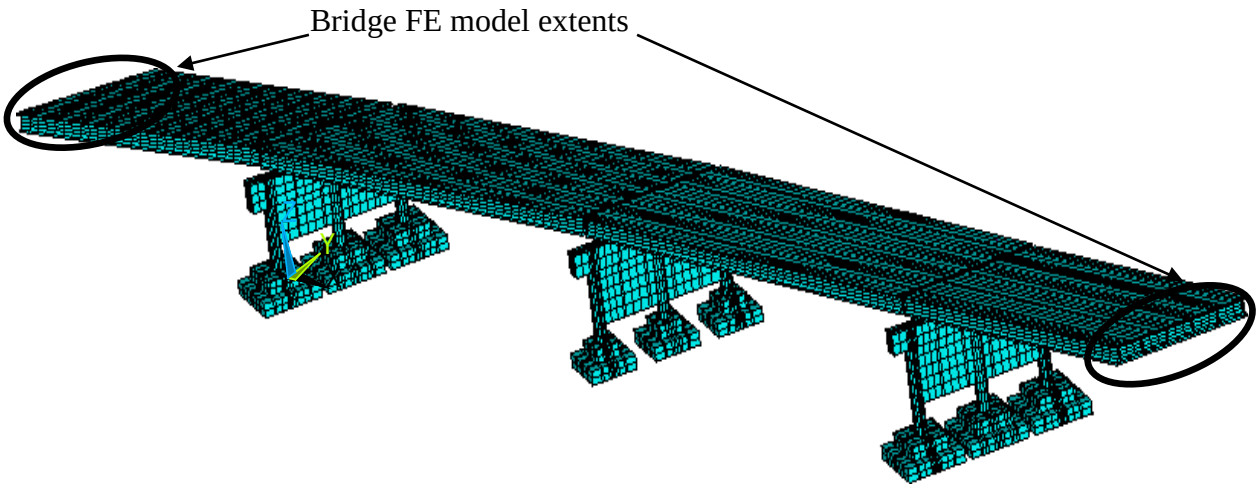

(a)

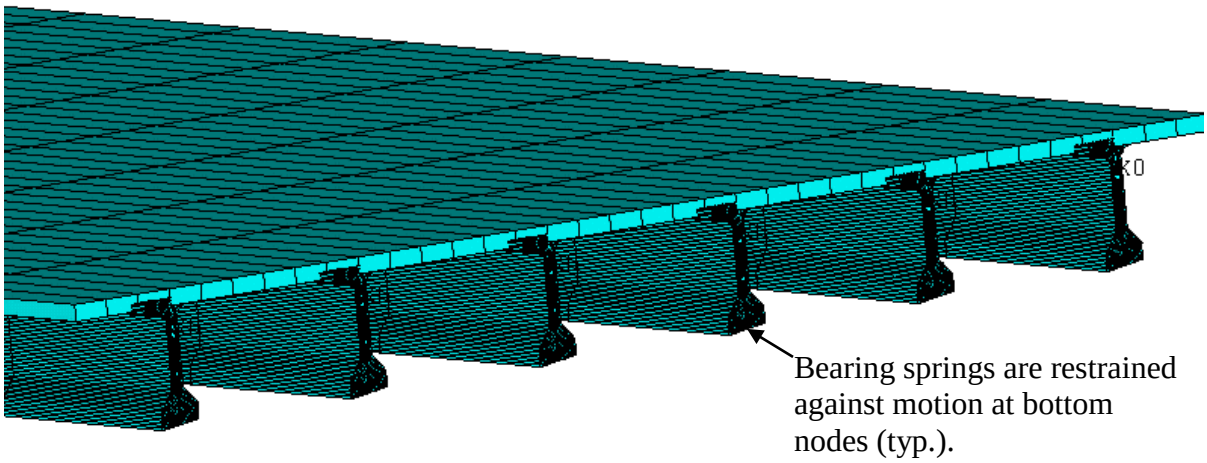

(b)

Fig. 4.8: Bridge FE model extents: a) Relative to entire model; b) Detailed view of span at right extent

4.3 Calibration and Validation of Bridge FE Model Under Gravity Loads

For the purposes of the FE model calibration and validation under gravity loading, two stages of the New Trammel Creek Bridge construction process were considered:

1. Casting of the instrumented pier footings
2. Installation of the superstructure deck

Calibration offsets were applied to the raw pressure cell readings based on manual pressure calculations for the first stage. Importantly, the first construction considered was followed by a period of time when wet concrete was allowed to set. Immediately following the casting of the pier footings, the footings remained mutually isolated, and therefore, area-proportional distributions of footing pressures accumulated in the pressure cells underlying the freshly poured bridge pier components. Consequently, manually calculated estimates of foundation pressures can be made and used as benchmark values for the first stage of construction considered.

To calibrate the FE bridge model, comparisons were made between the FE model results and the calibrated field readings of footing pressures for instances where bridge model components were subjected to gravity loading. By comparing the FEA foundation response quantities with measurements of foundation pressures (taken immediately following the second stage of construction) the following were considered: 1) FE model validation under gravity loading was carried out; and, 2) The validity of the pressure cell readings was assessed. Results obtained from FEA of the full bridge model, when subjected to combined gravity and temperature loading, are presented in a comparative manner (with corresponding field measurements) in Chapter 5.

4.3.1 FE Model Calibration

As discussed above, material properties were explicitly listed in the structural drawings for the various bridge structural members and the underlying limestone layers (recall Tables 4.2-4.4). However, mechanical properties (particularly the effective elastic moduli) associated with the 9 inch layers of crushed stone were not given in the bridge structural drawings. Furthermore, the literature gives widely varying magnitudes of 'effective stiffness' when estimating the mechanical properties of crushed stone layers, where aggregate type and size, layer thickness, level of compaction, confinement, and overburden stresses can affect stiffness magnitudes (Allen et al., 1999; Theyse, 2002). Further complicating any estimative calculations of the crushed stone moduli, was that the area footprint of each crushed stone layer was relatively small (compared to roadway bases) and was bounded below and along each side by relatively high-quality limestone. Additionally, a substantial volume of filler concrete was placed around the perimeter of each footing, where these latter two aspects of the bridge structural configuration confined the crushed stone layers.

Given the uncertainties associated with estimating the effective stiffnesses (i.e., elastic moduli) of the 9 inch layers of crushed stone beneath the instrumented pier footings, the elastic moduli of each layer were not directly calculated. Instead, trial values of the elastic moduli supplied for the crushed stone layers in the bridge FE model were incrementally varied so as to produce numerical gravity-load foundation responses that were in-line with those measured at the physical bridge site. Specifically, trial values of elastic moduli were defined for the crushed stone layers, and then the bridge FE model was subjected to gravity loading. Critically, all trial values of elastic modulus selected for the crushed stone layers were bounded between the corresponding range of values recommended in Hopkins et al. (2007) for crushed stone in Kentucky infrastructure construction (14 ksi to 77 ksi).

For each set of trial values of the elastic moduli, foundation pressures (obtained from using the trial FE model) were then compared to the foundation pressures measured at the physical bridge site, immediately following placement of the superstructure deck. Upon obtaining good

agreement between FE model results and the physically measured quantities, the corresponding elastic moduli were used in all subsequent analyses. To reflect the fact that all of the crushed stone placed at the bridge site was of the same type (No. 10), thickness (9 in.) and (approximate) compaction level, trial elastic modulus values were held equal across all crushed stone layers.

Material properties specified for the relatively thin layer of crushed stone located between the instrumented reinforced concrete pier footings and the thick limestone layers are listed in Table 4.5, where the elastic moduli obtained from the calibration process are included. The Poisson's ratio used in this study was taken from (NCHRP 2004), and the unit weight was taken as an average value for crush stone used in Kentucky infrastructure construction (Hopkins et al., 2007).

Table 4.5 Constitutive parameters for the crushed stone layers

Model component	Elastic modulus (ksi)	Poisson's ratio	Unit weight (pcf)
Crushed stone under instrumented footing of Pier 1	65	0.35	130
Crushed stone under instrumented footing of Pier 3	65	0.35	130

4.3.2 Casting of the Instrumented Pier Footings

Fig. 4.9 shows the instrumented footing of Pier 1 immediately after the footing concrete was poured. Readings were taken from the underlying pressure cells at this time. Correspondingly, a manual calculation of the anticipated uniform pressure over the plan area of the footing, and gravity-load FEA of the instrumented footing component were also carried out. For the FEA carried out, stress-points were identified at nodal locations that matched the spatial configuration of the physical system. A mapping of the Pier 1 footing pressure cell layout is shown in Fig. 4.10.

Fig. 4.9: Structural configuration associated with Stage 1 of bridge construction.

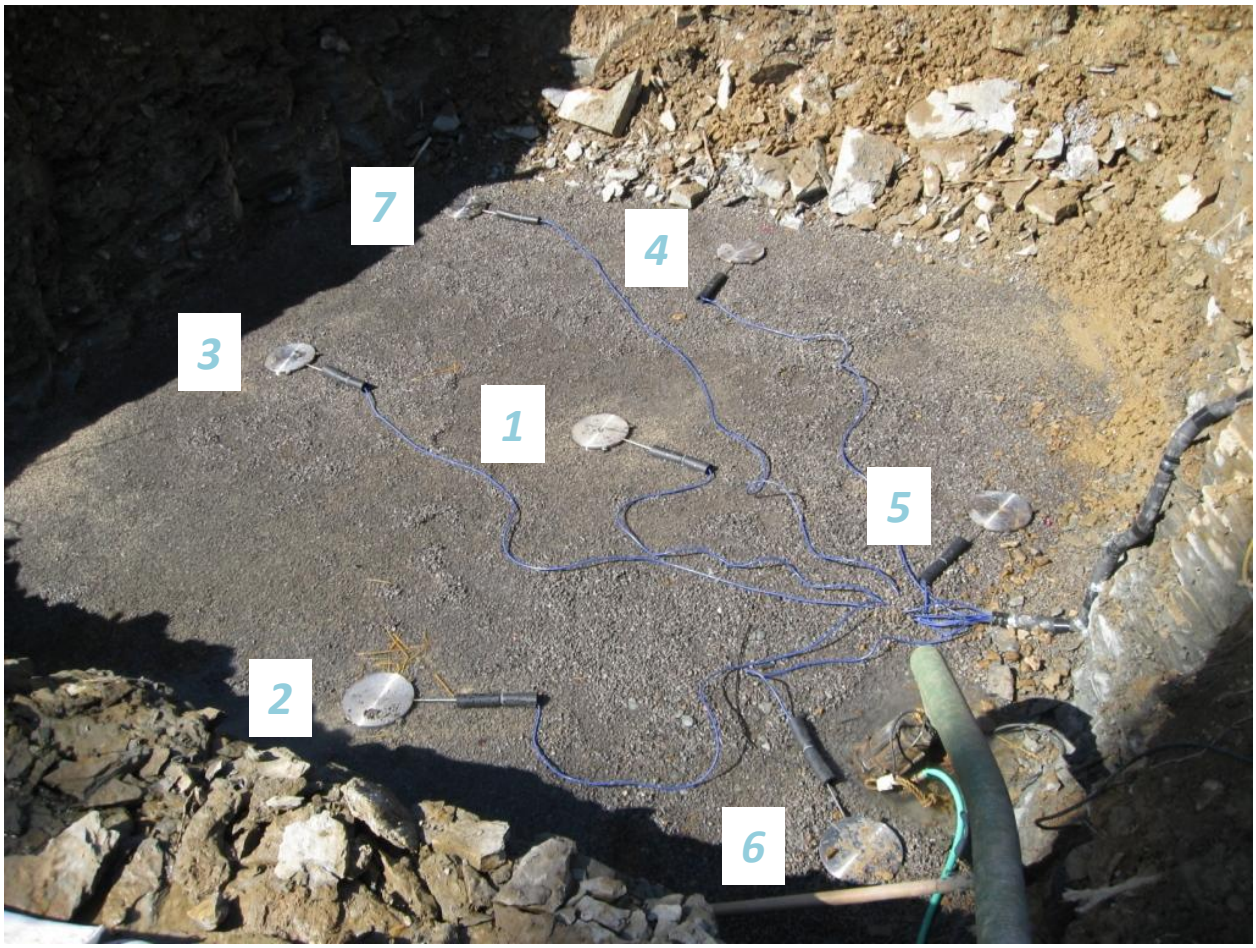

Fig. 4.10: Pressure cell layout beneath the southernmost footing of Pier 1 (picture taken prior to pouring of footing concrete).

Compressive pressure cell activity generated by the wet footing concrete, as derived from manual calculation and readings of the pressure cells at the bridge site are presented in Table 4.6. The manual calculation included the weight of the 12 ft x 12 ft x 3.5 ft reinforced concrete spread footing as well as 3 inches of #10 crushed stone cover above the pressure cells. The total weight of the wet reinforced concrete (150 pcf) and the crushed stone (130 pcf) divided by the footing (plan view) area (144 ft^2) yielded a manual calculation of approximately 3.90 psi at each pressure cell. An examination of the field measurements revealed variations among the pressure cells relative to the manual estimate of 3.90 psi (this issue is addressed below).

On-site pressure cell readings were taken after the footing concrete was poured; variations in readings were influenced by two factors: 1) An uneven limestone layer elevation within the footing pit; and, 2) Placement of masonry units beneath certain locations of the mild steel reinforcement cages. Variations in the limestone layer, in turn, produced variations in the strata stiffness beneath each pressure cell. The masonry units placed throughout the footing pit prior to placement of the mild steel reinforcement cage contributed to localized bearing concentration points between the footing concrete and the underlying pressure cells.

Calibrating adjustments were applied to all subsequent pressure cell readings to account for the differences between the 'benchmark' manually calculated pressures and the field measurements listed in Table 4.6. Namely, the pressure cell reading calibration consisted of adjusting on-site pressure data by magnitudes equal to the cell-specific differences from Table 4.6. The adjustment magnitudes are listed for each pressure cell in Table 4.7. After applying the adjustment amounts, the on-site readings and manual calculations of cell pressures associated with Stage 1 of construction gave exact agreement (i.e., the adjusted pressure magnitudes are uniformly taken as 3.90 psi).

Table 4.6 Pressure cell compressive pressures following pouring of the instrumented footing beneath Pier 1.

Pressure cell	Manual calculation (psi)	Field measurement (psi)
1	3.90	5.05
2	3.90	4.78
3	3.90	4.47
4	3.90	4.00
5	3.90	3.71
6	3.90	4.04
7	3.90	4.71
Average	3.90	4.39

Table 4.7 Adjustments applied to on-site pressure cell readings for the instrumented footing located beneath Pier 1.

Pressure cell	Adjustment pressure (psi)	Adjusted measurement (psi)
1	-1.15	3.90
2	-0.88	3.90
3	-0.57	3.90
4	-0.10	3.90
5	0.19	3.90
6	-0.14	3.90
7	-0.81	3.90

An analogous procedure was carried out for pressure cells of the instrumented footing of Pier 3, in association with the same stage of construction, and the results are presented in Table 4.8. On-site pressure cell reading variations and calibration offsets applied to readings of the pressure cells located beneath the Pier 3 footing are given in Table 4.9 (as discussed below). Calibrating adjustments were made to readings taken from the pressure cells physically located beneath the instrumented footing of Pier 3 in the same manner as those described above for the Pier 1 footing. After applying the calibration offsets, the on-site readings and manual calculations of cell pressures associated with Stage 1 of construction gave exact agreement (i.e., the adjusted pressure magnitudes are uniformly taken as 3.90 psi).

Table 4.8 Pressure cell compressive pressures following pouring of the instrumented footing beneath Pier 3.

Pressure cell	Manual calculation (psi)	Field measurement (psi)
1	3.90	5.45
2	3.90	5.47
3	3.90	6.37
4	3.90	4.94
5	3.90	4.66
6	3.90	3.56
7	3.90	3.20
Average	3.90	4.81

Table 4.9 Adjustments applied to on-site pressure cell readings for the instrumented footing located beneath Pier 3.

Pressure cell	Adjustment pressure (psi)	Adjusted measurement (psi)
1	-1.55	3.90
2	-1.57	3.90
3	-2.47	3.90
4	-1.04	3.90
5	-0.76	3.90
6	0.34	3.90
7	0.70	3.90

4.3.3 Installation of the Superstructure Deck: Measurements of Foundation Pressures

After the superstructure deck is emplaced, manually calculated estimates of individual footing pressures, which maintain reasonable levels of accuracy, are impractical. Specifically, integration of the individual piers with the superstructure and integral end bents leads to a highly statically indeterminate structural system, where foundation reactions can be strongly influenced by relative stiffnesses of the two integral end-bent foundations and the three intermediate pier footings. Therefore, verification of the FE bridge model is carried out by comparing the manually calculated, total weight of the bridge (i.e., the four spans, diaphragms, piers and footings, totaling 5.19E+03 kips) to the respective summation of boundary condition vertical reactions given by subjecting the full-bridge FE model to gravity loading (5.33E+06 kips). A comparison of the full-bridge reaction summation obtained from manual calculation and from FE bridge analysis with gravity loading (with a percent difference of less than 3%) indicated that the bridge FE model component masses were properly defined.

Footing pressures obtained from the full-bridge FE model (when subjected to gravity loading) are additionally compared to corresponding, physically measured pressure cell readings in Table 4.12 and 4.13, where the physical readings were taken immediately after the final roadway (deck) concrete pour. Specifically, a comparative listing of data is given for the instrumented footing beneath Pier 1 in Table 4.10. Reasonable agreement is shown for the data

pertaining to Pier 1, where the averages of the physically measured pressures and numerically generated pressures differ by less than 14.9%. As listed in Table 4.13 comparative data pertaining to the pressures generated beneath the footing of Pier 3 show good agreement between the physical measurements and the FEA results. Namely, the average pressure magnitudes differ by 2.3%.

Table 4.10 Pier 1 pressure cell compression pressures following placement of the deck concrete.

Pressure cell	Adjusted measurement (psi)	FEA (psi)
1	24.5	29.8
2	24.0	30.6
3	22.5	15.9
4	28.3	11.8
5	22.3	17.6
6	16.0	13.7
7	N/A[a]	16.7
Average	22.8	19.4

[a] - Data are not available for pressure cell 7, and so it is not included in the averaging.

Table 4.11 Pier 3 pressure cell compression pressures following placement of the deck.

Pressure cell	Adjusted measurement (psi)	FEA (psi)
1	13.5	15.9
2	16.8	20.7
3	17.0	14.3
4	8.3	5.6
5	N/A[a]	15.5
6	14.3	15.0
7	8.1	2.1
Average	13.0	12.7

[a] - Data are not available for pressure cell 5, and so it is not included in the averaging.

4.3.4 Installation of the Superstructure Deck: Measurements of Bridge Pier Tilt

The New Trammel Creek Bridge was constructed such that tiltmeters were not installed until several months after its was built. Therefore, comparisons between inclinations recorded from the tiltmeters and bridge pier motions obtained from FEA must account for temperature effects. The bridge pier inclinations and the effect of temperature on bridge pier motion are discussed in Chapter 5.

5 COMPARISON OF AASHTO DESIGN TEMPERATURE PRESSURES TO THERMAL PRESSURES MEASURED IN THE NEW TRAMMEL CREEK BRIDGE SUBSTRUCTURE

5.1 General

This chapter discusses bridge foundation response quantities obtained from subjecting the New Trammel Creek Bridge finite element (FE) model to combined gravity-temperature loading. Results acquired from using the FE model in combined gravity-temperature loading simulations were validated using corresponding, physically-measured bridge response quantities, where such measurements were taken on-site at the in-service New Trammel Creek Bridge (as discussed in Chapter 3). Further, the channel describes mechanisms by which changes in superstructure temperature lead to pier motion, and correspondingly, changes in pier foundation response (i.e., foundation bearing pressures) for integral abutment bridges were delineated.

Another topic explored in this chapter is the significance of the foundation pressures that were predicted for integral abutment bridges as a result of implementing the AASHTO superstructure temperature loading provisions. The extreme (i.e., design) temperatures that can be applied to the study bridge, as given by the AASHTO provisions, were determined. The corresponding FE bridge model was then exposed to gravity-temperature loading over a wide range of temperatures (including the design temperatures). Based on the analysis results and physical measurements taken at the bridge site, design-level temperature-induced bridge foundation response quantities were investigated. This process revealed that extreme changes in the bridge superstructure temperature induced pier rotations, which in turn, can lead to substantial increases in foundation bearing pressures. Design-level temperature-induced bearing pressures that developed beneath intermediate pier foundations of the integral abutment bridge were significant compared to those foundation bearing pressures associated with gravity loading.

5.2 AASHTO Temperature Loading: Procedure B

As discussed in Chapter 1, AASHTO bridge design provisions (AASHTO 2012) supply three different methods for making design-based estimates of bridge response quantities that can arise due to temperature changes at the superstructure level. Of these three variants, the New Trammel Creek Bridge was designed using, in part, the AASHTO temperature loading scheme termed “Procedure B”. Therefore, the loading procedure detailed in Procedure B (as given in Sec. 3.12 of AASHTO 2012) was of primary interest in the current study.

AASHTO’s Procedure B prescribes uniform, longitudinal deformations exclusively to superstructure members to integrate temperature loading into the bridge during the design phase. The bridge response stemming from these deformations was then calculated. In determining the prescribed superstructure deformations, minimum and maximum design temperatures were selected from temperature maps ($T_{MinDesign}$ and $T_{MaxDesign}$, as shown in Figs. 5.1-5.2, respectively). Then, to conduct a bridge structural analysis, a bridge FE (or structural analysis) model was formed, and the superstructure elements of the bridge model were subjected to uniform, longitudinal deformations to account for extreme changes in temperature. Specifically, uniform longitudinal deformations were prescribed in association with (design) uniform decreases (or

increases) in temperature relative to the base construction temperature for the bridge. For the current study, temperature values of interest were prescribed directly and uniformly throughout the superstructure elements in the bridge FE model (as opposed to employing the temperature loading indirectly through prescribed longitudinal deformations in the superstructure elements).

5.2.1 Design-Relevant Temperatures for the New Trammel Creek Bridge Site

The minimum design temperature ($T_{MinDesign}$) for the New Trammel Creek Bridge, per the AASHTO contour map (Fig. 5.1), is 10° F while the maximum design temperature ($T_{MaxDesign}$, per Fig. 5.2) is 110° F. These two temperatures constitute, respectively, the minimum and maximum temperatures that are anticipated to develop in the superstructure over the lifetime of the bridge.

Integral to the investigation of temperature effects on the foundation pressures developed in the New Trammel Creek Bridge was the determination of a base construction temperature. In this context, "base construction temperature" is defined as the ambient air temperature at which the overall bridge structure develops a minimum amount of thermally induced stresses. Further, the base construction temperature serves as a datum. When temperatures depart from the datum, either through increases or decreases in temperature, thermal stresses develop throughout the bridge. The limited guidance available in the literature recommends values of base construction temperature, including the use of simple or weighted averages of the extreme temperature values derived from the AASHTO provisions (e.g., Roeder, 2003).

Bridges that are integrated by pouring concrete at each pier top (diaphragm) location and at integral end abutments (span to wing wall) are affected by the ambient air temperatures present when the freshly poured concrete sets and cure (Klieger, 1958). The final concrete pours on the New Trammel Creek Bridge (above each pier and at the end bent locations) occurred in mid-January 2011. Given that the integrating portions of the bridge were poured in a winter month, selecting the average temperature over the 28-day period following these final pours (37.5° F) as the base construction temperature was appropriate. As discussed below, the good agreement found between the numerical and field measurements of bridge foundation response further supported the suitability of the chosen base construction temperature.

Fig. 5.1: Location of bridge site on contour map for minimum design temperatures ($T_{MinDesign}$) for concrete girder bridges with concrete decks (AASHTO 2012).

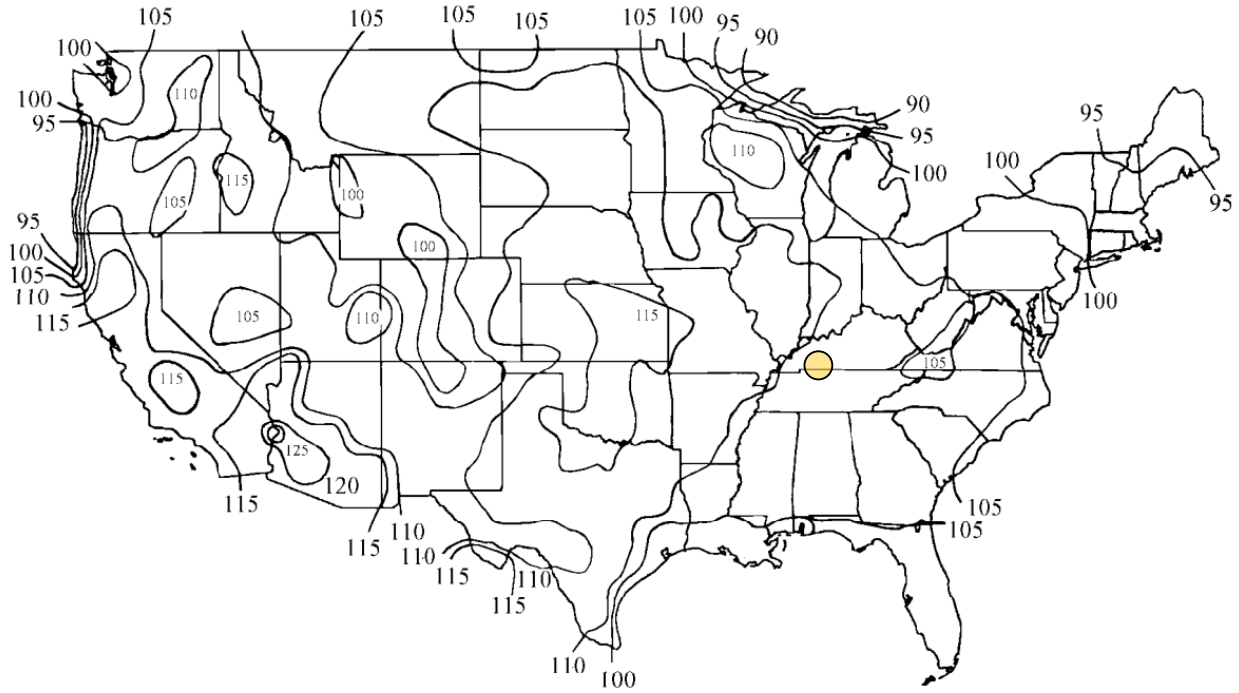

Fig. 5.2: Location of bridge site on contour map for maximum design temperatures ($T_{MaxDesign}$) for concrete girder bridges with concrete decks (AASHTO 2012).

5.3 Combined Gravity-Temperature Analysis

Based on the extreme temperature values ($T_{MinDesign}$ and $T_{MaxDesign}$), a series of combined gravity-temperature finite element analyses were carried out to investigate temperature-induced bridge foundation response. For each case, spatial points of interest within the bridge FE model were monitored, where these spatial points correspond to instrumented locations throughout Pier 1 and Pier 3 of the New Trammel Creek Bridge (Fig. 5.3). The load application techniques and specific temperature values considered are identified below.

5.3.1 Analysis Cases

The combined gravity-temperature loading analysis cases that were investigated used staged loading to identify bridge response quantities that were a direct response to application of each load type. At the onset of each analysis, gravity loads were statically applied (as body forces to all solid elements and surface pressures to all shell elements). Here, the individual element gravity force contributions were based on the respective element unit weight (as specified for each bridge model component in Chapter 4). After applying the gravity loads, all members of the superstructure (i.e., all elements above the bearing springs placed atop each pier) were subjected to a temperature change (Fig. 5.4); this change was measured relative to the base construction temperature.

Given the above staged-load application approach, the temperature loading domain was divided evenly among the AASHTO $T_{MinDesign}$ and $T_{MaxDesign}$ (10° F and 110° F, respectively) temperatures in 10° F increments. For each increment, the research team performed a separate, combined gravity-temperature load analysis. Analysis results were calculated for each of 11 cases, where after gravity loading was applied to the entire FE model, the bridge superstructure elements were additionally exposed to uniform temperature changes in the absolute domain of 10° F to 110° F. All temperatures were applied to the superstructure elements relative to the base construction temperature of 37.5° F. For instance, for the combined gravity-temperature analysis executed at the 30° F increment, a temperature of -7.5° F (i.e., a contraction or temperature decrease) was applied to all superstructure elements. Of particular interest in each analysis were the bridge pier tilts and footing bearing pressures at the locations indicated in Fig. 5.4.

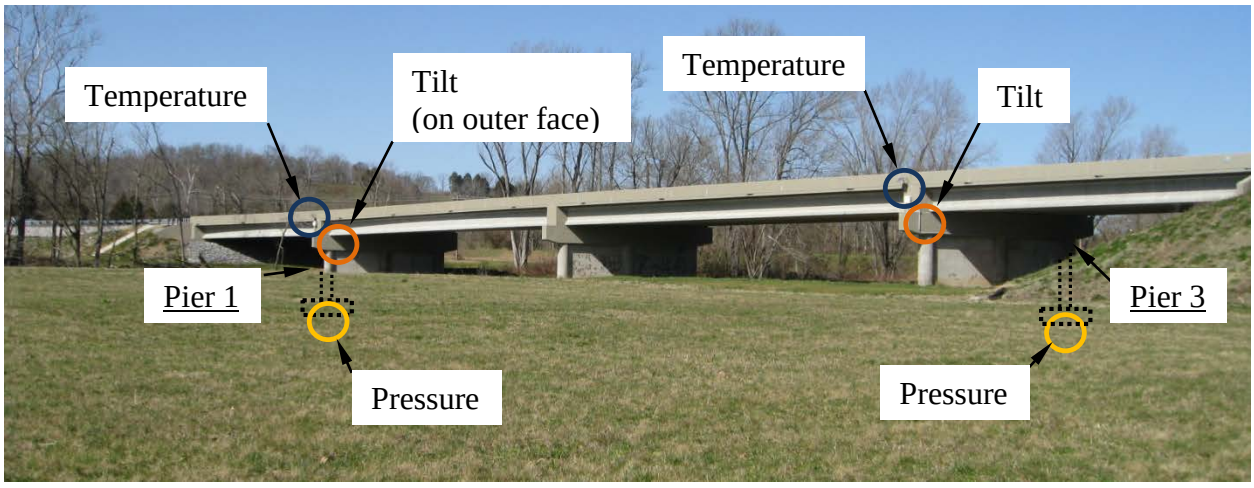

Fig. 5.3: Instrumented locations at the New Trammel Creek Bridge.

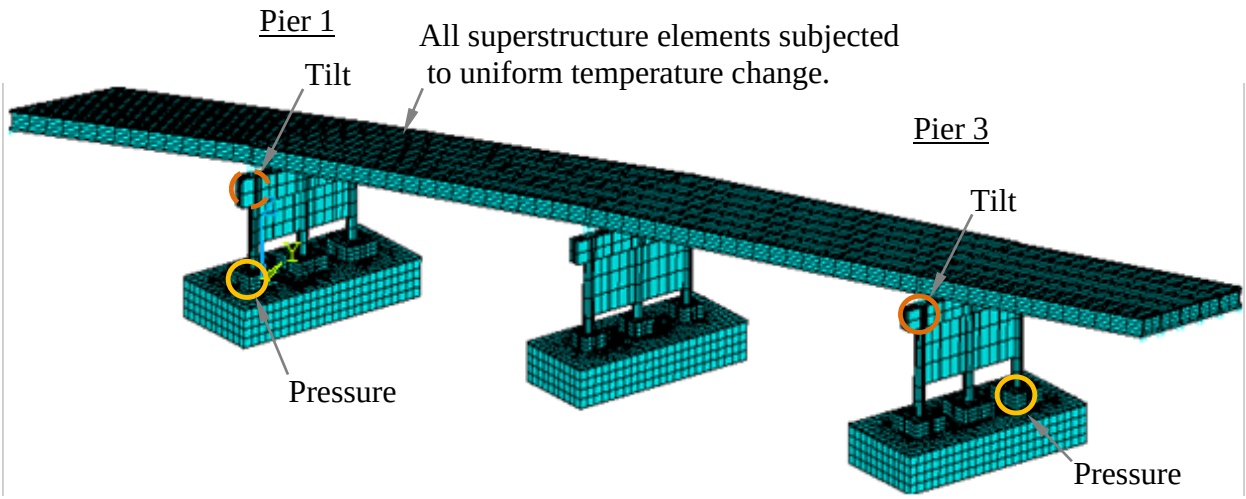

Fig. 5.4: Locations of interest throughout the finite element model of the New Trammel Creek Bridge.

5.3.2 Bridge Pier Tilt Data

Fig. 5.5 and Fig. 5.6 show the numerically generated pier tilts for Pier 1 and Pier 3, as related to superstructure temperature, where the pier inclinations are taken at the pier cap locations shown above in Fig. 5.4 (detailed placement of instrumentation on the pier caps is discussed in Chapter 3). Also shown in Fig. 5.5 and Fig. 5.6 are the physical on-site measurements of pier tilt, recorded from May 11, 2011 to May 11, 2012. Note that the FEA tilt values and tiltmeter inclinations are such that positive inclinations indicate that the Pier 1 and Pier 3 pier caps lean *toward* the center of the bridge (as illustrated in Fig. 5.7). In other words, for positive-valued inclinations, the horizontal distance from the footing (bottom of the pier) to the center of the bridge is *less* than the horizontal distance from the pier cap (top of the pier) to the center of the bridge.

Both the FEA pier tilt values and the on-site tiltmeter readings indicated that when temperatures (T) at the superstructure level rose above the base construction temperature, (37.5° F), Pier 1 and Pier 3 underwent restorative (centrifugal, relative to the center of the bridge) rotations toward fully upright, non-inclined orientations. That is, the positive inclinations in each pier, which indicate pier-top inclination toward the bridge center (Fig. 5.7), declined with increasing superstructure temperature. As shown below, the temperature-dependent, centrifugal tilt corresponded to increases in bearing pressure throughout outer portions of the pier footings.

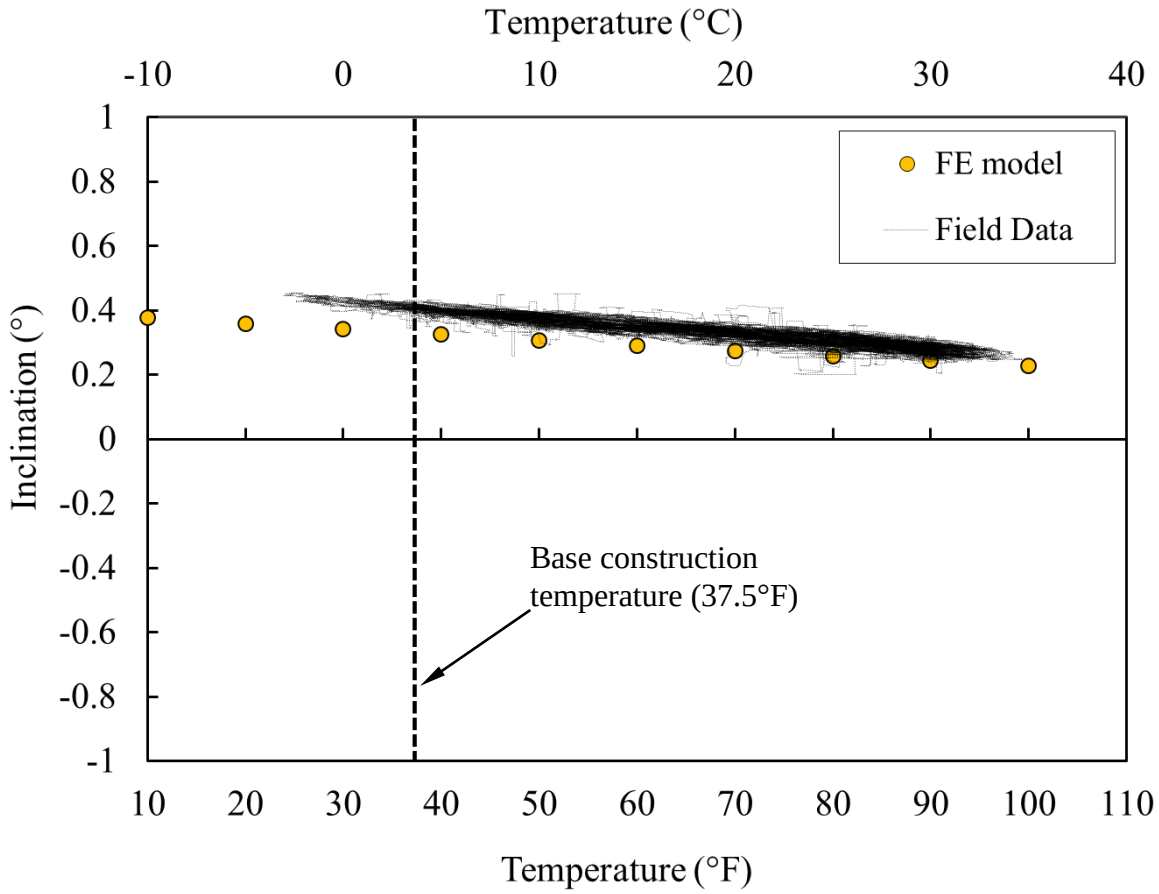

Fig. 5.5: Pier inclination versus temperature at Pier 1 pier cap.

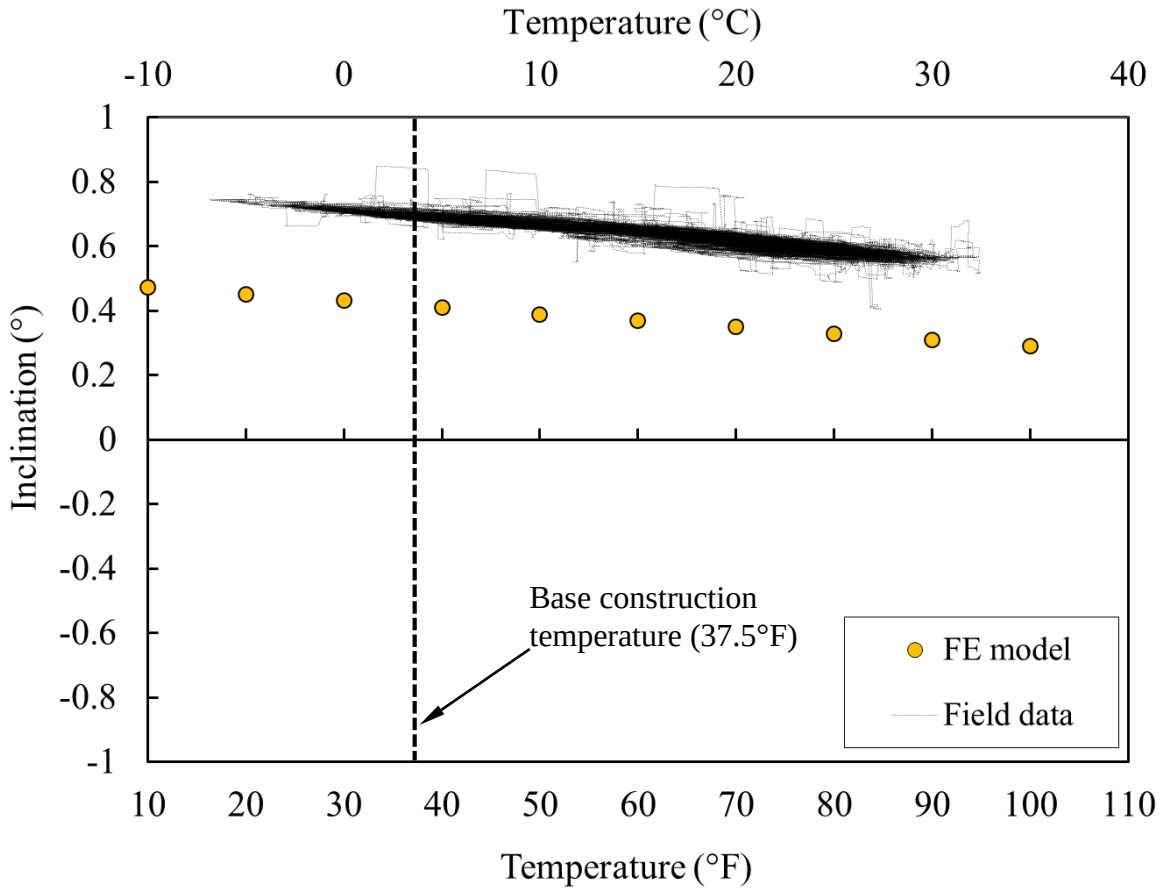

Fig. 5.6: Pier inclination versus temperature at Pier 3 pier cap.

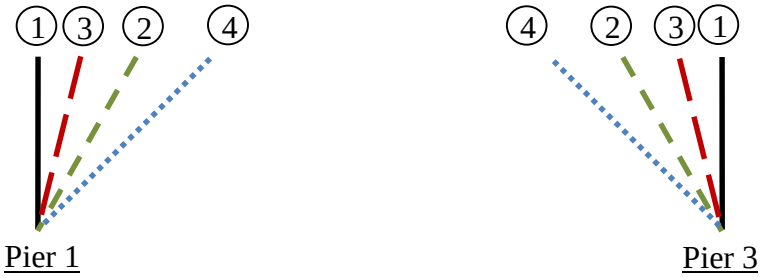

(1) Pier inclination prior to placement of superstructure.

(2) Pier inclination when superstructure diaphragms are poured, $T \sim 37.5°$ F.

(3) Pier inclination for T > 37.5° F.

(4) Pier inclination for T < 37.5° F.

Fig. 5.7: Bridge elevation schematic of longitudinal pier rotations versus temperature.

5.3.3 Design-Level Foundation Pressures Predicted using AAHSTO Procedure B

Given the correlations observed between the numerical (FEA) and physically-measured bridge pier tilts relative to changes in superstructure temperature, an analogous procedure was employed to illustrate the effect of superstructure temperature changes on foundation bearing pressures. For each pressure cell location installed on-site beneath footings of Pier 1 and Pier 3, the respective spatial points were monitored using the bridge FE model for each combined gravity-temperature analyses. In this context, "monitoring" signifies the extraction of vertical, compressive pressures throughout each analysis. By pairing the pier footing bearing pressures with the prescribed superstructure temperatures, correlations between superstructure temperature and foundation pressures emerged. By presenting the data in this way, the AASHTO Procedure B design-level foundation pressures specific to each pressure cell location were identified.

For example, Fig. 5.8 depicts the foundation bearing pressures obtained from FEA (over the domain of temperatures considered) corresponding to pressure cell 4 beneath Pier 1. Here, the domain of temperatures plotted were split into 10° F increments from 10° F and 110° F – the extreme temperature values specified by AASHTO Procedure B of ($T_{MinDesign}$ and $T_{MaxDesign}$). The non-zero slope of the pressure-temperature data acquired by introducing combined gravity-temperature loading to the FE model indicated that the pressures generated at cell 4 of Pier 1 were sensitive to changes in superstructure temperature.

Footing design must account for the pressures that arose throughout the footing when the superstructure was subjected to the AASHTO extreme temperature values ($T_{MinDesign}$ and $T_{MaxDesign}$). The corresponding footing bearing pressures are highlighted for cell 4 in Fig. 5.8. Further, the pressures that developed at cell 4 (when the AASHTO extreme temperatures are applied uniformly to the overlying superstructure) superseded all other temperature-dependent pressures that occurred at that location. This is because, in design applications that employ AASHTO Procedure B, only the $T_{MinDesign}$ and $T_{MaxDesign}$ values are considered. Therefore, the range of pressures corresponding to $T_{MinDesign}$ and $T_{MaxDesign}$ observed at cell 4 constituted the cell-specific envelope of design-foundation pressures (for AASHTO Procedure B).

As discussed below, pressures that develop throughout the footing (at the AASHTO Procedure B extreme temperature values) can be significant relative to pressures generated in response to other loads. Therefore, temperature-induced foundation bearing pressures can strongly influence the sizing of footing members. As a means of elucidating this phenomenon, cell-specific envelopes of design-foundation pressures were calculated for each pressure cell under the footings of Pier 1 and Pier 3. Specifically, pressures associated with $T_{MinDesign}$ and $T_{MaxDesign}$ are listed, respectively, in Table 5.1 and Table 5.2 for Pier 1. Those pressures were used later to inform estimates of the portion of bearing pressures that arose from temperature loading, in comparison to those that arose due to gravitational loads.

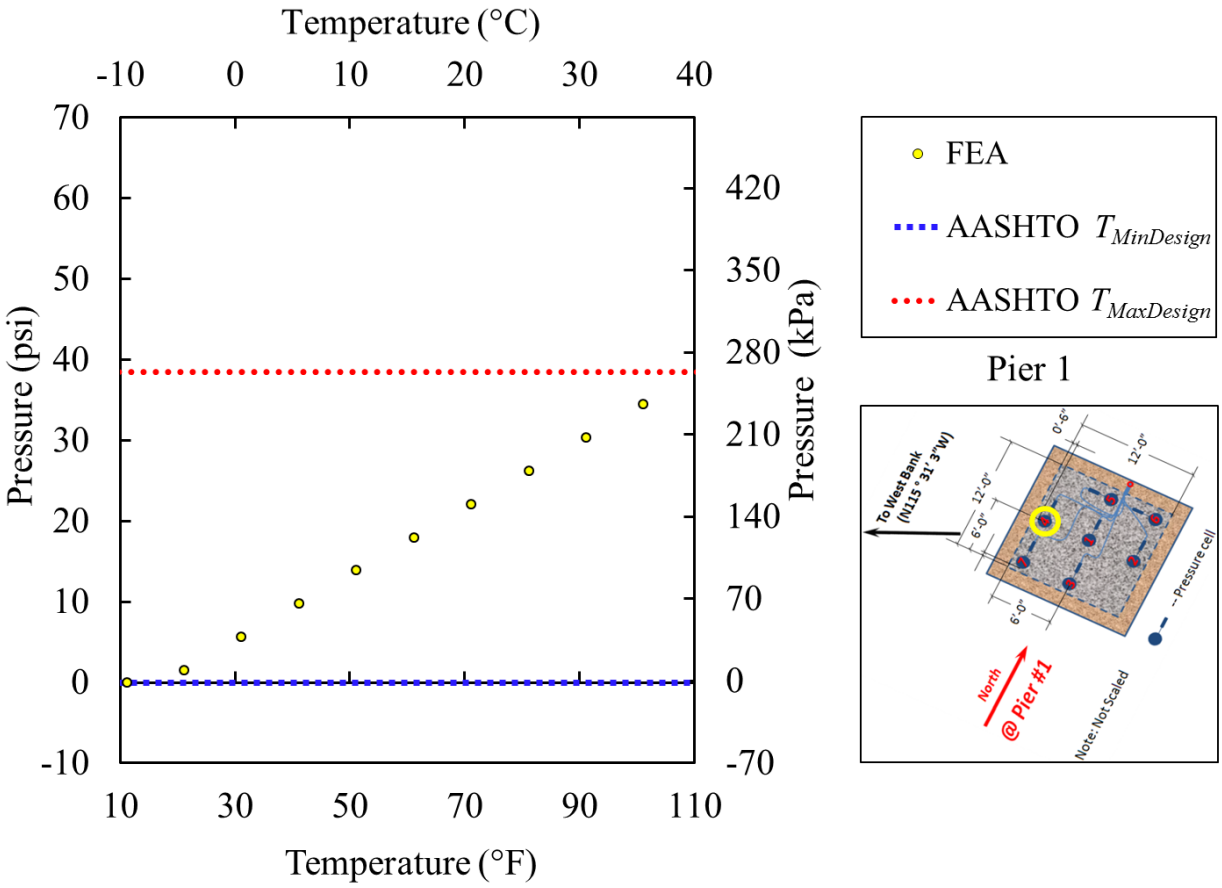

Fig. 5.8: FEA bearing pressures at Pier 1, cell 4 under combined gravity-temperature loading.

Table 5.1 FEA bearing pressures at Pier 1 cell locations for AASHTO $T_{MinDesign}$.

Pressure cell	Pressure (psi)
1	30.4
2	33.4
3	5.2
4	0.0
5	19.6
6	14.5
7	8.2

Table 5.2 FEA bearing pressures at Pier 1 cell locations for AASHTO $T_{MaxDesign}$.

Pressure cell	Pressure (psi)
1	28.5
2	25.5
3	35.7
4	38.5
5	13.8
6	12.3
7	32.9

Given the centrifugal manner in which both Pier 1 and Pier 3 rotated (recall Fig. 5.7) in response to superstructure level temperature increases, either of the pressures corresponding to $T_{MinDesign}$ and $T_{MaxDesign}$ may constitute the maximum pressure for a given pressure cell location. That is, the temperature at which the maximum magnitude pressure occurred for a given pressure cell depended on the pressure cell location within the footing. For example, as listed in Table 5.1, the Pier 1, cell 4 pressure at $T_{MinDesign}$ (0.0 psi) is less than the Pier 1, cell 4 pressure at $T_{MaxDesign}$ (38.5 psi, as listed in Table 5.2). The opposite is true for pressure cell 6 of Pier 1, however. This behavior occurred because superstructure temperature increase (from $T_{MinDesign}$ to $T_{MaxDesign}$) caused Pier 1 to rotate (in a relative sense) *away* from the bridge center. As Fig. 5.7 illustrates, cell 7 of Pier 1 is located at the southwest corner (farthest from bridge center) of the footing, and therefore, underwent an increase in pressure with increasing temperature. In contrast, cell 6 of Pier 1 is located at the northeast corner (closest to bridge center) of the footing, and therefore, underwent a decrease in pressure increasing temperature. The same phenomenon was observed among the pressures associated with $T_{MinDesign}$ and $T_{MaxDesign}$ for Pier 3, as listed respectively, in Table 5.3 and Table 5.4.

Table 5.3 FEA bearing pressures at Pier 3 cell locations for $T_{MinDesign}$.

Pressure cell	Pressure (psi)
1	14.1
2	21.1
3	5.8
4	0.3
5	16.1
6	18.1
7	0.0

Table 5.4 FEA bearing pressures at Pier 3 cell locations for $T_{MaxDesign}$.

Pressure cell	Pressure (psi)
1	19.8
2	19.6
3	32.5
4	17.0
5	14.1
6	8.4
7	16.3

5.4 Comparison of FEA Temperature-Dependent Foundation Pressures to Field Measurements

Before using the temperature-induced foundation bearing pressures obtained from FEA in exploring the associated effects on foundation member design, it was critical to demonstrate that the bridge FE model was capable of undergoing bridge responses that show agreement with the available field measurements for the New Trammel Creek Bridge. For example, Fig. 5.9 shows a comparative plot of numerically generated (using FEA) and physically measured foundation bearing pressures for pressure cell 4 beneath Pier 1. The plot includes cell-specific envelopes of pressure, which correspond to the FEA results of vertical, compressive pressures under the footings when the overlying superstructure elements were subjected to uniform temperature changes of $T_{MinDesign}$ and $T_{MaxDesign}$. The field data consisted of measurements recorded from May 11, 2011 to May 11, 2012.

There was agreement between the range of cell pressures obtained from FEA and the respective range of field-measured pressures across all the pressure cells of Pier 1 and Pier 3, which are given in Fig. 5.9 and Appendix C. Importantly, the slopes of the FEA pressure-temperature curves generally showed agreement with the field data in terms of the direction of correlation at every pressure cell location. Alternatively stated, for pressure cell locations that physically showed positive correlations with temperature (as indicated by the general, positive trend of the field-measured data), positive correlations were also observed in the FEA results (as shown in Fig. 5.9 and Appendix C).

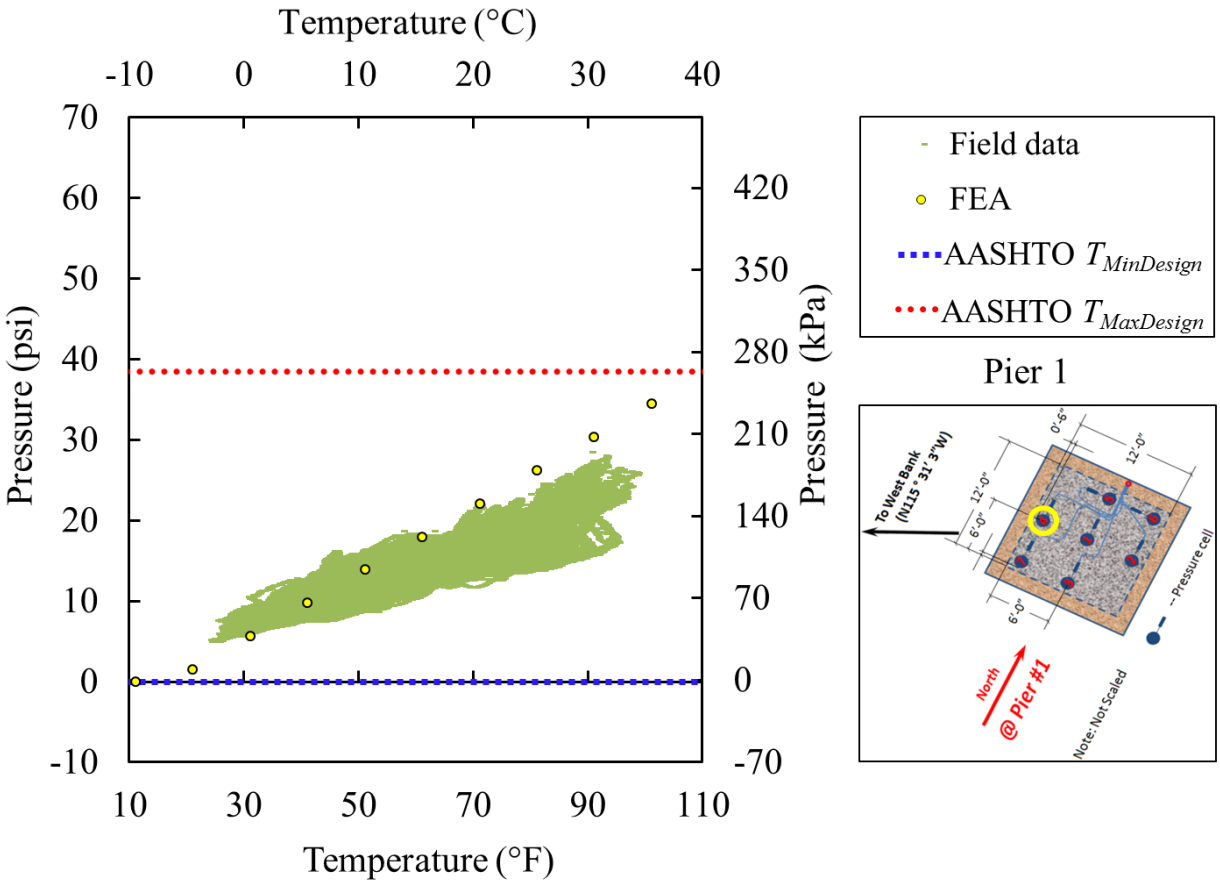

Fig. 5.9: Pier 1, Cell 4 field measurements and numerical estimates of substructure response to gravity-temperature loading.

5.4.1 Summary Comparison of Numerical and Physical Foundation Pressures

Fig 5.10 and Fig 5.11 contain plots of the physically measured data for all pressure cells beneath the footings of Pier 1 and Pier 3. Pier 1 field data showed that pressures ranged from 5 psi to 36 psi. Similarly, the physically measured pressures associated with Pier 3 ranged from 2 psi to 29 psi. Overall, the collective pressures fell within a range that is approximately one-half or less than that of the allowable soil (limestone) bearing capacity (P_a) of 65.3 psi. Consequently, the available field measurements indicated that the bridge foundation design and bearing pressures conferred a bearing safety factor of approximately 2 or greater. This value is consistent with the recommended safety factor for allowable bearing capacity of spread footings in the state of Kentucky (KyTC, 2005), and supports the assertion that the field measurements consisted of valid pressure readings.

Fig. 5.10 and Fig. 5.11 also show the minimum and maximum foundation bearing pressures (P_{FEAmin} and P_{FEAmax}, respectively) that arose due to combined gravity-temperature analysis of the bridge FE model. While the FEA-generated overall maximum footing pressures were conservative for the pressure cell groups in both the Pier 1 and Pier 3 footings, the level of conservatism was such that the FEA-based envelopes gave maximum pressure magnitudes that differred by 7.5% (38.5 psi from FEA, 35.8 psi from field measurements) and 12% (32.5 psi from FEA, 28.9 psi from field measurements), respectively.

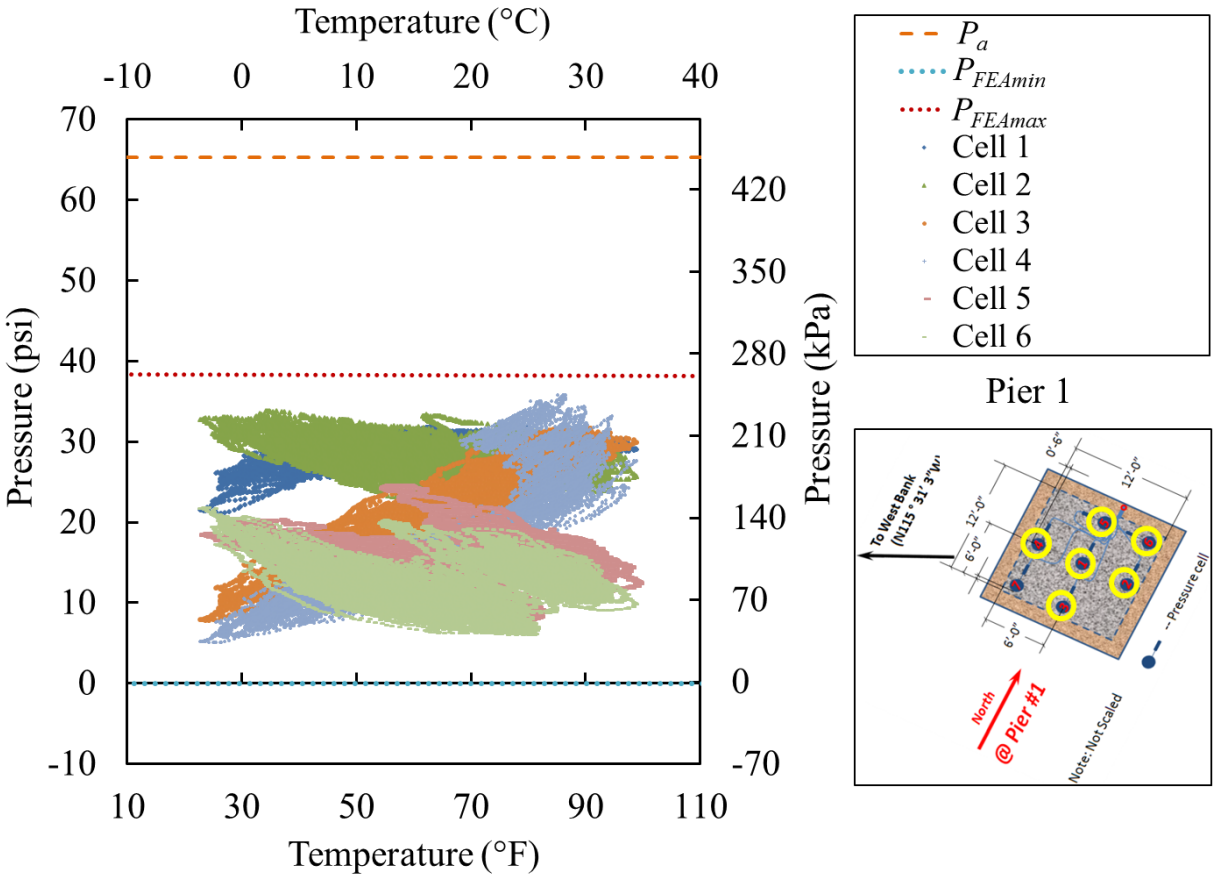

Fig. 5.10: Summary of Pier 1 foundation bearing pressures (Note: Cell 7 data are not available).

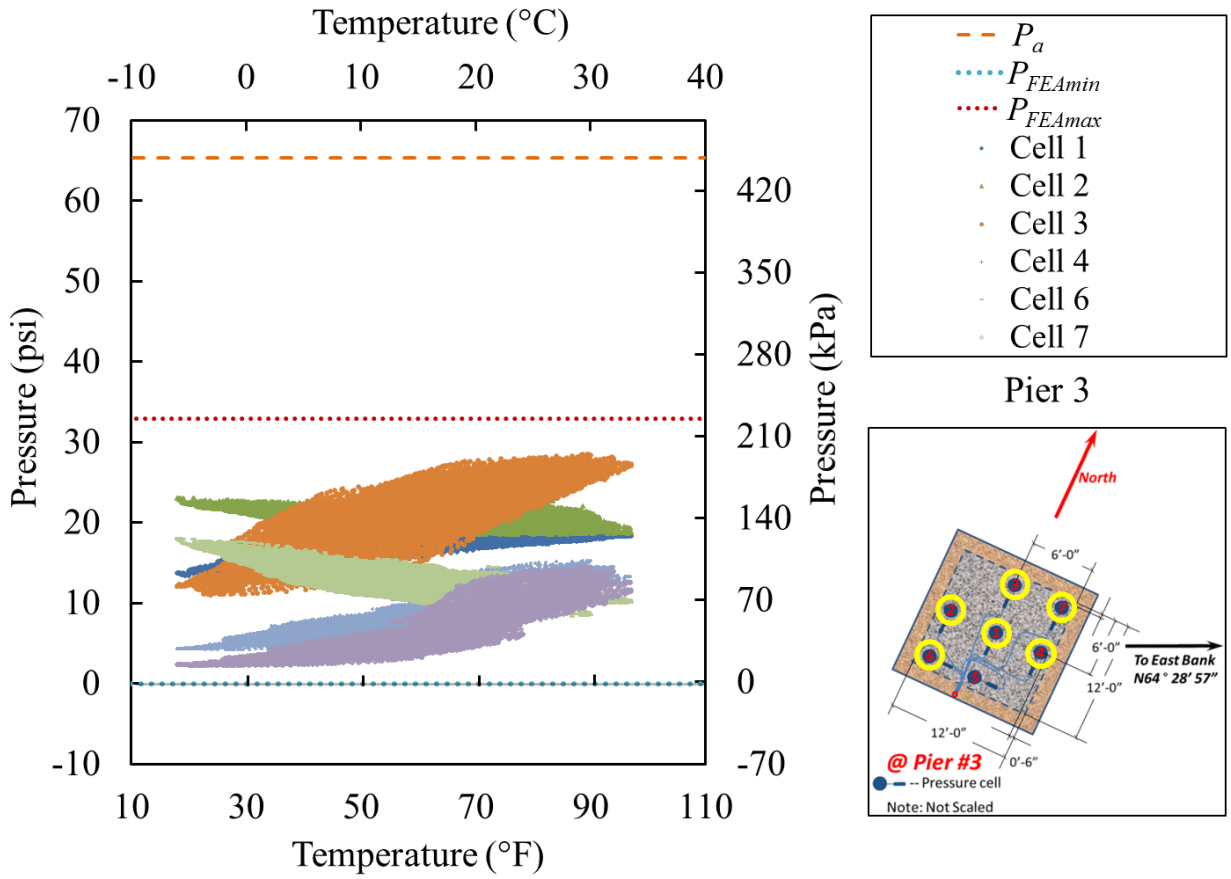

Fig. 5.11: Summary of Pier 3 foundation bearing pressures (Note: Cell 5 data are not available).

5.5 Effect of Superstructure Temperature Changes on Foundation Pressures

This study produced the following conclusions about FEA temperature-induced bridge responses and the on-site measurements recorded for footings beneath Pier 1 and Pier 3 of the New Trammel Creek Bridge:

1. For superstructure temperatures cooler than the base construction temperature (37.5° F), rotations were induced in Pier 1 and Pier 3 such that the piers rotated (relatively) away from the center of the bridge (recall Fig. 5.7).
2. For superstructure temperatures warmer than the base construction temperature (37.5° F), rotations were induced in Pier 1 and Pier 3 such that the piers rotated (relatively) toward the center of the bridge (recall Fig. 5.7).
3. The pier rotations, in turn, induced changes in bearing pressure beneath the footings of Pier 1 and Pier 3.
4. For each pressure cell beneath the footings of Pier 1 and Pier 3, general agreement was found between the numerical (FEA) and physical (on-site) range of foundation bearing pressure magnitudes (Fig. 5.9 and Appendix C).
5. For each pressure cell, agreement was universally observed among the FEA and on-site correlation directions for a given pressure cell, when pressures were compared to changes in superstructure temperature (Fig. 5.9 and Appendix C).

Given the above observations, and further taking into consideration that the datum (i.e., physical measurements) for the bridge FE model responses were representative of the physical conditions beneath the instrumented footings of Pier 1 and Pier 3, the FE model can be used to further elucidate the temperature-induced responses of the footings in the New Trammel Creek Bridge. Introducing gravity-only loading to the bridge FE model, and extracting the vertical, compressive pressures at the spatial points that correspond to the pressure cell locations in the physical bridge, it is possible to quantify the cell-specific pressure contribution associated with gravity loading. Second, by subjecting the bridge FE model to combined gravity-temperature loading, and again extracting the vertical, compressive pressures at the pressure cell locations beneath the footings of Pier 1 and Pier 3, the total (combined) gravity-temperature stress at each pressure cell can be quantified. Lastly, subtracting the gravitational component of vertical, compressive pressure from the combined gravity-temperature pressure value yields the portion of the total pressure associated with temperature changes at the superstructure level.

This process was carried out using the bridge FE model, where the maximum magnitude pressure obtained from subjecting the bridge FE model to combined gravity-temperature loading, separately, at the AASHTO Procedure B extreme temperatures ($T_{MinDesign}$ and $T_{MaxDesign}$) was taken as the maximum pressure in Table 5.5. and Table 5.6 for Pier 1 and Pier 3, respectively. For example, the maximum pressure column in Table 5.5 (pertaining to Pier 1) contains the maximum of the cell-specific $T_{MinDesign}$ pressure values from Table 5.1 and the $T_{MaxDesign}$ pressure values from Table 5.2. Similarly, the maximum pressure values listed in Table 5.6 for Pier 3 are derived from Table 5.3 and Table 5.4.

The next step to determine the components of the vertical, compressive pressures in each pressure cell entailed identifying the component of pressure due to gravity; those values were

taken directly from Chapter 4 (Table 4.10 and 4.11 for Pier 1 and Pier 3, respectively). The component of vertical, compressive pressure that developed in the pressure cell locationswas associated exclusively with temperature changes in the superstructure. The calculation for each pressure celldetermined the difference in maximum pressure and the pressure due to gravity. The temperature-induced pressures are listed in Table 5.5 and Table 5.6 for Pier 1 and Pier 3, respectively.

Table 5.5 FEA estimates of gravity-induced pressures and temperature-induced pressures for Pier 1.

Pressure cell	Maximum pressure (psi)	Due to gravity (psi)	Due to temperature (psi)
1	30.4	29.8	0.6
2	33.4	30.6	2.8
3	35.7	15.9	19.8
4	38.5	11.8	26.7
5	19.6	17.6	2.0
6	14.5	13.7	0.8
7	32.9	16.7	16.2
Average	29.2	19.4	9.8

Table 5.6 FEA estimates of gravity-induced pressures and temperature-induced pressures for Pier 3.

Pressure cell	Maximum pressure (psi)	Due to gravity (psi)	Due to temperature (psi)
1	19.8	15.9	3.9
2	21.1	20.7	0.4
3	32.5	14.3	18.2
4	17.0	5.6	11.4
5	16.1	15.5	0.6
6	18.1	15.0	3.1
7	16.3	2.1	14.2
Average	20.1	12.7	7.4

The maximum pressures listed in Table 5.5 and Table 5.6 represent footing design pressures attributed to combined gravity-temperature loading. One conservative approach to design of the footings would be to take the greatest-magnitude maximum pressure (38.5 psi for Pier 1, 32.5 psi for Pier 3) and design the footing dimensions such that these pressure levels are never exceeded (with consideration of the applicable design and resistance factors). In this scenario, the maximum gravity-induced and temperature-induced pressures for Pier 1 would be 11.8 psi and 26.7 psi, respectively. Hence, the component of foundation pressure attributed to temperature changes in the superstructure would far outweigh that associated with gravity (where the temperature-induced pressure is 2.3 times larger than the gravity-induced pressure).

An inspection of the average contribution of temperature-induced pressures beneath the footings of Pier 1 and Pier 3 indicated that temperature-induced vertical, compressive pressures

components were significant. For Pier 1, the average temperature-induced contribution was 50.5 of that attributed to gravity loading. For Pier 3, the temperature-induced contribution to stress was 51.1%.

Further insights can be gained into bridge response to temperature loads at the superstructure by graphically examining the distribution of temperature-induced and gravity-induced stresses across each footing. Accordingly, the quantities listed in Table 5.5 and Table 5.6 are mapped in Fig. 5.12 and Fig. 5.13 across the Pier 1 and Pier 3 footing surfaces, respectively. From these plots, it is apparent that the portions of the footing directly beneath the pier column were not strongly affected by design-level changes in temperature (those associated with use of AASHTO Procedure B) at the superstructure level.

Due to the rotation of Pier 1 and Pier 3 in conjunction with the orientation of the pier footings, pressure was alleviated from pressure cells 2, 5, and 6 of each footing. Consequently, the contribution of the design-level vertical, compressive pressures in cells 2, 5, and 6, which can be attributed to temperature changes at the superstructure level, were relatively small. In contrast, pier rotations away from the center of the bridge lead to increases in pressure throughout regions of the footings that have been instrumented with cells 3, 4, and 7. As a result, dominant portions (50% or greater) of the design-level combined gravity-temperature loading pressures can be attributed to temperature changes at the superstructure level.

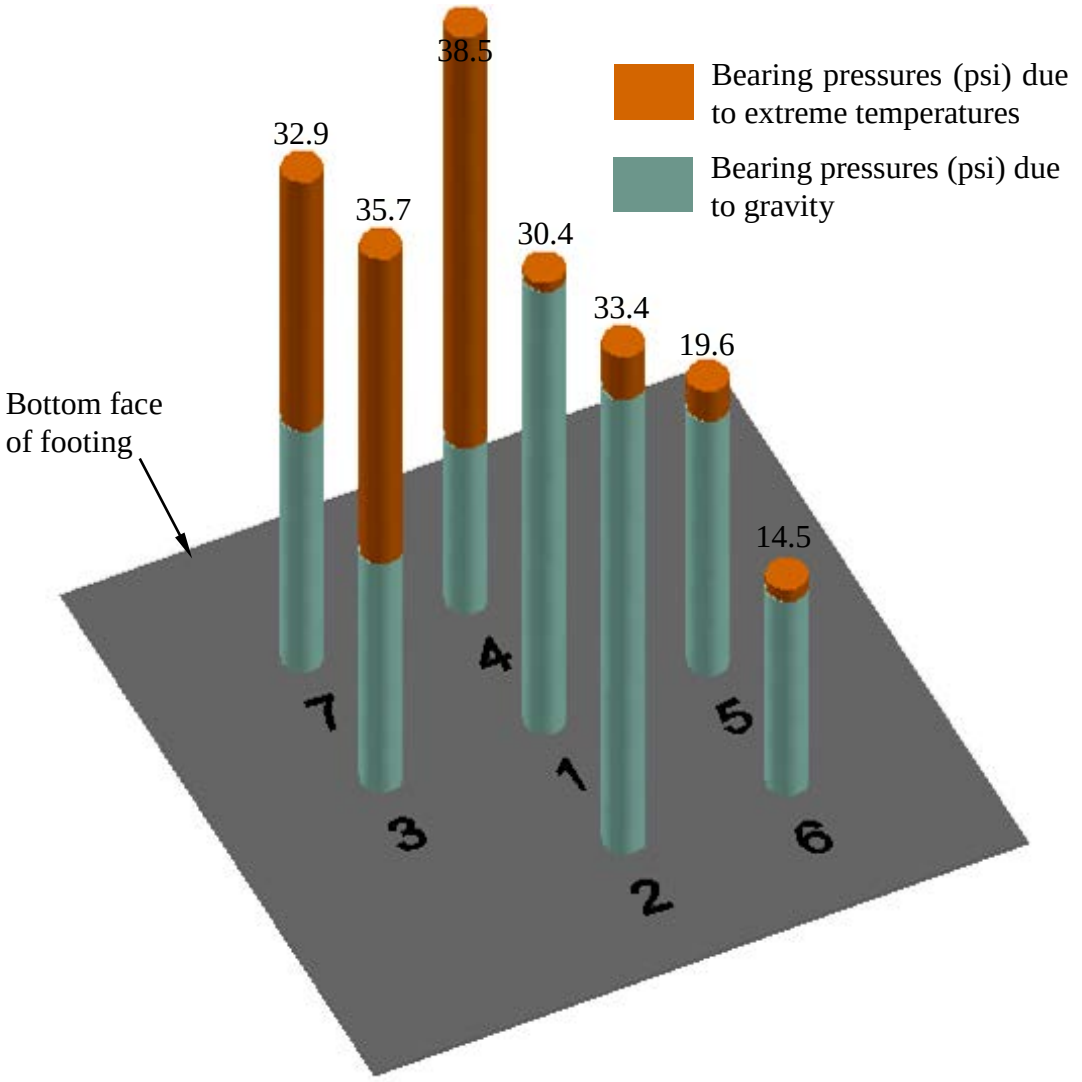

Fig. 5.12: Distribution of gravity and extreme-temperature bearing pressures on the bottom face of the instrumented Pier 1 footing (based on FEA results).

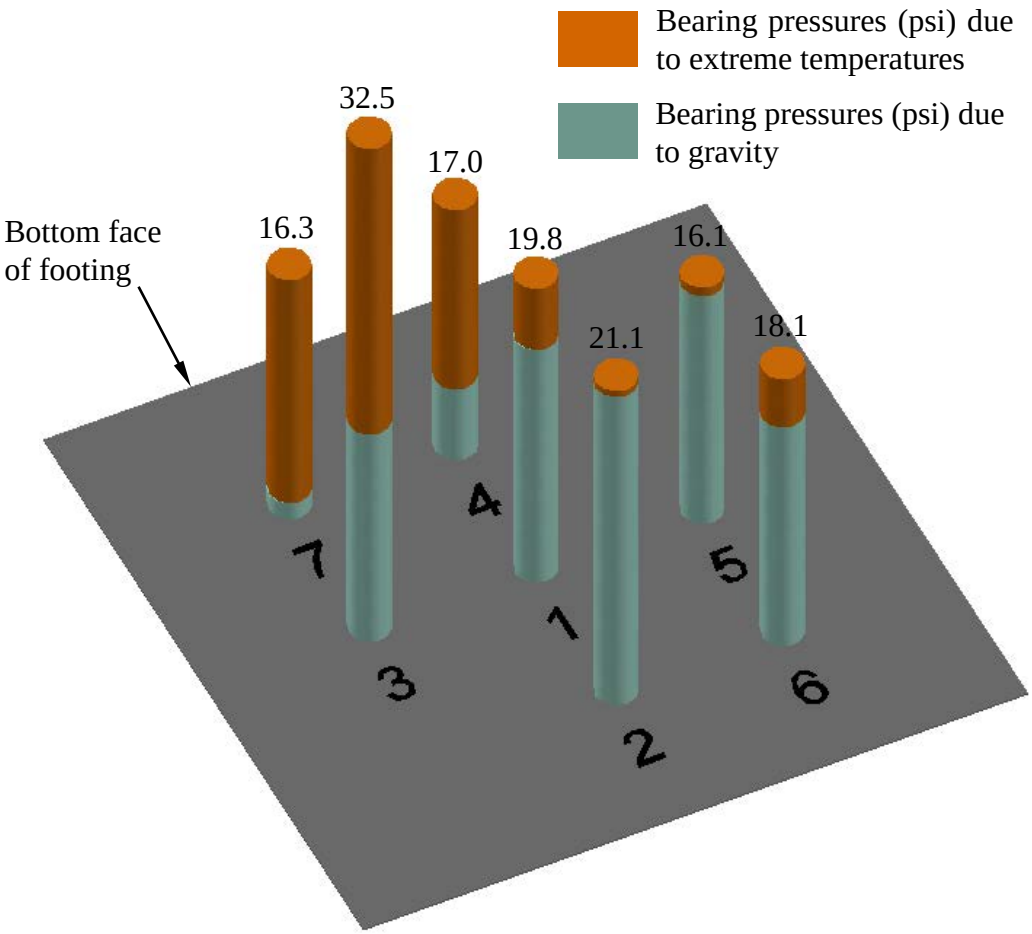

Fig. 5.13: Distribution of gravity and extreme-temperature bearing pressures on the bottom face of the instrumented Pier 3 footing (based on FEA results).

6 SUMMARY AND CONCLUSIONS

6.1 Summary of Research Activities

This study focused on the New Trammel Creek Bridge on KY-100 in Allen County, in southwest Kentucky. The team investigated foundation response quantities that are attributable to temperature changes at the superstructure level. The New Trammel Creek Bridge is a four-span (two-lane) integral abutment bridge; its spans range from 80 ft to 120 ft in length. The bridge spans are supported at the bridge far ends by integral end bents made of reinforced concrete wing walls, wall stems, and steel h-piles, where these latter members are driven into the underlying limestone bedrock at the bridge site. Three evenly spaced (at 120 ft) reinforced concrete bridge piers support the intermediate spans of the integral abutment bridge, where each pier contains a large shear wall and three pier columns. Each pier column span terminates below onto thick reinforced concrete spread footings. All bridge foundation members rest on limestone bedrock that is of good to relatively high quality.

6.1.1 AASHTO Provisions for Superstructure Temperature Loading

Of critical interest for this study were the AASHTO LRFD Bridge Design Specifications (AASHTO, 2012) and their guidance related to designing foundation members so they can resist superstructure temperature loading. This research, which used the New Trammel Creek Bridge as a case study, investigated the efficacy and precision associated with the use of these AASHTO design provisions. Those portions of the AASHTO provisions concerned with superstructure temperature loading have been reviewed. Of the three techniques available in the AASHTO provisions to determine temperature-load effects on bridges, AASHTO Procedure B was used in the design of the New Trammel Creek Bridge. Therefore, foundation design pressures that arose from the use of Procedure B in assessing temperature-load effects for the New Trammel Creek Bridge have been of primary interest in the current study.

As required by AASHTO Procedure B for superstructure temperature loading, the research team used temperature maps to identify the two extreme values of temperature impacting the site. Researchers used these temperatures to calculate their difference, which was used to determine the superstructure's design-level elongation or contraction that underlying substructure members must be able to adequately resist. The use of AASHTO Procedure B involves applying uniform temperature effects throughout the bridge spans.

On-site and analytical investigations were carried out (as summarized below) to directly measure bridge superstructure temperatures and bridge foundation response quantities. Once the research team had these in hand, these quantities were collectively used to estimate the contribution of foundation bearing pressures resulting exclusively from temperature changes in the New Trammel Creek Bridge's substructure. The design-level pressures predicted using Procedure B were also compared to the temperature-induced foundation bearing pressures.

6.1.2 Bridge Instrumentation and Monitoring

To collect bridge response data, the New Trammel Creek Bridge was instrumented with temperature measurement and bridge response monitoring devices both prior and subsequent to construction. Before select spread footings were poured beneath the outermost bridge piers (first and third), workers placed, leveled, and compacted layers of crushed stone within the footing excavation pits. Pressure cells were placed atop the crushed stone layers; these cells quantified the bearing pressures that developed beneath each of the instrumented footings. After placement, the pressure cell arrays were covered with another thin layer of crushed stone that was leveled and compacted.

After installing pressure cell arrays and pouring and setting the bridge pier spread footings, pier columns, and pier caps, additional instrumentation was placed at the outermost piers (Pier 1 and Pier 3). Tiltmeters were installed on the outermost faces of pier caps. Following installation of the prestressed concrete superstructure girders and pouring reinforced concrete diaphragms atop each pier, thermocouples were installed on the south face of the superstructure rails, where placement locations lie directly above Pier 1 and Pier 3. Solar panels were installed alongside the thermocouples above Pier 1 and Pier 3.

The pressure cell arrays, tiltmeters, and thermocouples data transmission lines, as well as the power transmission cables from the solar panels, terminated at data acquisition boxes located near the soil surface, directly above each of the instrumented spread footings. The solar panels generated sufficient electricity to enable the wireless transmission of data readings for all of the instrumentation; this allowed for remote monitoring activities. In addition to providing data that were integral to the completion of the current study, the in-service response of the bridge can now be monitored and use for future investigations based on the continuously updated dataset of superstructure temperatures, pier tilts, and foundation pressures. Accordingly, real-time in-service foundation and pier motion (tilt) data records are available to view on the KTC website: http://www.ktc.uky.edu/kytc/RemoteBridgeMonitoringInKY/ky100Allen.html.

6.1.3 Finite Element Modeling and Analysis

In conjunction with the on-site instrumentation program, the research team performed an analytical study on the New Trammel Creek Bridge. A bridge finite element model (FE) was created using structural drawings; the model represented the bridge superstructure roadway, prestressed concrete girders, bridge diaphragms, elastomeric bearing devices, reinforced concrete bridge piers, and reinforced concrete spread footings. Using the site-specific geotechnical report, underlying bedrock limestone was modeled beneath each of the three integral end abutment bridge piers. The general purpose FE software ANSYS (2012) was used to execute modeling tasks.

The bridge model incorporated twenty-node solid elements – four-node shell elements were used to model the bridge roadway, and spring elements represented the various stiffness contributions associated with the elastomeric bearing pads atop each pier as well as the span ends. The model integrated soil-structure interaction using surface-to-surface contact definitions between the pier bottommost faces and the immediately underlying crushed stone (or limestone) element top-faces.

Gravity loads and uniform superstructure temperature loads were applied as part of the FE analyses (FEA) performed. Due to the use of soil-structure interaction contact definitions, a staged loading was carried out. Gravity loading was applied globally to the structure, and then uniform temperature changes were applied (uniformly) to all superstructure members (all elements making up the girder and roadway members).

Bridge response quantities obtained from the bridge FE model were compared to full-scale physical measurements of bridge response, which were taken from instrumentation at the New Trammel Creek Bridge. In particular, it has been demonstrated that the bridge FE model is capable of developing gravity-induced bearing pressures that agree with physical pressure cell readings over the various stages of bridge construction. Additionally, this study verified that – under combined gravity and temperature loadings (as applied in the model) – the bridge motion and foundation bearing pressures obtained from FEA align with data readings taken from the bridge site.

6.1.4 AASHTO Temperature Load Effects on Bridge Substructures

This study sought to determine the effects of bridge superstructure temperature changes on bridge substructure response. The bridge FE model for the New Trammel Creek location proved instrumental in isolating these effects. After demonstrating that the bridge FE model gave gravity responses consistent with response quantities measured at the bridge site, the bridge FE model was subjected to gravity-only loading; foundation bearing pressures were recorded at locations corresponding to the pressure cell array locations at the bridge site. The bridge FE model was also subjected to combined gravity-temperature loading over a range of temperatures bounded by the extreme temperatures derived from AASHTO Procedure B. The maximum pressure that occurs over the full range of combined gravity-temperature load analyses was recorded at each pressure cell location with the bridge FE model. For all pressure cell locations, maximum bearing pressures were developed for the analyses involving extreme superstructure temperatures (i.e., those temperatures determined using the extreme temperature maps from Procedure B).

By subjecting the bridge FE model to gravity-only loading, and extracting the vertical, compressive pressures at the spatial points that correspond to the pressure cell locations in the physical bridge, the cell-specific pressure contribution associated with gravity loading was quantified. By subsequently exposing the bridge FE model to combined gravity-temperature loading, and again extracting the vertical, compressive pressures at the pressure cell locations beneath the instrumented footings of Pier 1 and Pier 3, the effect of combined gravity-temperature loading upon each pressure cell was quantified. Finally, by subtracting the gravitational component of vertical, compressive pressure from the combined gravity-temperature pressure, the portion of the total pressure associated with temperature changes at the superstructure level were calculated.

6.2 Conclusions

The research activities have generated the following conclusions:

- The research team gained understanding of the mechanism by which bearing pressures are affected by temperature changes at the superstructure level for the New Trammel Creek Bridge. Changes in temperature of the superstructure members initiate a tendency for the superstructure to elongate or contract. Due to the monolithic nature of the bridge superstructure (from the pier-top diaphragms), and the bearing restraint present at the bridge extents (from the integral end bents and the diaphragms), the temperature-induced elongation was restrained. Instead, curvature developed throughout the span. In response to the introduced span curvature, the bridge piers rotated. Because of the relative rigidity of the shear-wall reinforced bridge piers, the ensuing pier motions were rigid-body rotation. This rigid-body rotation resulted in increased bearing pressure beneath portions of the underlying footings, and in decreased pressure along the opposite-edged portions of the footings.
- The in-service foundation bearing pressures measured for the New Trammel Creek Bridge indicated that its design is consistent with the recommended safety factor for allowable bearing pressures in the spread footings.
- Using the AASHTO Procedure B and the New Trammel Creek Bridge FE model, the combined gravity-temperature load foundation bearing pressures generated were conservative relative to the range of pressures that constitute the available, physical data record.
- The components of vertical, compressive bearing pressure attributed to temperature changes at the superstructure level can be significant relative to those pressures that were traced to gravity loading. On the study bridge, portions of the footing developed temperature-induced bearing pressures that were equal to or greater than pressures associated with gravity-loading.

6.2.1 Future Research

Future research can leverage and expand upon this study's findings. The following aspects of bridge temperature loading and bridge foundation merit additional investigation:

- The methodology specified by AASHTO Procedure B for determining superstructure load effects was of primary interest in the current study. However, further insights could be gained into foundation response to temperature loading by investigating bridges that have been designed using one of the other two methodologies given in the AASHTO provisions.
- The study findings are specific to integral abutment bridges, which are constructed with relatively high levels of superstructure restraint. Similar instrumentation and analytical tasks could be carried out on bridges containing other superstructure types to facilitate a more general understanding of temperature-induced bridge foundation response.

- The soil modeling included in the current study was site-specific. However, soil-structure interaction plays an important role in determining the distribution of loads to substructures such as individual piers. Therefore, a parametric study of soil strengths and types should be carried out to further examine the importance that soil-structure interaction plays in dictating substructure response to temperature loads.
- Very little research has addressed the issue of how to determine the base construction temperature for reinforced concrete structures. This temperature is critical to establish a datum for bridge response, which can be used to isolate the effect of temperature loads on substructure response.

7 REFERENCES

AASHTO. (2012). *LRFD Bridge Design Specifications 6th Edition*, Washington D.C.

ACI. (1992). State of the Art Report on High-Strength Concrete (ACI Committee 363). Detroit, Michigan: ACI.

ACI. (2011). Building Code Requirements for Structural Concrete and Commentary (ACI 318-11). Farmington Hills, Michigan: ACI.

Allen, J. J., Stokoe, K. H., Bueno, J. L., Kalinski, M. E., & Myers, M. L. (1999). In-Situ Stiffness Measurements of Thick-Life Unbound Aggregate Bases. *International Center for Aggregates Research (ICAR), 7th Annual Symposium Research Papers.*

ANSYS. (2012). *Command Reference*. Release 14.0, Cannonsburg, Pennsylvania.

Arsoy, S., Barker, R. M., Duncan, J.M., & Via, C. E. (1999). The Behavior of Integral Abutment Bridges. Virginia Transportation Research Council. Charlottesville, Virginia.

Barr, P. J., Stanton, J. F. & Eberhard, M. O. (2005). Effects of Temperature Variations on Precast, Prestressed Concrete Bridge Girders. *ASCE JBE*, 10(2), 186-194.

Byerlee, J. (1978). Friction of Rocks. *Pure Appl. Geophysics*, 116, 615-626.

Cobb, F. (2009). *Structural Engineer's Pocket Book, 2nd Edition.* London, UK: Butterworth-Heinemann.

Connal, J. (2004). Integral Abutment Bridges: Australian and U.S. Practice. *Fifth Austroads Bridge Conference, May 2004: Hobart, Tasmania: Bridges Another Dimension: Design, Construction, Procurement, Maintenance*. Hobart, Tasmania; Australia.

Gastineau, A., Johnson, T., & Schultz, A. (2009). Bridge and Health Monitoring and Inspections – A Survey of Methods. *Minnesota Department of Transportation, MN/RC 2009-29.*

Hawkins, A. B. (1986). Rock Descriptions, Site Investigation Practice: Assessing BS 5930. London, UK: Geological Society.

Hopkins, T. C., Beckham, T. L., & Sun, C. (2007). Resilient Modulus of Compacted Crushed Stone Aggregate Bases. *Kentucky Transportation Center Research Report KTC-05-27/SPR-229-01-1F*. University of Kentucky, Lexington, Kentucky.

Kappayil, S. & Reed, D. (1996). Microzonation for Temperature and Wind for the State of Washington. *Washington State Department of Transportation WA-RD 402.1*. Seattle, Washington.

Kentucky Transportation Cabinet (KyTC). (2005). *Geotechnical Guidance Manual.* Frankfort, Kentucky.

Kim, W. & Laman, J. A. (2010). Integral Abutment Bridge Response Under Thermal Loading. *Engineering Structures*, 32, 1495-1508.

Klieger, P. (1958). Effect of Mixing and Curing Temperature on Concrete Strength. *American Concrete Institute (ACI) Journal Proceedings*, 54, (6), 1063-1081.

Kuiper, J., Van Ryen, W. M., & Koefoed, O. (1959). Laboratory Determinations of Elastic Properties of Some Limestones. *Geophysical Prospecting*, 7, (1), 38-44.

NCHRP. (2004). Guide for Mechanistic-Empirical Design of new and Rehabilitated Pavement Structures-Part 4. Low Volume Roads. NCHRP, Washington D.C.

Paul, M., Laman, J. A., & Linzell, D. G. (2005). Thermally Induced Superstructure Stresses in Prestressed Girder Integral Abutment Bridges. *Transportation Research Record: Journal of the Transportation Research Board, CD 11-S*, 287-297.

Podolny, W., Jr., & Muller, J. M. (1982). *Construction and design of prestressed concrete segmental bridges*. New York: Wiley.

Precast/Prestress Concrete Institute (PCI). (2010). *PCI Design Handbook: Precast and Prestressed Concrete, 7th Edition.* Chicago, Illinois: PCI.

Rodriguez, L. E. (2012). *Temperature Effects on Integral Abumtnet Bridges for the Long-Term Bridge Performance Program*. (Master's Thesis, Paper 1221). Utah State University, Logan, Utah.

Roeder, C. W. (2002). Thermal Movement Design Procedure for Steel and Concrete Bridges. *NCHRP 20-07/106*. Washington, D.C.

Roeder, C. W. (2003). Proposed Design Method for Thermal Bridge Movements. *ASCE JBE*, 8, (1), 12-19.

Schultz, A. E., Scheevel, C. J., & Morris, M. K. (2011). Evaluation of AASHTO-LRFD Design Methods for Thermal Loads in Fixed-Flexible Twin-Walled R/C Bridge Piers. *ASCE JBE*, 16, 890-899.

Takayama, T. (1992). Estimation of Sliding Failure Probability of Present Breakwaters for Probabilistic Design. *Report of Port and Harbour Research Institute*, 31, (5).

Theyse, H. L. (2002). Stiffness, Strength, and Performance of Unbound Aggregate Material: Application of South African HVS and Laboratory Results to California Flexible Pavements. University of California-Davis, Pavement Research Center, Davis, California.

Turner, J. (2006). Rock-Socketed Shafts for Highway Structure Foundations. *NCHRP Synthesis 360*. Washington, D.C.

APPENDIX A: PRESSURE CELL READINGS

Presented in the following are the readings for those pressure cells installed beneath the selected footings of Pier 1 and Pier 3. Specifically, seven pressure cells were installed beneath the southernmost footing of Pier 1 and seven pressure cells were installed beneath the northernmost footing of Pier 3. Data are presented for each cell in 5-minute intervals starting on May 11, 2011. Note that data are not available for pressure cell 7 beneath the Pier 1 footing, nor are data available for the pressure cell 5 beneath the Pier 3 footing. Also, note that the pressure cell readings for pressure cell 1 beneath the Pier 1 footing are given in Chapter 3.

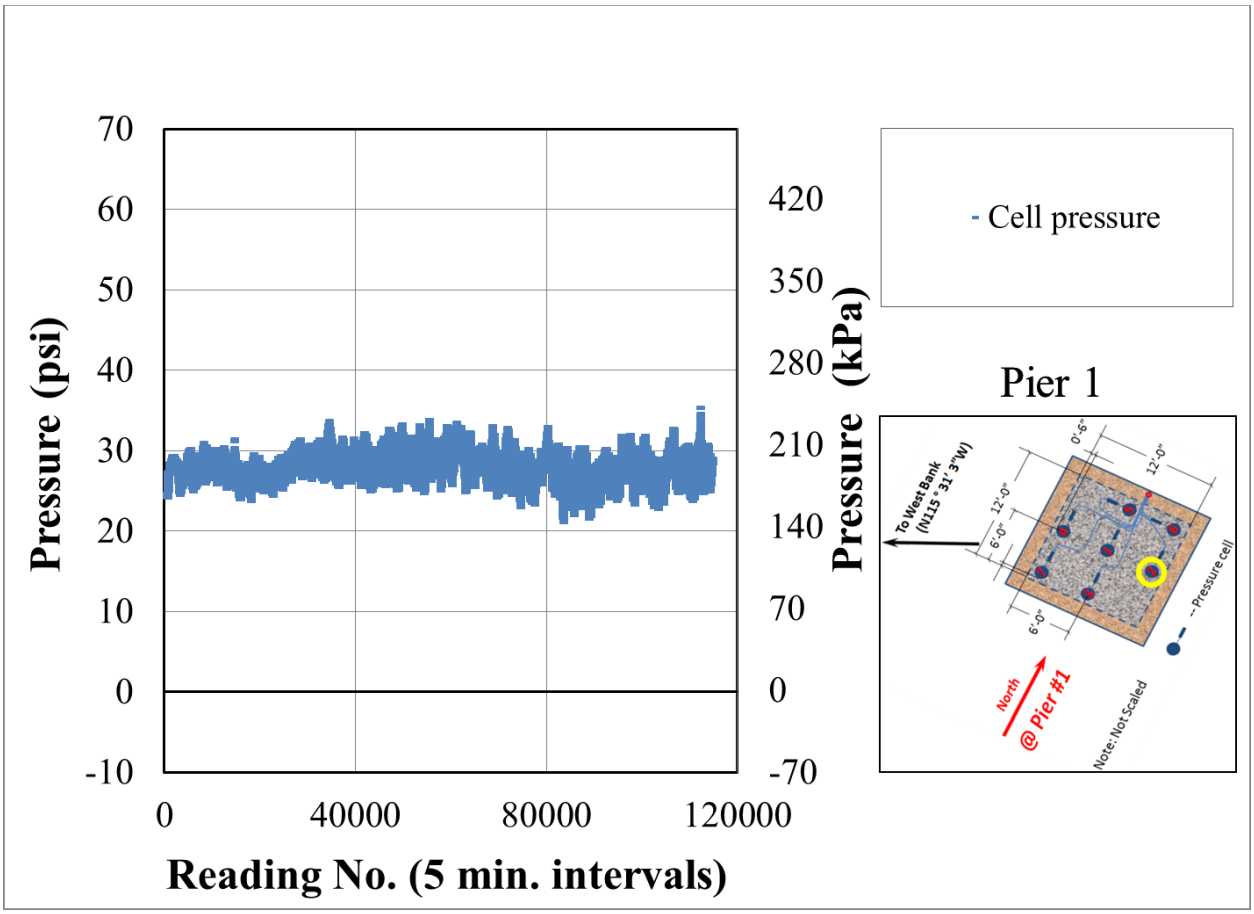

Fig. A.1: Time-history of foundation pressures at Cell 2 of Pier 1 (note: reading No. 0 corresponds to May 11, 2011).

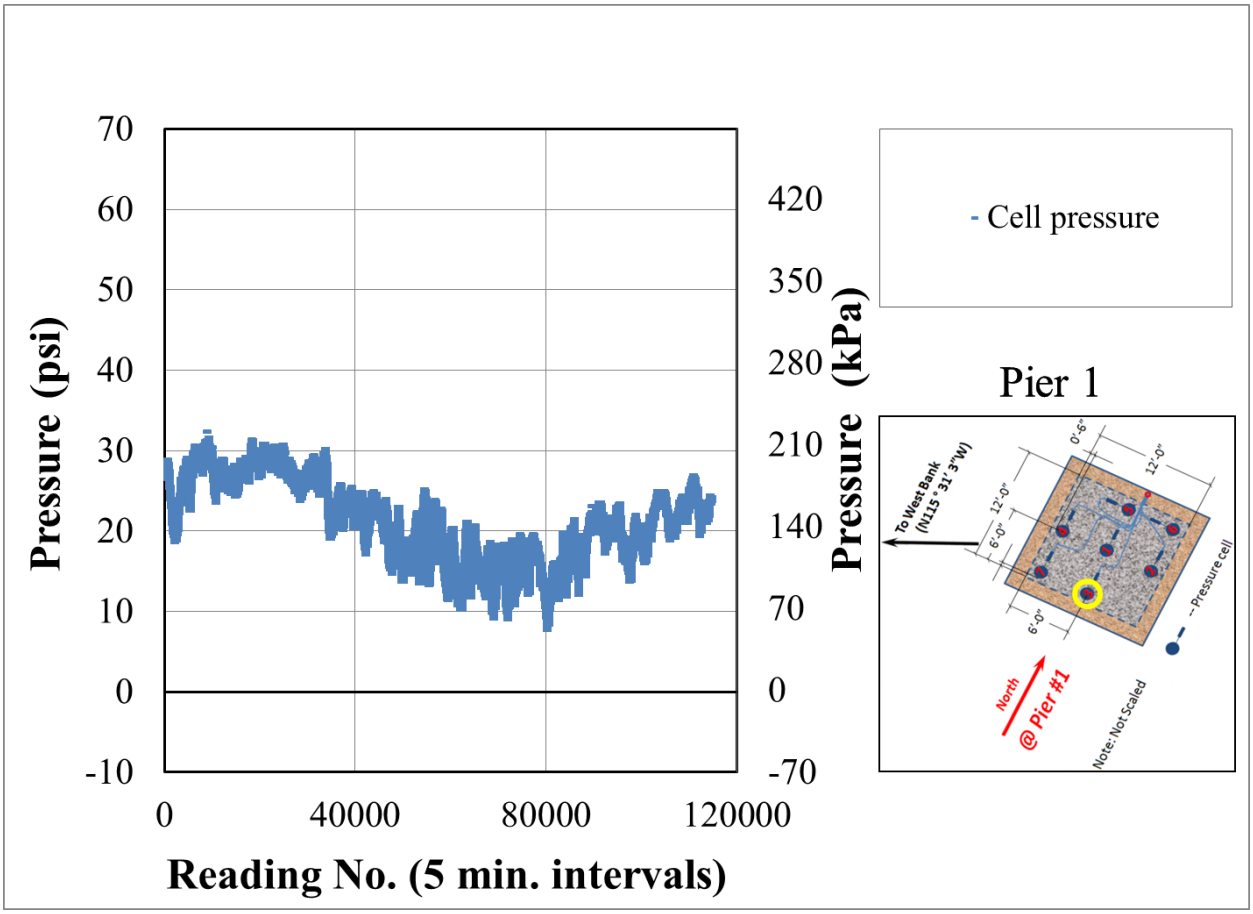

Fig. A.2: Time-history of foundation pressures at Cell 3 of Pier 1 (note: reading No. 0 corresponds to May 11, 2011).

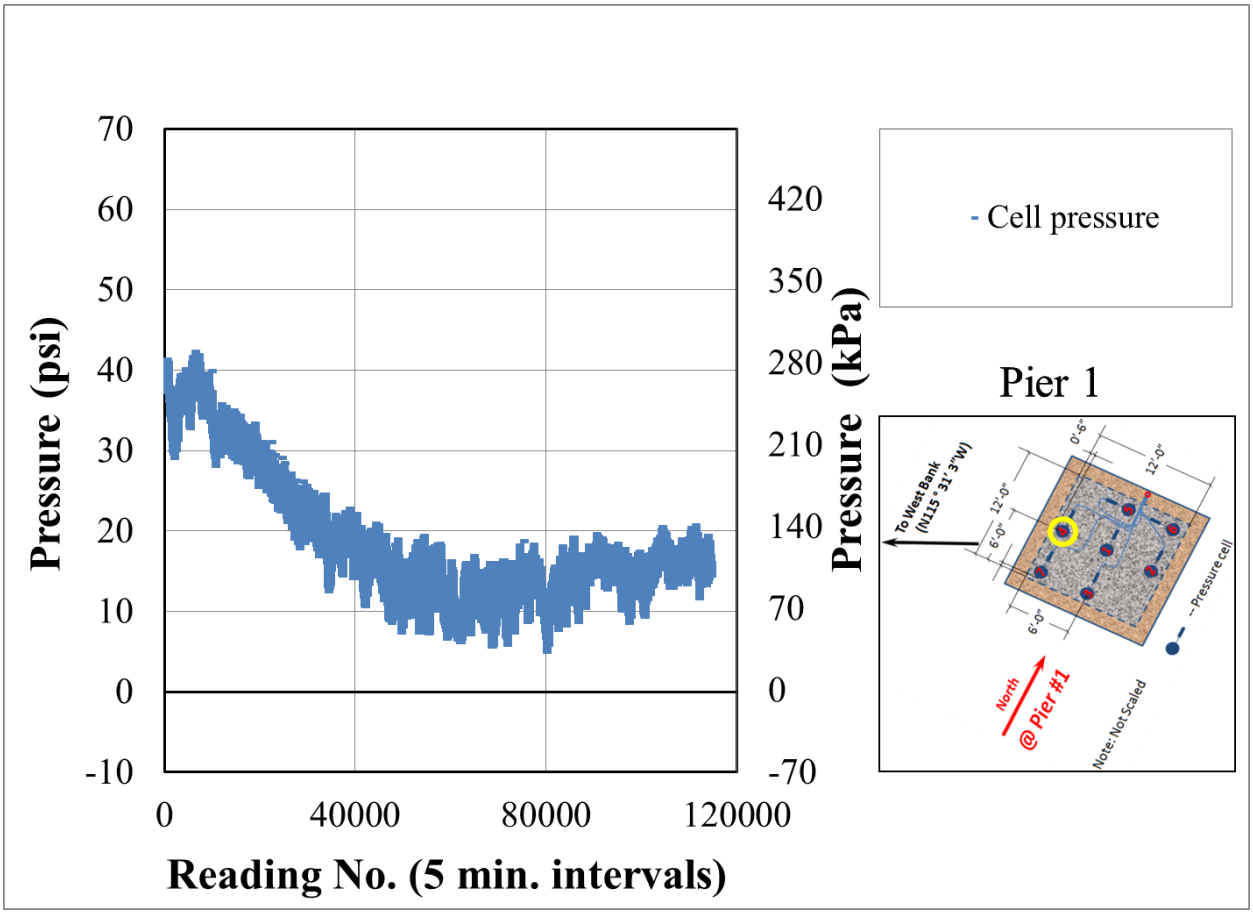

Fig. A.3: Time-history of foundation pressures at Cell 4 of Pier 1 (note: reading No. 0 corresponds to May 11, 2011).

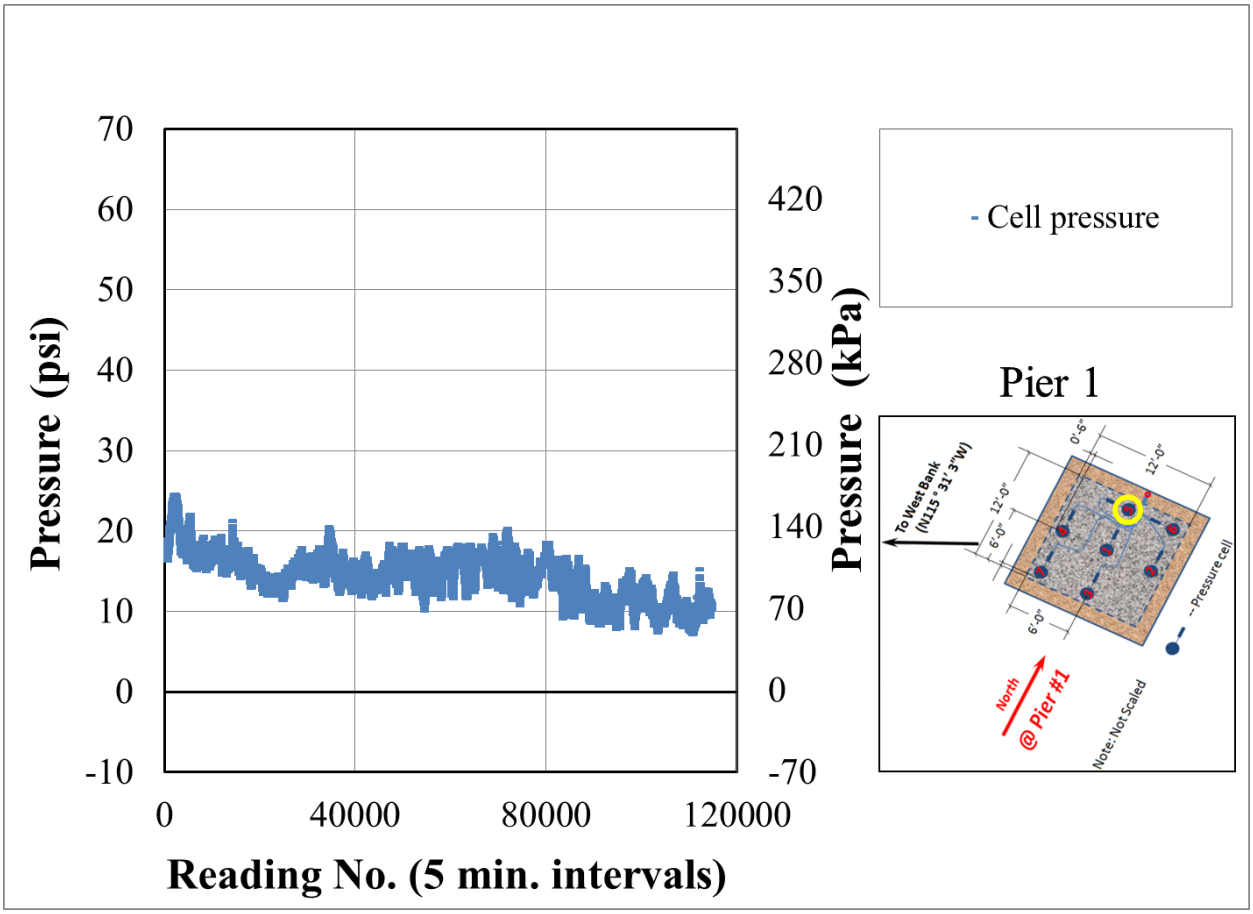

Fig. A.4: Time-history of foundation pressures at Cell 5 of Pier 1 (note: reading No. 0 corresponds to May 11, 2011).

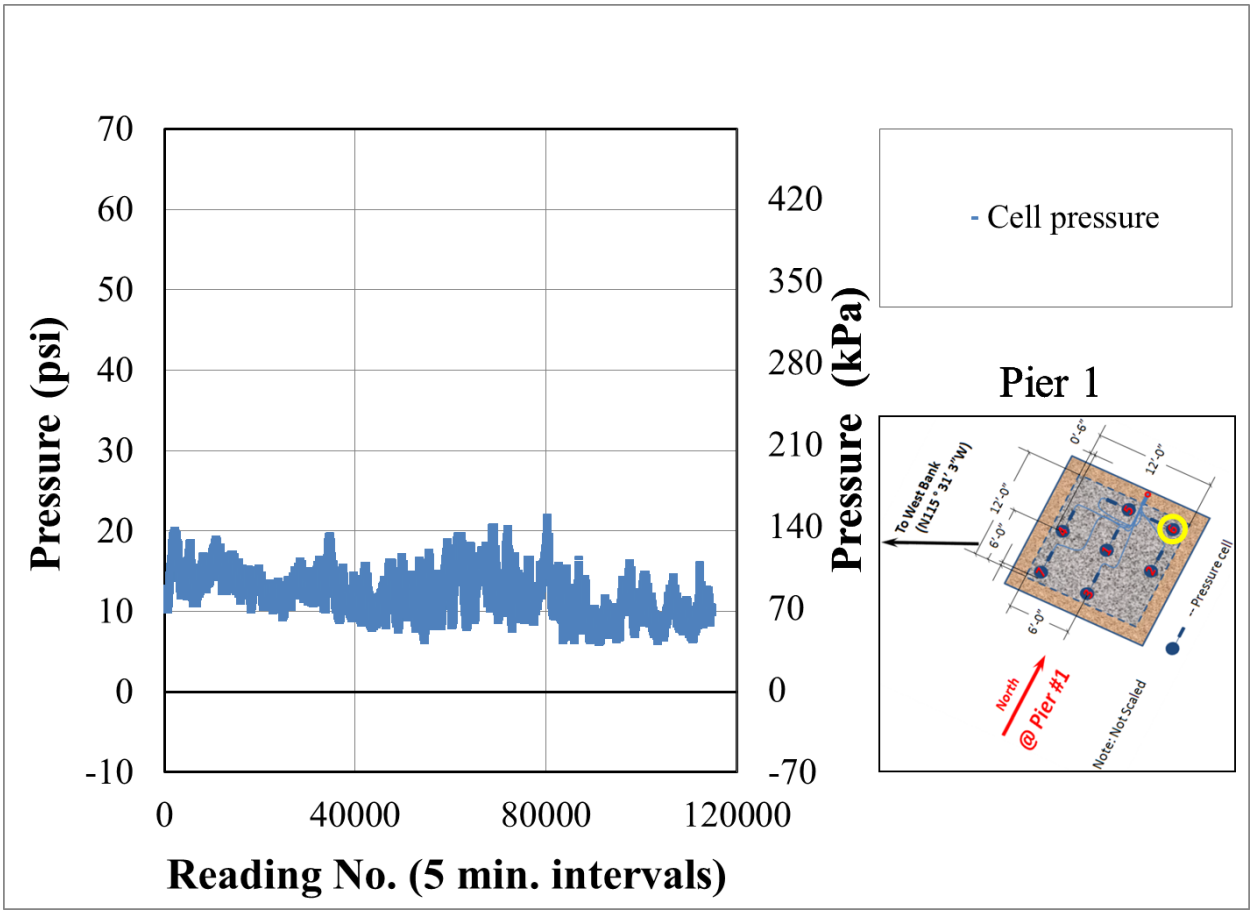

Fig. A.5: Time-history of foundation pressures at Cell 6 of Pier 1 (note: reading No. 0 corresponds to May 11, 2011).

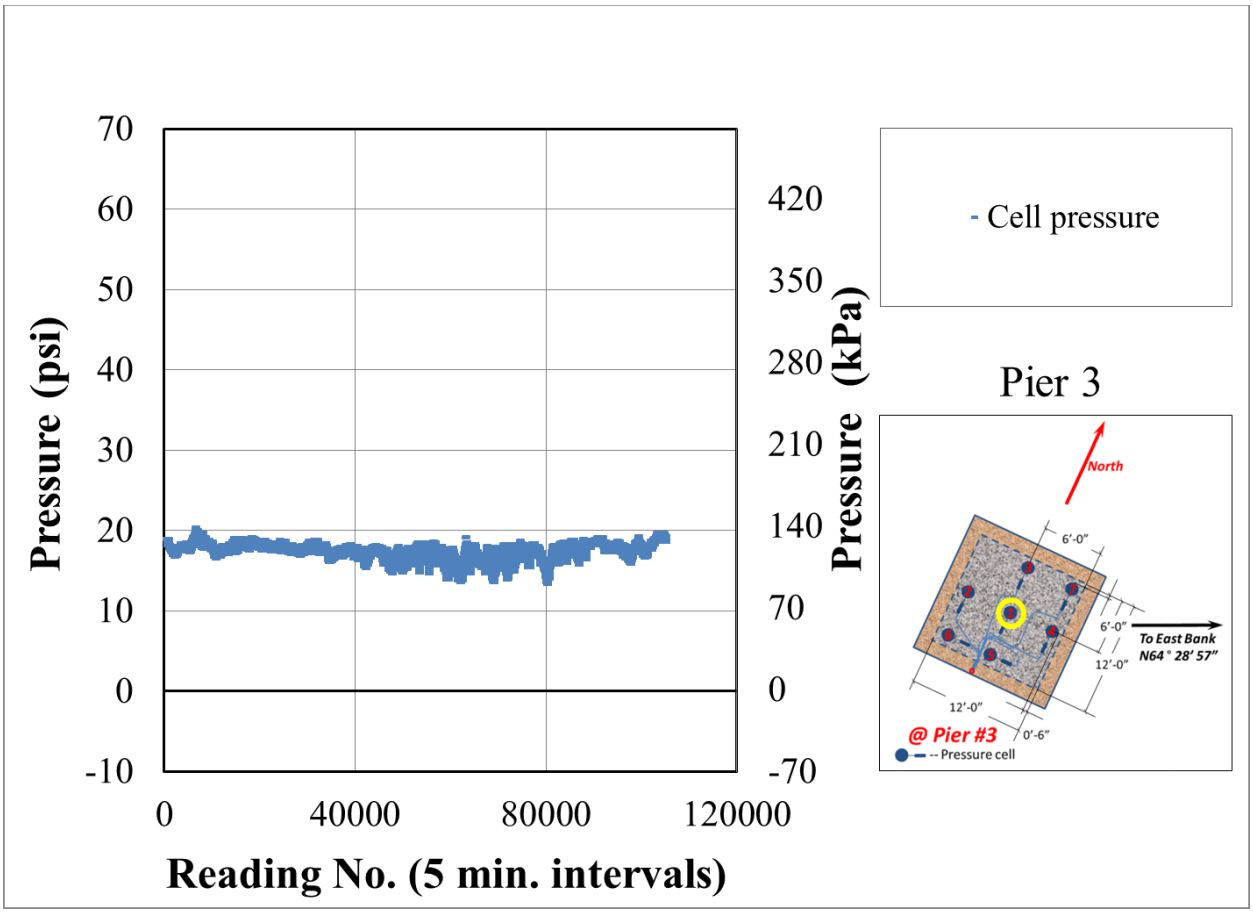

Fig. A.6: Time-history of foundation pressures at Cell 1 of Pier 3 (note: reading No. 0 corresponds to May 11, 2011).

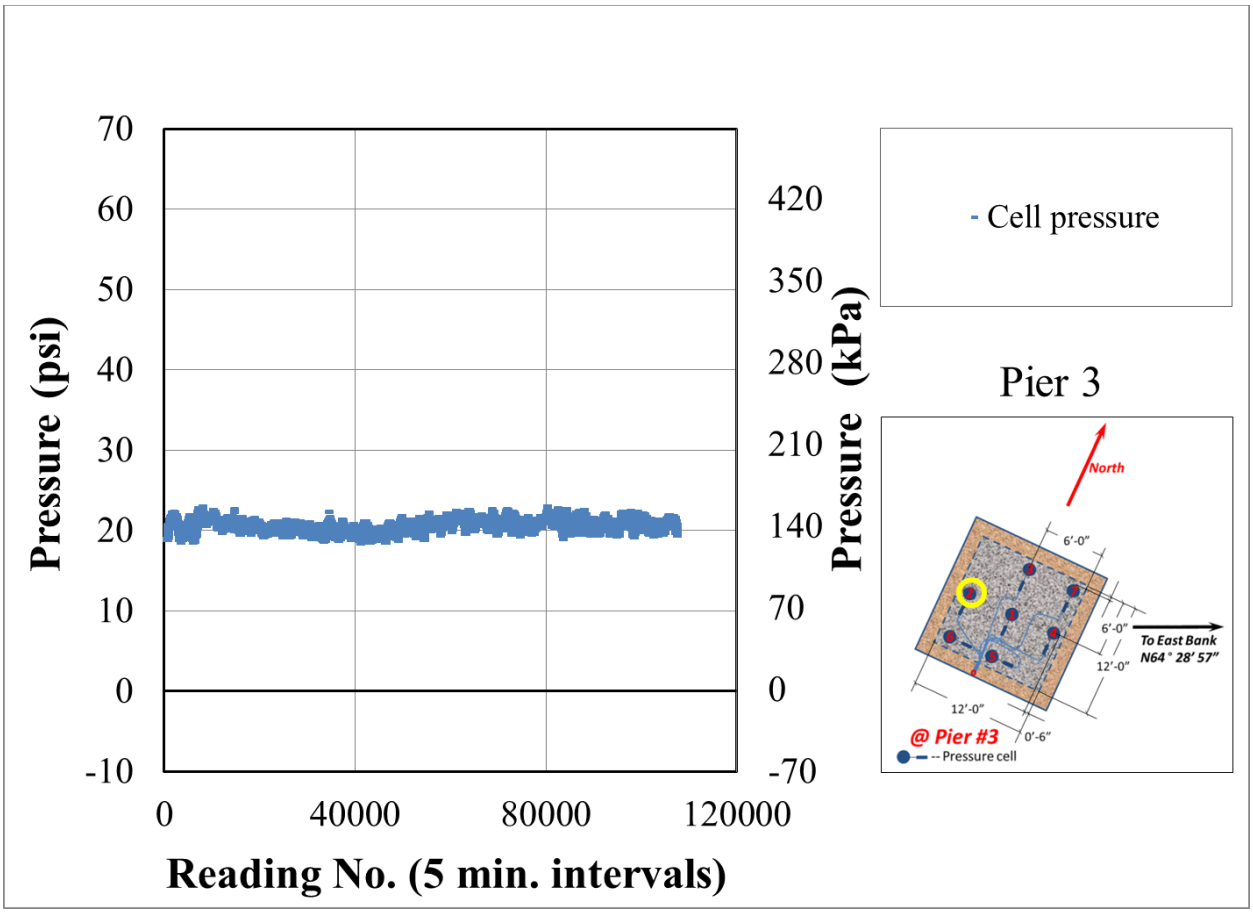

Fig. A.7: Time-history of foundation pressures at Cell 2 of Pier 3 (note: reading No. 0 corresponds to May 11, 2011).

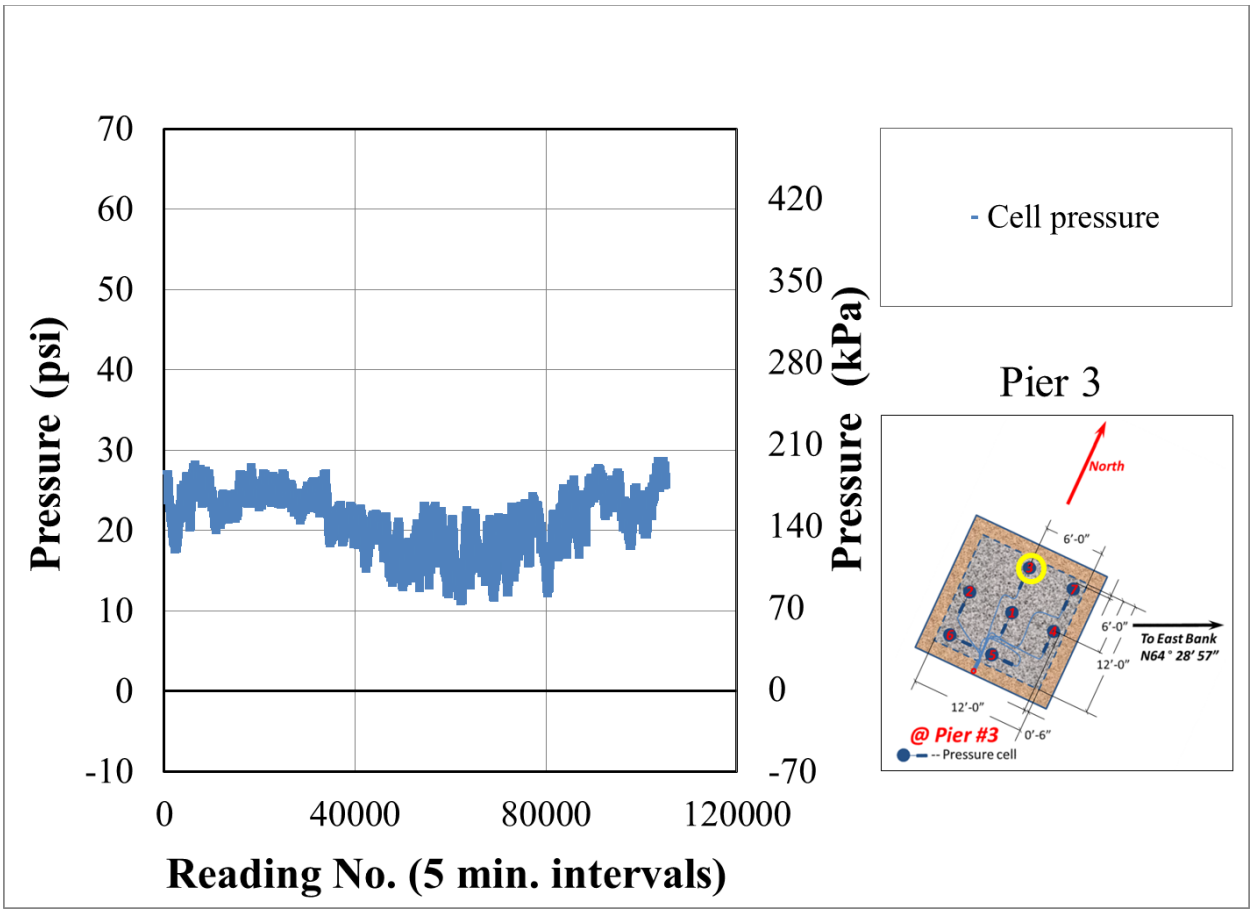

Fig. A.8: Time-history of foundation pressures at Cell 3 of Pier 3 (note: reading No. 0 corresponds to May 11, 2011).

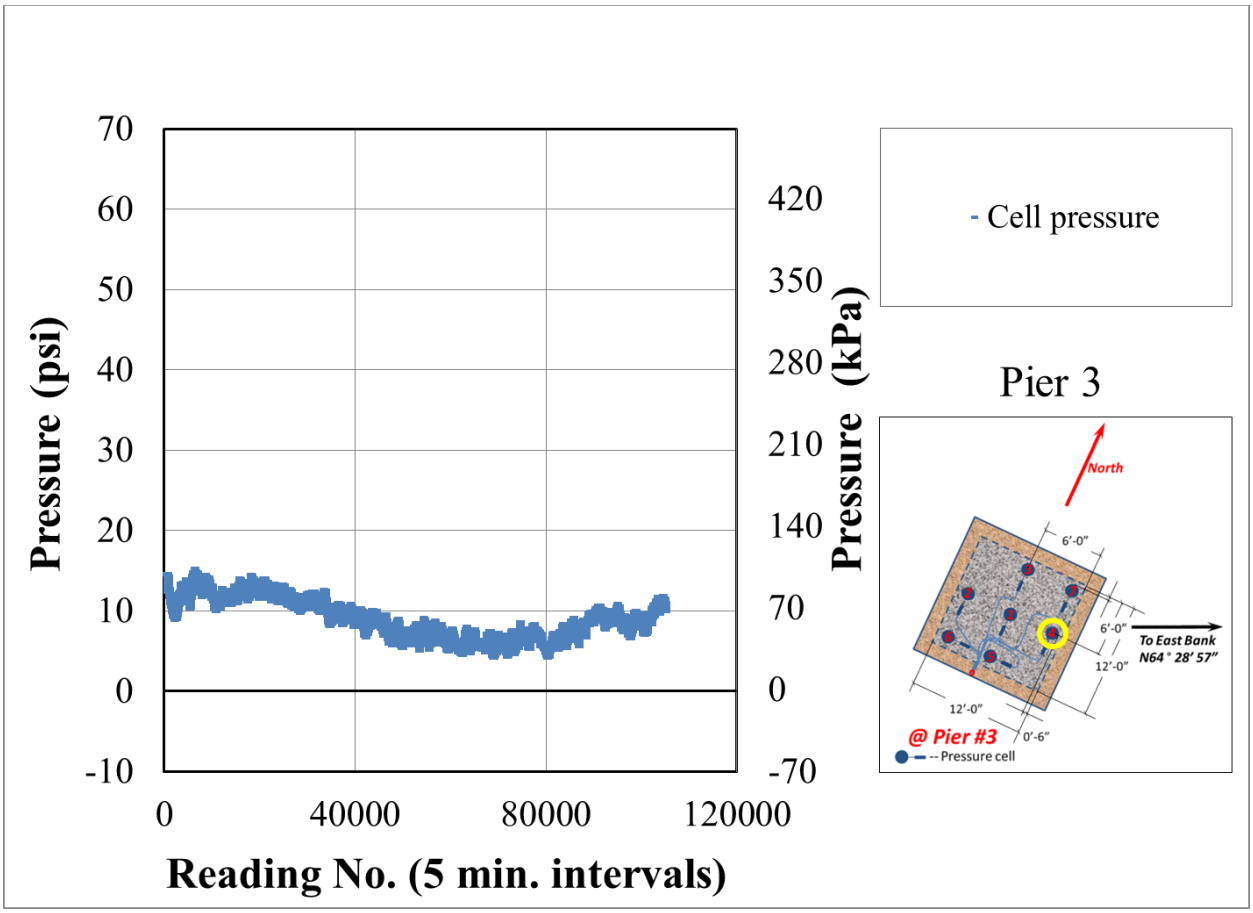

Fig. A.9: Time-history of foundation pressures at Cell 4 of Pier 3 (note: reading No. 0 corresponds to May 11, 2011).

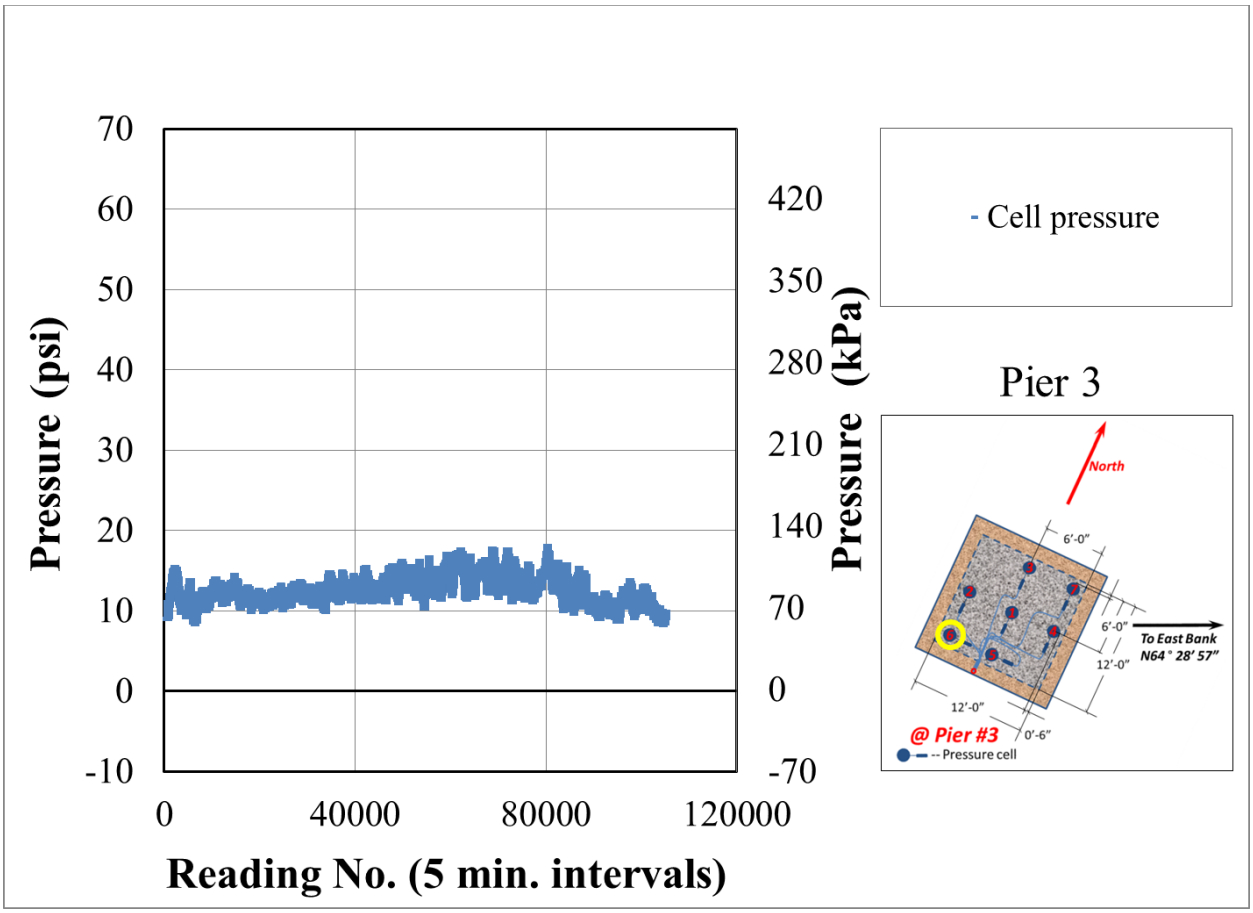

Fig. A.10: Time-history of foundation pressures at Cell 6 of Pier 3 (note: reading No. 0 corresponds to May 11, 2011).

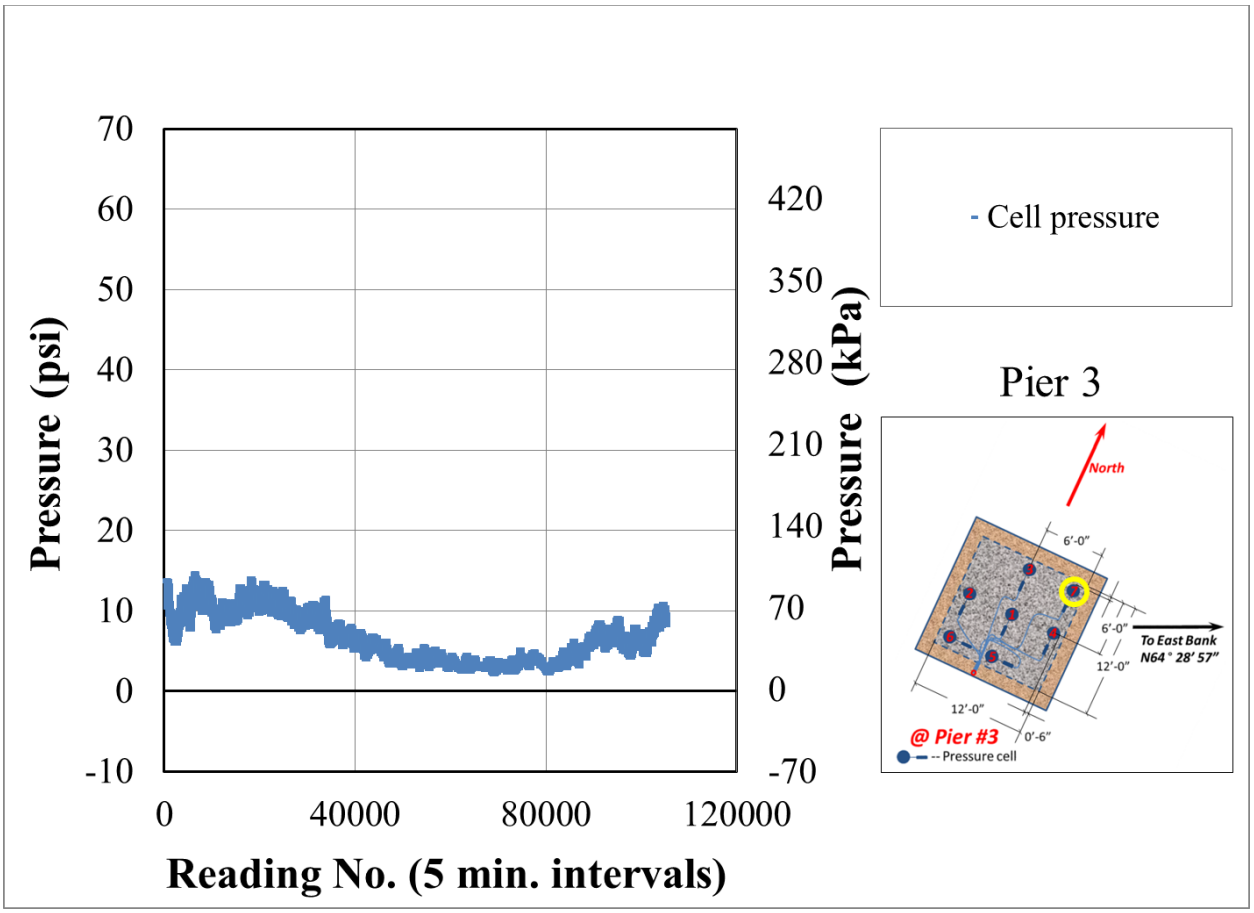

Fig. A.11: Time-history of foundation pressures at Cell 7 of Pier 3 (note: reading No. 0 corresponds to May 11, 2011).

APPENDIX B: LAYOUT OF BRIDGE MONITORING WEB-SITE

Presented in the following are the layout guidelines for the bridge monitoring website dedicated to monitoring of ambient temperatures, pier rotation, and substructure foundation response for the New Trammel Creek Bridge in Allen Co., Kentucky. The layout guidelines are ordered by link-depth, where the homepage of the website is presented first, and webpages that emanate therefrom are subsequently presented. Note that preliminary data are supplied for the plots in Appendix B, where the current data are presented in the main body of the current report, and the most recent data presentation layout for the bridge monitoring website can be accessed at: http://www.ktc.uky.edu/kytc/RemoteBridgeMonitoringInKY/.

Screen 1. Site map of monitored bridges

Effect of Thermal Loads on Substructure of New Trammel Creek Bridge: Allen Co., Kentucky

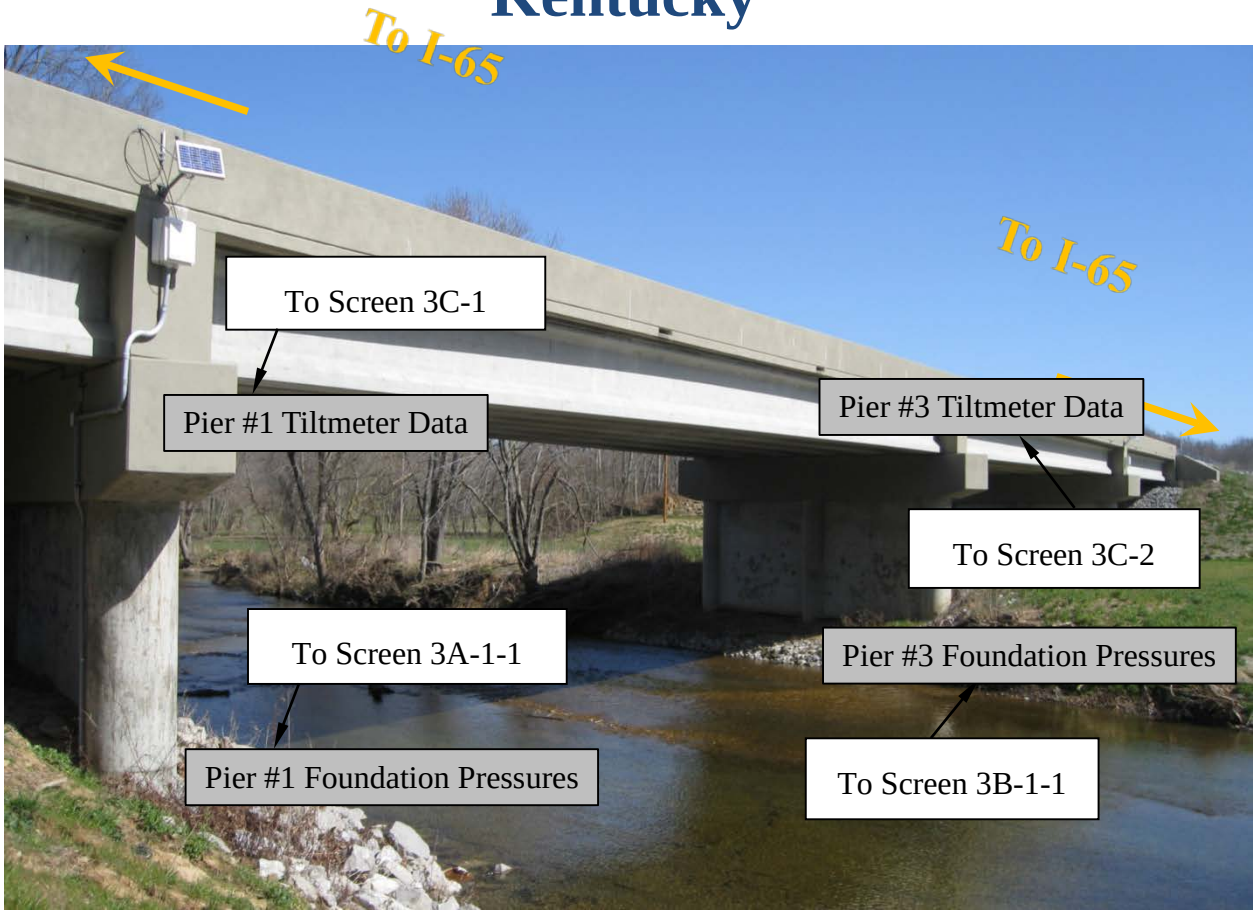

Trammel Creek Bridge in Allen Co. Kentucky

Screen 2. Introduction [continued on next page]

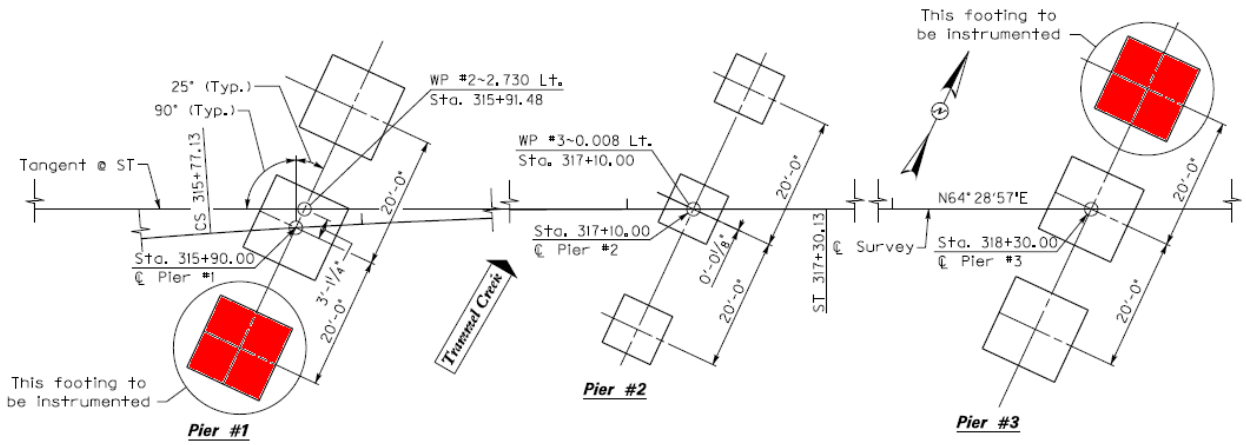

Introduction

The design of footings for short bridge piers is primarily controlled by the AASHTO thermal loads requirements. Accurate estimates of the thermal loads on footings is essential for proper design and can be achieved by instrumenting footings in new bridges, monitoring the soil pressure on the footing under different ambient conditions for a period of three or more years, and by comparing the actual soil pressure with ones estimated by the AASHTO code equations.

To Screen 3D

Screen 2. Introduction

Click on any cell in the figure below to view data for that cell.

Specify Date Range: _____ to _____

Note that data are available from May 11, 2011.

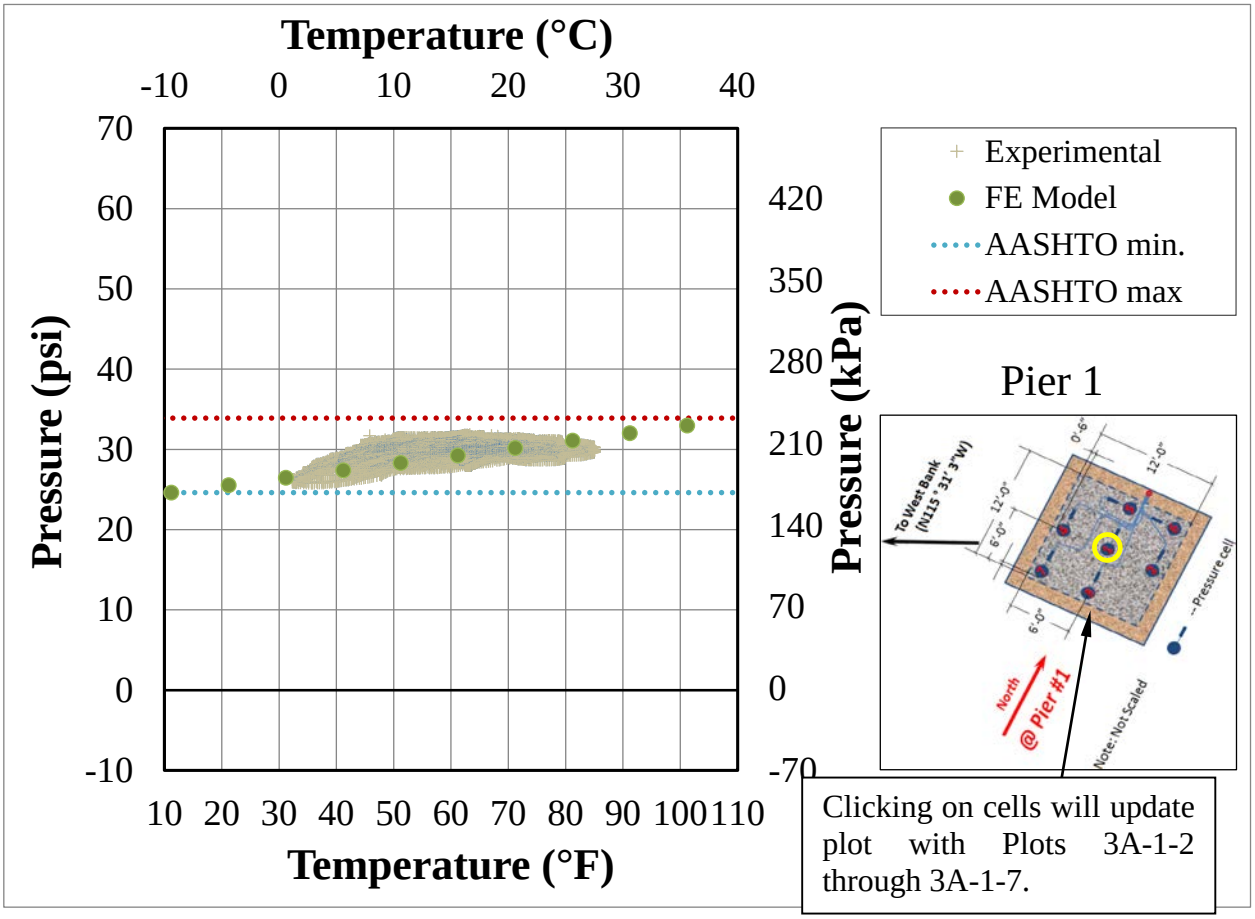

	Magnitude	Date Range	Sensor
Min. Temp °F			
Max. Temp °F			
Min. Pressure (psi)			
Max. Pressure (psi)			

Pier 1 Summary Plot → To Screen 3A-1-8

Tiltmeter Data Plots → To Screen 3C-1

Pier 3 Data Plots → To Screen 3B-1-1

Project Background → To Screen 3D

Screen 3A-1-1. Pressure cell 1 of Pier 1

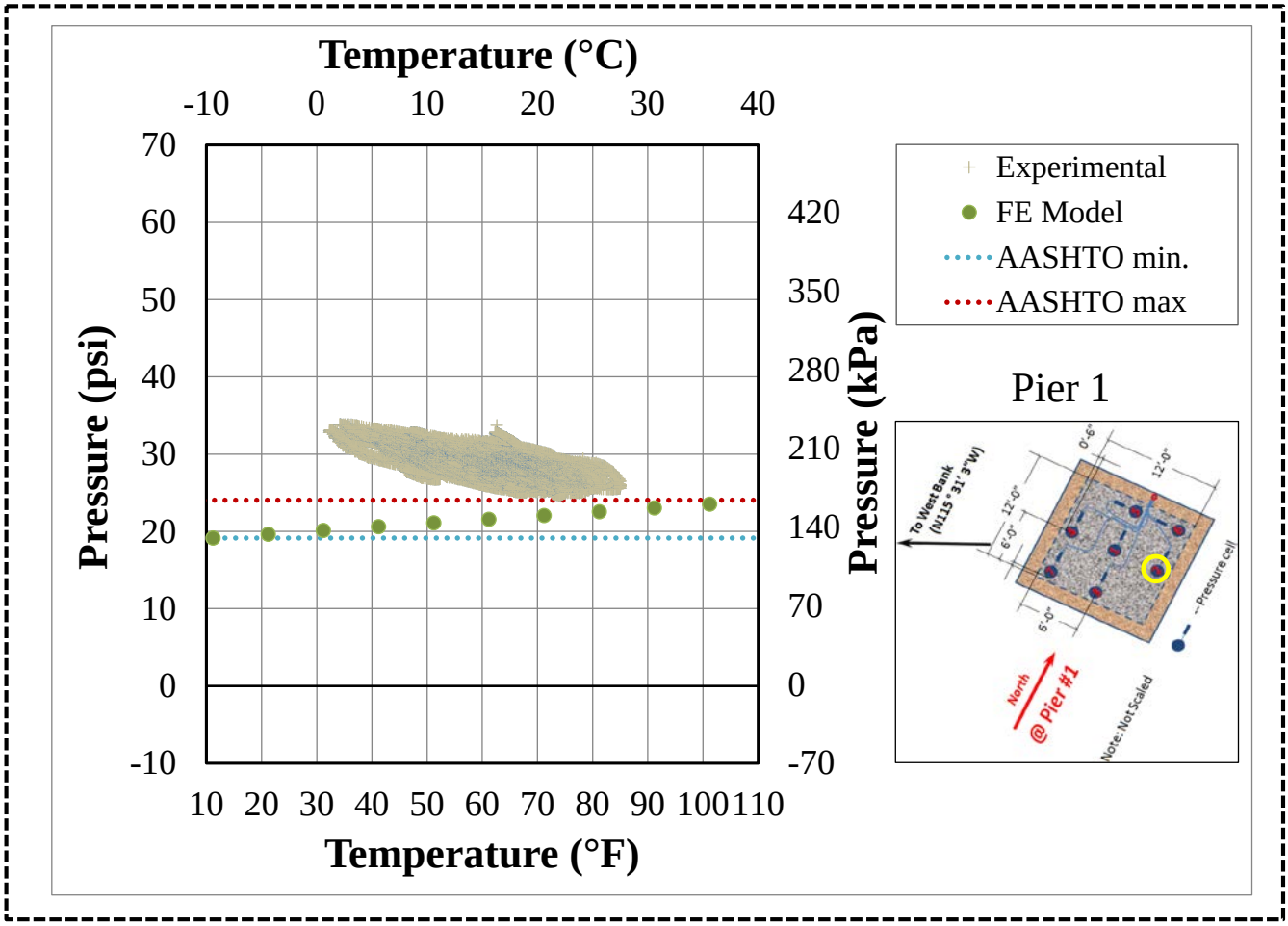

Plot 3A-1-2. Pressure cell 2 of Pier 1

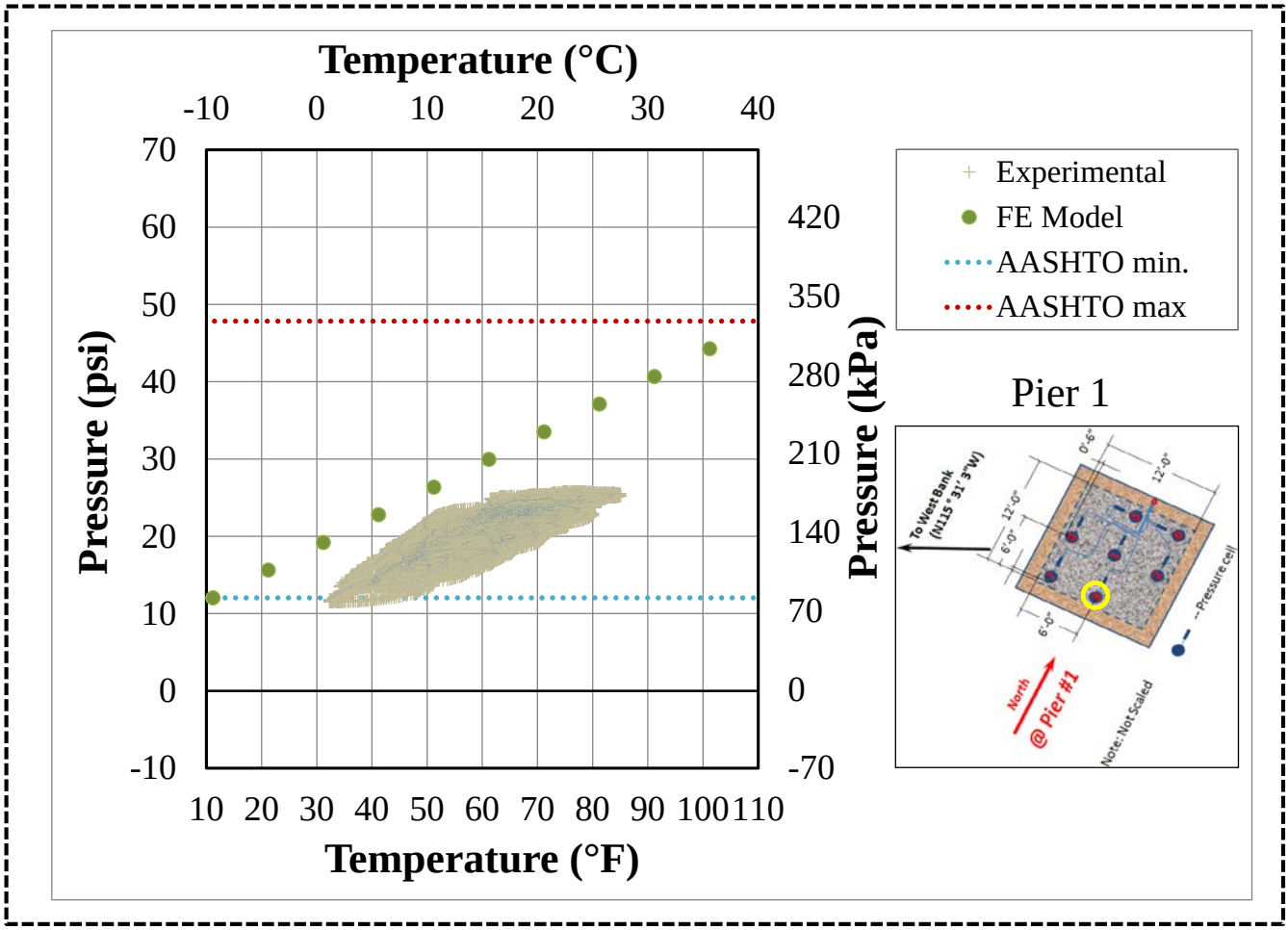

Plot 3A-1-3. Pressure cell 3 of Pier 1

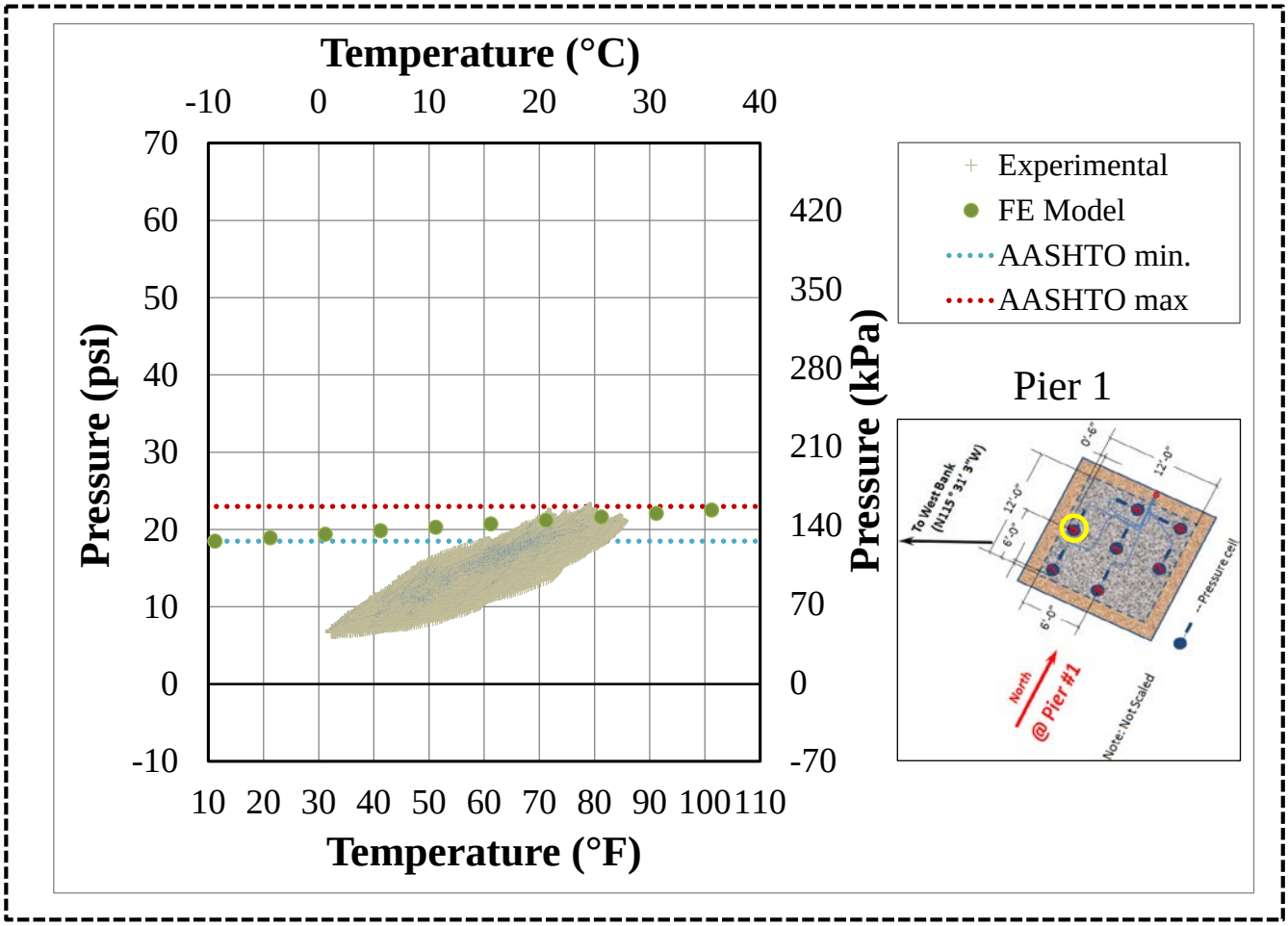

Plot 3A-1-4. Pressure cell 4 of Pier 1

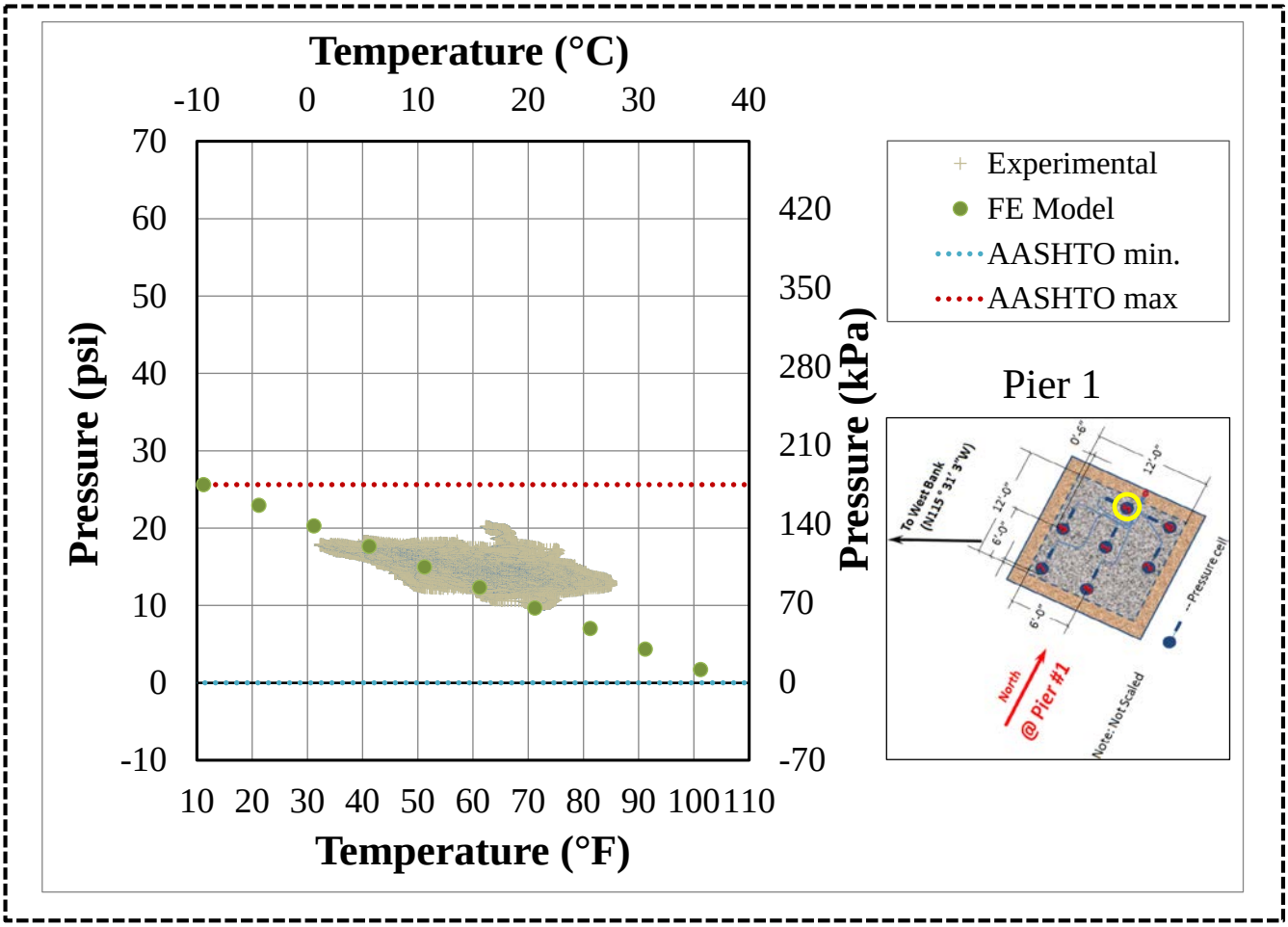

Plot 3A-1-5. Pressure cell 5 of Pier 1

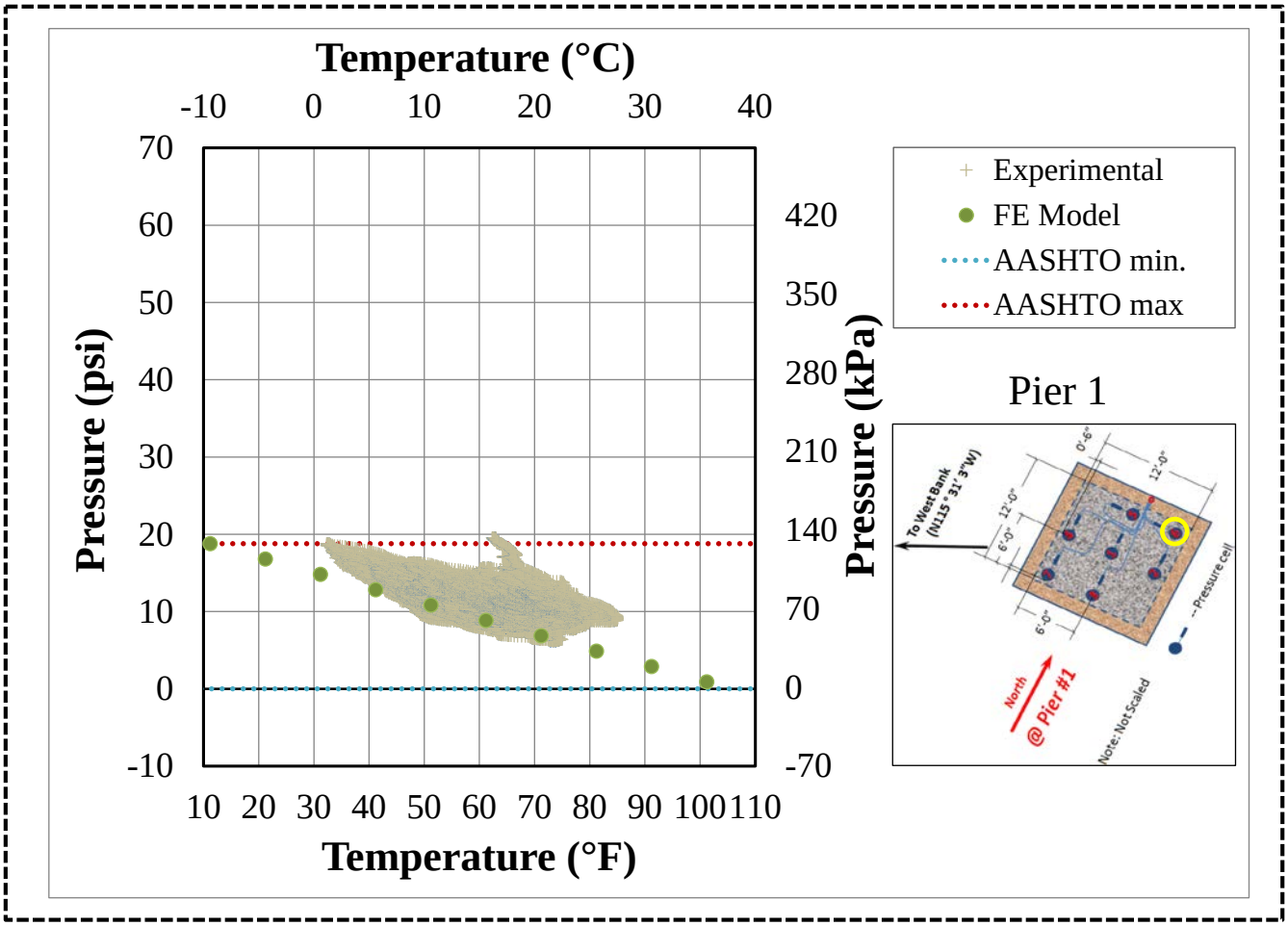

Plot 3A-1-6. Pressure cell 6 of Pier 1

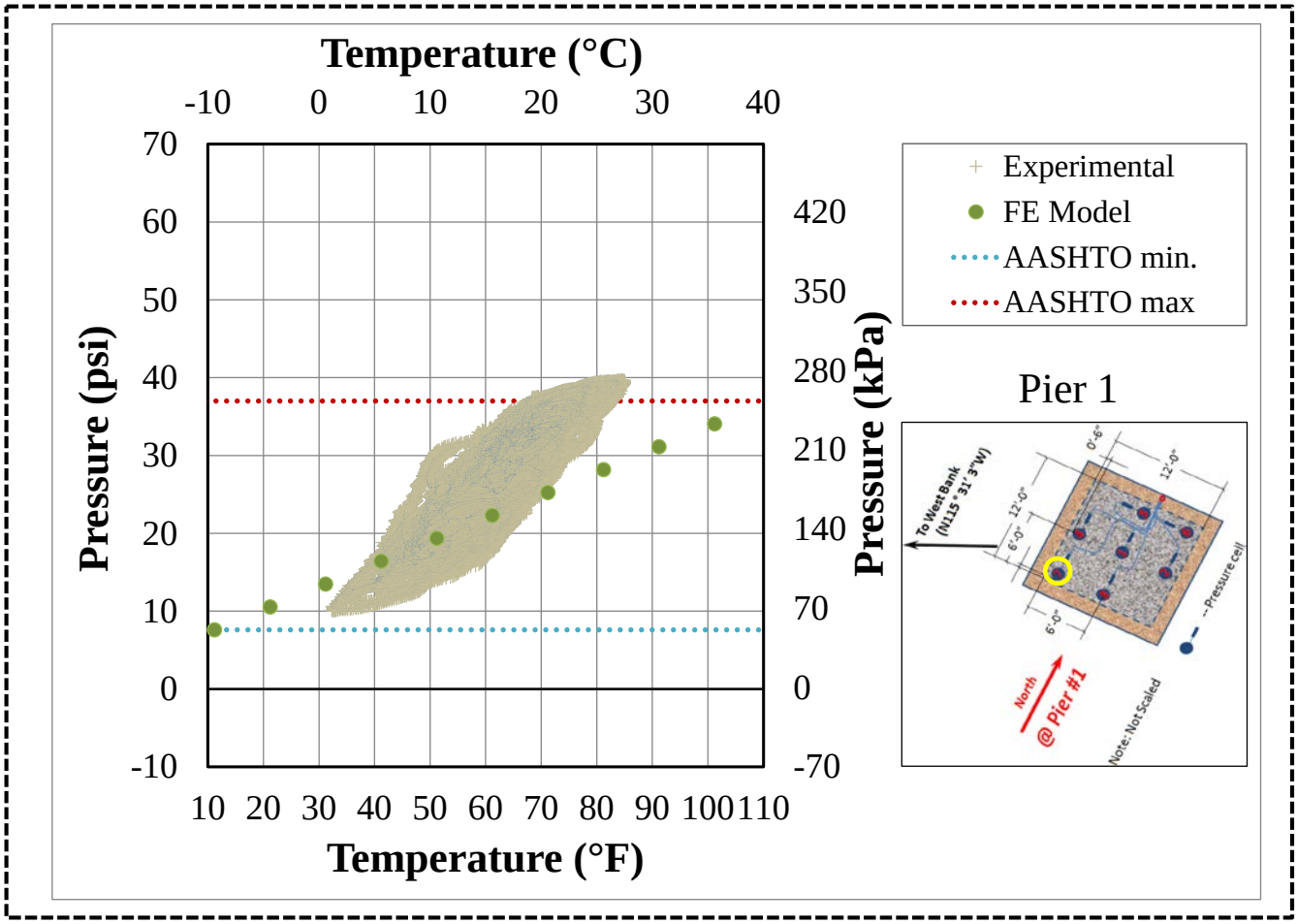

Plot 3A-1-7. Pressure cell 7 of Pier 1

Specify Date Range: _____ to _____

Note that data are available from May 11, 2011.

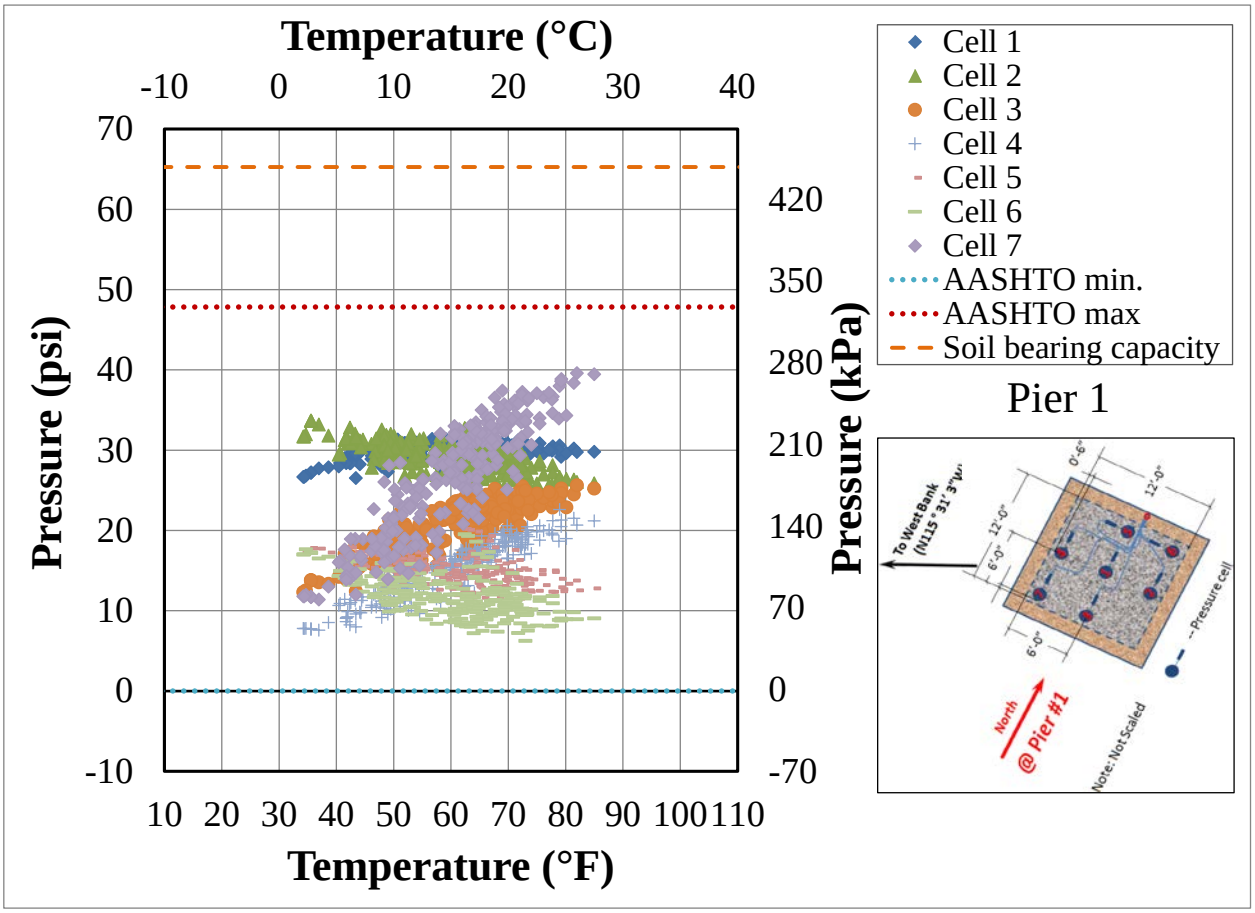

	Magnitude	Date Range	Sensor
Min. Temp °F			
Max. Temp °F			
Min. Pressure (psi)			
Max. Pressure (psi)			

Individual Cell Plots → To Screen 3A-1-8

Tiltmeter Data Plots → To Screen 3C-1

Pier 3 Data Plots → To Screen 3B-1-1

Project Background → To Screen 3D

Screen 3A-1-8. Summary for Pier 1 [continued on next page]

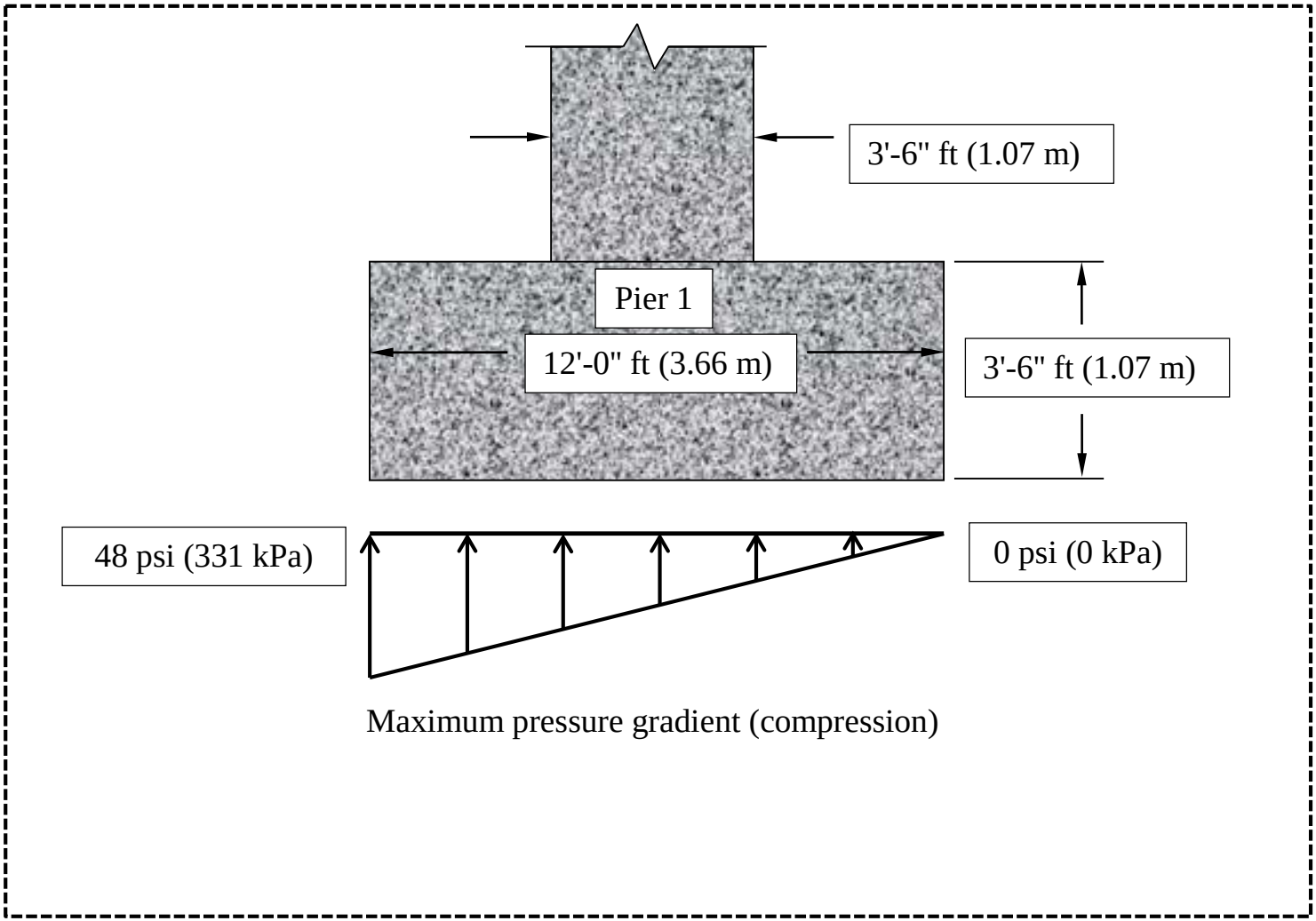

Screen 3A-1-8. Summary for Pier 1

Click on any cell in the figure below to view data for that cell.

Specify Date Range: _____ to _____

Note that data are available from May 11, 2011.

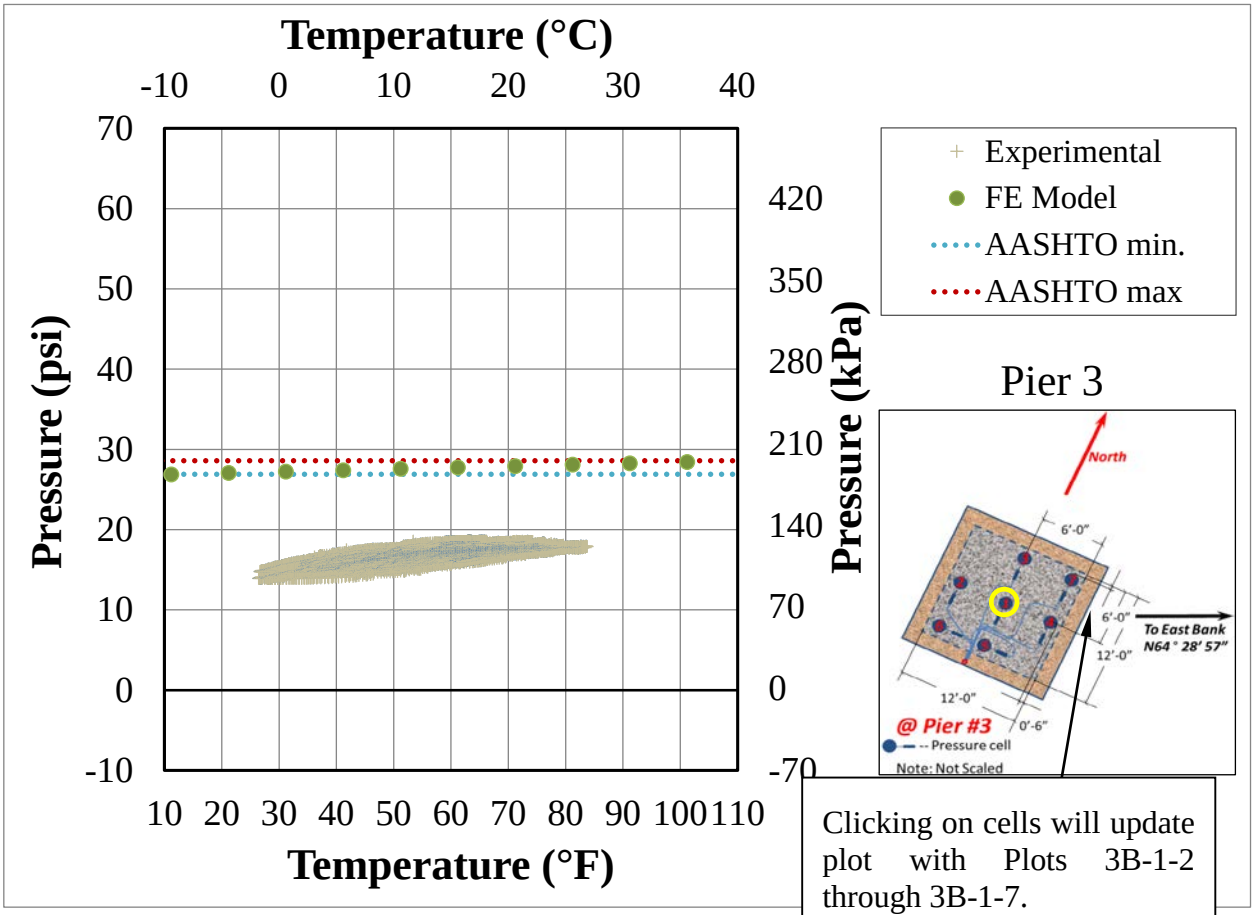

	Magnitude	Date Range	Sensor
Min. Temp °F			
Max. Temp °F			
Min. Pressure (psi)			
Max. Pressure (psi)			

Pier 3 Summary Plot

To Screen 3B-1-8

To Screen 3A-1-1

Tiltmeter Data Plots

To Screen 3C-2

To Screen 3D

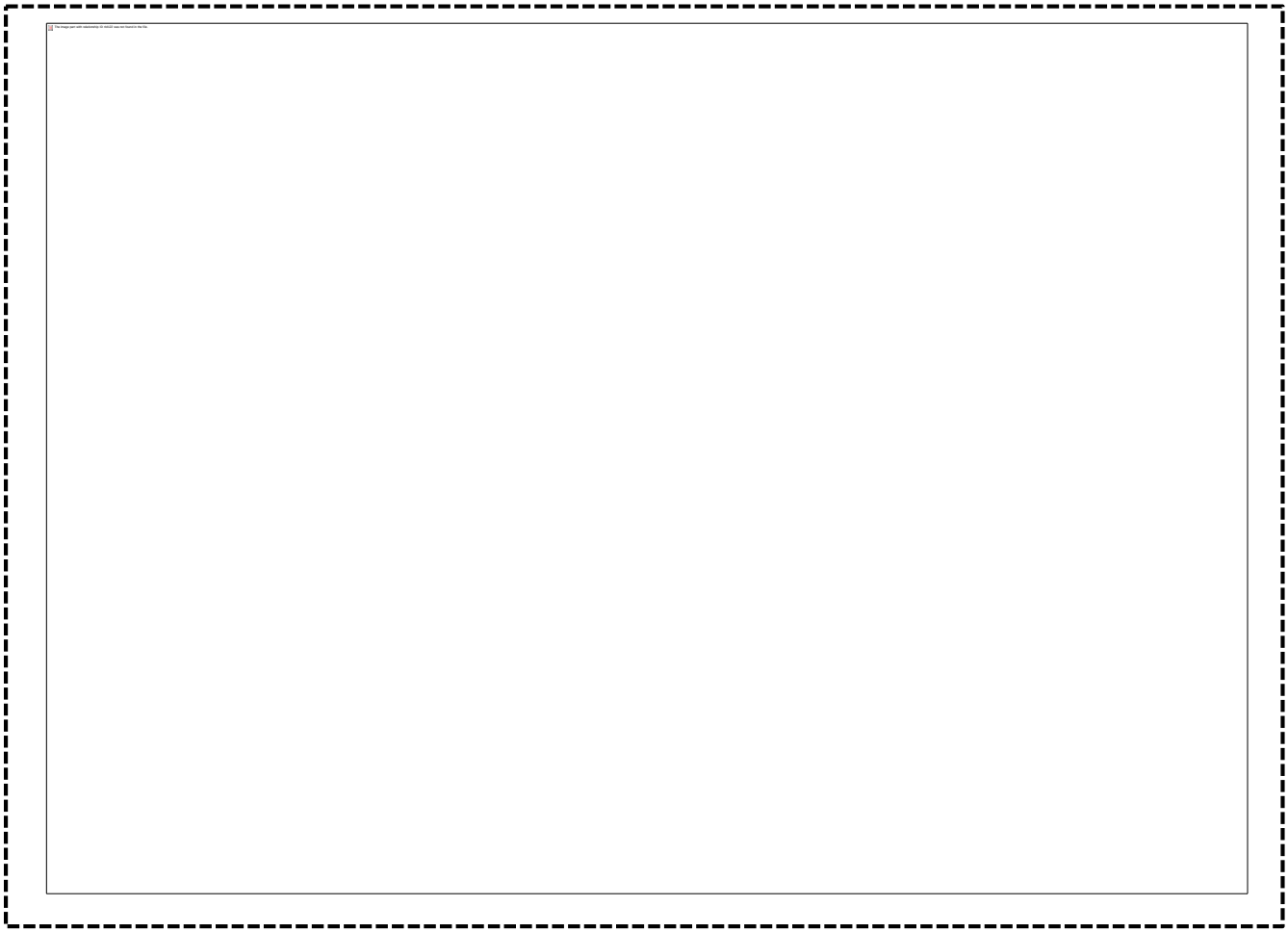

Plot 3B-1-2. Pressure cell 2 of Pier 3

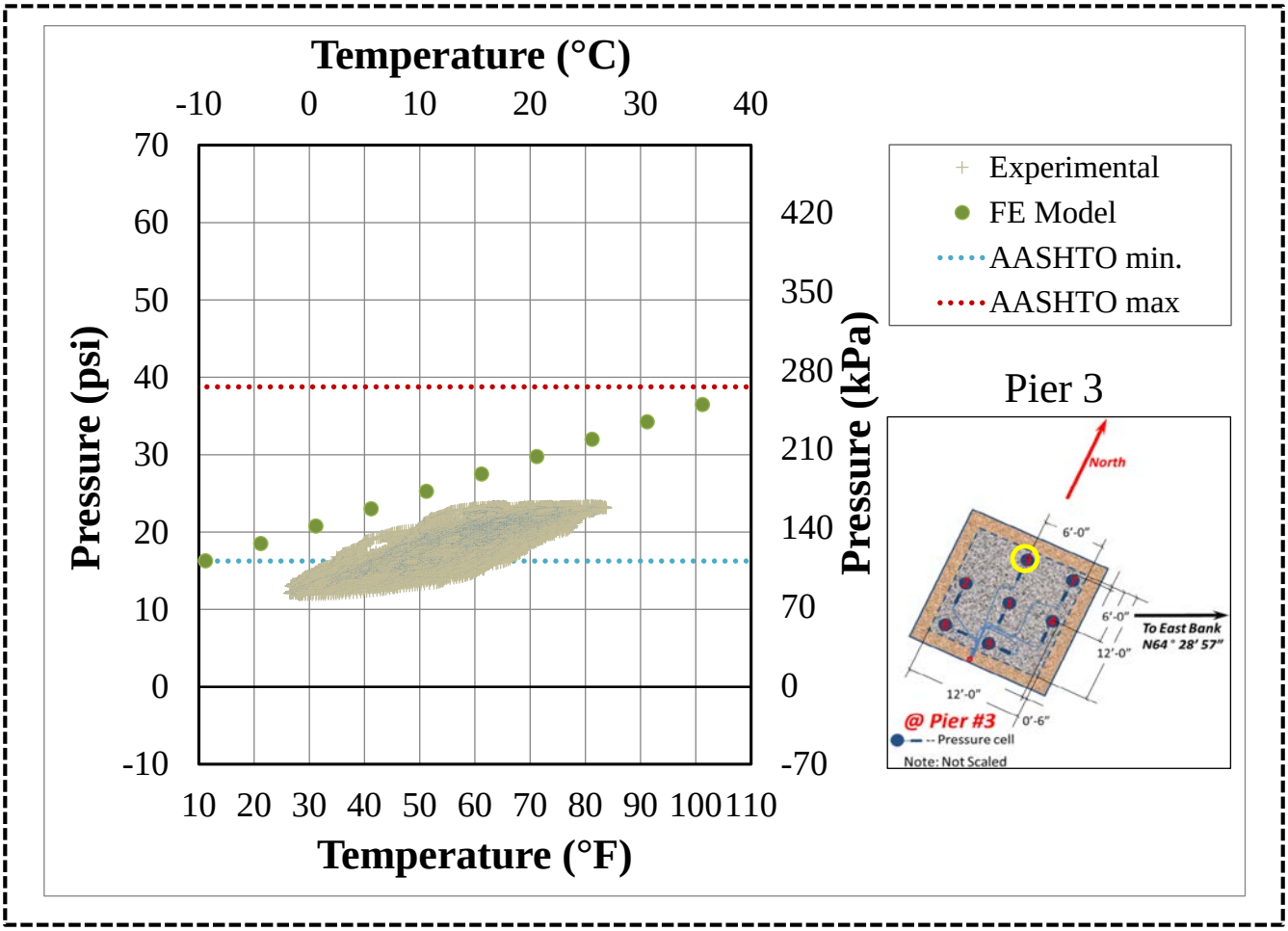

Plot 3B-1-3. Pressure cell 3 of Pier 3

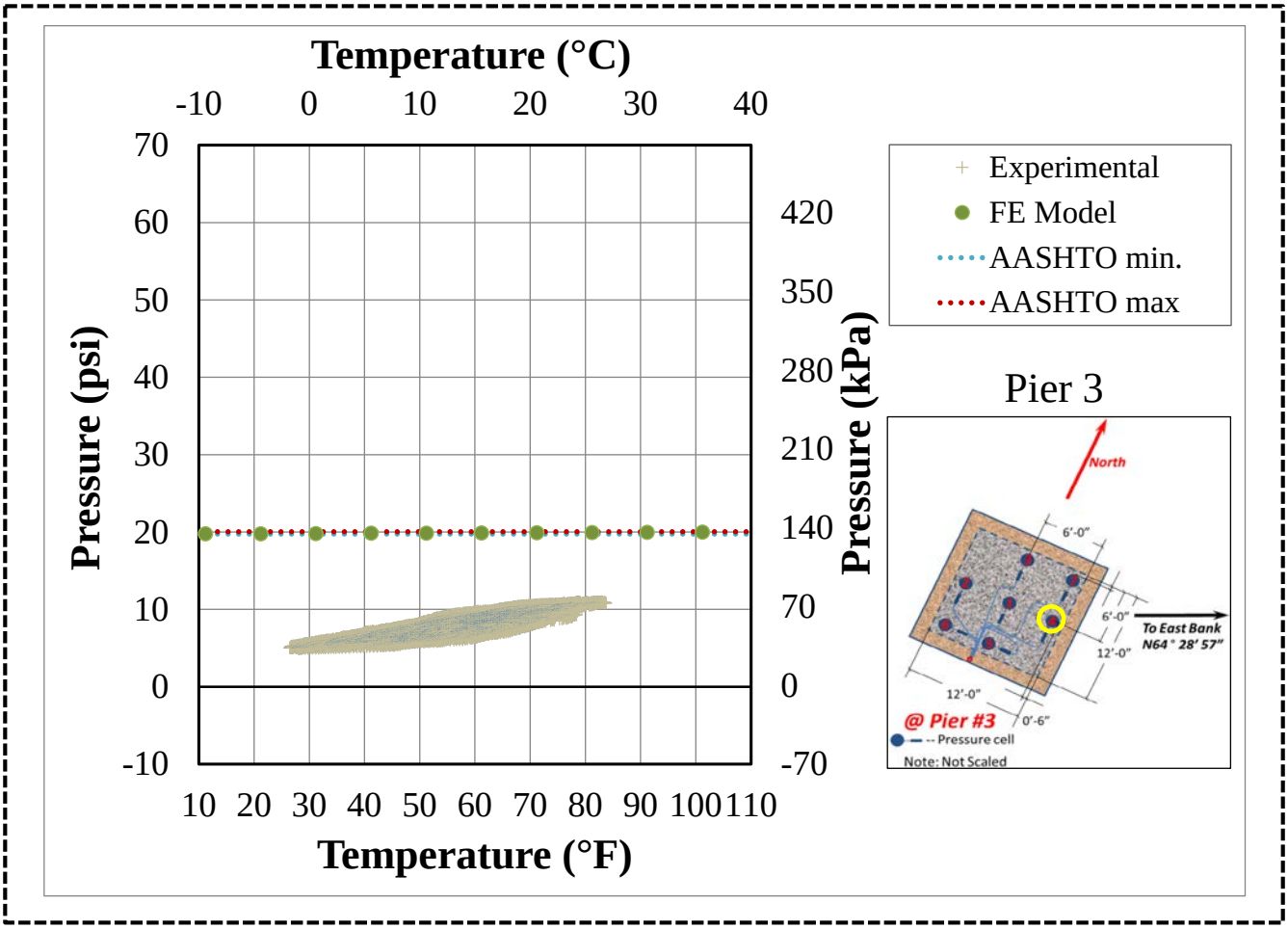

Plot 3B-1-4. Pressure cell 4 of Pier 3

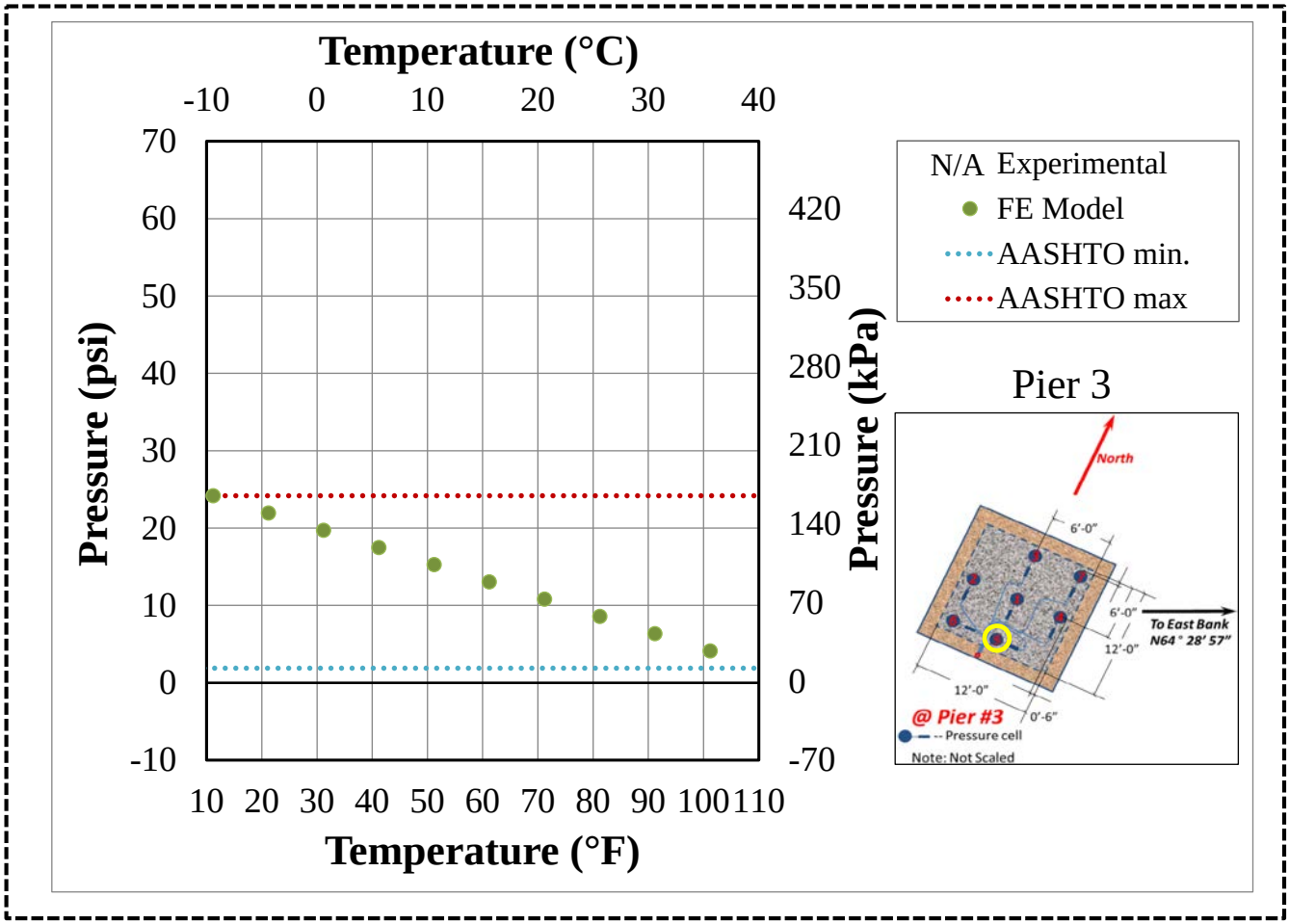

Plot 3B-1-5. Pressure cell 5 of Pier 3

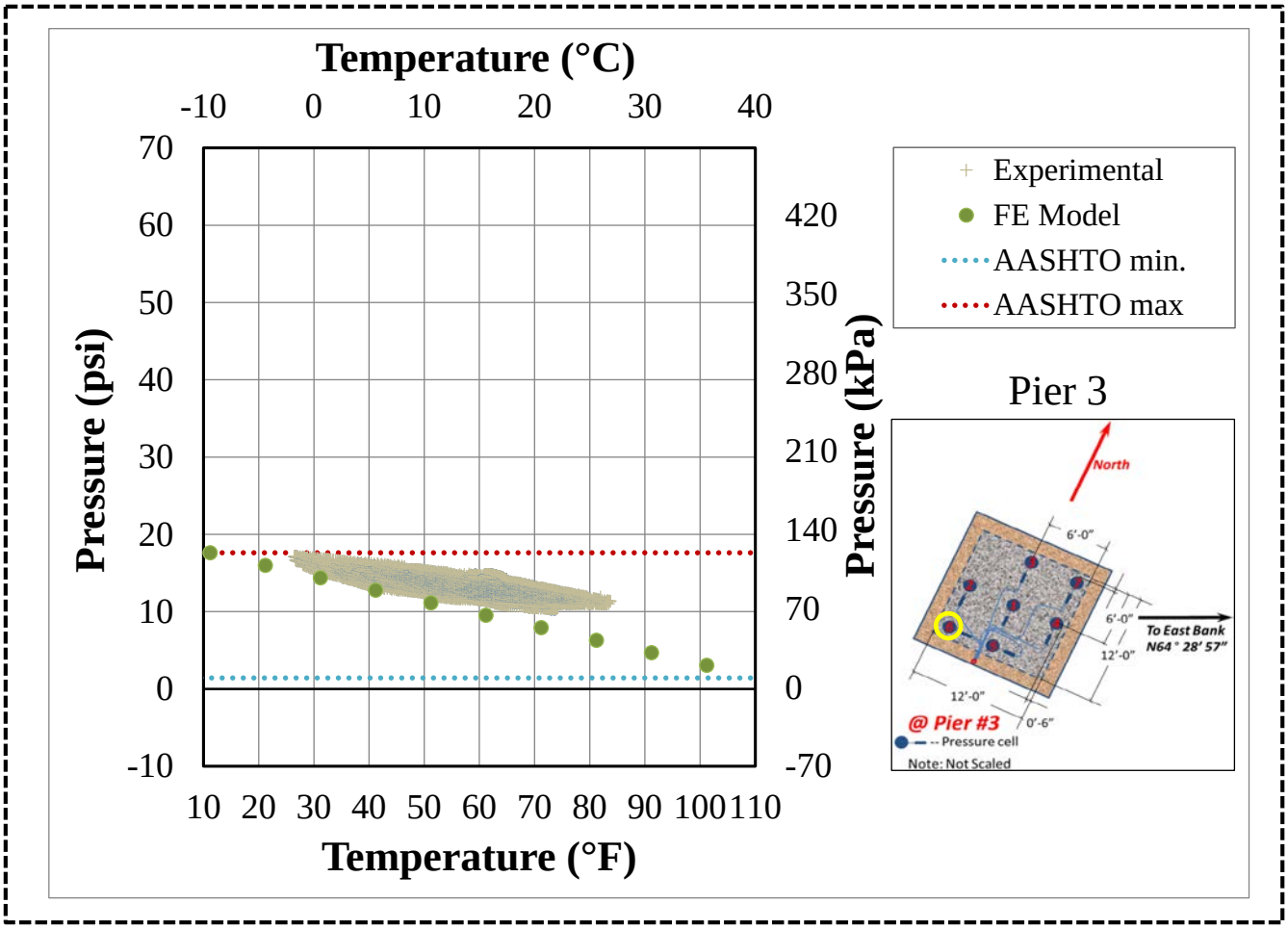

Plot 3B-1-6. Pressure cell 6 of Pier 3

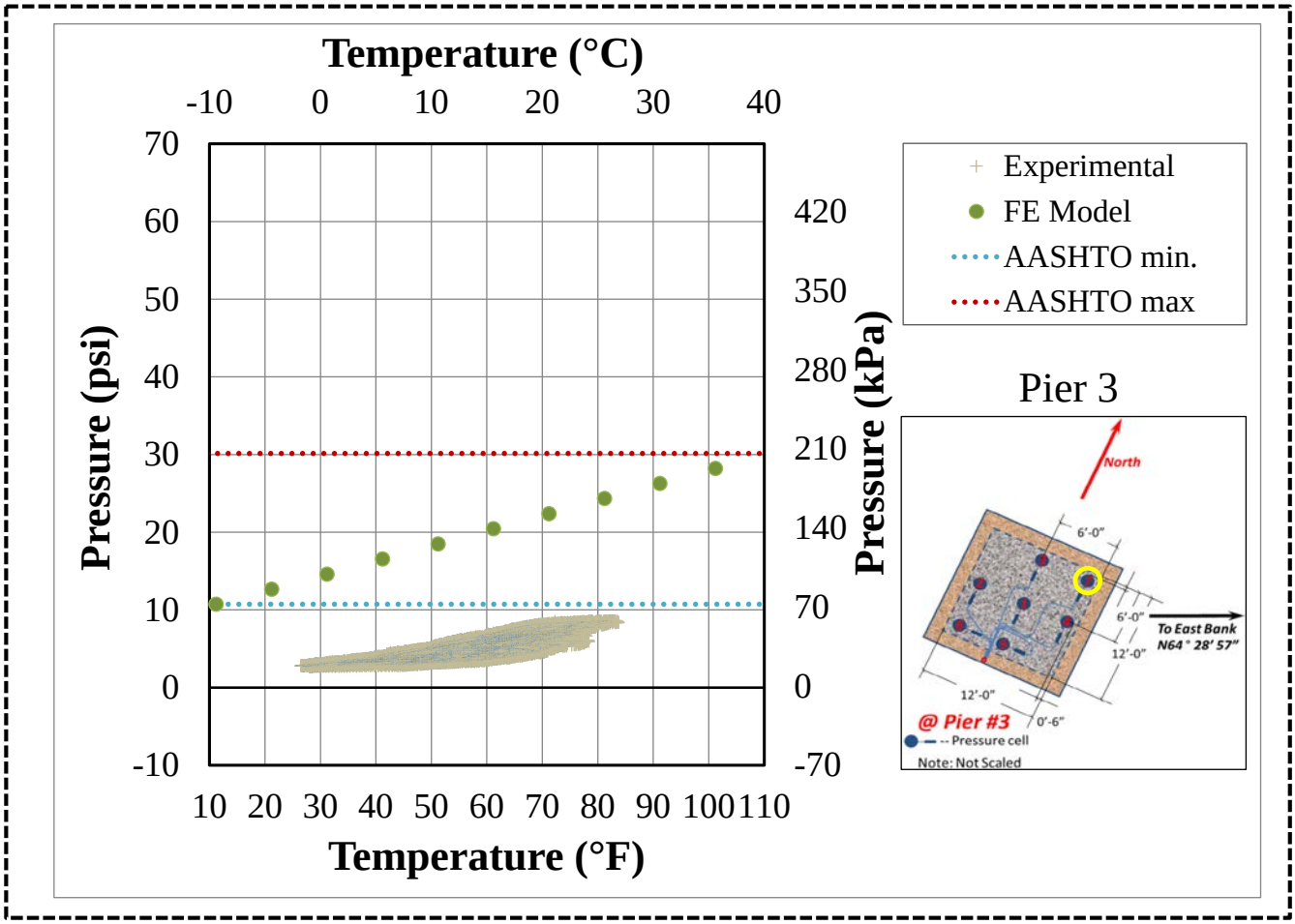

Plot 3B-1-7. Pressure cell 7 of Pier 3

Specify Date Range: _____ to _____

Note that data are available from May 11, 2011.

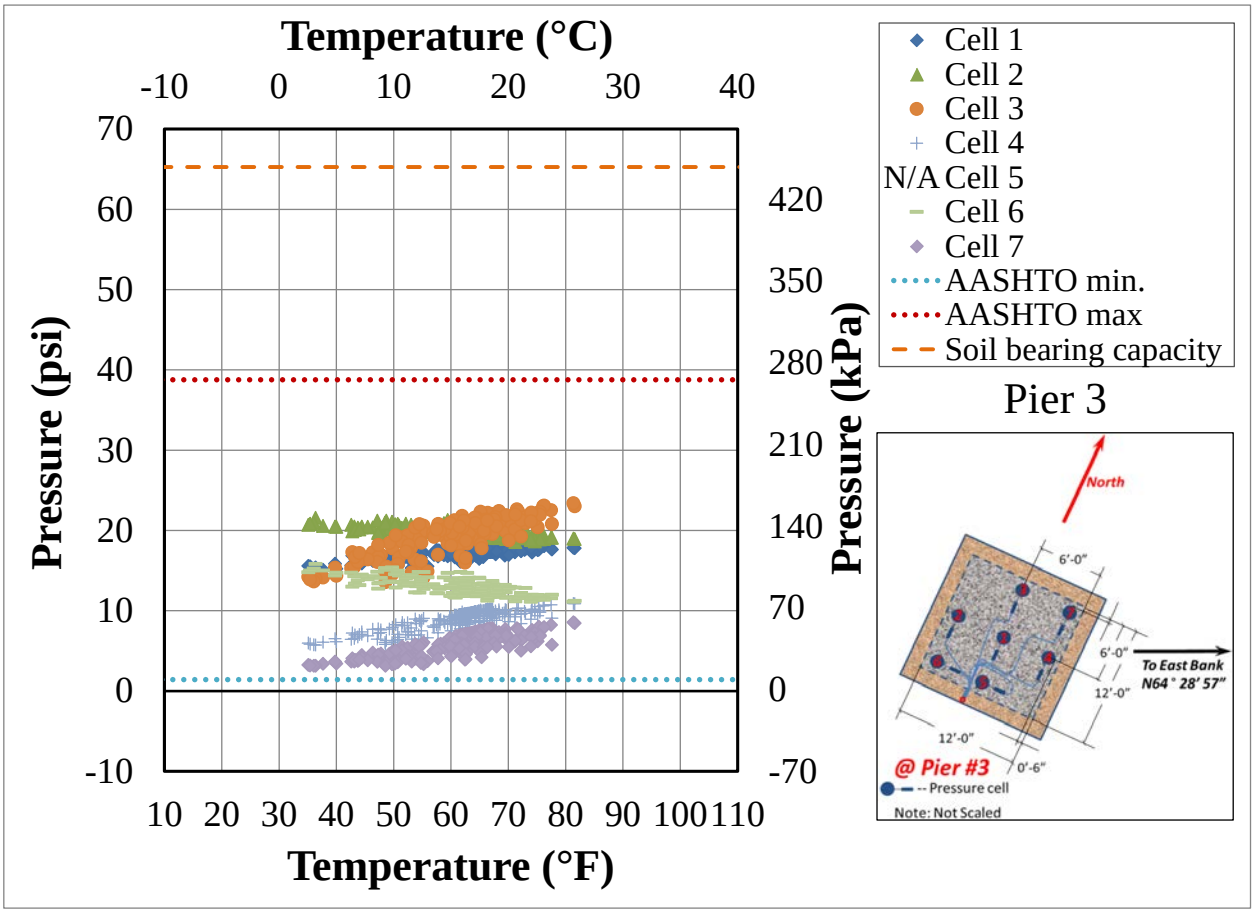

	Magnitude	Date Range	Sensor
Min. Temp °F			
Max. Temp °F			
Min. Pressure (psi)			
Max. Pressure (psi)			

Individual Cell Plots → To Screen 3B-1-1

Pier 1 Data Plots → To Screen 3A-1-1

Tiltmeter Data Plots → To Screen 3C-2

Project Background → To Screen 3D

Screen 3B-1-8. Summary for Pier 3 [continued on next page]

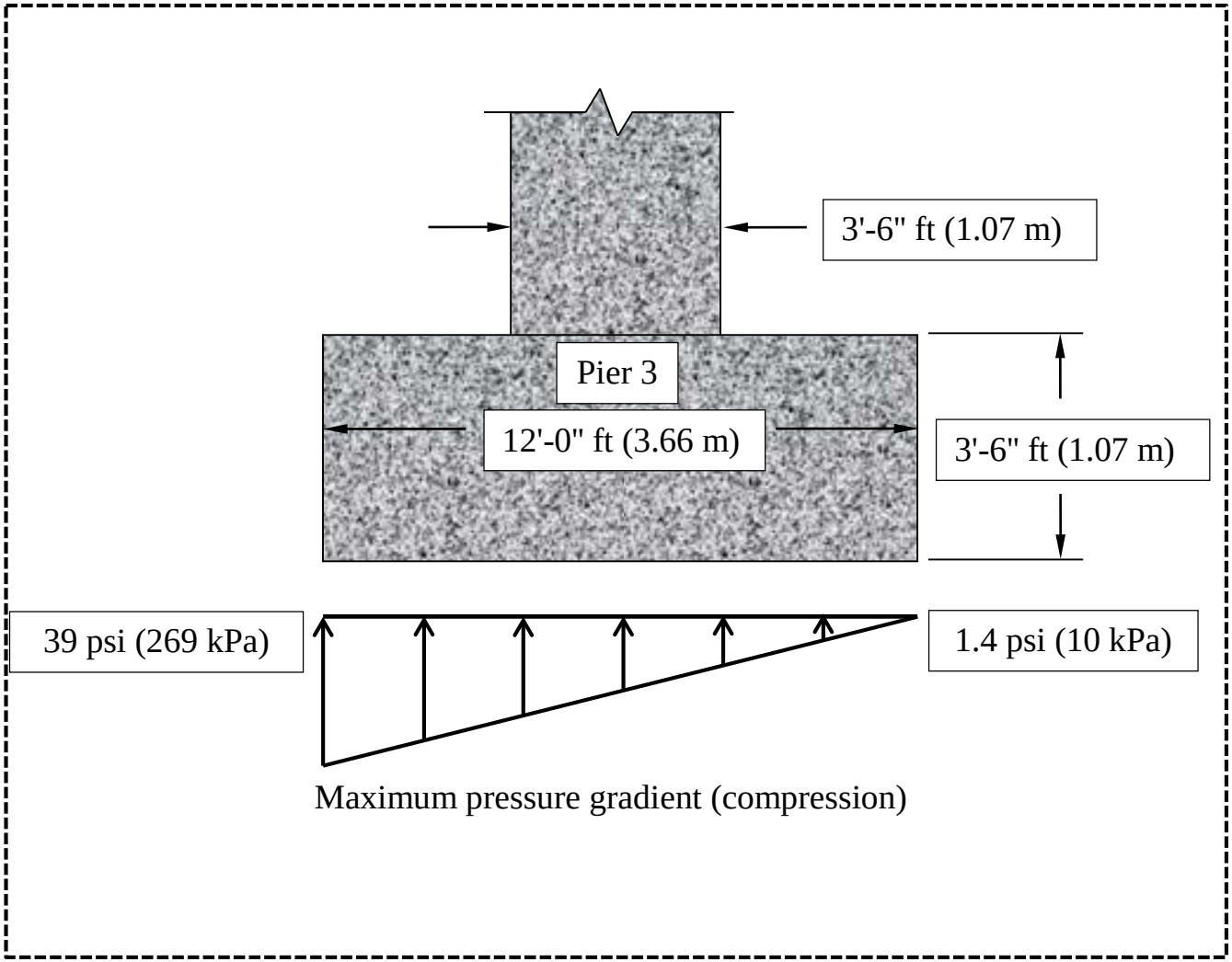

Screen 3B-1-8. Summary for Pier 3

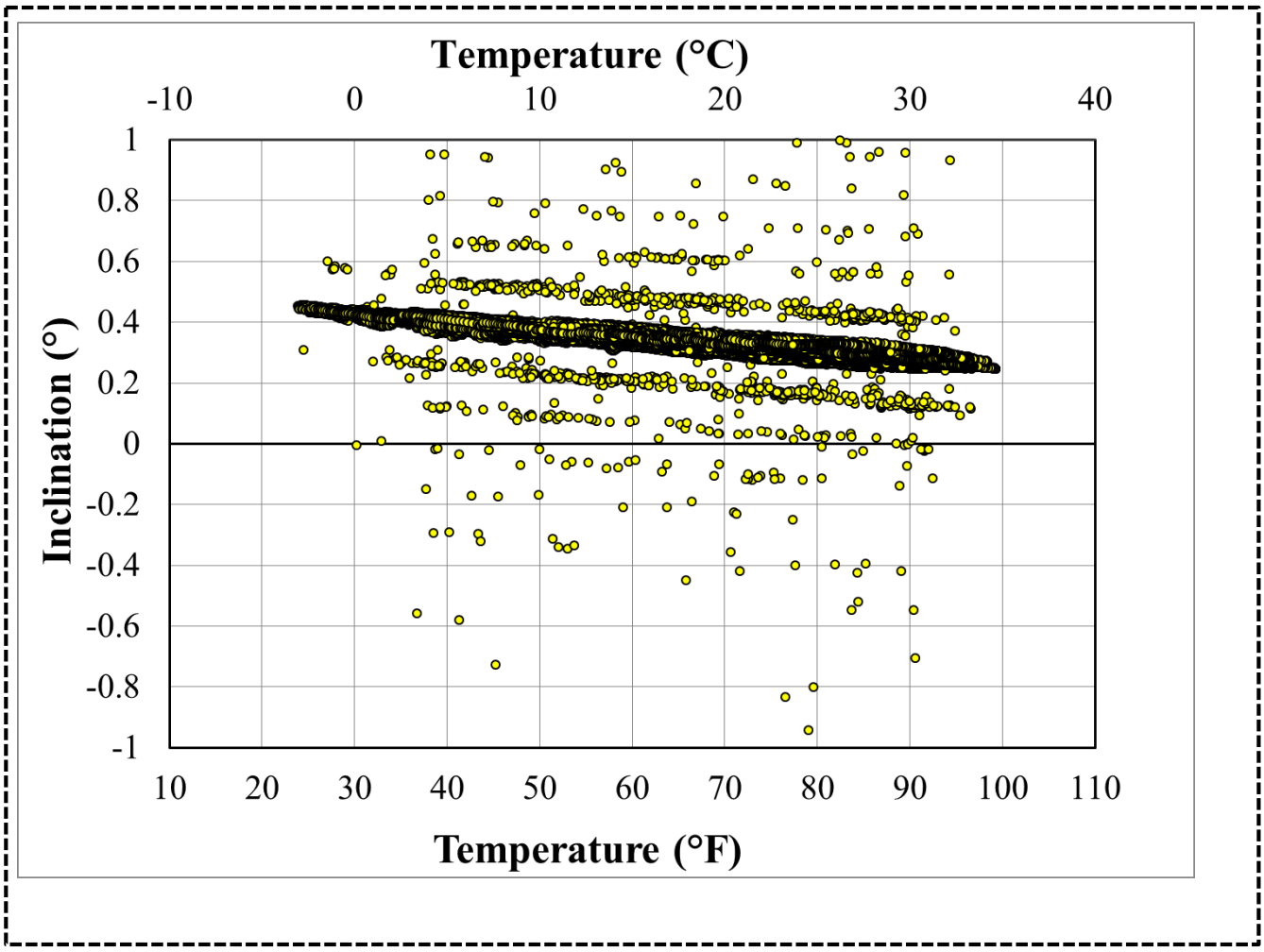

Screen 3C-1. Rotations at Top of Pier 1 Pier Cap

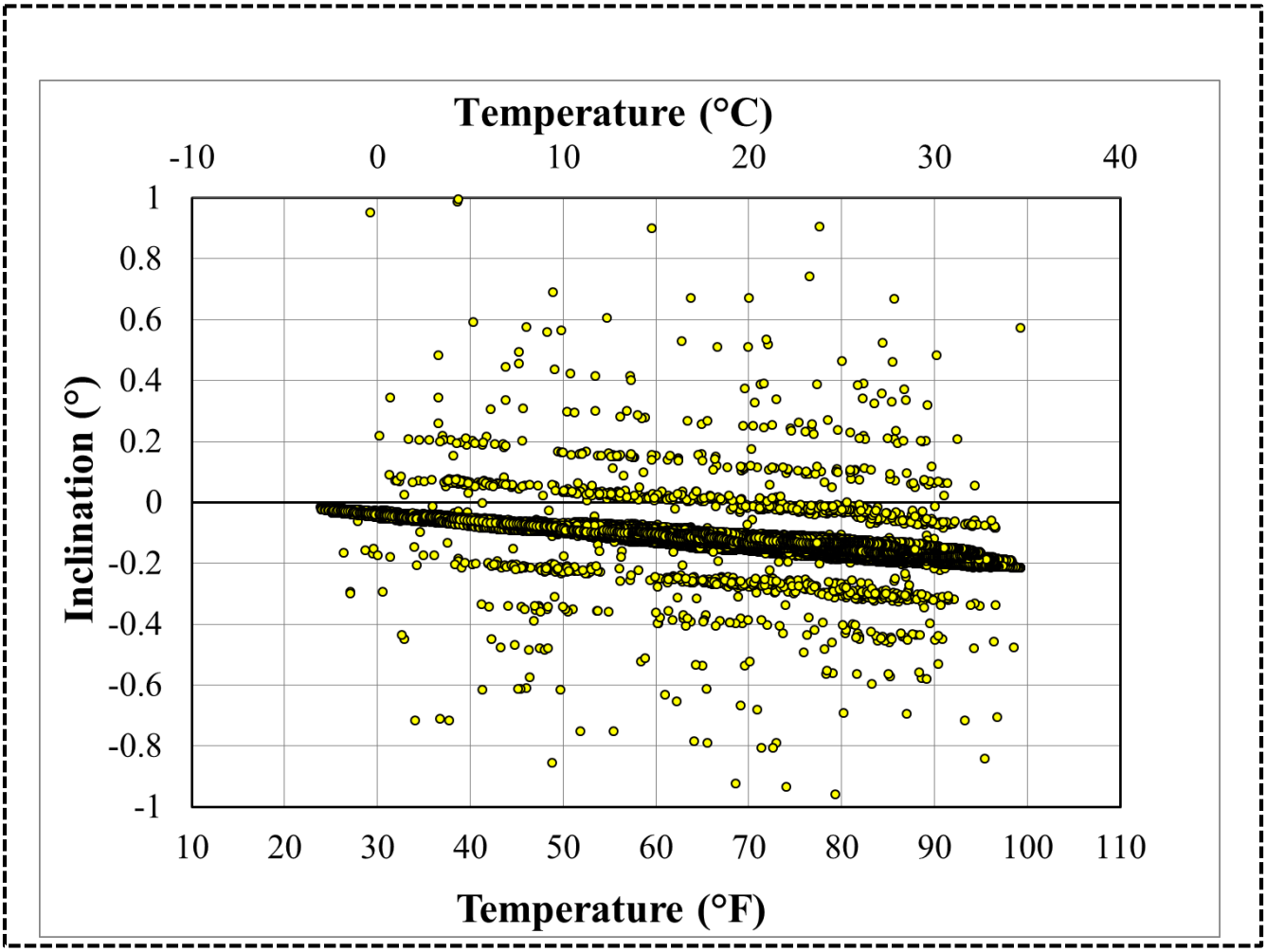

Screen 3C-2. Rotations at Bottom of Pier 1 Pier Cap

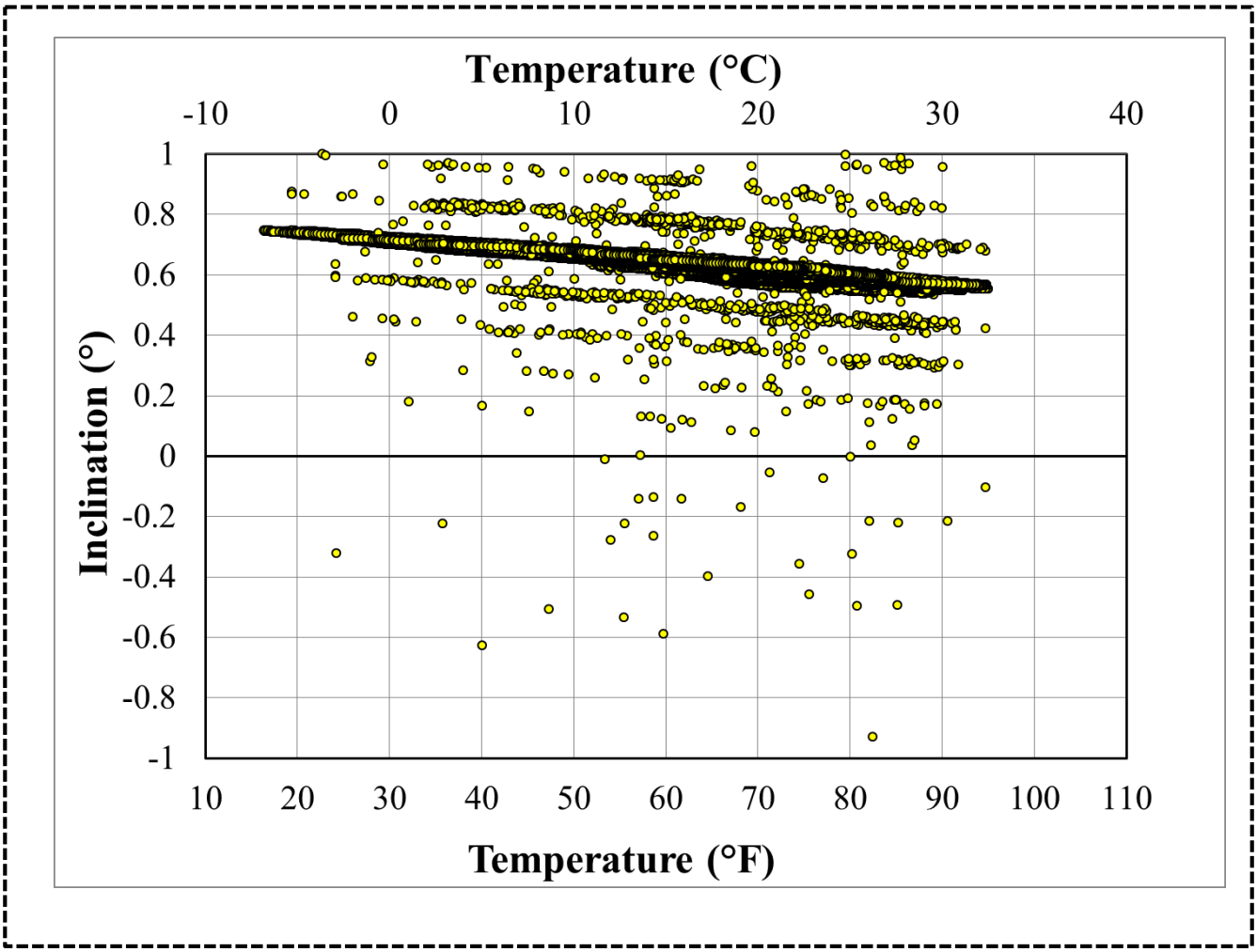

Screen 3C-3. Rotations at Bottom of Pier 3 Pier Cap

Project Objective

The objective of this study is to instrument, on a multi-span bridge, the bottom horizontal surface at the base of the footing of the pier with soil pressure cells and temperature gages, and instrument the vertical face of the footing and pier with three temperature gages each, and to continuously monitor the soil pressure and temperatures and compare the soil pressures with ones derived using the AASHTO code.

Trammel Creek Bridge

Located within the state of Kentucky, in Allen Co., the newly constructed Trammel Creek Bridge afforded the opportunity to enact the study objective through instrumenting selected footings of a (subsequently) in-service bridge, for the purpose of monitoring pier foundation pressures in response to changes in temperature at the superstructure level.

State-location of bridge site (source: Google Maps)

Screen 3D. Project background [continued on next page]

The Trammel Creek Bridge, spanning Trammel Creek near Scottsville in south-central Kentucky. The bridge contains three piers, with each pier resting on three mat foundation footings, and two integral end abutments, each supported by drive h-piles. The two-lane concrete slab deck is supported along two 120 ft (36.6 m) spans (between the three piers) and two 80 ft (24.4 m) spans between piers and abutments. The roadway slab is supported by six prestressed concrete girders of varying reinforcement configurations.

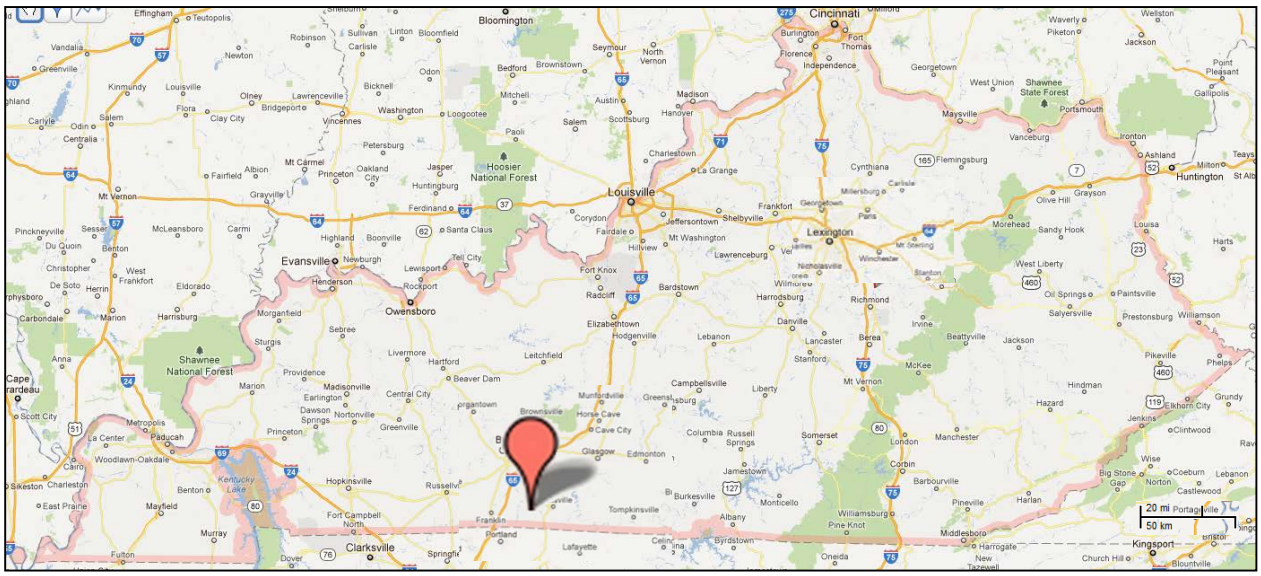

Location of bridge within Kentucky (source: Google Maps)

Screen 3D. Project background [continued on next page]

Screen 3D. Project background [continued on next page]

Areal view of Trammel Creek Bridge in Allen Co. Kentucky (source: Google Maps)

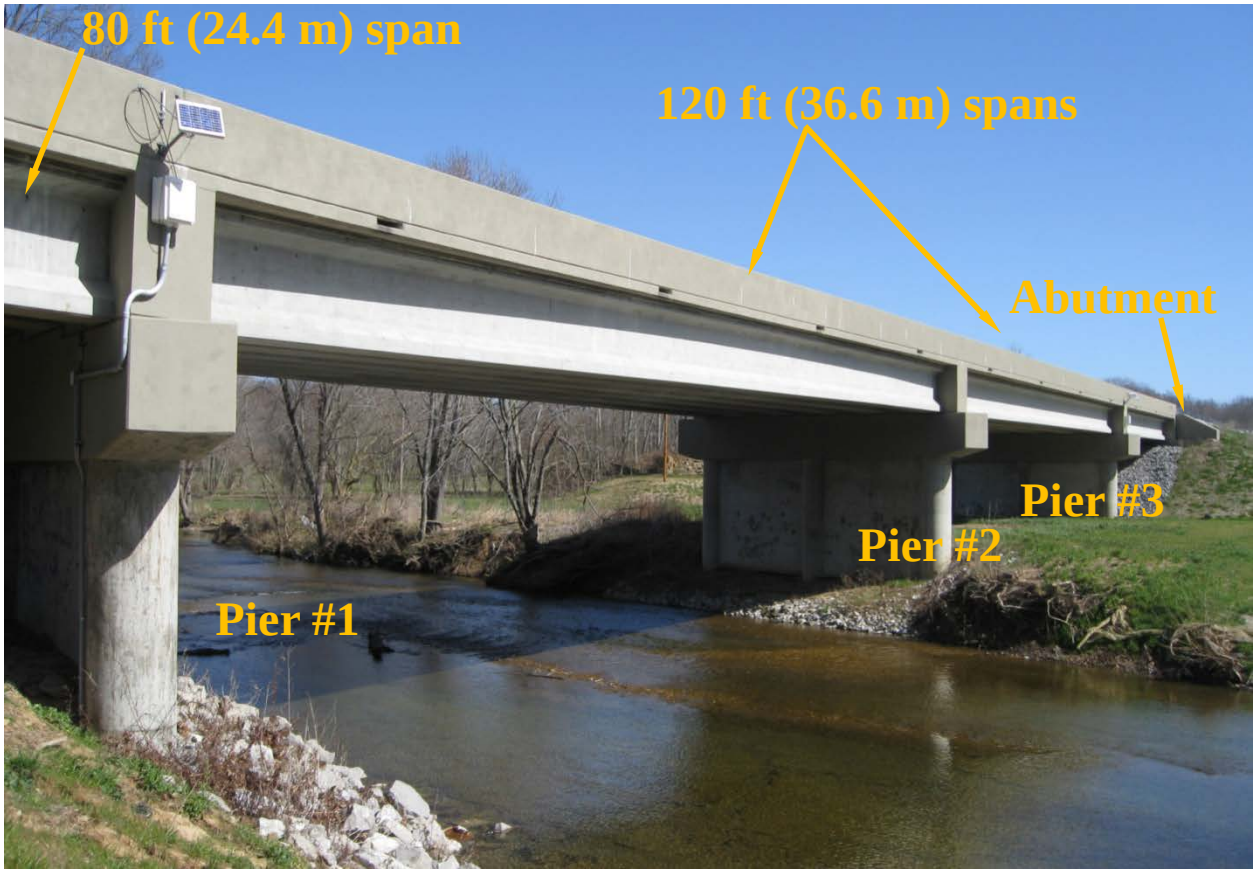

Pier enumeration for Trammel Creek Bridge in Allen Co. Kentucky

Instrumentation

During construction of the pier foundations, seven pressure cells were installed in the gravel subsurface immediately below the pier footings, as depicted schematically below. The pressure cells, as installed in the Pier 1 gravel bed, are shown below. Simultaneous to pouring and curing of the overlying pier members, data transmission lines were installed to allow real-time, long-term monitoring of foundation pressures. Additionally, subsequent to installation of the bridge superstructure (consisting of a concrete slab cast integrally atop prestressed concrete girders), thermocouples were installed along the tops of Pier 1 and Pier 3 to facilitate monitoring of temperatures at the superstructure level in real-time. By pairing (through time) pressure cell activity at Pier 1 and Pier 3 (i.e., foundation pressures) with measurements of temperatures atop the respective piers, relationships between thermal loads at the superstructure level and the resulting foundation pressures will be examined for the Trammell Creek Bridge.

Screen 3D. Project background [continued on next page]

As shown in the figure below, the southernmost footing of Pier 1 and northernmost footing of Pier 3 were each instrumented with seven pressure cells, and the experimental measurements of foundation pressures will be continually updated over the next three years. In the following figures, the pressures (those measured experimentally, and those obtained from finite element analysis) are depicted.

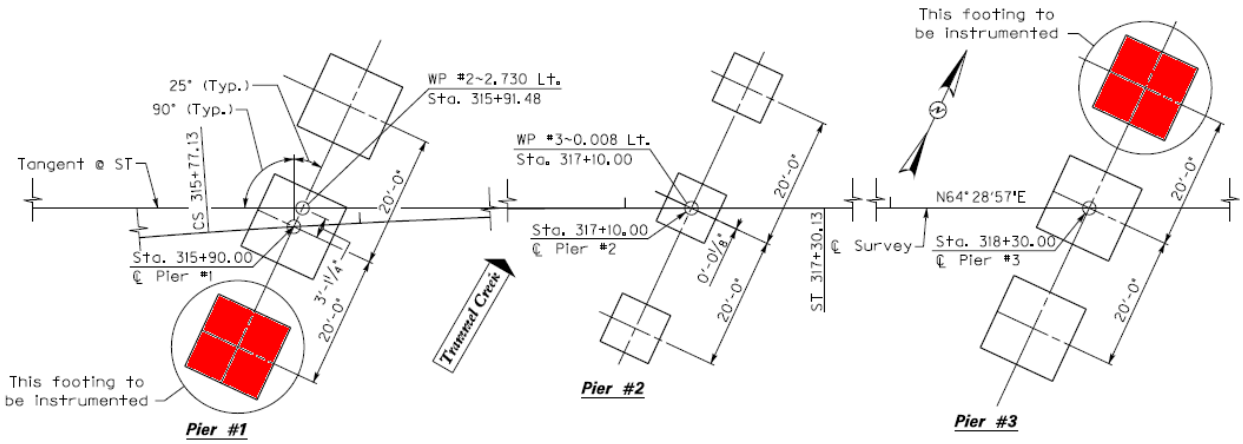

Plan view of Trammel Creek Bridge (instrumented footings are highlighted)

Pier 1

Shown below is the pressure cell layout for the southernmost footing of Pier 1. Click on individual cells in the figure to access plots of the experimental, analytical, and estimated AASHTO design load pressures found in the individual pressure cells as a function of temperature. The plots will be continually updated throughout the project. Note that the abscissa axis of the plots contains superstructure temperature, where the base construction temperature is taken as the mean-ambient temperature (41.2 °F) in the vicinity of the bridge superstructure 28 days after the pouring of the bridge deck.

Summary plots of the available experimental measurements of pressure at the Pier 1 footing level are also available below. The summary plot depicts extreme values of pressures predicted by subjecting the superstructure elements of the bridge finite element model to the minimum (10 °F) and maximum (110 °F) design temperatures, as selected from Sec. 3.12 of the AASHTO design provisions. The predicted pressures predicted across all cells located in the Pier 1 footing (in association with the minimum and maximum design temperatures) are used to determine the AASHTO lower bound and AASHTO upper bound stress levels in the Trammell Creek Bridge Pier 1 foundation. For example, as shown in the summary plot, the lower bound pressure predicted to occur in the Pier 1 footing, which is produced by subjecting the bridge model superstructure to the AASHTO minimum design temperature (10 °F), is approximately 0 psi. The respective maximum design temperature (110 °F) produces a pressure (taken as the maximum across all cells) is 47.8 psi. Also, included in the summary is the maximum bearing capacity for the soil underlying the footing located at Pier 1 (as obtained from structural drawings), which is 65.3 psi.

Screen 3D. Project background [continued on next page]

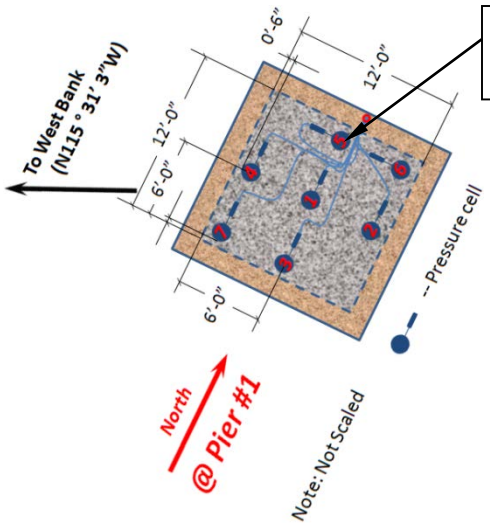

Instrumentation layout for Pier 1

Finally, a plot of the overturning pressure gradient (estimated from finite element analysis) is given beneath the summary plot.

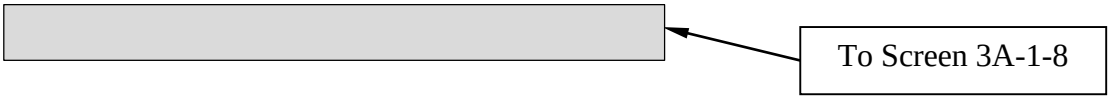

Screen 3D. Project background [continued on next page]

Pier 3

Shown below is the pressure cell layout for the northernmost footing of Pier 3. Clicking on individual pressure cells gives access to plots of the experimental, analytical, and estimated AASHTO design load pressures found in the respective, individual pressure cells of the Pier 3 footing as a function of temperature. The plots will be continually updated throughout the project. Note that the abscissa axis of the plots contains superstructure temperature, where the base construction temperature is taken as the mean-ambient temperature (41.2 °F) in the vicinity of the bridge superstructure 28 days after the pouring of the bridge deck.

A summary of the available experimental measurements of pressure at the Pier 3 footing level and estimates of stresses associated with the low and high AASHTO extreme temperatures are additionally available below. Additionally shown is the maximum bearing capacity for the soil underlying the footing located at Pier 3 (as obtained from structural drawings).

Also given in the summary plot are the extreme values of pressures predicted by subjecting the superstructure elements of the bridge finite element model to the minimum (10 °F) and maximum (110 °F) design temperatures, as selected from Sec. 3.12 of the AASHTO design provisions. The predicted pressures predicted across all cells located in the Pier 3 footing (in association with the minimum and maximum design temperatures) are used to determine the AASHTO lower bound and AASHTO upper bound stress levels in the Trammell Creek Bridge Pier 3 foundation. For example, as shown in the summary plot, the lower bound pressure predicted to occur in the Pier 3 footing, which is produced by subjecting the bridge model superstructure to the AASHTO minimum design temperature (10 °F), is approximately 1.4 psi. The respective maximum design temperature (110 °F) produces a pressure (taken as the maximum across all cells) is 39 psi.

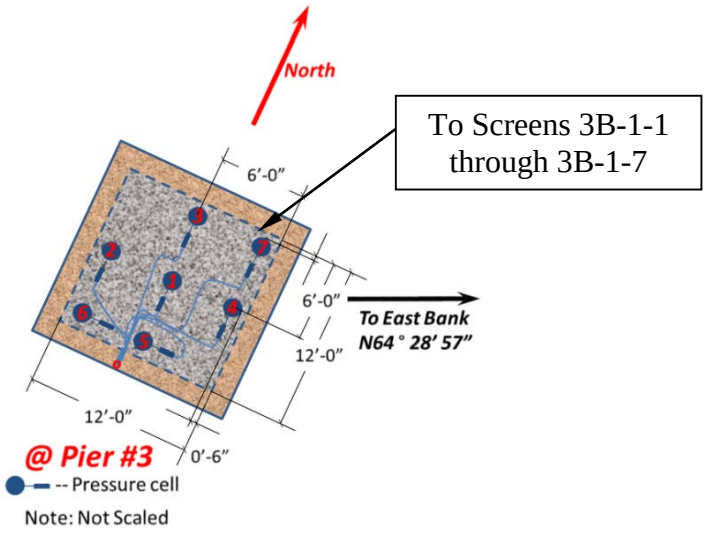

Instrumentation layout for Pier 3

Screen 3D. Project background [continued on next page]

Finally, a plot of the overturning pressure gradient (estimated from finite element analysis) is given beneath the summary plot.

To Screen 3B-1-8

Screen 3D. Project background [continued on next page]

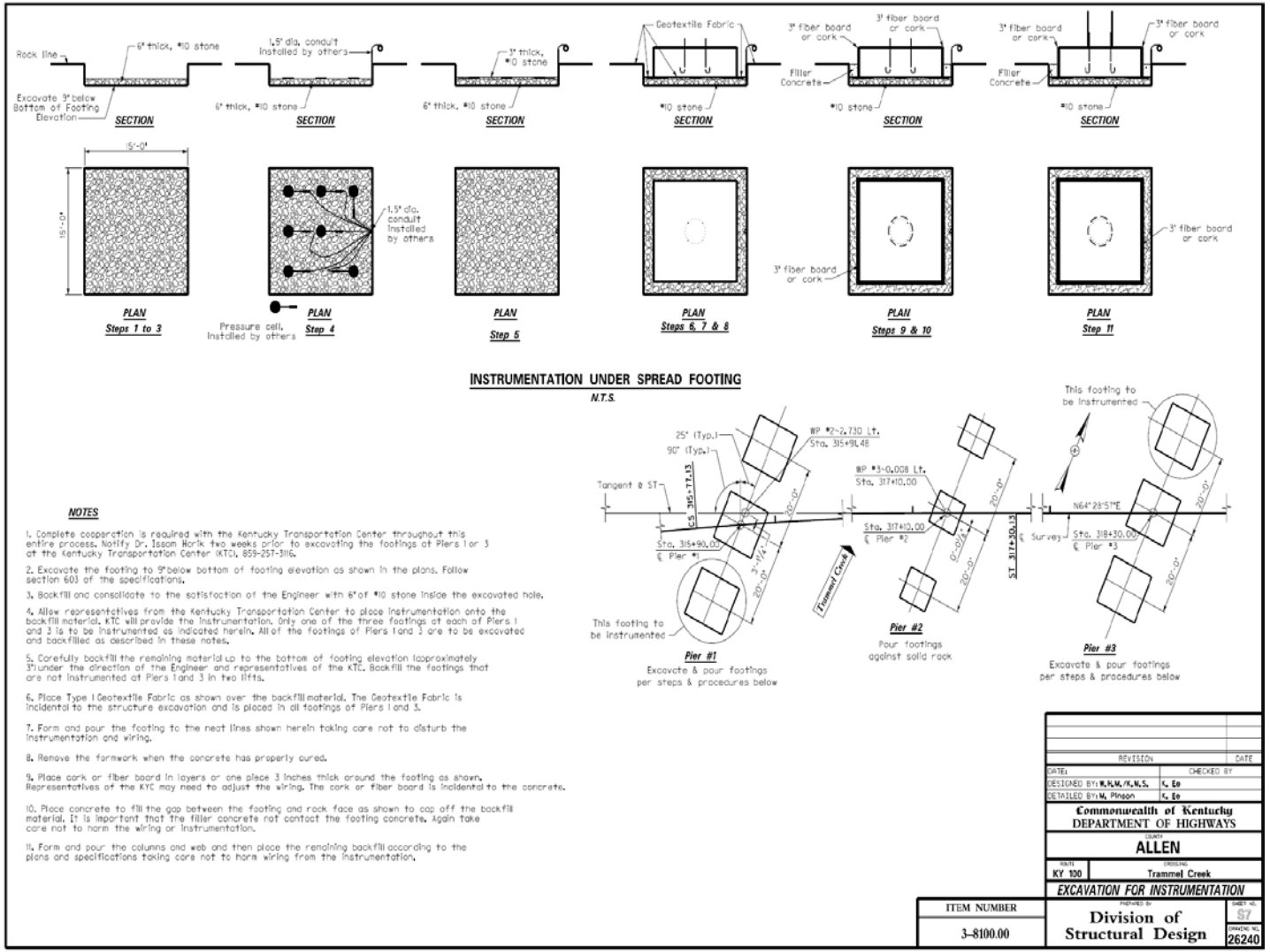

Schematic and construction notes for installation of pressure cells in footings

Screen 3D. Project background [continued on next page]

Installation of pressure cells beneath pier footings

Screen 3D. Project background [continued on next page]

Placement of foundation reinforcement and column reinforcement over pressure cells

Screen 3D. Project background [continued on next page]

Pier 1 with pressure cell instrumentation installed

Screen 3D. Project background [continued on next page]

Location of thermocouples on Pier 1 and Pier 3

Finite Element Modeling

As a supplement to the experimental program, a high-resolution finite element model of the bridge was created based on structural drawings using the ANSYS general-purpose finite element software. Based on site soil conditions and available experimental measurements of foundation response, the finite element model was calibrated to facilitate agreement between analytical predictions of bridge response and experimental measurements at the bridge site.

The calibrated model includes discrete modeling of bearing stiffnesses at the substructure-superstructure interface as well as fully discrete modeling of superstructure members. Using the calibrated model, estimates of the bridge response (when subjected to the relatively more extreme design conditions associated with AASHTO superstructure-thermal loading) can then be made.

Screen 3D. Project background [continued on next page]

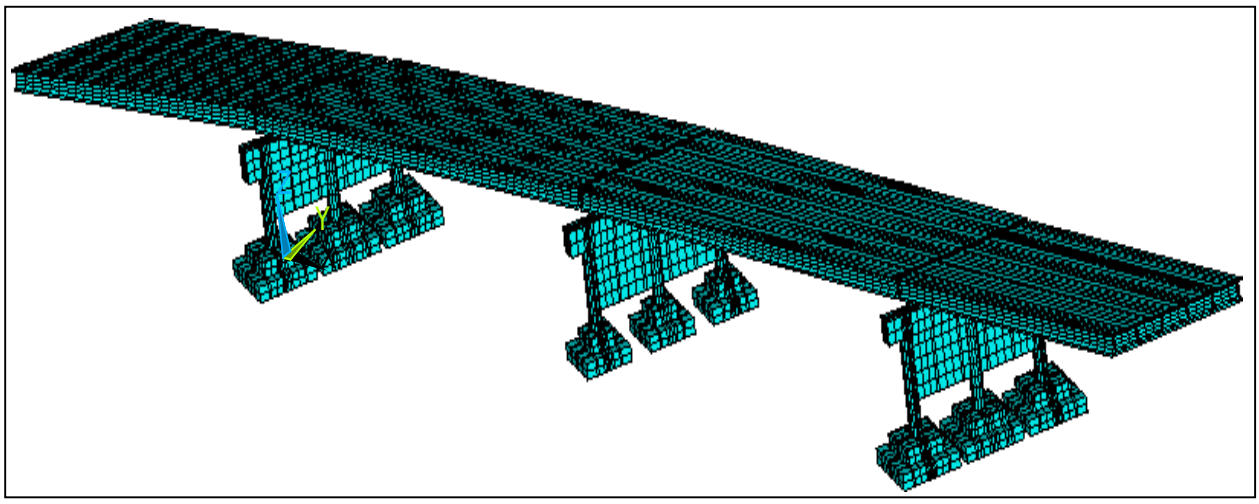

Finite element model of Trammel Creek Bridge

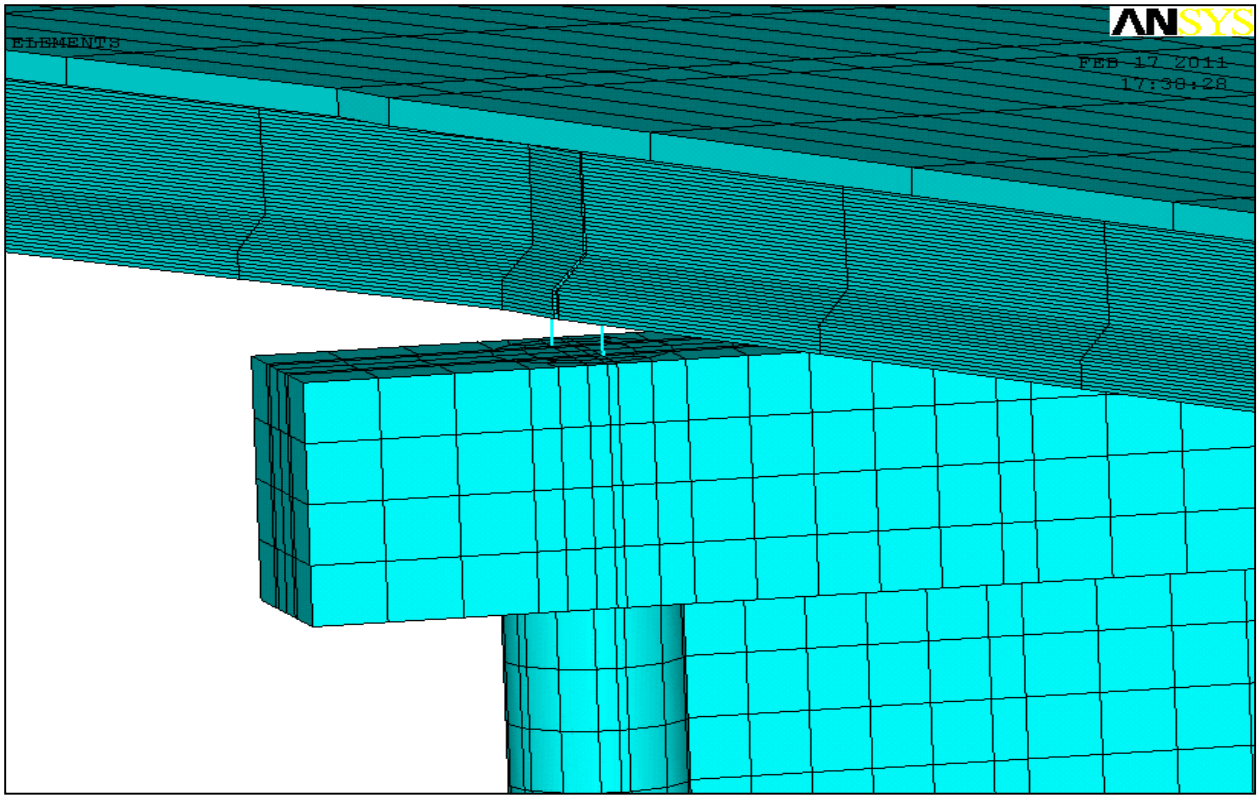

Modeling of substructure-superstructure interaction

Screen 3D. Project background [continued on next page]

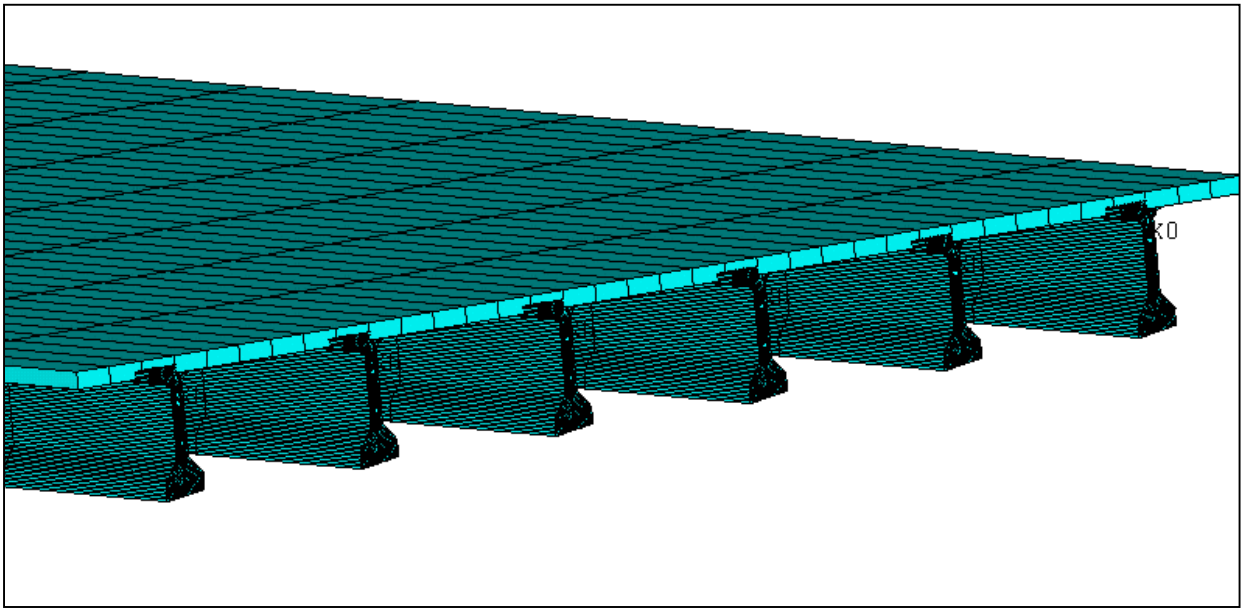

Discrete modeling of superstructure

AASHTO Thermal Loads on Bridge Superstructures

In the AASHTO design provisions pertaining to thermal loading, one commonly employed method of incorporating thermal loading into the bridge during the design phase is through prescribed longitudinal displacements at the superstructure level. In determining the prescribed displacements, minimum and maximum design temperatures are selected from temperature maps (excerpted from Sec. 3.12 of the AASHTO design provisions, below). Then, for the purposes of conducting a bridge structural analysis, a bridge model is formed, and the superstructure elements of the bridge model are subjected to displacements to account for temperature loading. Specifically, uniform longitudinal displacements in association with (design) uniform decreases (or increases) in temperature, relative to the base construction temperature for the superstructure.

For the Trammell Creek Bridge, located in Allen Co. in south-central Kentucky, the minimum design temperature per the AASHTO contour maps is 10 °F. Likewise, the AASHTO maximum design temperature is 110 °F. Furthermore, the base construction temperature for the superstructure is 41.2 °F, where this temperature is the mean air temperature in the vicinity of the bridge on the day corresponding to 28 days following the pouring of the bridge deck.

Screen 3D. Project background [continued on next page]

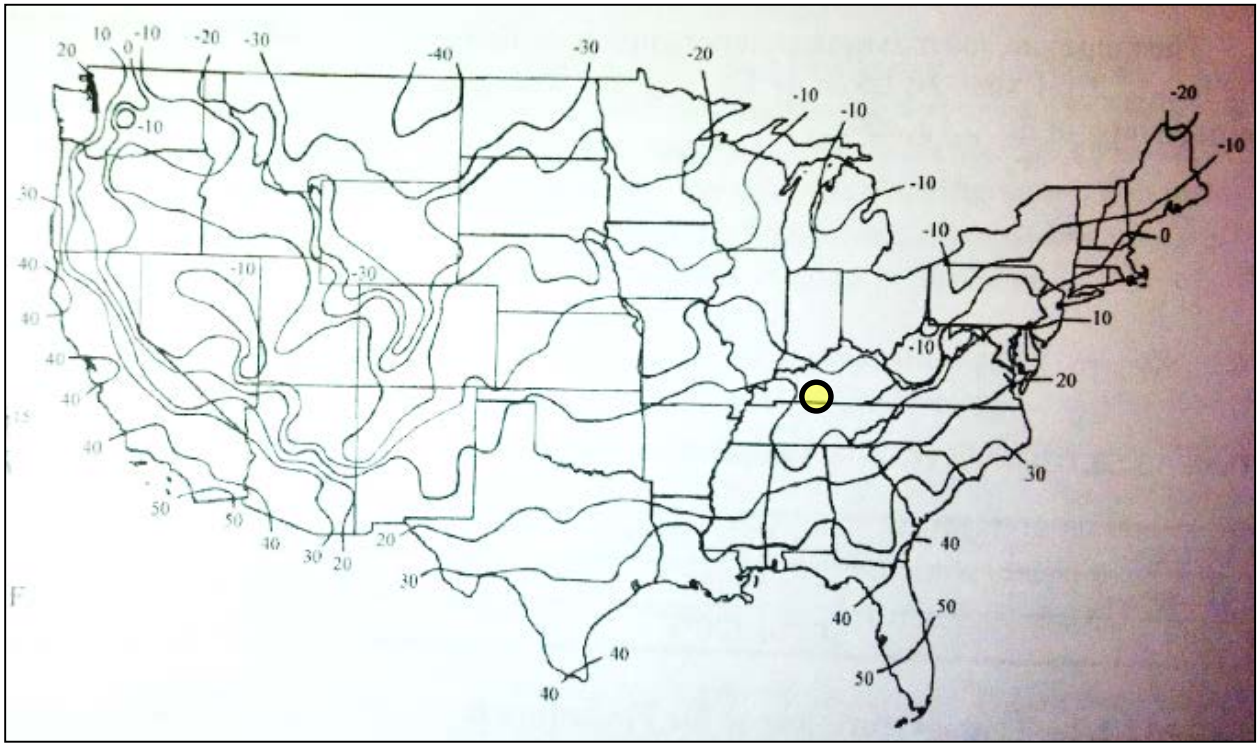

Contour map for minimum design temperatures for concrete girder bridges with concrete decks (from Sec. 3.12 of the AASHTO LRFD code)

Screen 3D. Project background [continued on next page]

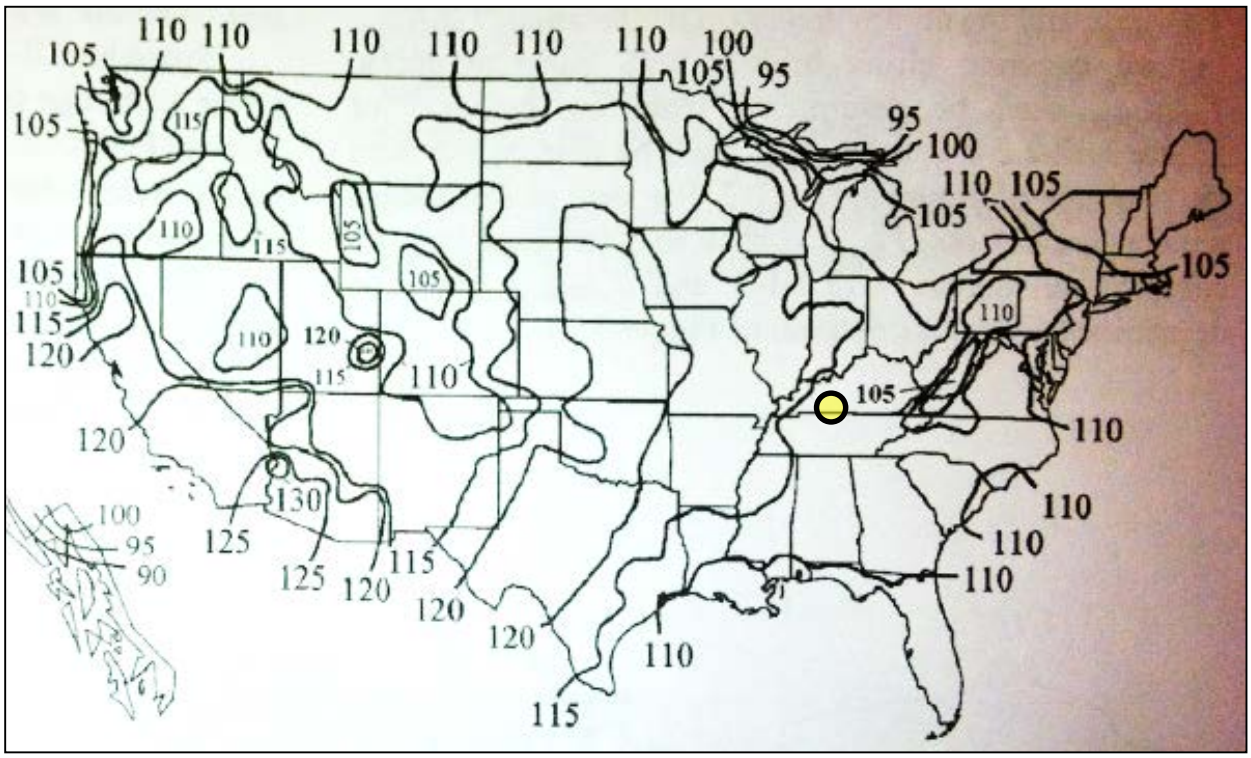

Contour map for maximum design temperatures for concrete girder bridges with concrete decks (from Sec. 3.12 of the AASHTO LRFD code)

Screen 3D. Project background

APPENDIX C: COMPARISON OF FEA RESULTS TO FIELD MEASUREMENTS OF FOUNDATION PRESSURES

Presented in the following are the FEA generated foundation pressures and the on-site readings for those pressure cells installed beneath the selected footings of Pier 1 and Pier 3. Specifically, seven pressure cells were installed beneath the southernmost footing of Pier 1 and seven pressure cells were installed beneath the northernmost footing of Pier 3. In the Appendix C plots, foundation pressure data are paired with corresponding superstructure temperatures, for a range of temperatures stipulated in the AASHTO Method B for superstructure temperature loading. The field data consist of readings taken from May 11, 2011 to May 11, 2012. Note that data are not available for pressure cell 7 beneath the Pier 1 footing, nor are data available for pressure cell 5 beneath the Pier 3 footing. Also, note that the analogous plot pressure cell 4 beneath the Pier 1 footing is given in Chapter 5.

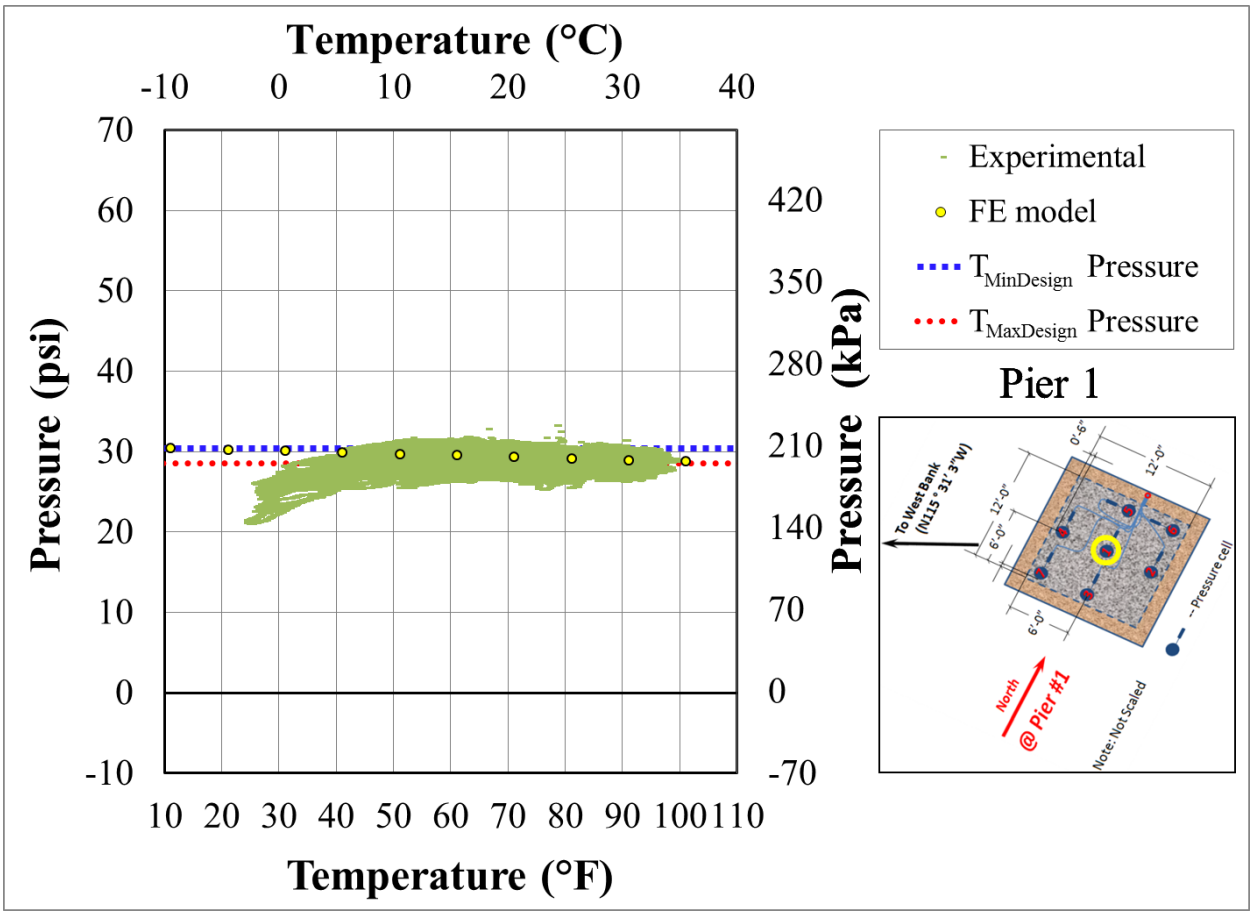

Fig. C.1: Pier 1, Cell 1 field measurements and numerical estimates of substructure response to gravity-temperature loading.

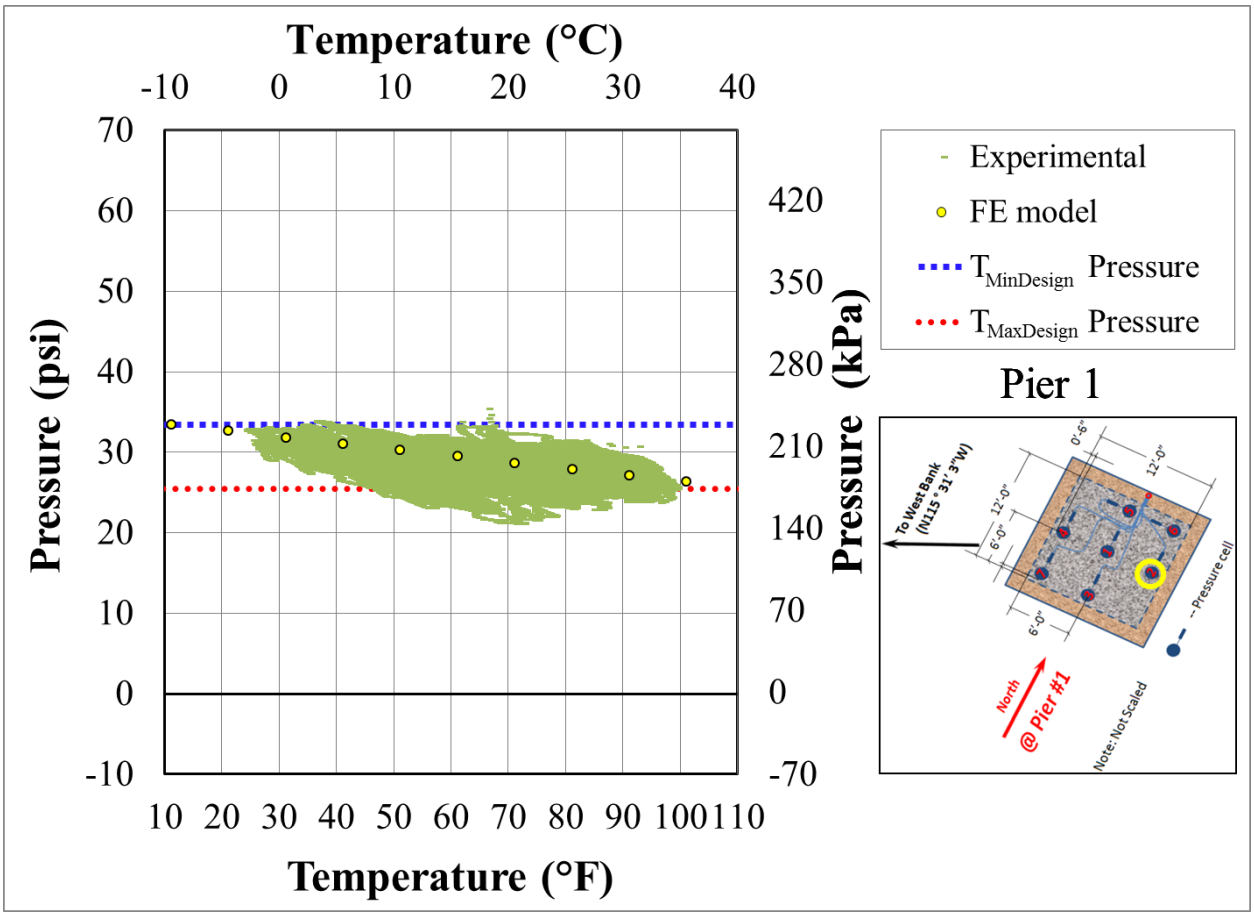

Fig. C.2: Pier 1, Cell 2 field measurements and numerical estimates of substructure response to gravity-temperature loading.

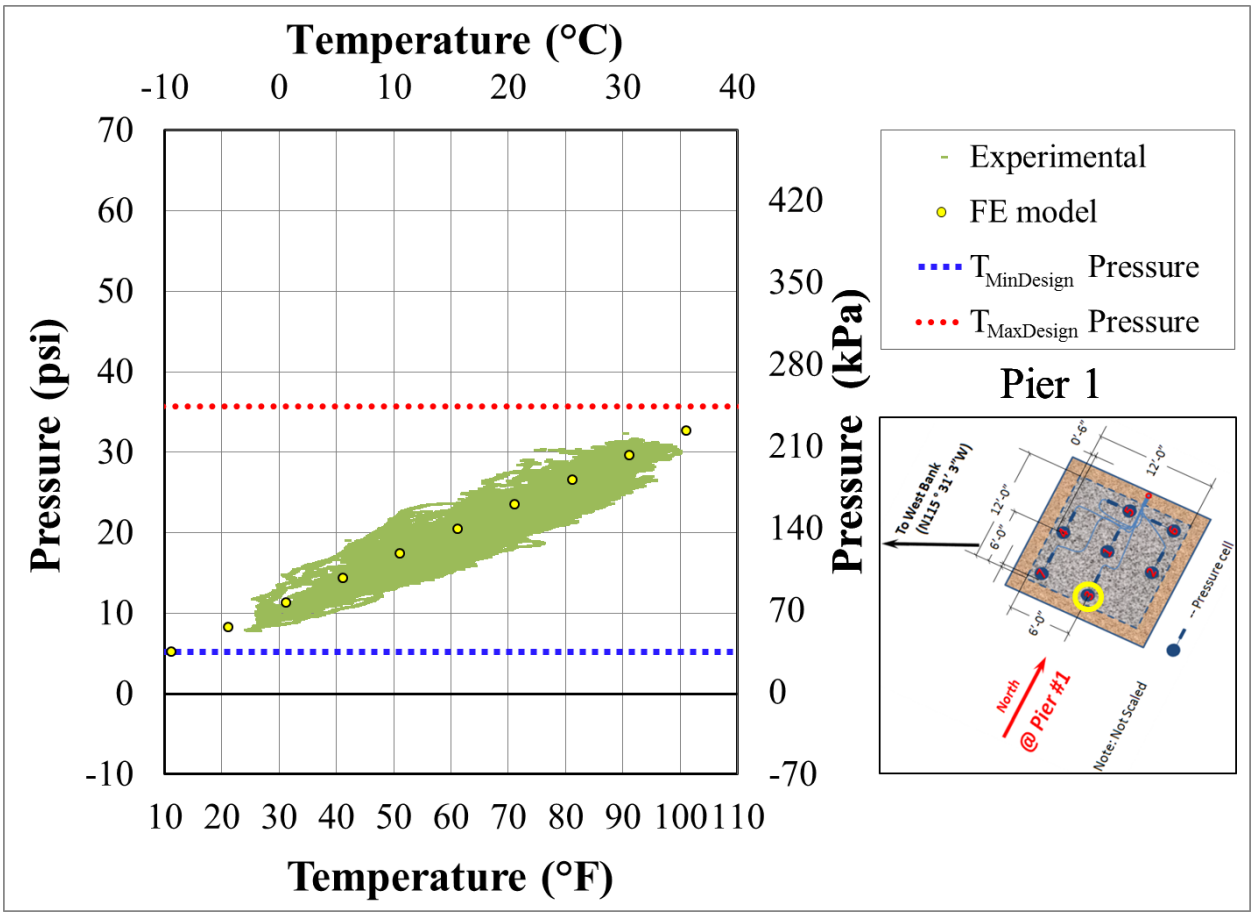

Fig. C.3: Pier 1, Cell 3 field measurements and numerical estimates of substructure response to gravity-temperature loading.

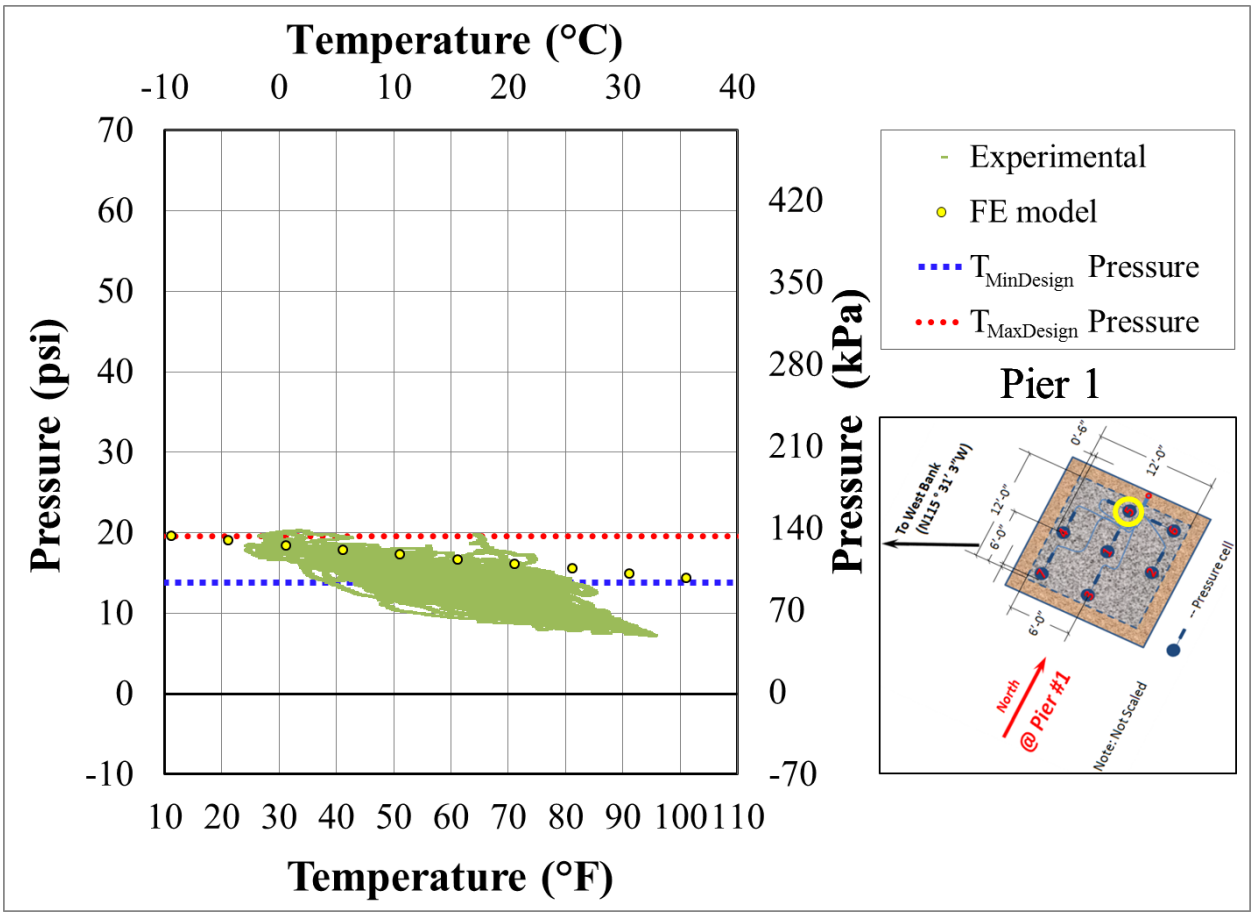

Fig. C.4: Pier 1, Cell 5 field measurements and numerical estimates of substructure response to gravity-temperature loading.

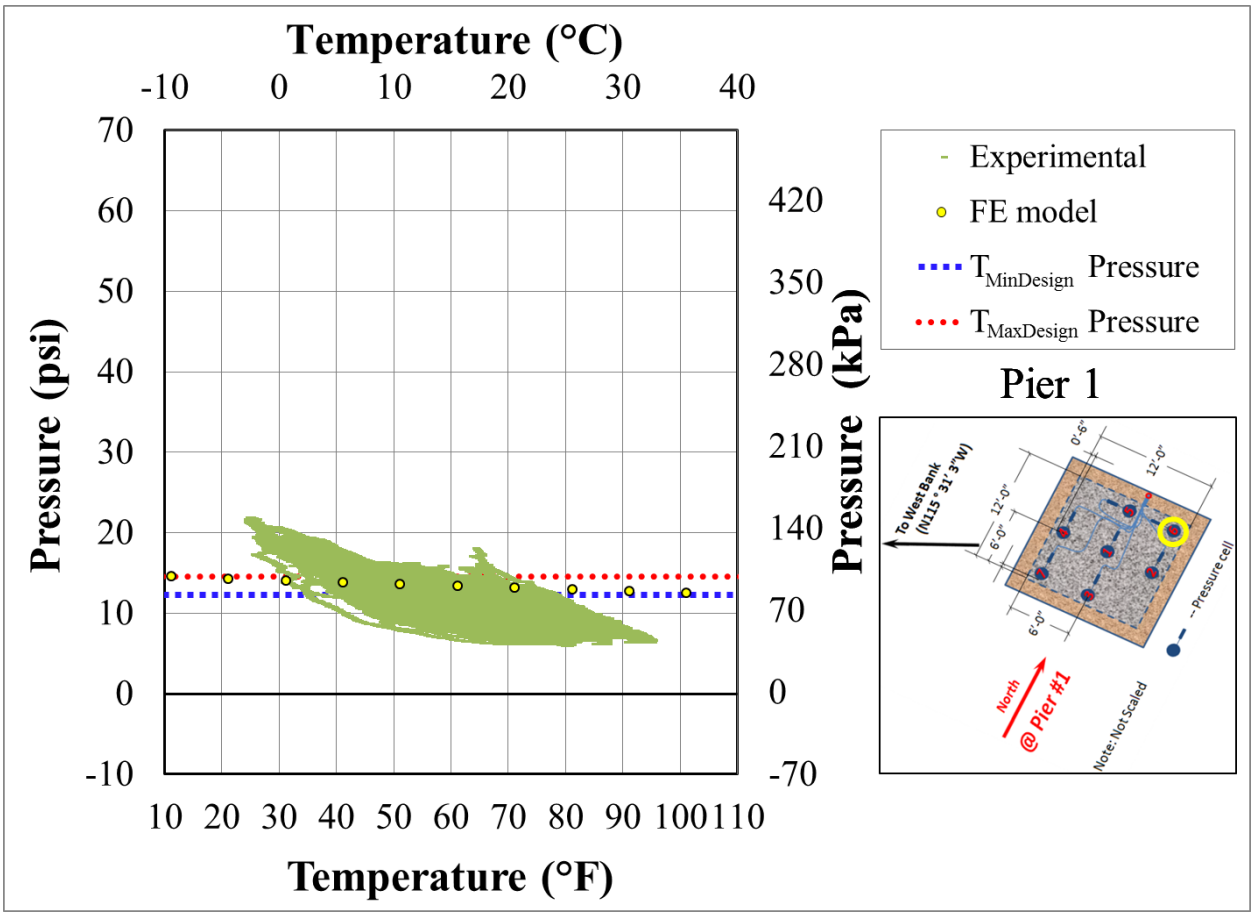

Fig. C.5: Pier 1, Cell 6 field measurements and numerical estimates of substructure response to gravity-temperature loading.

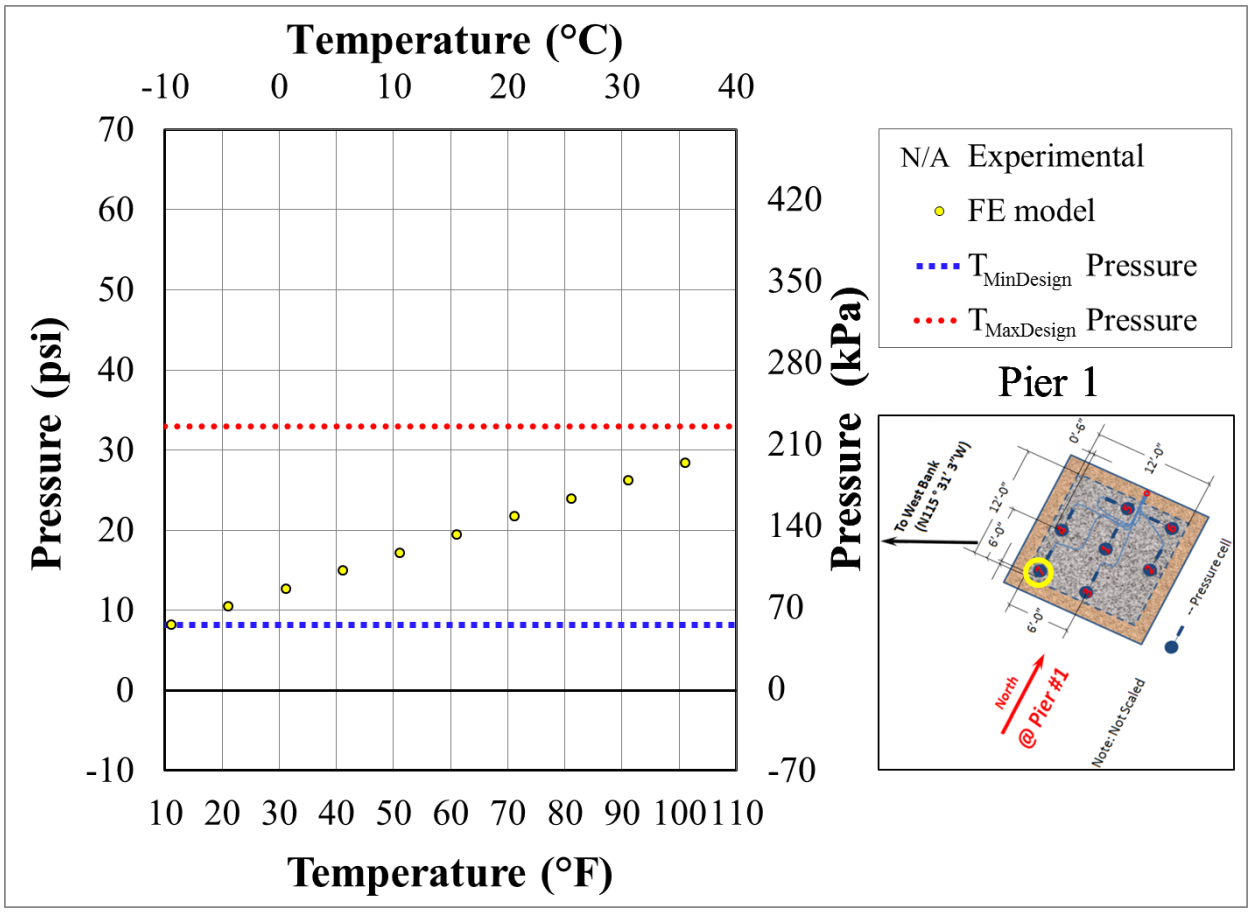

Fig. C.6: Pier 1, Cell 7 numerical estimates of substructure response to gravity-temperature loading (Note: Cell 7 field data are not available).

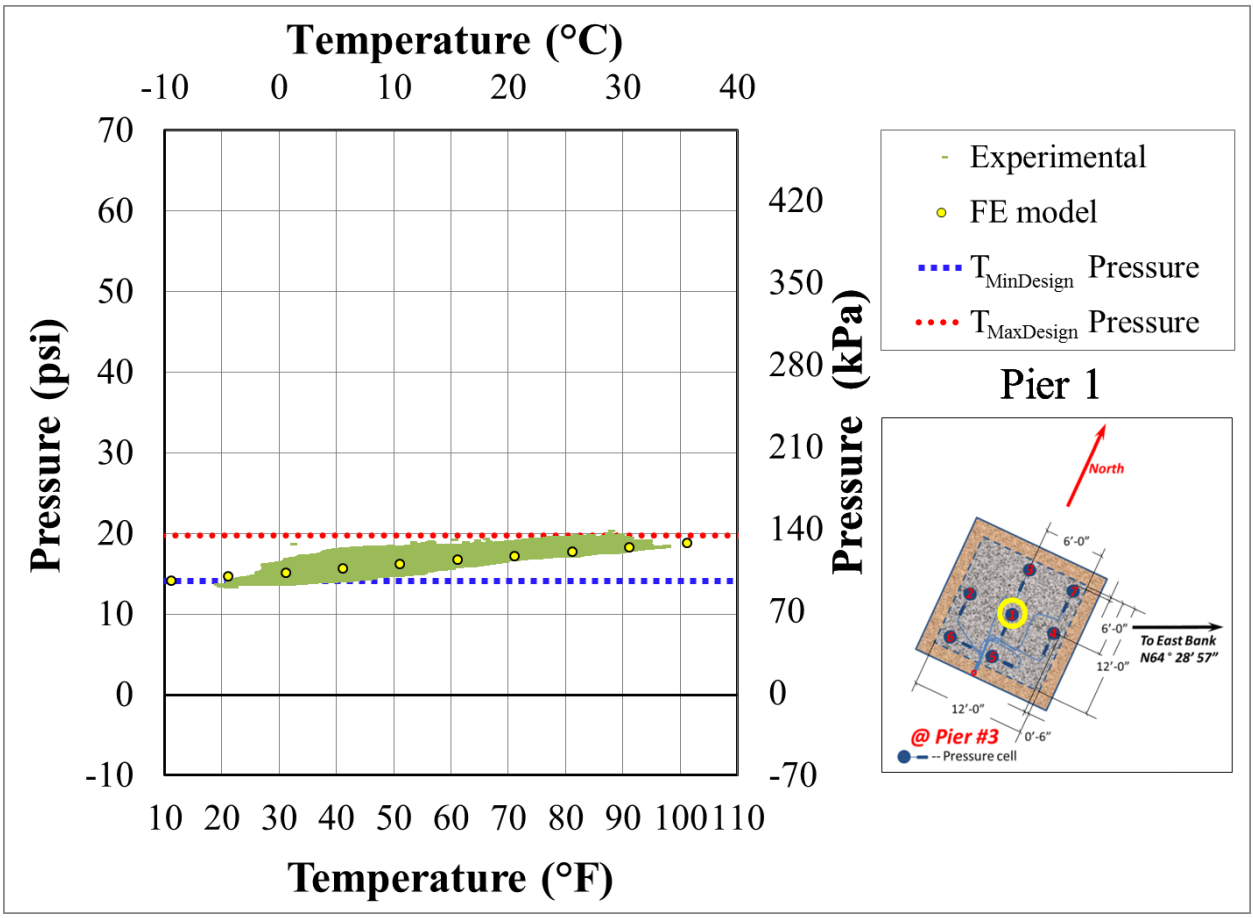

Fig. C.7: Pier 3, Cell 1 field measurements and numerical estimates of substructure response to gravity-temperature loading.

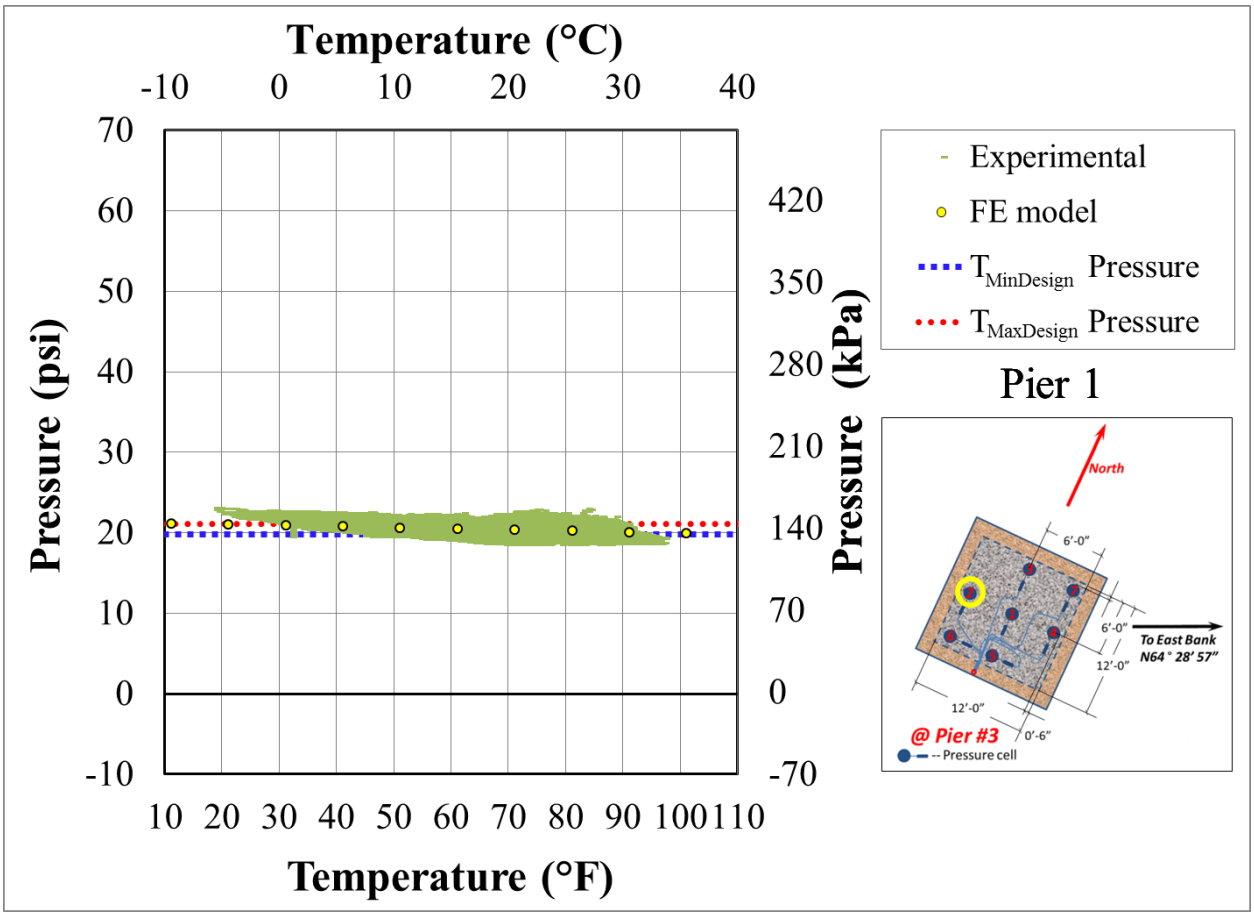

Fig. C.8: Pier 3, Cell 2 field measurements and numerical estimates of substructure response to gravity-temperature loading.

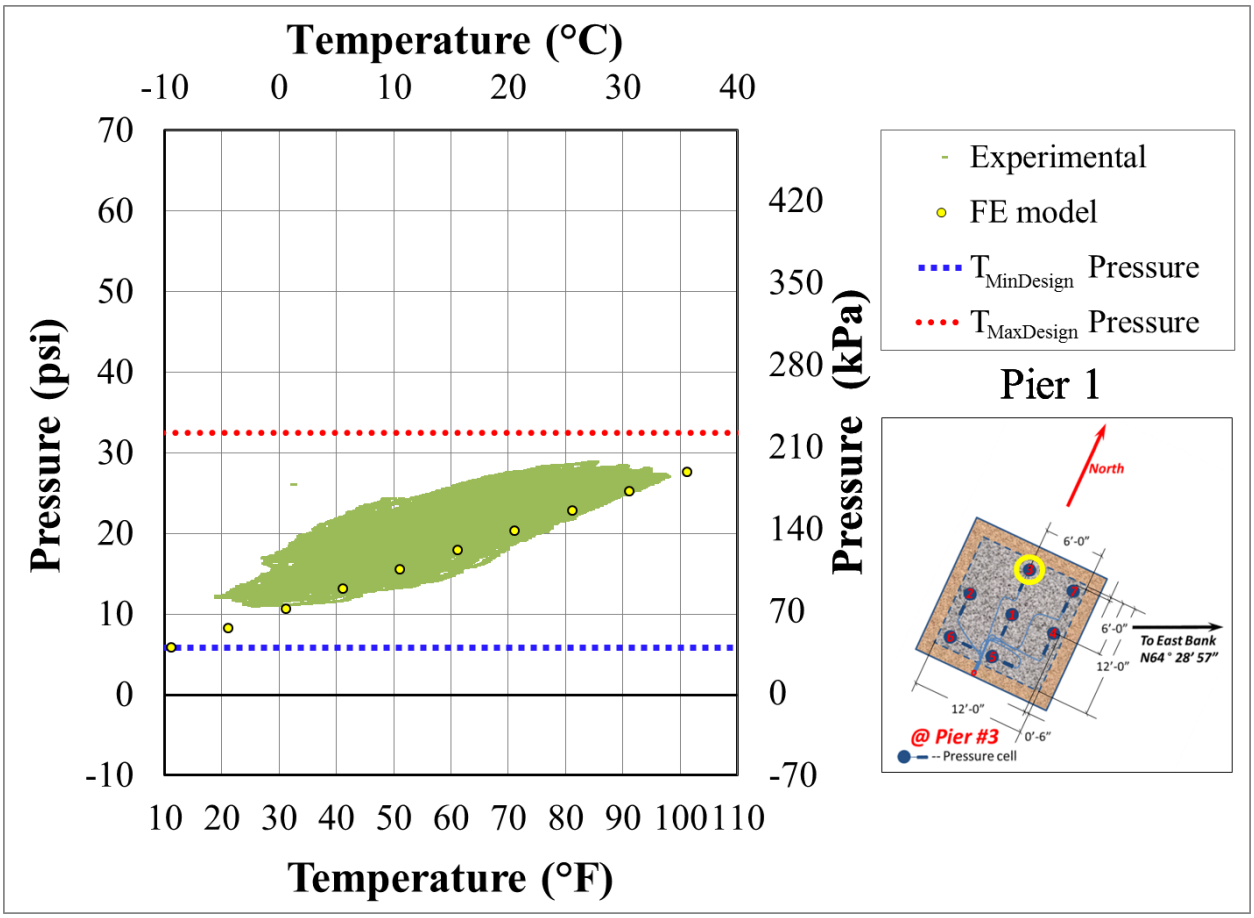

Fig. C.9: Pier 3, Cell 3 field measurements and numerical estimates of substructure response to gravity-temperature loading.

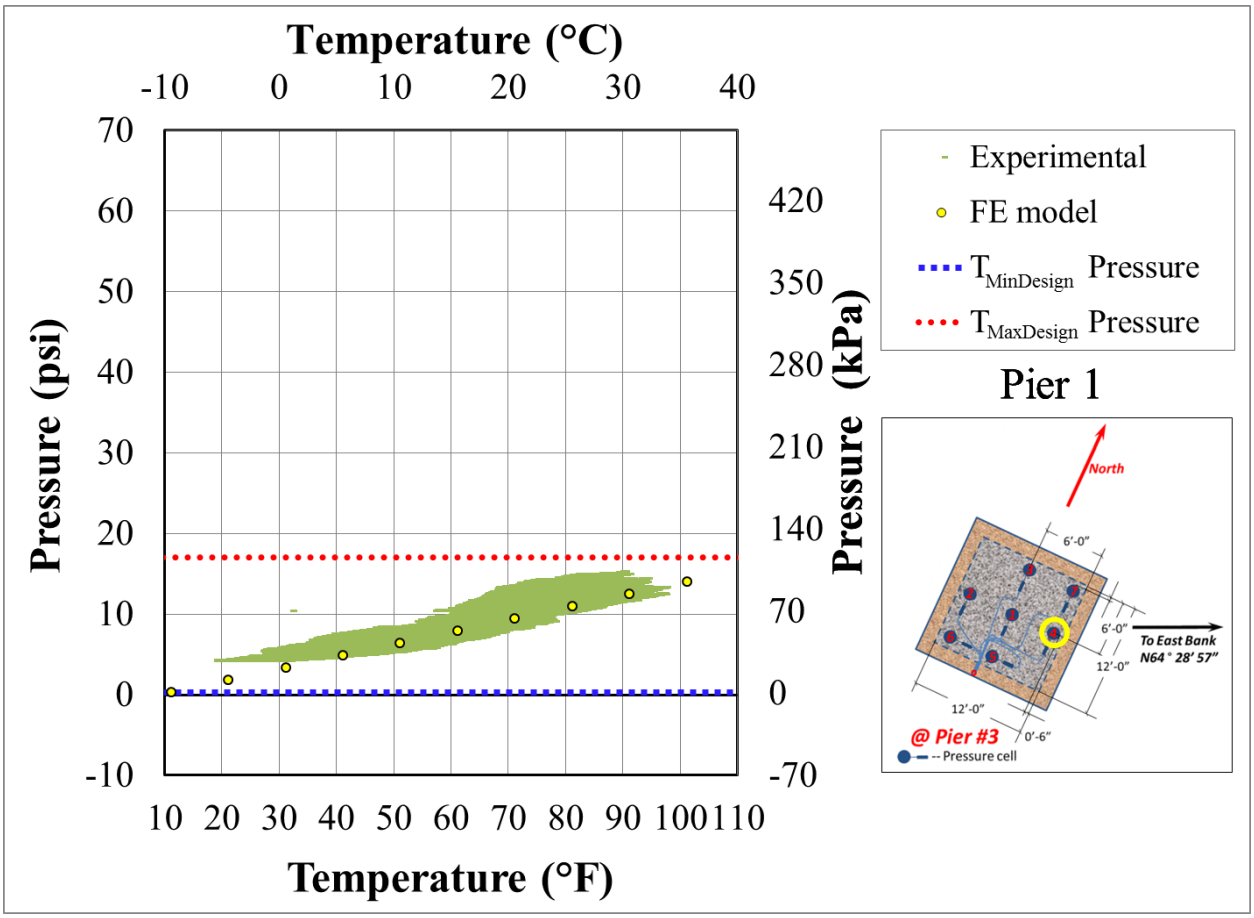

Fig. C.10: Pier 3, Cell 4 field measurements and numerical estimates of substructure response to gravity-temperature loading.

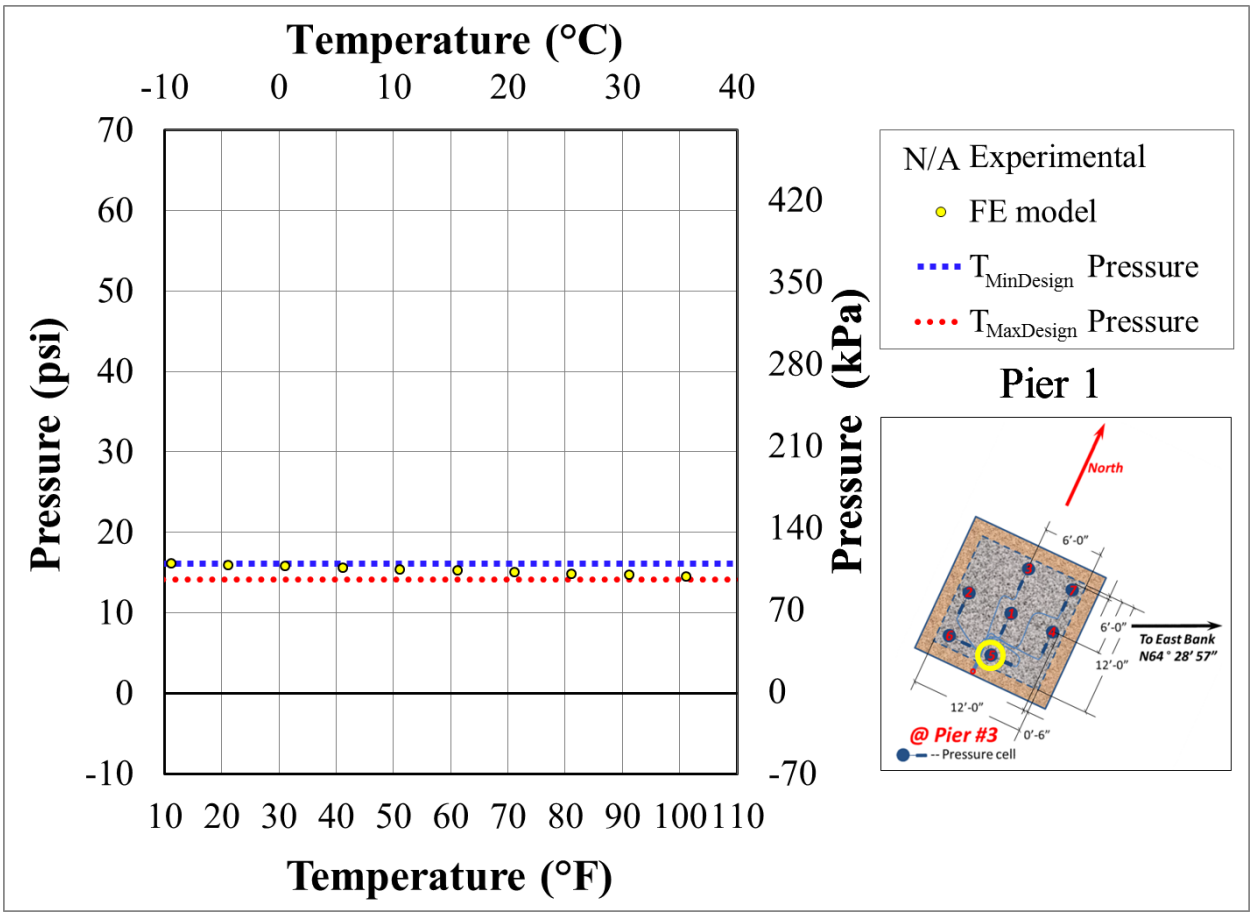

Fig. C.11: Pier 3, Cell 5 numerical estimates of substructure response to gravity-temperature loading (Note: Cell 5 field data are not available).

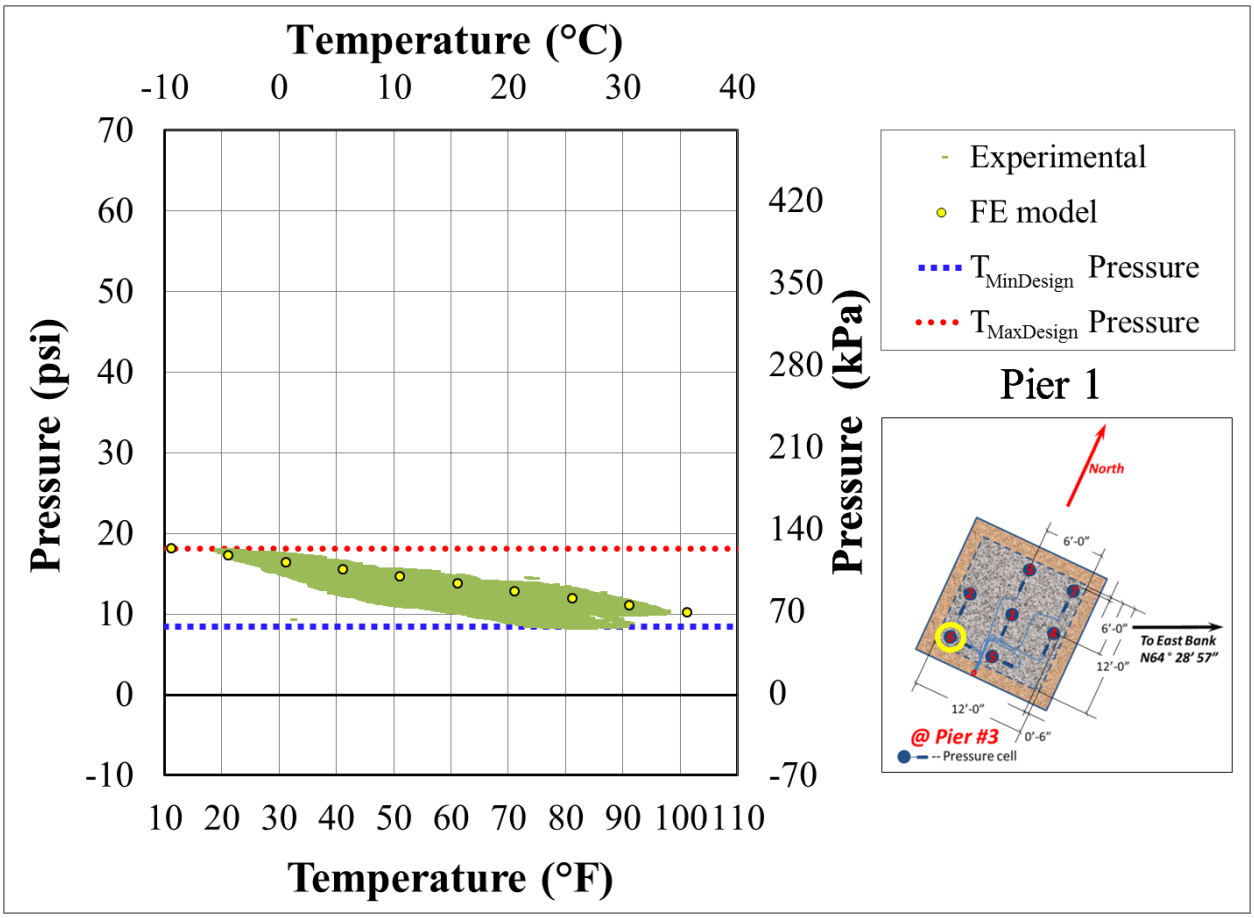

Fig. C.12: Pier 3, Cell 6 field measurements and numerical estimates of substructure response to gravity-temperature loading.

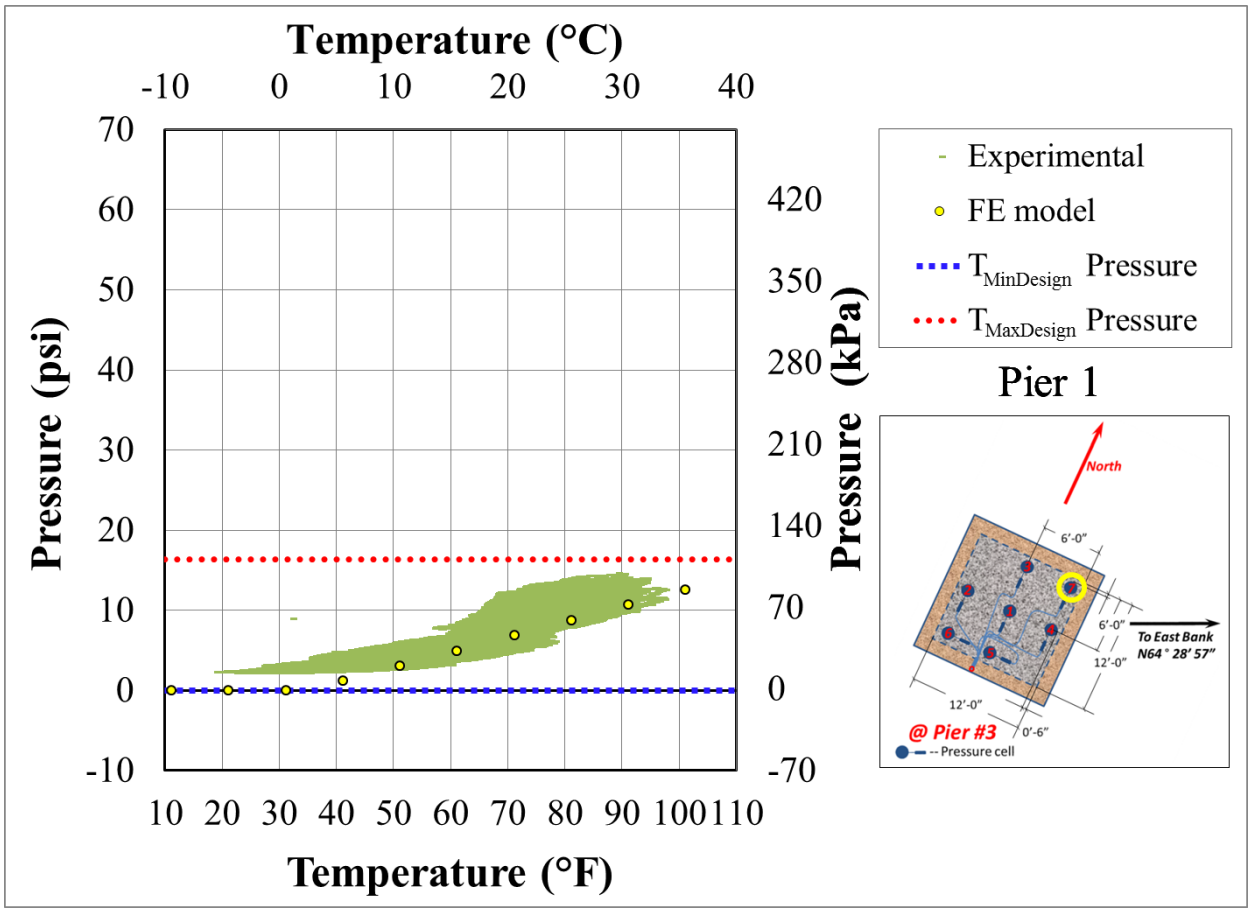

Fig. C.13: Pier 3, Cell 7 field measurements and numerical estimates of substructure response to gravity-temperature loading.